

# Mixed Convection Flows of Nonlinear Fluids



*By*

*Muhammad Bilal Ashraf*

**Department of Mathematics  
Quaid-i-Azam University  
Islamabad, Pakistan  
2015**

# Mixed Convection Flows of Nonlinear Fluids



*By*

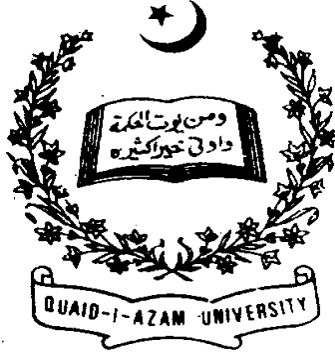
*Muhammad Bilal Ashraf*

Supervised By

*Prof. Dr. Tasawar Hayat*

Department of Mathematics  
Quaid-i-Azam University  
Islamabad, Pakistan  
2015

# Mixed convection flows of nonlinear fluids



*By*

*Muhammad Bilal Ashraf*

A THESIS SUBMITTED IN THE PARTIAL FULFILLMENT OF THE REQUIREMENT  
FOR THE DEGREE OF  
DOCTOR OF PHILOSOPHY  
IN  
MATHEMATICS

Supervised By

*Prof. Dr. Tasawar Hayat*

Department of Mathematics  
Quaid-i-Azam University  
Islamabad, Pakistan  
2015

# Mixed Convection Flows of Nonlinear Fluids


By


*Muhammad Bilal Ashraf*


## CERTIFICATE

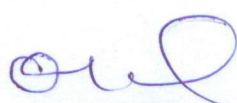
A THESIS SUBMITTED IN THE PARTIAL FULFILLMENT OF THE  
REQUIREMENTS FOR THE DEGREE OF THE DOCTOR OF  
PHILOSOPHY

**We accept this dissertation as conforming to the required standard**

1.   
Prof. Dr. Tasawar Hayat  
(Supervisor)

2.   
Prof. Dr. Tasawar Hayat  
(Chairman)

3.   
Prof. Dr. Nazir Ahmed Mir  
(External Examiner)

4.   
Dr. Qamar Ul Haq  
(External Examiner)

**Department of Mathematics  
Quaid-i-Azam University  
Islamabad, Pakistan  
2015**

## Preface

The boundary layer flows over a moving surface have vital importance due to their ever increasing usage in the industries. In such industrial processes, the kinematics of stretching and heat transfer through rate of cooling have substantial impact in the improvement of final product of better quality. No doubt, the thermal buoyancy force arising due to cooling or heating of a moving surface may alter significantly the flow and thermal fields and thereby the heat transfer behavior in the manufacturing process. In several practical applications, the order of magnitudes of buoyancy and viscous forces are comparable for moderate flow velocities and large surface temperature differences and convective heat transfer process is thus called as mixed convection. The buoyancy forces due to temperature and concentration differences are significant in mixed convection thermal and concentration diffusions. In fact the buoyancy forces causing a pressure gradient in the boundary layer modify the velocity, temperature and concentration distributions and consequently the rate of heat and mass transfer between the surface and fluid. Specifically the mixed convection flows are encountered in industrial processes like solar central receivers exposed to the wind currents, nuclear reactors called during emergency shutdown, electronic devices cooled by fans and heat exchangers etc. The mixed convection flows with heat and mass transfer are relevant to energy related engineering problems that include both metal and polymer sheets. Mostly, the fluids in industrial processes are non-Newtonian. Certain oils, paints, blood at low shear rate, shampoos, cosmetic products body fluids, pasta, ice cream, ice, mud etc are few examples of non-Newtonian fluids. Keeping all the aforementioned facts in mind, the present thesis is structured as follows.

Chapter one covers literature survey and laws of conservation of mass, linear momentum and energy. Boundary layer equations of second grade, Maxwell, Oldroyd-B and thixotropic fluids are presented. Basic idea of homotopy analysis method is also given.

Chapter two deliberates the mixed convection boundary layer flow of thixotropic fluid with thermophoresis over a stretched sheet. Fluid is electrically conducting in the presence of constant applied magnetic field. Heat and mass transfer effects are considered in the presence of Joule heating and thermal radiation. Series solutions are obtained to analyze the velocity, temperature and concentration fields. Numerical values of local Nusselt and Sherwood numbers for different values of emerging parameters are computed and analyzed. A comparative study with the previous solutions in a limiting sense is made. The leading results of this problem are published in "**Journal of Thermophysics and Heat Transfer 27 (2013) 733-740**".

Three-dimensional mixed convection flow of second grade fluid over an exponentially stretching surface are studied in chapter three. Convective boundary conditions are utilized for the heat transfer analysis. Analysis is carried out in the presence of thermal radiation. The series solutions are established through a newly developed method recognized as

the homotopy analysis method. The convergent analysis of velocity components and temperature are derived. Graphs are plotted and analyzed for interesting physical parameters. A systematic study is performed to analyze the impacts of the significant parameters on the velocity and temperature, the skin friction coefficients and the local Nusselt number. The contents of this chapter are published in **"Plos One 9 (2014) e90038"**.

Chapter four reports the heat and mass transfer effects in three-dimensional mixed convection flow of viscoelastic fluid with internal heat source/sink and chemical reaction. An exponential stretching surface is employed for flow generation. Magnetic field normal to the direction of flow is taken under consideration. Convective conditions at boundary surface are also encountered. An analytical approach homotopy analysis method is used to develop the solution expressions of the problem. Impacts of different controlling parameters such as stretching ratio parameter, Hartman number, internal heat source/sink, chemical reaction, mixed convection, concentration buoyancy parameter and Biot numbers on the velocity, temperature and concentration profiles are analyzed graphically. The local Nusselt number and Sherwood numbers are sketched and examined. The results of present chapter are accepted for publication in **"Computational Mathematics and Mathematical Physics"**.

Chapter 5 provides the three-dimensional mixed convection flow of viscoelastic fluid over a stretching surface in presence of thermophoresis. Soret and Dufour effects are also taken into account. Series solutions are constructed. Dimensionless velocity, temperature and concentration distributions are shown graphically for different values of involved parameters. Numerical values of local Nusselt and Sherwood numbers are computed and analyzed. The contents of this chapter are submitted for possible publication in **"International Journal of Nonlinear Sciences and Numerical Simulation"**.

Three-dimensional flow of Maxwell fluid over a stretching surface is addressed in chapter six. Analysis is prepared in presence of concentration and thermal buoyancy effects. Convective boundary conditions for heat and mass transfer are explored. Series solutions of the resulting problem are established. Results are displayed to examine the influence of physical parameters on the velocity, temperature and concentration fields. Main observations of this chapter are published in **"Journal of Central South University 22 (2015) 717-726"**.

Chapter seven is prepared to examine the heat and mass transfer effects in three-dimensional flow of Maxwell fluid over a stretching surface with convective boundary conditions. Mass transfer is considered in the presence of first order chemical reaction. Conservation laws of energy and concentration are based upon the Soret and Dufour effects. Convergent series solutions to the resulting nonlinear problems are developed. The relevant results are published in **"International Journal of Numerical Method for Heat and Fluid Flow 25 (2015) 98 - 120"**.

Mixed convection flow by an inclined stretching surface with thermal radiation is investigated in chapter eight. The boundary layer equations of an Oldroyd-B fluid in the presence of heat transfer are used. Suitable transformations reduce the partial differential equations into the ordinary differential equations. Computational analysis is implemented

for the convergent series solutions. The values of local Nusselt number are numerically analyzed. Effects of various parameters involved in the velocity and temperature are discussed. The contents of this chapter are accepted for publication in "**Journal of Applied Mechanics and Technical Physics**".

Chapter nine provides the mixed convection flow of an Oldroyd-B fluid bounded by a stretching surface with suction/injection. Mathematical formulation is developed in the presence of heat source and power law heat flux. Velocity and temperature are computed. Numerical values of local Nusselt number are examined. Results are computed in a limiting sense with existing literature. The contents of this chapter are published in "**Journal of the Brazilian Society of Mechanical Sciences and Engineering 37 (2015) pp 423-430**".

Chapter ten investigates the effects of heat and mass transfer in the mixed convection flow of an Oldroyd-B fluid over a stretching surface with convective boundary conditions. Stress is given to the analysis of Soret and Dufour effects. Related problems are first modeled and then computed by homotopy analysis method (HAM). Velocity, temperature and concentration fields are given. In addition, the local Nusselt and Sherwood numbers are examined through numerical values. These observations are submitted for publication in "**Thermophysics and Aeromechanics**".

Falkner-Skan flow of rate type non-Newtonian fluid is analyzed in chapter eleven. Expressions of an Oldroyd-B fluid are used in the development of relevant equations. Analysis has been carried out in presence of mixed convection and thermal radiation. Expressions of flow and heat transfer are assembled. Convergence of derived nonsimilar series solutions is provided. This research is submitted for publication in "**Journal of Aerospace Engineering**".

.

# Contents

<b>1</b>	<b>Literature survey and methodology</b>	<b>5</b>
1.1	Introduction . . . . .	5
1.2	Background . . . . .	5
1.3	Fundamental laws . . . . .	12
1.3.1	Law of conservation of mass . . . . .	12
1.3.2	Law of conservation of linear momentum . . . . .	12
1.3.3	Equation of heat transfer . . . . .	13
1.3.4	Diffusion equation . . . . .	13
1.4	Boundary layer equations of nonlinear fluids . . . . .	14
1.4.1	Second grade fluid . . . . .	14
1.4.2	Maxwell fluid . . . . .	15
1.4.3	Oldroyd-B fluid . . . . .	16
1.4.4	Thixotropic fluid . . . . .	17
1.5	Homotopy analysis method (HAM) . . . . .	18
<b>2</b>	<b>MHD mixed convection flow of thixotropic fluid with thermophoresis, Joule heating and thermal radiation</b>	<b>21</b>
2.1	Mathematical formulation . . . . .	21
2.2	Series solutions . . . . .	25
2.3	Convergence analysis and discussion . . . . .	28
2.4	Closing remarks . . . . .	40



<b>3</b>	<b>Three-dimensional mixed convection flow of viscoelastic fluid with thermal radiation and convective conditions</b>	<b>41</b>
3.1	Mathematical analysis . . . . .	42
3.2	Solutions development . . . . .	45
3.3	Convergence analysis . . . . .	49
3.4	Discussion of results . . . . .	50
3.5	Conclusions . . . . .	58
<b>4</b>	<b>Convective heat and mass transfer in three-dimensional mixed convection flow of viscoelastic fluid with chemical reaction and heat source/sink</b>	<b>60</b>
4.1	Mathematical modeling . . . . .	61
4.2	Series solutions . . . . .	63
4.3	Convergence analysis and discussion . . . . .	67
4.4	Closing remarks . . . . .	75
<b>5</b>	<b>Thermophoresis and MHD mixed convection flow with Soret and Dufour effects</b>	<b>76</b>
5.1	Mathematical analysis . . . . .	76
5.2	Construction of solutions . . . . .	79
5.3	Analysis . . . . .	83
5.4	Conclusions . . . . .	90
<b>6</b>	<b>Three-dimensional flow of Maxwell fluid over a stretching surface with heat source and convective conditions</b>	<b>92</b>
6.1	Governing problems . . . . .	92
6.2	Series solutions . . . . .	95
6.3	Convergence analysis and discussion . . . . .	98
6.3.1	Conclusions . . . . .	105
<b>7</b>	<b>Soret and Dufour effects in three-dimensional flow of Maxwell fluid with chemical reaction and convective condition</b>	<b>106</b>
7.1	Problems formulation . . . . .	106

7.2	Homotopy analysis solutions . . . . .	109
7.3	Analysis and discussion . . . . .	113
7.4	Conclusions . . . . .	125
<b>8</b>	<b>Radiative mixed convection flow of an Oldroyd-B fluid by an inclined stretching surface</b>	<b>127</b>
8.1	Mathematical analysis . . . . .	127
8.2	Convergence of the series solutions . . . . .	132
8.3	Discussion . . . . .	133
8.4	Concluding remarks . . . . .	138
<b>9</b>	<b>Mixed convection flow of an Oldroyd-B fluid with power law heat flux and heat source</b>	<b>139</b>
9.1	Development of problems . . . . .	139
9.2	Homotopy analysis solutions . . . . .	142
9.3	Convergence of the homotopy solutions . . . . .	144
9.4	Graphical results and discussion . . . . .	145
9.5	Final remarks . . . . .	150
<b>10</b>	<b>Soret and Dufour effects in mixed convection flow of an Oldroyd-B fluid with convective boundary conditions</b>	<b>151</b>
10.1	Mathematical model . . . . .	151
10.2	Series solutions . . . . .	153
10.2.1	Zeroth and mth order deformation problems . . . . .	154
10.3	Convergence of the homotopy solutions . . . . .	156
10.4	Discussion . . . . .	157
10.5	Conclusions . . . . .	163
<b>11</b>	<b>Mixed convection Falkner-Skan wedge flow of an Oldroyd-B fluid in presence of thermal radiation</b>	<b>164</b>
11.1	Problems development . . . . .	164
11.2	Series solutions . . . . .	167

11.2.1	Zeroth order problem . . . . .	167
11.2.2	$m$ th-order deformation problems . . . . .	168
11.3	Convergence . . . . .	170
11.4	Discussion . . . . .	170
11.5	Conclusions . . . . .	175

# Chapter 1

## Literature survey and methodology

### 1.1 Introduction

This chapter contains the literature review related to the considered flow problems. Boundary layer equations of thixotropic, second grade, Maxwell and Oldroyd-B fluids are presented. Brief idea of homotopy analysis method (HAM) are also provided.

### 1.2 Background

External flows around streamlined bodies have viscous (shear and no-slip) effects confined close to the body surfaces and its wake but are nearly inviscid far from the body are termed as boundary layer flows [1] which occur in aerodynamics (airplanes, rockets, projectiles), hydrodynamics (ships, submarines, torpedoes), transportation (automobiles, trucks, cycles), wind engineering (buildings, bridges, water towers) and ocean engineering (buoys, breakwaters, cables). The boundary layer flow problem over stretching sheet have many industrial applications such as polymer sheet or filament extrusion from a dye or long thread between feed roll or wind-up roll, glass fiber and paper production, drawing of plastic films and liquid films in condensation process. Due to the high applicability of this problem in such industrial phenomena, Sakiadis [2] initiated the work for flow by moving surface. After the pioneering work of Sakiadis, researchers have studied the flow over stretching surfaces under various aspects for viscous and nonlinear fluids. A similarity solution of viscous fluid over a stretching surface which is stretched with

the velocity proportional to the distance from origin was presented by Crane [3]. Chakrabarti and Gupta [4] analyzed the hydromagnetic flow over a stretching surface. Heat transfer over a continuous stretching surface with suction and injection was analyzed by Chen and Char [5]. Vajravelu and Hadjinicolaou [6] reported the heat transfer features in the laminar boundary layer flow of viscous fluid over a linearly stretching surface with variable wall temperature. Effects of suction and injection are present. They attained the solutions of the problem in Kumar functions. Andersson et al. [7] found the solutions over a stretching surface in presence of first order chemical reactions. Similarity solutions of the boundary layer equations over stretching wall was obtained by Banks [8]. Closed form solution of magnetohydrodynamic (MHD) flow under slip condition over a permeable stretching surface was obtained by Fang et al. [9]. Mukhphadhyay et al. [10] obtained the solution of MHD boundary layer flow over a heated stretching sheet with variable viscosity. Wang [11] extended the boundary layer flow of Crane [3] for three-dimensional stretching surface. Devi et al. [12] extended the flow of ref. [11] for unsteady stretching surface in presence of heat and mass transfer effects. An approximate analytical solutions of the steady, laminar three-dimensional flow for an incompressible viscous fluid past a stretching sheet were proposed by Ariel [13,14]. Hayat and Javed [15] analyzed the three-dimensional flow of an incompressible viscous fluid over a porous stretching surface in presence of magnetic field by employing homotopy analysis method. Kumari and Nath [16] discussed the unsteady magnetohydrodynamic viscous fluid with heat transfer induced by a bilateral stretching surface. An analysis for heat transfer over a non-linearly stretching surface for a viscous fluid was provided by Vajravelu [17]. Cortell [18] extended the work of ref. [17] in presence of thermal radiation and viscous dissipation over a non-linearly stretching surface. Two-dimensional magnetohydrodynamic stagnation point flow of an incompressible micropolar fluid over a non-linearly stretching surface was explored by Hayat et al. [19]. The laminar boundary layer flow over an axisymmetric plane was provided by Afzal [20]. It has been noted by Gupta and Gupta [21] that stretching mechanism in all realistic situation is not linear. For instance the stretching is not linear in plastic and paper production industries. Besides these the flow and heat transfer by an exponentially stretching surface has been studied by Magyari and Keller [22]. In this attempt the two-dimensional flow of an incompressible viscous fluid is considered. The solutions of laminar boundary layer equations describing heat and flow in a

quiescent fluid driven by an exponentially permeable stretching surface were numerically analyzed by Elbashbasha [23]. Al- Odat et al. [24] numerically discussed the thermal boundary layer flow with an exponential temperature distribution. Here magnetohydrodynamic flow was addressed. Liu et al. [25] studied the three-dimensional boundary layer flow of a viscous fluid over an exponentially stretching surface by using the Ackroyd and Runge-Kutta methods.

Analysis of non-linear fluids is an active area of research for the last few years. In many fields such as food industry, drilling operations and bioengineering, the fluids, either synthetic or natural, are mixtures of different stuffs such as water, particle, oils, red cells and other long chain molecules. Such combination imparts strong rheological properties to the resulting liquids. The dynamic viscosity in non-linear materials varies non-linearly with the shear rate. These fluids in terms of their different rheological features cannot be described by a single constitutive relationship. Hence several relationships for the non-linear fluids are proposed. In fact the additional parameters in such non-linear fluids are the main culprit which makes the resulting systems more nonlinear, higher order and complex than the Navier-Stokes equations. The rheological fluids in general have been classified into three categories known as the differential, integral and rate types. Second grade fluid is a subclass of differential type fluids which exhibits the normal stress effects. To predict these effects many researchers studied second grade fluid under various aspects. Dandapat and Gupta [26] discussed the flow of an incompressible second-order fluid due to stretching surface under boundary layer assumptions. Chen et al. [27] delivered the temperature distribution in viscoelastic fluid of Walters' B Model over a horizontal stretching plate. The velocity of the plate is proportional to the distance from the slit. Vajravelu and Rollins [28] carried out the heat transfer effects in viscoelastic fluid over a stretching surface with frictional heating and internal heat generation or absorption. Hayat et al. [29] studied the three-dimensional flow over stretching surface in a viscoelastic fluid by applying homotopy analysis method. Liu [30] presented analytical solutions for the flow and heat transfer in steady laminar boundary flow of an electrically conducting fluid of second grade subject to transverse uniform magnetic field past a semi-infinite stretching sheet with power-law surface temperature or power-law surface heat flux. The effects of viscous dissipation, internal heat generation or absorption, work done due to deformation and Joule heating were also considered in the energy equation. Flow and heat transfer characteristics of viscoelastic fluid with porous medium over

a stretching surface with viscous dissipation was governed by Nandeppanavar et al. [31]. Differential type models do not predict the relaxation and retardation time effects while these effects can be anticipated by rate type fluids. Maxwell fluid is a simplest subclass of rate type fluids. Channel flow of an upper convected Maxwell fluid (UCM) induced by suction was presented by Choi et al. [32]. Sadeghy [33] discussed the flow of an upper-convected Maxwell (UCM) fluid above a rigid plate moving steadily. Pahlavan et al. [34] studied the MHD flows of UCM fluids above porous stretching sheets using two-auxiliary-parameter homotopy analysis method. Maxwellian MHD flow induced by a linearly stretched with thermal radiations was investigated by Aliakbar et al. [35]. Unsteady flow of generalized Maxwell fluid with fractional derivative induced by an accelerating plate was provided by Fetecau et al. [36]. Kumari and Nath [37] analyzed the Maxwell fluid over stretching sheet in presence of mixed convection. Abel et al. [38] proposed the MHD flow and heat transfer for the upper-convected Maxwell fluid over a stretching sheet. Hayat et al. [39] presented the three-dimensional Maxwell fluid over stretching surface with convective boundary conditions. Bhatanagar et al. [40] initiated to analyze the boundary layer flow of rate type fluids. They obtained the solutions of two-dimensional flow over a stretching surface with variable free stream velocity. Exact solutions of unidirectional flow of an Oldroyd-B fluid between two parallel plates was presented by Rajagopal [41]. Exact solutions for flows of an electrically conducting Oldroyd-B fluid over an infinite oscillatory plate in the presence of a transverse magnetic field when the entire system rotates about an axis normal to the plate was obtained by Hayat et al. [42]. The linear stability of the flow of an Oldroyd-B fluid through a linear array of cylinders confined in a channel was analyzed by Smith et al. [43]. They computed solutions for both the steady state and linear stability of these states by employing finite element analysis. Exact solutions for the influence of Hall current and rotation in the oscillatory flows by an infinite plate were obtained by Asghar et al. [44]. Fetecau and Fetecau [45] analyzed the unsteady flows of Oldroyd-B fluids in a channel of rectangular cross-section. A linear stability analysis determining the onset of oscillatory convection of an Oldroyd-B fluid in a two-dimensional rectangular porous medium generated by Newtonian heating was presented by Niu et al. [46].

In nonlinear fluids sometimes nonlinearity introduced by their shear-dependent viscosity and/or elasticity often gives rise to a formidable mathematical task which cannot be solved.

Obviously, the situation becomes much more complicated when the viscosity of the fluid is time-dependent. Time-dependent fluid systems are quite frequent in industrial applications with the common effect being a drop in viscosity by the progress of time. Complex fluid systems such as drilling muds, foodstuff, paints, cosmetics, pharmaceuticals, suspensions, grease, and the like belong to this class of fluids-the so-called thixotropic fluids. Physiological fluids such as blood, synovial fluid, and mucus may also exhibit thixotropic behavior depending on the time scale of the observation. A common effect among thixotropic fluids is that their viscosity is decreased even when the shear rate is constant [47,48]. Harris [49,50] tried to address boundary layer flows of thixotropic fluids. Harris presented a simple thixotropic fluid model (the so called Harris model) to investigate the effects of a fluid's thixotropic behavior on the characteristics of the momentum boundary layer formed above a fixed plate [50]. Two-dimensional flow of an incompressible thixotropic fluid obeying Harris rheological model over a fixed semi-infinite plate was investigated by Sadeqi et al. [51].

Mixed convection flows or combined free and forced convection flows occur in many technological and industrial applications and in nature for example, in solar receivers exposed to wind currents, electronic devices cooled by fans, nuclear reactors cooled during emergency shutdown, heat exchanges placed in a low-velocity environment, flows in the ocean and in the atmosphere, and many more. Finite element method was utilized for detailed analysis of mixed-convection flow in a horizontal channel heated from the side walls were computed by Sillekens [52]. Heat transfer enhancement by air injection in upward heated mixed-convection flow of water was studied by Celata et al. [53]. Barletta [54] provided the analysis of the laminar and fully developed mixed convection flow in a vertical rectangular duct with one or more isothermal walls. Magyari et al. [55] analyzed the boundary layer mixed convection flow over a permeable horizontal plate. The unsteady mixed convection boundary layer flow near the region of a stagnation point on a vertical surface embedded in a Darcian fluid-saturated porous medium was investigated by Nazar et al. [56]. They employed Keller-Box method to obtain the solutions. Laminar two-dimensional unsteady mixed convection boundary-layer flow of viscous incompressible fluid past a sharp wedge was developed by Hussain et al. [57]. Perturbation solutions were obtained for small and large dimensionless time. Experimental investigation was presented on mixed (free and forced) convection to study the local and average heat transfer



for hydrodynamically and thermally developed laminar air flow in a horizontal circular cylinder was analyzed by Mohammed and Salman [58]. Laminar mixed convection heat transfer for assisted and opposed air flows in the entrance region of a vertical circular tube with wall heat flux boundary condition had been experimentally investigated by Mohammed [59]. Kotouc et al. [60] also provided the loss of axisymmetry in the mixed convection assisting flow past a heated sphere. A transient laminar mixed convection flow of viscous incompressible fluid generated by thermal buoyancy force over a horizontal porous sensor surface placed inside a squeezing channel was discussed by Mahmood et al. [61]. The implicit finite difference approximation together with Keller box method was employed for the solution of small and large time regimes. Heat and mass transfer characteristics in mixed convection boundary layer flow past a linearly stretching vertical surface in a porous medium filled with a viscoelastic fluid with Dufour and Soret effects was governed by Hayat et al. [62].

Radiative mixed convection has gained much importance amongst the recent researchers due to number of applications in geophysical and energy storage problems such as in furnaces, ovens and boilers and the interest in our environment and in no conventional energy sources, such as the use of salt gradient solar ponds for energy collection and storage. Similarity equations governing steady hydromagnetic boundary-layer flow over an accelerating permeable surface in the presence of thermal radiation, thermal buoyancy and heat generation or absorption effects were obtained by Chamka [63]. Buoyancy force and thermal radiation effects in MHD boundary layer viscoelastic fluid flow over continuously moving stretching surface was investigated by Abel et al. [64]. Mukhopadhyay and Layek [65] presented the free convective boundary layer flow and heat transfer of a fluid with variable viscosity over a porous stretching vertical surface in presence of thermal radiation. Results were obtained by Lie group transformations. Also Mukhopadhyay [66] analyzed the effects of thermal radiation on unsteady boundary layer mixed convection heat transfer problem from a vertical porous stretching surface embedded in porous medium. Magnetohydrodynamic mixed convective flow and heat transfer of an electrically conducting power-law fluid past a stretching surface in the presence of heat generation/absorption and thermal radiation was studied by Chen [67]. Numerical solutions were generated by an implicit finite-difference technique for the non-similar coupled flow.

A study of utilizing heat source or sink in moving fluids has been a subject of interest of many

researchers. This is because of its possible application to geophysical sciences, astrophysical sciences, and in cosmic studies. Such flows arise either due to unsteady motion of the boundary or the boundary temperature. The study of fluctuating flow is important in the paper industry and many other technological fields. Many investigators stressed on the magnetohydrodynamic flow of an electrically conducting fluid because of numerous applications in metallurgical industry such as in drawing, annealing, in the purification of molten metals from non-metallic inclusions, electromagnetic pumps, MHD generators etc. Several studies have been presented by the authors in presence of transverse magnetic field and heat source/sink over a stretching surface. Heat transfer characteristics in an electrically conducting fluid over a stretching sheet with variable wall temperature and heat source/sink was investigated by Vajravelu and Rollins [68]. Abel et al. [69] presented the study of momentum and heat transfer characteristics in hydromagnetic flow of viscoelastic liquid over a stretching sheet with non-uniform heat source, where the flow was generated due to a linear stretching of the sheet and influenced by uniform magnetic field applied vertically. Beg et al. [70] examined the magnetohydrodynamic free convection from a sphere embedded in an electrically-conducting fluid-saturated porous regime with heat generation.

The present trend in the field of chemical reaction analysis is to give a mathematical model for the system to predict the reactor performance. A large amount of research work has been reported in this field. In particular, the study of heat and mass transfer with chemical reaction is of considerable importance in chemical and hydrometallurgical industries. MHD flow with heat and mass transfer characteristics of an incompressible viscous electrically conducting and Boussinesq fluid due to a vertical stretching surface with chemical reaction and thermal stratification effects was presented by Kandasamy et al. [71]. Mansour et al. [72] studied the effects of chemical reaction, thermal stratification, Soret and Dufour numbers on MHD free convective heat and mass transfer of a viscous incompressible and electrically conducting fluid over a vertical stretching surface embedded in a saturated porous medium. The combined effect of mixed convection with thermal radiation and chemical reaction on MHD flow of viscous and electrically conducting fluid past a vertical permeable surface in presence of porous medium was analyzed by Pal and Talukdar [73]. Mass transfer with chemical reaction in MHD mixed convective flow along a vertical stretching sheet was investigated by Singh et al. [74].

## 1.3 Fundamental laws

### 1.3.1 Law of conservation of mass

The equation of continuity (law of conservation of mass) can be represented by

$$\frac{\partial \rho}{\partial t} + \nabla \cdot (\rho \mathbf{V}) = 0, \quad (1.1)$$

where  $\rho$  is the density of fluid and  $\mathbf{V}$  is the fluid velocity.

For an incompressible fluid Eq. (1.1) can be expressed as follows:

$$\nabla \cdot \mathbf{V} = 0. \quad (1.2)$$

### 1.3.2 Law of conservation of linear momentum

Generalized equation of motion can be expressed as

$$\rho \frac{d\mathbf{V}}{dt} = \nabla \cdot \boldsymbol{\tau} + \rho \mathbf{b}. \quad (1.3)$$

For an incompressible flow

$$\boldsymbol{\tau} = -p\mathbf{I} + \mathbf{S} \quad (1.4)$$

in which  $\boldsymbol{\tau}$  is the Cauchy stress tensor,  $p$  is the pressure,  $\mathbf{I}$  is the identity tensor,  $\mathbf{S}$  is the extra stress tensor,  $\mathbf{b}$  is the body force and  $d/dt$  is the material time derivative. The Cauchy stress tensor and the velocity field for three-dimensional flow can be described in the forms

$$\boldsymbol{\tau} = \begin{bmatrix} \sigma_{xx} & \tau_{xy} & \tau_{xz} \\ \tau_{yx} & \sigma_{yy} & \tau_{yz} \\ \tau_{zx} & \tau_{zy} & \sigma_{zz} \end{bmatrix}, \quad (1.5)$$

$$\mathbf{V} = [u(x, y, z), v(x, y, z), w(x, y, z)], \quad (1.6)$$

where  $\sigma_{xx}$ ,  $\sigma_{yy}$  and  $\sigma_{zz}$  represent the normal stresses,  $\tau_{xy}$ ,  $\tau_{xz}$ ,  $\tau_{yx}$ ,  $\tau_{yz}$ ,  $\tau_{zx}$  and  $\tau_{zy}$  show the shear stresses and  $u$ ,  $v$ ,  $w$  are the velocity components along the  $x$ ,  $y$  and  $z$ -directions respectively.

Equation (1.3) in component form can be written as follows:

$$\rho \left( \frac{\partial u}{\partial t} + u \frac{\partial u}{\partial x} + v \frac{\partial u}{\partial y} + w \frac{\partial u}{\partial z} \right) = \frac{\partial (\sigma_{xx})}{\partial x} + \frac{\partial (\tau_{xy})}{\partial y} + \frac{\partial (\tau_{xz})}{\partial z} + \rho b_x, \quad (1.7)$$

$$\rho \left( \frac{\partial v}{\partial t} + u \frac{\partial v}{\partial x} + v \frac{\partial v}{\partial y} + w \frac{\partial v}{\partial z} \right) = \frac{\partial (\tau_{yx})}{\partial x} + \frac{\partial (\sigma_{yy})}{\partial y} + \frac{\partial (\tau_{yz})}{\partial z} + \rho b_y, \quad (1.8)$$

$$\rho \left( \frac{\partial w}{\partial t} + u \frac{\partial w}{\partial x} + v \frac{\partial w}{\partial y} + w \frac{\partial w}{\partial z} \right) = \frac{\partial (\tau_{zx})}{\partial x} + \frac{\partial (\tau_{zy})}{\partial y} + \frac{\partial (\sigma_{zz})}{\partial z} + \rho b_z, \quad (1.9)$$

where  $b_x$ ,  $b_y$  and  $b_z$  show the components of body force along the  $x$ ,  $y$  and  $z$ -axes, respectively.

The above equations for two-dimensional flow become

$$\rho \left( \frac{\partial u}{\partial t} + u \frac{\partial u}{\partial x} + v \frac{\partial u}{\partial y} \right) = \frac{\partial (\sigma_{xx})}{\partial x} + \frac{\partial (\tau_{xy})}{\partial y} + \rho b_x, \quad (1.10)$$

$$\rho \left( \frac{\partial v}{\partial t} + u \frac{\partial v}{\partial x} + v \frac{\partial v}{\partial y} \right) = \frac{\partial (\tau_{yx})}{\partial x} + \frac{\partial (\sigma_{yy})}{\partial y} + \rho b_y. \quad (1.11)$$

### 1.3.3 Equation of heat transfer

According to first law of thermodynamics the heat transfer equation can be written as

$$\rho \frac{d\varepsilon}{dt} = \boldsymbol{\tau} \cdot \mathbf{L} - \boldsymbol{\nabla} \cdot \mathbf{q}_1 + \rho r_h, \quad (1.12)$$

where  $\varepsilon = C_p T$  is the internal energy,  $C_p$  the specific heat,  $T$  the temperature,  $\mathbf{L} = \boldsymbol{\nabla} \mathbf{V}$  the velocity gradient,  $\mathbf{q}_1 = -k \boldsymbol{\nabla} T$  the heat flux,  $k$  the thermal conductivity and  $r_h$  the radiative heating. The above equation in absence of radiative heating is given below

$$\rho C_p \frac{dT}{dt} = \boldsymbol{\tau} \cdot \boldsymbol{\nabla} \mathbf{V} + k \boldsymbol{\nabla}^2 T. \quad (1.13)$$

### 1.3.4 Diffusion equation

Mass transfer occurs whenever fluid flows that is some mass is transferred from one place to another. According to Fick's law

$$\frac{dC}{dt} = D_e \boldsymbol{\nabla}^2 C - k_n C_n \quad (1.14)$$

where  $C$  is the concentration,  $D_e$  is the coefficient of mass diffusivity and  $k_n$  is the reaction rate diffusing species.

## 1.4 Boundary layer equations of nonlinear fluids

### 1.4.1 Second grade fluid

Extra stress tensor  $\mathbf{S}$  for a second grade fluid can be expressed as

$$\mathbf{S} = \mu \mathbf{A}_1 + \alpha_1 \mathbf{A}_2 + \alpha_2 \mathbf{A}_1^2, \quad (1.15)$$

where  $\mathbf{A}_1$  is the first Rivlin-Erickson tensor can be defined by

$$\mathbf{A}_1 = \text{grad } \mathbf{V} + (\text{grad } \mathbf{V})^{transpose}. \quad (1.16)$$

For three-dimensional flow one obtains

$$\mathbf{A}_1 = \begin{bmatrix} 2\frac{\partial u}{\partial x} & \frac{\partial u}{\partial y} + \frac{\partial v}{\partial x} & \frac{\partial u}{\partial z} + \frac{\partial w}{\partial x} \\ \frac{\partial u}{\partial y} + \frac{\partial v}{\partial x} & 2\frac{\partial v}{\partial y} & \frac{\partial v}{\partial z} + \frac{\partial w}{\partial y} \\ \frac{\partial u}{\partial z} + \frac{\partial w}{\partial x} & \frac{\partial v}{\partial z} + \frac{\partial w}{\partial y} & 2\frac{\partial w}{\partial z} \end{bmatrix} \quad (1.17)$$

and the second Rivlin-Erickson tensor  $\mathbf{A}_2$  can be computed through

$$\mathbf{A}_n = \frac{d\mathbf{A}_{n-1}}{dt} + \mathbf{A}_{n-1}\mathbf{L} + \mathbf{L}^{transpose}\mathbf{A}_{n-1}. \quad (1.18)$$

For thermodynamic stability the second grade model should obey the inequality given below:

$$\mu \geq 0, \alpha_1 \geq 0, \alpha_1 + \alpha_2 = 0. \quad (1.19)$$

From the boundary layer theory [1], the order of  $u, v, x$  and  $y$  are 1 while the order of  $w$  and  $z$  are  $\delta$ . Three-dimensional boundary layer equations for second grade fluid can be written as

$$u\frac{\partial u}{\partial x} + v\frac{\partial u}{\partial y} + w\frac{\partial u}{\partial z} = \nu\frac{\partial^2 u}{\partial z^2} + \frac{\alpha_1}{\rho} \left( \begin{aligned} &u\frac{\partial^3 u}{\partial x\partial z^2} + w\frac{\partial^3 u}{\partial z^3} - \\ &\left( \frac{\partial u}{\partial x}\frac{\partial^2 u}{\partial z^2} + \frac{\partial u}{\partial z}\frac{\partial^2 w}{\partial z^2} + 2\frac{\partial u}{\partial z}\frac{\partial^2 u}{\partial x\partial z} + 2\frac{\partial w}{\partial z}\frac{\partial^2 u}{\partial z^2} \right) \end{aligned} \right), \quad (1.20)$$

$$u \frac{\partial v}{\partial x} + v \frac{\partial v}{\partial y} + w \frac{\partial v}{\partial z} = \nu \frac{\partial^2 v}{\partial z^2} + \frac{\alpha_1}{\rho} \left( \begin{aligned} &v \frac{\partial^3 v}{\partial y \partial z^2} + w \frac{\partial^3 v}{\partial z^3} - \\ &\left( \frac{\partial v}{\partial y} \frac{\partial^2 v}{\partial z^2} + \frac{\partial v}{\partial z} \frac{\partial^2 w}{\partial z^2} + 2 \frac{\partial v}{\partial z} \frac{\partial^2 v}{\partial y \partial z} + 2 \frac{\partial w}{\partial z} \frac{\partial^2 v}{\partial z^2} \right) \end{aligned} \right). \quad (1.21)$$

### 1.4.2 Maxwell fluid

The extra stress tensor  $\mathbf{S}$  for Maxwell fluid can be expressed by the following relation

$$\left(1 + \lambda_1 \frac{D}{Dt}\right) \mathbf{S} = \mathbf{S} + \lambda_1 \frac{D\mathbf{S}}{Dt} = \mu \mathbf{A}_1, \quad (1.22)$$

in which  $\lambda_1$  is the relaxation time,  $D/Dt$  the covariant differentiation,  $\mu$  denotes the kinematic viscosity and  $\mathbf{A}_1$  the first Rivlin-Erickson tensor. For a tensor  $\mathbf{S}$  of rank two, a vector  $\mathbf{b}_1$  and a scalar  $\varphi$ , we get

$$\frac{D\mathbf{S}}{Dt} = \frac{\partial \mathbf{S}}{\partial t} + (\mathbf{V} \cdot \nabla) \mathbf{S} - \mathbf{S}(\text{grad } \mathbf{V})^{\text{transpose}} - (\text{grad } \mathbf{V}) \mathbf{S}, \quad (1.23)$$

$$\frac{D\mathbf{b}_1}{Dt} = \frac{\partial \mathbf{b}_1}{\partial t} + (\mathbf{V} \cdot \nabla) \mathbf{b}_1 - (\text{grad } \mathbf{V}) \mathbf{b}_1, \quad (1.24)$$

$$\frac{D\varphi}{Dt} = \frac{\partial \varphi}{\partial t} + (\mathbf{V} \cdot \nabla) \varphi. \quad (1.25)$$

Implementation of  $(1 + \lambda_1 \frac{D}{Dt})$  on Eq. (1.3), we have the following relations in the absence of body force

$$\rho \left(1 + \lambda_1 \frac{D}{Dt}\right) \frac{d\mathbf{V}}{dt} = - \left(1 + \lambda_1 \frac{D}{Dt}\right) \nabla p + \left(1 + \lambda_1 \frac{D}{Dt}\right) (\nabla \cdot \mathbf{S}). \quad (1.26)$$

By adopting the procedure

$$\frac{D}{Dt}(\nabla \cdot) = \nabla \cdot \left(\frac{D}{Dt}\right). \quad (1.27)$$

Hence the above relations in absence of pressure gradient is

$$\rho \left(1 + \lambda_1 \frac{D}{Dt}\right) \frac{d\mathbf{V}}{dt} = \mu (\nabla \cdot \mathbf{A}_1). \quad (1.28)$$

By using the boundary layer theory [1], the order of  $u$ ,  $v$ ,  $x$  and  $y$  is 1 and order of  $w$  and  $z$  is  $\delta$ . The  $w$ -momentum equation vanishes identically because it has order  $\delta$ . Hence the boundary

layer equations for three-dimensional flow of Maxwell fluid are

$$u \frac{\partial u}{\partial x} + v \frac{\partial u}{\partial y} + w \frac{\partial u}{\partial z} + \lambda_1 \left( \begin{aligned} &u^2 \frac{\partial^2 u}{\partial x^2} + v^2 \frac{\partial^2 u}{\partial y^2} + w^2 \frac{\partial^2 u}{\partial z^2} \\ &+ 2uv \frac{\partial^2 u}{\partial x \partial y} + 2vw \frac{\partial^2 u}{\partial y \partial z} + 2uw \frac{\partial^2 u}{\partial x \partial z} \end{aligned} \right) = \nu \frac{\partial^2 u}{\partial z^2}, \quad (1.29)$$

$$u \frac{\partial v}{\partial x} + v \frac{\partial v}{\partial y} + w \frac{\partial v}{\partial z} + \lambda_1 \left( \begin{aligned} &u^2 \frac{\partial^2 v}{\partial x^2} + v^2 \frac{\partial^2 v}{\partial y^2} + w^2 \frac{\partial^2 v}{\partial z^2} \\ &+ 2uv \frac{\partial^2 v}{\partial x \partial y} + 2vw \frac{\partial^2 v}{\partial y \partial z} + 2uw \frac{\partial^2 v}{\partial x \partial z} \end{aligned} \right) = \nu \frac{\partial^2 v}{\partial z^2}. \quad (1.30)$$

The boundary layer equation for two-dimensional flow of Maxwell fluid are given below

$$u \frac{\partial u}{\partial x} + v \frac{\partial u}{\partial y} + \lambda_1 \left( u^2 \frac{\partial^2 u}{\partial x^2} + v^2 \frac{\partial^2 u}{\partial y^2} + 2uv \frac{\partial^2 u}{\partial x \partial y} \right) = \nu \frac{\partial^2 u}{\partial y^2}. \quad (1.31)$$

### 1.4.3 Oldroyd-B fluid

The extra stress tensor for an Oldroyd-B fluid model can be expressed as

$$\left( 1 + \lambda_1 \frac{D}{Dt} \right) \mathbf{S} = \mathbf{S} + \lambda_1 \frac{D\mathbf{S}}{Dt} = \mu \left( 1 + \lambda_2 \frac{D}{Dt} \right) \mathbf{A}_1, \quad (1.32)$$

where  $\lambda_2$  denotes the retardation time and law of conservation of momentum in absence of pressure gradient and body force can be written as follows:

$$\rho \left( 1 + \lambda_1 \frac{D}{Dt} \right) \frac{d\mathbf{V}}{dt} = \mu \left( 1 + \lambda_2 \frac{D}{Dt} \right) (\nabla \cdot \mathbf{A}_1). \quad (1.33)$$

The scalar forms of boundary layer equations in this case are

$$\begin{aligned} &u \frac{\partial u}{\partial x} + v \frac{\partial u}{\partial y} + w \frac{\partial u}{\partial z} + \lambda_1 \left( \begin{aligned} &u^2 \frac{\partial^2 u}{\partial x^2} + v^2 \frac{\partial^2 u}{\partial y^2} + w^2 \frac{\partial^2 u}{\partial z^2} \\ &+ 2uv \frac{\partial^2 u}{\partial x \partial y} + 2vw \frac{\partial^2 u}{\partial y \partial z} + 2uw \frac{\partial^2 u}{\partial x \partial z} \end{aligned} \right) \\ &= \nu \left( \frac{\partial^2 u}{\partial z^2} + \lambda_2 \left( \begin{aligned} &u \frac{\partial^3 u}{\partial x \partial z^2} + v \frac{\partial^3 u}{\partial y \partial z^2} + w \frac{\partial^3 u}{\partial z^3} \\ &- \frac{\partial u}{\partial x} \frac{\partial^2 u}{\partial z^2} - \frac{\partial u}{\partial y} \frac{\partial^2 v}{\partial z^2} - \frac{\partial u}{\partial z} \frac{\partial^2 w}{\partial z^2} \end{aligned} \right) \right), \end{aligned} \quad (1.34)$$

$$\begin{aligned}
& u \frac{\partial v}{\partial x} + v \frac{\partial v}{\partial y} + w \frac{\partial v}{\partial z} + \lambda_1 \left( \begin{aligned} & u^2 \frac{\partial^2 v}{\partial x^2} + v^2 \frac{\partial^2 v}{\partial y^2} + w^2 \frac{\partial^2 v}{\partial z^2} \\ & + 2uv \frac{\partial^2 v}{\partial x \partial y} + 2vw \frac{\partial^2 v}{\partial y \partial z} + 2uw \frac{\partial^2 v}{\partial x \partial z} \end{aligned} \right) \\
& = \nu \left( \frac{\partial^2 u}{\partial z^2} + \lambda_2 \left( \begin{aligned} & u \frac{\partial^3 v}{\partial x \partial z^2} + v \frac{\partial^3 v}{\partial y \partial z^2} + w \frac{\partial^3 v}{\partial z^3} \\ & - \frac{\partial v}{\partial x} \frac{\partial^2 v}{\partial z^2} - \frac{\partial v}{\partial y} \frac{\partial^2 v}{\partial z^2} - \frac{\partial v}{\partial z} \frac{\partial^2 w}{\partial z^2} \end{aligned} \right) \right), \tag{1.35}
\end{aligned}$$

and the governing boundary layer equation for two-dimensional flow is

$$u \frac{\partial u}{\partial x} + v \frac{\partial u}{\partial y} + \lambda_1 \left( u^2 \frac{\partial^2 u}{\partial x^2} + v^2 \frac{\partial^2 u}{\partial y^2} + 2uv \frac{\partial^2 u}{\partial x \partial y} \right) = \nu \left( \frac{\partial^2 u}{\partial y^2} + \lambda_2 \left( \begin{aligned} & u \frac{\partial^3 u}{\partial x \partial y^2} + v \frac{\partial^3 u}{\partial y^3} \\ & - \frac{\partial u}{\partial x} \frac{\partial^2 u}{\partial y^2} - \frac{\partial u}{\partial y} \frac{\partial^2 v}{\partial y^2} \end{aligned} \right) \right). \tag{1.36}$$

#### 1.4.4 Thixotropic fluid

Stress tensor  $\boldsymbol{\tau}$  for thixotropic fluid model

$$\tau_{ij} = 2\mu(II_{2d}(t))d_{ij},$$

where the viscosity is allowed to be time-dependent through allowing the second invariant of the deformation-rate tensor to be time-dependent,  $II_{2d}$  is the second invariant of the deformation-rate tensor and

$$2d_{ij} = (\partial u_i / \partial x_j + \partial u_j / \partial x_i). \tag{1.37}$$

In the simple Harris model, a quadratic form is used for the  $II_{2d}$  so that we have,

$$II_{2d} = (2d_{ij})^2 = 4 \left( \left( \frac{\partial u}{\partial x} \right)^2 + \frac{1}{2} \left( \frac{\partial u}{\partial y} + \frac{\partial v}{\partial x} \right)^2 + \left( \frac{\partial v}{\partial y} \right)^2 \right) > 0. \tag{1.38}$$

For the viscosity function, in the SH model we have [49,50]

$$\mu = \mu_0 - R_1 II_{2d} + R_2 \frac{dII_{2d}}{dt}, \tag{1.39}$$

where  $\frac{d}{dt}$  is the material derivative defined as

$$\frac{d}{dt} = \frac{\partial}{\partial t} + (V \cdot \nabla). \tag{1.40}$$



In equation (1.39)  $R_1$  and  $R_2$  are the material constants.

For boundary layer analysis the viscosity function becomes

$$\mu = \mu_0 - 2R_1 \left( \frac{\partial u}{\partial y} \right)^2 + 4R_2 \left( u \frac{\partial u}{\partial y} \frac{\partial^2 u}{\partial x \partial y} + v \frac{\partial u}{\partial y} \frac{\partial^2 u}{\partial y^2} \right). \quad (1.41)$$

By using boundary layer analysis the  $y$ -momentum equation is completely dropped for two-dimensional flow. On the other hand, the  $x$ -momentum equation is reduced to

$$u \frac{\partial u}{\partial x} + v \frac{\partial u}{\partial y} = \nu \frac{\partial^2 u}{\partial y^2} - \frac{6R_1}{\rho} \left( \frac{\partial u}{\partial y} \right)^2 \left( \frac{\partial^2 u}{\partial y^2} \right) + \frac{4R_2}{\rho} \left( 2 \left( \frac{\partial u}{\partial y} \right) \left( \frac{\partial^2 u}{\partial y^2} \right) \left( u \frac{\partial^2 u}{\partial x \partial y} + v \frac{\partial^2 u}{\partial y^2} \right) + \left( \frac{\partial u}{\partial y} \right)^2 \left( u \frac{\partial^3 u}{\partial x \partial y^2} + v \frac{\partial^3 u}{\partial y^3} + \frac{\partial u}{\partial y} \frac{\partial^2 u}{\partial x \partial y} + \frac{\partial v}{\partial y} \frac{\partial^2 u}{\partial y^2} \right) \right). \quad (1.42)$$

## 1.5 Homotopy analysis method (HAM)

In the absence of analytical solutions before the advent of computers, the researchers mainly directed their efforts at obtaining some forms of approximate solutions. One of the key issues of approximate solutions has always been the accuracy of the solutions. The accuracy, generally speaking, is measured in terms of the norm of the error in Banach space. The error being the difference of the approximate solution from the exact solution. In the absence of an exact solution (analytical or numerical) a heuristic approach consisting of the convergence of successive approximations has been chosen to judge the merit of an approximate solution. With the advent of computers the approximate solutions in fluid dynamics have lost some of their importance as more and better numerical algorithms have been developed to solve the increasingly realistic, but more complicated problems numerically. Nevertheless, approximate analytical solutions still have their relevance for the following reasons: Firstly, they give the solutions for each point within the domain of interest unlike the numerical solutions which are available for a particular run only for a set of discrete points in the domain. Secondly, compared to a numerical solution a nicely produced approximate solution, requiring a minimal effort and having a reasonable amount of accuracy is always handy for an engineer, scientist or an applied mathematician, who can obtain a solution completely, thereby gaining a valuable

insight into the essentials of the problem. Thirdly, even with most of the scientific packages, some initial guess is required for the solution, as the algorithms, in general are not globally convergent. In such situations, approximate solutions can provide an excellent starting guess, which can be rapidly refined to the exact numerical solution in a few iterations. Homotopy analysis method is proposed by Liao [75, 76] and is very useful to obtain the series solutions of the nonlinear ordinary and partial differential equations [77-85]. According to Liao [75, 76], this method distinguishes itself from other analytical methods in the following five aspects

1. HAM is not dependent on physical parameters. Therefore the technique can be used for both strong/weak nonlinear problems.
2. It is valid for strongly nonlinear problems even if a given nonlinear problem does not contain any small/large parameter.
3. It provides us with a convenient way to adjust the convergence region and rate of approximation of the series solution.
4. HAM provides freedom to chose base functions to approximate the solution of nonlinear problem.
5. This method can be coupled with many other mathematical methods such as integral transform methods, series expansion methods, numerical methods and so on.

This technique is applicable in the development of results to numerous problems [78 – 88]. Idea behind the HAM is as follows.

Nonlinear differential equation can be written as follows:

$$C(w) + c(r) = 0, \quad (1.43)$$

where  $C$  is a nonlinear operator,  $w(r)$  is an unknown function to be determined and  $c(r)$  is a known function. The homotopic equation is

$$(1 - p)\mathcal{L}[\bar{w}(r, p) - w_0(r)] = p\hbar \{C[\bar{w}(r, p) - c(r)]\}, \quad (1.44)$$

where  $w_0(r)$  is initial guess,  $\mathcal{L}$  is auxiliary linear operator,  $\hbar$  is auxiliary parameter or convergence control parameter,  $p \in [0, 1]$  is an embedding parameter and  $\bar{w}(r, p)$  is an unknown function. By expanding Taylor's series about  $p$  one obtains

$$\bar{w}(r, p) = w_0(r) + \sum_{k=1}^{\infty} w_k(r) p^k, \quad u_k(r) = \frac{1}{k!} \frac{\partial^k \bar{w}(r, p)}{\partial p^k} \Big|_{p=0}. \quad (1.45)$$

The convergence of above series firmly depends upon  $\hbar$ . The value of  $\hbar$  is chosen in such a way that series solution is convergent at  $p = 1$ . Substituting  $p = 1$  one obtains

$$w(r) = w_0(r) + \sum_{k=1}^{\infty} w_k(r). \quad (1.46)$$

The  $k$ -th order deformation problems are

$$\mathcal{L}[w_k(r) - \chi_k w_{k-1}(r)] = \hbar \mathcal{R}_k(r), \quad (1.47)$$

where

$$\chi_k = \begin{cases} 0, & k \leq 1, \\ 1, & k > 1, \end{cases} \quad (1.48)$$

$$\mathcal{R}_k(r) = \frac{1}{(k-1)!} \times \left\{ \frac{d^{k-1}}{dp^{k-1}} B \left[ w_0(r) + \sum_{k=1}^{\infty} w_k(r) p^k \right] \right\}_{p=0}. \quad (1.49)$$

## Chapter 2

# MHD mixed convection flow of thixotropic fluid with thermophoresis, Joule heating and thermal radiation

This chapter deals with the magnetohydrodynamic (MHD) mixed convection flow of thixotropic fluid over a moving surface. Heat transfer is considered in the presence of thermophoresis, Joule heating and radiative effects. Dimensionless nonlinear problem is computed by homotopy analysis method (HAM). The convergent solutions are plotted and examined for various parameters of interest. Numerical values of wall shear stress and heat transfer rate are computed and discussed.

### 2.1 Mathematical formulation

We consider Cartesian coordinate system in such a way that  $x$ -axis is along the stretching surface and  $y$ -axis is perpendicular to it. The magnetohydrodynamic boundary layer flow of thixotropic fluid is taken into account. Heat and mass transfer characteristics are accounted in the presence of thermal radiation and thermophoresis effects. Uniform temperature of the

surface  $T_w$  is higher than the ambient fluid temperature  $T_\infty$ . Further the species concentration at the surface is taken uniform  $C_w = 0$  while the ambient concentration is  $C_\infty$ . A constant magnetic field of strength  $\mathbf{B}_0$  is applied in the  $y$ -direction. The flow is steady and the magnetic Reynolds number is taken small so that an induced magnetic field is negligible in comparison to applied magnetic field. Taking into account the Rosseland approximation for radiative heat flux, the mass, linear momentum, energy and concentration equations are simplified to the following expressions:

$$\frac{\partial u}{\partial x} + \frac{\partial v}{\partial y} = 0, \quad (2.1)$$

$$\begin{aligned} u \frac{\partial u}{\partial x} + v \frac{\partial u}{\partial y} = & \nu \frac{\partial^2 u}{\partial y^2} - \frac{6R_1}{\rho} \left( \frac{\partial u}{\partial y} \right)^2 \left( \frac{\partial^2 u}{\partial y^2} \right) - \frac{\sigma^* B_0^2}{\rho} u \\ & + \frac{4R_2}{\rho} \left( \begin{aligned} & 2 \left( \frac{\partial u}{\partial y} \right) \left( \frac{\partial^2 u}{\partial y^2} \right) \left( u \frac{\partial^2 u}{\partial x \partial y} + v \frac{\partial^2 u}{\partial y^2} \right) \\ & + \left( \frac{\partial u}{\partial y} \right)^2 \left( u \frac{\partial^3 u}{\partial x \partial y^2} + v \frac{\partial^3 u}{\partial y^3} + \frac{\partial u}{\partial y} \frac{\partial^2 u}{\partial x \partial y} + \frac{\partial v}{\partial y} \frac{\partial^2 u}{\partial y^2} \right) \end{aligned} \right) \\ & + g[\beta_T(T - T_\infty) + \beta_c(C - C_\infty)], \end{aligned} \quad (2.2)$$

$$\begin{aligned} u \frac{\partial T}{\partial x} + v \frac{\partial T}{\partial y} = & \frac{k}{\rho c_p} \frac{\partial^2 T}{\partial y^2} + \frac{16\sigma_s T_\infty^3}{3k_e} \frac{\partial^2 T}{\partial y^2} - \frac{2\mu R_1}{\rho c_p} \left( \frac{\partial u}{\partial y} \right)^4 + \frac{4\mu R_2}{\rho c_p} u \frac{\partial u}{\partial y} \frac{\partial^2 u}{\partial x \partial y} \left( \frac{\partial u}{\partial y} \right)^2 \\ & + \frac{4\mu R_2}{\rho c_p} v \frac{\partial u}{\partial y} \frac{\partial^2 u}{\partial y^2} \left( \frac{\partial u}{\partial y} \right)^2 + \frac{\mu}{\rho c_p} \left( \frac{\partial u}{\partial y} \right)^2 + \frac{\sigma^* B_0^2}{\rho c_p} u^2, \end{aligned} \quad (2.3)$$

$$u \frac{\partial C}{\partial x} + v \frac{\partial C}{\partial y} = D \frac{\partial^2 C}{\partial y^2} - \frac{\partial}{\partial y} (V_T (C - C_\infty)), \quad (2.4)$$

where  $(u, v)$  are the velocity components parallel to the  $x$ - and  $y$ -axes,  $R_1$  and  $R_2$  are the constants,  $\nu$  the dynamic viscosity of fluid,  $\rho$  the density of fluid,  $\sigma^*$  the electrical conductivity,  $g$  the gravitational acceleration,  $\beta_T$  and  $\beta_c$  the thermal and concentration expansion coefficients respectively,  $T$  the temperature,  $c_p$  the specific heat,  $\sigma_s$  the Stefan-Boltzmann constant,  $k_e$  the

mean absorption coefficient,  $D$  the diffusion coefficient and  $V_T$  the thermophoretic velocity.

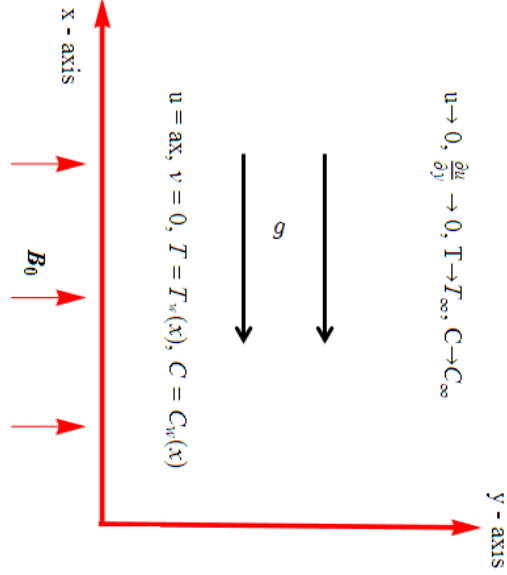


Fig. 2. 1: Physical model

Equations (2.1)-(2.4) are solved subject to the boundary conditions

$$\begin{aligned} u &= u_w = ax, \quad v = 0, \quad T = T_w(x), \quad C = C_w(x) \quad \text{at } y = 0, \\ u &\rightarrow 0, \quad \frac{\partial u}{\partial y} \rightarrow 0, \quad T \rightarrow T_\infty, \quad C \rightarrow C_\infty \quad \text{as } y \rightarrow \infty. \end{aligned} \quad (2.5)$$

The thermophoretic term  $V_T$  in Eq. (2.4) can be defined as

$$V_T = -k_2 \frac{\nu}{T_r} \frac{\partial T}{\partial y}. \quad (2.6)$$

Here  $k_2$  is the thermophoretic coefficient and  $T_r$  is the reference temperature. A thermophoretic parameter  $\tau$  is defined by the following relation

$$\tau = -\frac{k_2(T_w - T_\infty)}{T_r}. \quad (2.7)$$

The wall temperature and concentration fields are

$$T_w = T_\infty + bx, \quad C_w = C_\infty + cx, \quad (2.8)$$

where  $a$ ,  $b$  and  $c$  are the positive constants. Introducing

$$u = axf'(\eta), \quad v = -\sqrt{av}f(\eta), \quad \eta = y\sqrt{\frac{a}{\nu}}, \quad \theta(\eta) = \frac{T - T_\infty}{T_w - T_\infty}, \quad (2.9)$$

incompressibility condition (2.1) is automatically satisfied and the Eqs. (2.2)-(2.5) become

$$f''' + ff'' - f'^2 + K_1(x)f''^2f''' + K_2(x) \begin{pmatrix} 2f'f''^2f''' + f''^4 \\ -2ff''f'''^2 - ff''^2f^{iv} \end{pmatrix} - M^2f' + \lambda(\theta + N\phi) = 0, \quad (2.10)$$

$$\begin{aligned} & \left(1 + \frac{4}{3}R\right)\theta'' + Pr(f\theta' - \theta f') + PrEc f''^2 + \frac{1}{3}K_1PrEc f''^4 \\ & + K_2PrEc(f'f''^4 - f f''^3 f''') + M^2PrEc f'^2 = 0, \end{aligned} \quad (2.11)$$

$$\phi'' + Sc(f\phi' - \phi f') - Sc\tau(\phi'\theta' - \phi\theta'') = 0, \quad (2.12)$$

$$\begin{aligned} f &= 0, \quad f' = 1, \quad \theta = 1, \quad \phi = 1 \text{ at } \eta = 0, \\ f' &\rightarrow 0, \quad f'' \rightarrow 0, \quad \theta \rightarrow 0, \quad \phi \rightarrow 0 \text{ as } \eta \rightarrow \infty, \end{aligned} \quad (2.13)$$

where the non-Newtonian parameters are  $K_1(x) = -\frac{6R_1a^3x^2}{\rho\nu^2}$  and  $K_2(x) = \frac{4R_2a^4x^2}{\rho\nu^2}$ ,  $M = \sigma^*B_0^2/\rho c$  the Hartman number,  $\lambda = Gr_x/Re_x^2$  the local buoyancy parameter,  $Gr_x = \frac{g\beta_T(T_w - T_\infty)x^3/\nu^2}{u_w^2x^2/\nu^2}$  the local Grashof number,  $N = \beta_c(C_w - C_\infty)/\beta_T(T_w - T_\infty)$  the constant dimensionless concentration buoyancy parameter,  $Pr = \frac{\mu c_p}{k}$  the Prandtl number,  $R = 4\sigma_s T_\infty^3/k_e k$  the radiation parameter,  $Ec = u_w^2/c_p(T_w - T_\infty)$  the Eckert number and  $Sc = \frac{\nu}{D}$  the Schmidt number. It is further seen that both  $K_1$  and  $K_2$  are functions of  $x$ . Hence the fluid flow in present situation lacks a self-similar solution. This is striking difference when compared present case with that of Blasius flow of viscous fluid i.e. in Blasius flow there is self-similar solution. Here  $K_2$  especially indicates the fluids' thixotropic behavior.

The skin friction coefficient, local Nusselt number and local Sherwood number in non-dimensional form can be written as follows:

$$Re_x^{1/2}C_f = f''(0) - K_1/6[f''(0)]^3, \quad Nu_x Re_x^{-1/2} = -\theta'(0) \text{ and } Sh Re_x^{-1/2} = -\phi'(0). \quad (2.14)$$

Here we noticed that the wall shear stress at given  $x$ -location is only affected by  $R_1$  but only indirectly by  $R_2$  (i.e. through  $f''(0)$ ) [51]. We have serious limitation in a simplified Harris model for representing true thixotropic fluid.

## 2.2 Series solutions

The homotopic solutions for  $f$  and  $\theta$  in a set of base functions

$$\{\eta^k \exp(-n\eta), k \geq 0, n \geq 0\} \quad (2.15)$$

are given by

$$f_m(\eta) = \sum_{n=0}^{\infty} \sum_{k=0}^{\infty} a_{m,n}^k \eta^k \exp(-n\eta), \quad (2.16)$$

$$\theta_m(\eta) = \sum_{n=0}^{\infty} \sum_{k=0}^{\infty} b_{m,n}^k \eta^k \exp(-n\eta) \quad (2.17)$$

$$\phi_m(\eta) = \sum_{n=0}^{\infty} \sum_{k=0}^{\infty} c_{m,n}^k \eta^k \exp(-n\eta) \quad (2.18)$$

where  $a_{m,n}^k$ ,  $b_{m,n}^k$  and  $c_{m,n}^k$  are the coefficients. The appropriate initial approximations and auxiliary linear operators are

$$f_0(\eta) = 1 - \exp(-\eta), \quad \theta_0(\eta) = \exp(-\eta), \quad \phi_0(\eta) = \exp(-\eta), \quad (2.19)$$

$$\mathcal{L}_f = f''' - f', \quad \mathcal{L}_\theta = f'' - f, \quad \mathcal{L}_\phi = f'' - f \quad (2.20)$$

with

$$\mathcal{L}_f(C_1 + C_2 e^\eta + C_3 e^{-\eta}) = 0, \quad \mathcal{L}_\theta(C_4 e^\eta + C_5 e^{-\eta}) = 0, \quad \mathcal{L}_\phi(C_6 e^\eta + C_7 e^{-\eta}). \quad (2.21)$$

in which  $C_i$  ( $i = 1-7$ ) denote the arbitrary constants and the zeroth order deformation problems are

$$(1-p) \mathcal{L}_f \left( \hat{f}(\eta; p) - f_0(\eta) \right) = p \hbar_f \mathcal{N}_f \left( \hat{f}(\eta; p), \hat{\theta}(\eta; p), \hat{\phi}(\eta; p) \right), \quad (2.22)$$

$$(1-p) \mathcal{L}_\theta \left( \hat{\theta}(\eta; p) - \theta_0(\eta) \right) = p \hbar_\theta \mathcal{N}_\theta \left( \hat{\theta}(\eta; p), \hat{f}(\eta; p), \hat{\phi}(\eta; p) \right), \quad (2.23)$$



$$(1-p)\mathcal{L}_\phi\left(\hat{\phi}(\eta;p)-\phi_0(\eta)\right)=p\hbar_\phi\mathcal{N}_\phi\left(\hat{\theta}(\eta;p),\hat{f}(\eta;p),\hat{\phi}(\eta;p)\right), \quad (2.24)$$

$$\begin{aligned} \hat{f}(0;p) &= 0, \quad \hat{f}'(0;p)=1, \quad \hat{f}'(\infty;p)=0, \quad \hat{f}''(\infty;p)=0, \\ \hat{\theta}(0;p) &= 1, \quad \hat{\theta}(\infty;p)=0, \quad \hat{\phi}(0;p)=1 \text{ and } \hat{\phi}(\infty;p)=0, \end{aligned} \quad (2.25)$$

where  $p$  shows embedding parameter,  $\hbar_f$ ,  $\hbar_\theta$  and  $\hbar_\phi$  the non-zero auxiliary parameters and the nonlinear operators  $\mathcal{N}_f$ ,  $\mathcal{N}_\theta$  and  $\mathcal{N}_\phi$  are

$$\begin{aligned} \mathcal{N}_f[\hat{f}(\eta,p),\hat{\theta}(\eta;p),\hat{\phi}(\eta;p)] &= \frac{\partial^3 \hat{f}(\eta,p)}{\partial \eta^3} + \hat{f}(\eta,p) \frac{\partial^2 \hat{f}(\eta,p)}{\partial \eta^2} - \left( \frac{\partial \hat{f}(\eta,p)}{\partial \eta} \right)^2 \\ &+ K_1(x) \left( \frac{\partial^2 \hat{f}(\eta,p)}{\partial \eta^2} \right)^2 \frac{\partial^3 \hat{f}(\eta,p)}{\partial \eta^3} \\ &+ K_2(x) \left( \frac{\partial \hat{f}(\eta,p)}{\partial \eta} \left( \frac{\partial^2 \hat{f}(\eta,p)}{\partial \eta^2} \right)^2 \frac{\partial^3 \hat{f}(\eta,p)}{\partial \eta^3} + \left( \frac{\partial^2 \hat{f}(\eta,p)}{\partial \eta^2} \right)^4 - \hat{f}(\eta,p) \right. \\ &\quad \left. - \frac{\partial^2 \hat{f}(\eta,p)}{\partial \eta^2} \left( \frac{\partial^3 \hat{f}(\eta,p)}{\partial \eta^3} \right)^2 - \hat{f}(\eta,p) \left( \frac{\partial^2 \hat{f}(\eta,p)}{\partial \eta^2} \right)^2 \frac{\partial^4 \hat{f}(\eta,p)}{\partial \eta^4} \right) \\ &+ \lambda(\hat{\theta}(\eta,p) + N\hat{\phi}(\eta;p) - M^2 \frac{\partial \hat{f}(\eta,p)}{\partial \eta}), \end{aligned} \quad (2.26)$$

$$\begin{aligned} \mathcal{N}_\theta[\hat{f}(\eta,p),\hat{\theta}(\eta;p),\hat{\phi}(\eta;p)] &= \left( 1 + \frac{4}{3}R \right) \frac{\partial^2 \hat{\theta}(\eta,p)}{\partial \eta^2} + PrEc \left( \frac{\partial^2 \hat{f}(\eta,p)}{\partial \eta^2} \right)^2 \\ &+ M^2 PrEc \left( \frac{\partial \hat{f}(\eta,p)}{\partial \eta} \right)^2 + \frac{1}{3}K_1 PrEc \left( \frac{\partial^2 \hat{f}(\eta,p)}{\partial \eta^2} \right)^4 \\ &- Pr\hat{\theta}(\eta,p) \frac{\partial \hat{f}(\eta,p)}{\partial \eta} + Pr\hat{f}(\eta,p) \frac{\partial \hat{\theta}(\eta,p)}{\partial \eta} \\ &+ K_2 PrEc \left( \frac{\partial \hat{f}(\eta,p)}{\partial \eta} \left( \frac{\partial^2 \hat{f}(\eta,p)}{\partial \eta^2} \right)^4 - \hat{f}(\eta,p) \frac{\partial^3 \hat{f}(\eta,p)}{\partial \eta^3} \left( \frac{\partial^2 \hat{f}(\eta,p)}{\partial \eta^2} \right)^3 \right), \end{aligned} \quad (2.27)$$

$$\begin{aligned} \mathcal{N}_\phi[\hat{f}(\eta,p),\hat{\theta}(\eta;p),\hat{\phi}(\eta;p)] &= \frac{\partial^2 \hat{\phi}(\eta,p)}{\partial \eta^2} + Sc \left( \hat{f}(\eta,p) \frac{\partial \hat{\phi}(\eta,p)}{\partial \eta} - \frac{\partial \hat{f}(\eta,p)}{\partial \eta} \hat{\phi}(\eta,p) \right) \\ &- Sc\tau \left( \frac{\partial \hat{\theta}(\eta,p)}{\partial \eta} \frac{\partial \hat{\phi}(\eta,p)}{\partial \eta} - \hat{\phi}(\eta,p) \frac{\partial^2 \hat{\theta}(\eta,p)}{\partial \eta^2} \right), \end{aligned} \quad (2.28)$$

When  $p = 0$  and  $p = 1$  then

$$\hat{f}(\eta; 0) = f_0(\eta) \text{ and } \hat{f}(\eta; 1) = f(\eta), \quad (2.29)$$

$$\hat{\theta}(\eta; 0) = \theta_0(\eta) \text{ and } \hat{\theta}(\eta; 1) = \theta(\eta), \quad (2.30)$$

$$\hat{\phi}(\eta; 0) = \phi_0(\eta) \text{ and } \hat{\phi}(\eta; 1) = \phi(\eta), \quad (2.31)$$

and when  $p$  increases from 0 to 1 then  $f(\eta, p)$ ,  $\theta(\eta, p)$  and  $\phi(\eta, p)$  vary from  $f_0(\eta)$  to  $f(\eta)$ ,  $\theta_0(\eta)$  to  $\theta(\eta)$  and  $\phi_0(\eta)$  to  $\phi(\eta)$ . Employing the Taylor's series expansion we have

$$f(\eta, p) = f_0(\eta) + \sum_{m=1}^{\infty} f_m(\eta) p^m, \quad f_m(\eta) = \frac{1}{m!} \left. \frac{\partial^m f(\eta; p)}{\partial p^m} \right|_{p=0}, \quad (2.32)$$

$$\theta(\eta, p) = \theta_0(\eta) + \sum_{m=1}^{\infty} \theta_m(\eta) p^m, \quad \theta_m(\eta) = \frac{1}{m!} \left. \frac{\partial^m \theta(\eta; p)}{\partial p^m} \right|_{p=0}, \quad (2.33)$$

$$\phi(\eta, p) = \phi_0(\eta) + \sum_{m=1}^{\infty} \phi_m(\eta) p^m, \quad \phi_m(\eta) = \frac{1}{m!} \left. \frac{\partial^m \phi(\eta; p)}{\partial p^m} \right|_{p=0}. \quad (2.34)$$

Convergence of series (2.32-2.34) is closely associated with  $\hbar_f$ ,  $\hbar_\theta$  and  $\hbar_\phi$ . The values of  $\hbar_f$ ,  $\hbar_\theta$  and  $\hbar_\phi$  are chosen such that the series (2.32-2.34) converge at  $p = 1$ . Hence

$$f(\eta) = f_0(\eta) + \sum_{m=1}^{\infty} f_m(\eta), \quad (2.35)$$

$$\theta(\eta) = \theta_0(\eta) + \sum_{m=1}^{\infty} \theta_m(\eta), \quad (2.36)$$

$$\phi(\eta) = \phi_0(\eta) + \sum_{m=1}^{\infty} \phi_m(\eta). \quad (2.37)$$

If we denote the special solutions  $f_m^*(\eta)$ ,  $\theta_m^*(\eta)$  and  $\phi_m^*(\eta)$  then the general solutions  $f_m(\eta)$ ,  $\theta_m(\eta)$  and  $\phi_m(\eta)$  are

$$f_m(\eta) = f_m^*(\eta) + C_1 + C_2 e^\eta + C_3 e^{-\eta}, \quad (2.38)$$

$$\theta_m(\eta) = \theta_m^*(\eta) + C_4 e^\eta + C_5 e^{-\eta}, \quad (2.39)$$

$$\phi_m(\eta) = \phi_m^*(\eta) + C_6 e^\eta + C_7 e^{-\eta}. \quad (2.40)$$

## 2.3 Convergence analysis and discussion

We recall that the auxiliary parameters  $\hbar_f$ ,  $\hbar_\theta$  and  $\hbar_\phi$  are useful in controlling and adjusting the convergence of the series solutions. We draw the  $\hbar$ -curves at 14th order of approximation in obtaining the ranges for  $\hbar_f$ ,  $\hbar_\theta$  and  $\hbar_\phi$ . It is noticed from Fig. 2.2 that the admissible values of  $\hbar_f$ ,  $\hbar_\theta$  and  $\hbar_\phi$  are  $-0.7 \leq \hbar_f \leq -0.25$ ,  $-0.95 \leq \hbar_\theta \leq -0.5$  and  $-0.95 \leq \hbar_\phi \leq -0.5$ . Further the series solutions converge in the whole region of  $\eta$  when  $\hbar_f = \hbar_\theta = \hbar_\phi = -0.6$ . Table 2.1 is presented to see the convergent values for different order of approximations at  $\hbar_f = \hbar_\theta = \hbar_\phi = -0.6$ . This Table indicates that the series solutions for velocity converge from 20th order of deformations and temperature and concentration converge from 25th order of deformations. Hence 25th order deformations are computed to find a convergent series solutions.

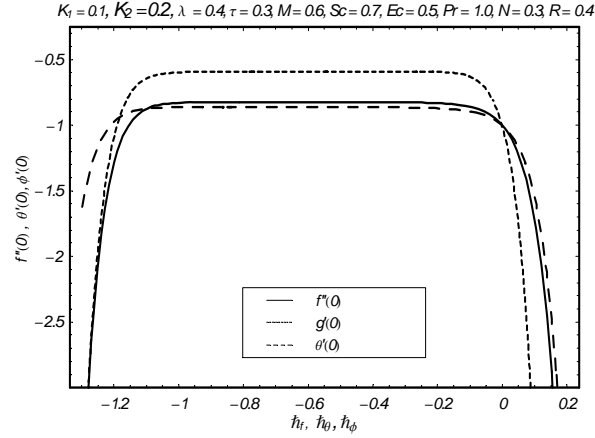


Fig. 2. 2:  $\hbar$ -curves for the functions  $f$ ,  $\theta$  and  $\phi$

**Table 2.1:** Convergence of series solutions for different order of approximations when  $K_1 = 0.1$ ,  $K_2 = 0.2$ ,  $\lambda = 0.4$ ,  $\tau = 0.3$ ,  $M = 0.6$ ,  $Sc = 0.7$ ,  $Ec = 0.5$ ,  $Pr = 1.0$ ,  $N = 0.3$ ,  $R = 0.4$

and  $\hbar_f = \hbar_\theta = \hbar_\phi = -0.6$ .

Order of approximations	$-f''(0)$	$-\theta'(0)$	$-\phi'(0)$
1	0.86800	0.63500	0.85000
5	0.82753	0.60365	0.71921
10	0.82461	0.60732	0.69473
20	0.82425	0.60872	0.68636
25	0.82425	0.60886	0.68578
30	0.82425	0.60886	0.68578
35	0.82425	0.60886	0.68578

Figs. 2.3- 2.7 are sketched to analyze the variations of thixotropic parameters  $K_1$  and  $K_2$ , local buoyancy parameter  $\lambda$ , Hartman number  $M$  and concentration buoyancy parameter  $N$  on the fluid velocity  $f'(\eta)$ . Figs. 2.3 and 2.4 depict that the fluid velocity and momentum boundary layer thickness are increasing functions of thixotropic parameters. By increasing thixotropic parameters, the values of material parameters  $R_1$  and  $R_2$  increase. An increase in the material parameters give rise to the fluid velocity and momentum boundary layer thickness. Fig. 2.5 shows that an increase in local buoyancy parameter gives rise to the fluid velocity and its associated boundary layer thickness. Increase in buoyancy parameter corresponds to stronger buoyancy force. Buoyancy force is an agent that causes an increase in the fluid flow and its related boundary layer thickness. An increase in Hartman number reduces the fluid velocity. Hartman number involves the Lorentz force and an increase in Lorentz force reduces the fluid velocity and boundary layer thickness (see Fig. 2.6). The Lorentz force provides a resistance to flow. From Fig. 2.7 it is observed that concentration buoyancy parameter enhances the velocity.

To see the impacts of different parameters on the temperature  $\theta(\eta)$ , Figs. 2.8-2.15 are portrayed. From Figs. 2.8 and 2.9, we have seen that the thixotropic parameters  $K_1$  and  $K_2$  are decreasing functions of temperature and thermal boundary layer thicknesses. Larger values of  $K_1$  and  $K_2$  correspond to stronger  $R_1$  and  $R_2$  showing a reduction in the temperature. We also noted that the thixotropic parameters have quite opposite effects on the fluid velocity and temperature. Figs. 2.10 and 2.11 present the effects of local buoyancy parameter and

concentration buoyancy parameter on the temperature. It is found that the temperature and thermal boundary layer thickness become smaller for larger values of local buoyancy parameter and concentration buoyancy parameter. Physically, both  $\lambda$  and  $N$  depend on the buoyancy force. Larger values of  $\lambda$  and  $N$  lead to the stronger buoyancy force. Such stronger buoyancy force reduced the temperature and thermal boundary layer thickness. Fig. 2.12 is plotted to analyze the influence of Eckert number on the temperature. Here it is revealed that the temperature and thermal boundary layer thickness are increased for larger Eckert number. This is because of the reason that heat energy is always stored in the liquid due to the frictional heating. Such increase in Eckert number enhances the temperature at any point in the thermal boundary layer region. From Fig. 2.13, one can see that temperature is an increasing function of Hartman number. Larger values of Hartman number posses stronger Lorentz force. This stronger Lorentz force enhances the temperature and thermal boundary layer thickness. Impact of Prandtl number  $Pr$  on the temperature  $\theta(\eta)$  is analyzed in Fig. 2.14. Thermal boundary layer thickness and temperature  $\theta(\eta)$  are decreasing functions of  $Pr$ . This is due to the fact that with an enhancement in Prandtl number  $Pr$ , thermal diffusivity decreases which leads to a reduction in temperature  $\theta(\eta)$ . Fig. 2.15 shows that temperature  $\theta(\eta)$  increases with an increase in radiation parameter  $R$ . Also thermal boundary layer thickness enhances with  $R$  which is due to the fact that as thermal radiation parameter increases, the mean absorption coefficient  $k_e$  decreases which in results give rise to the divergence of radiative heat flux. Hence the rate of radiative heat transferred to the fluid shoot up so that the fluid temperature increases.

Figs. 2.16-2.22 are plotted to see the variations of  $K_1$ ,  $K_2$ ,  $\lambda$ ,  $N$ ,  $Ec$ ,  $M$  and  $\tau$  on the concentration  $\phi(\eta)$ . Figs. 2.16 and 2.17 show the influence of thixotropic parameters on the concentration. From these Figs. we observed that increase in thixotropic parameters reduced the concentration and its related boundary layer thickness. We also analyzed that the effects of thixotropic parameters on the temperature and concentration are similar in a qualitative sense. A comparison of Figs. 2.8, 2.9, 2.16 and 2.17 show that the variation in temperature are dominant in comparison to variation in concentration due to thixotropic parameters. Local buoyancy parameter and concentration buoyancy parameter are decreasing functions of concentration (see Figs. 2.18 and 2.19). Fig. 2.20 shows that an increase in Eckert number leads to a decrease in the concentration and its related boundary layer thickness. For higher Eckert

number, concentration specie diffuses due to which the concentration field decreases. Fig. 2.21 illustrates the variations of Hartman number on the fluid concentration. It is revealed that concentration is a decreasing function of Hartman number. We conclude that the variations in temperature are more dominant when compared with the variations in the concentration. From Fig. 2.22 it is observed that the associated boundary layer thickness and concentration profile decrease when thermophoretic parameter  $\tau$  increases.

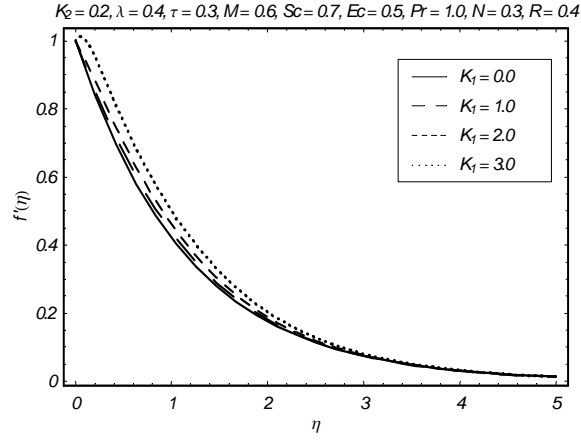


Fig. 2.3: Influence of  $K_1$  on  $f'(\eta)$

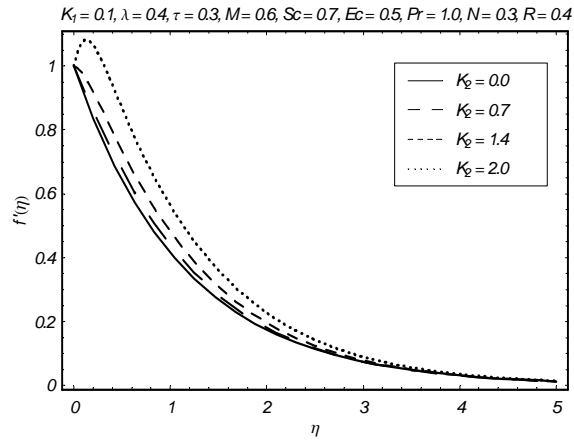


Fig. 2.4: Influence of  $K_2$  on  $f'(\eta)$

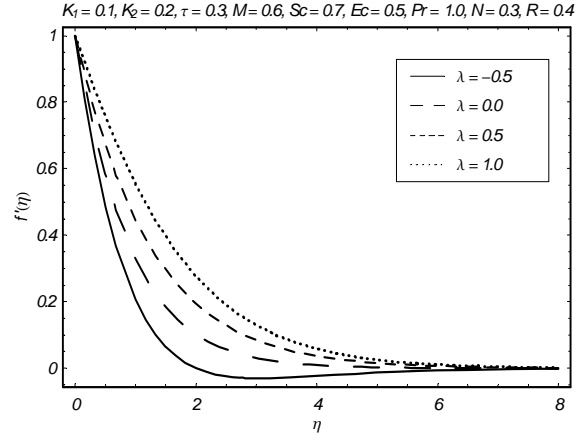


Fig. 2.5: Influence of  $\lambda$  on  $f'(\eta)$

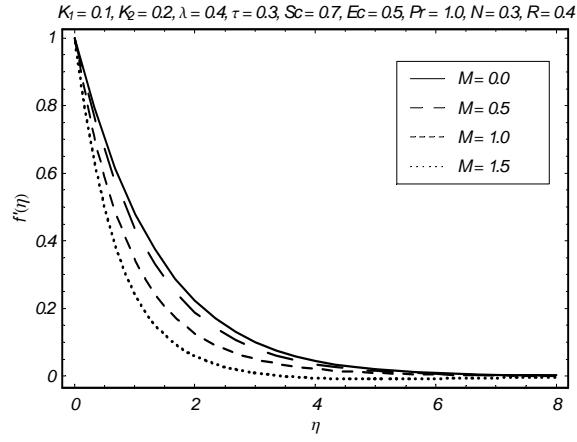


Fig. 2.6: Influence of  $M$  on  $f'(\eta)$

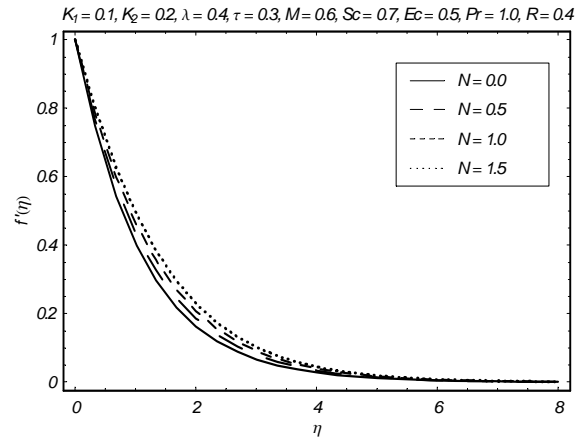


Fig. 2.7: Influence of  $N$  on  $f'(\eta)$

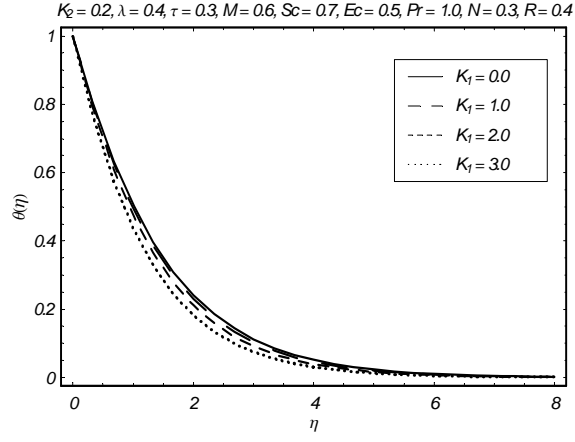


Fig. 2.8: Influence of  $K_1$  on  $\theta(\eta)$

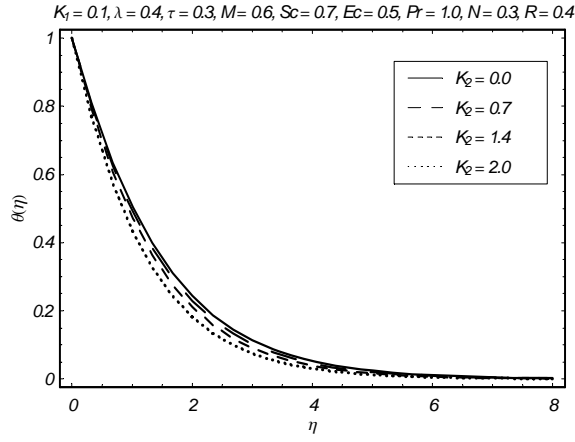


Fig. 2.9: Influence of  $K_2$  on  $\theta(\eta)$

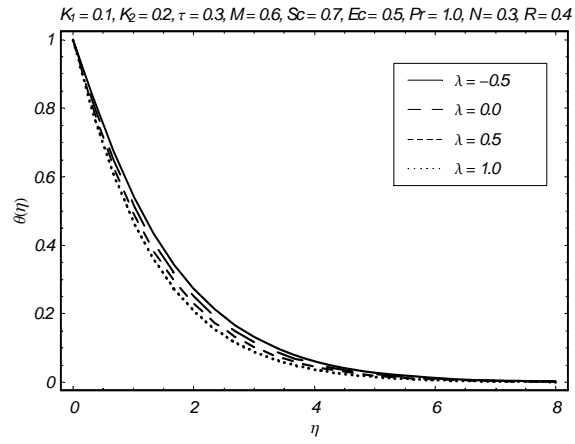


Fig. 2.10: Influence of  $\lambda$  on  $\theta(\eta)$



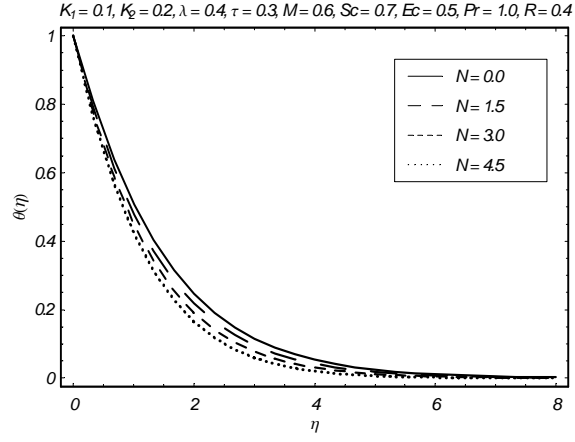


Fig. 2.11: Influence of  $N$  on  $\theta(\eta)$

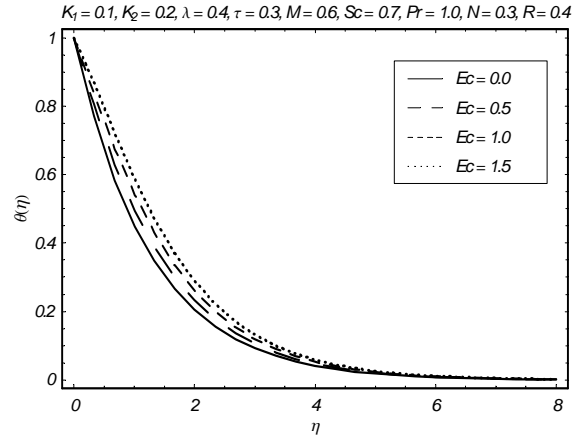


Fig. 2.12: Influence of  $Ec$  on  $\theta(\eta)$

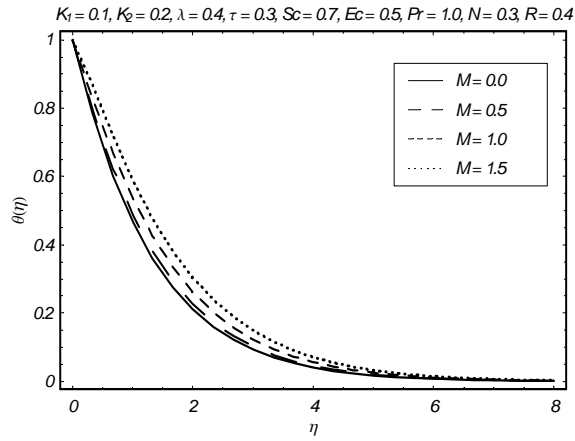


Fig. 2.13: Influence of  $M$  on  $\theta(\eta)$

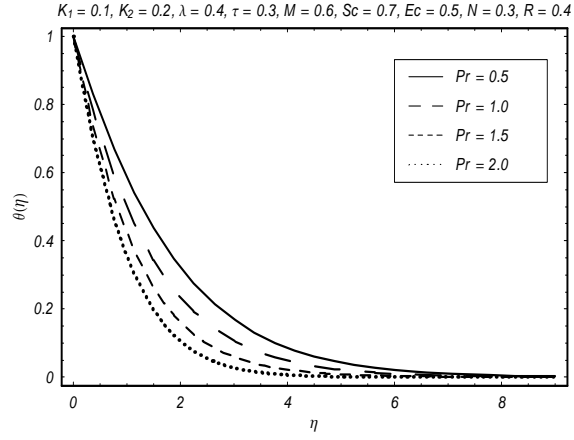


Fig. 2.14: Influence of  $Pr$  on  $\theta(\eta)$

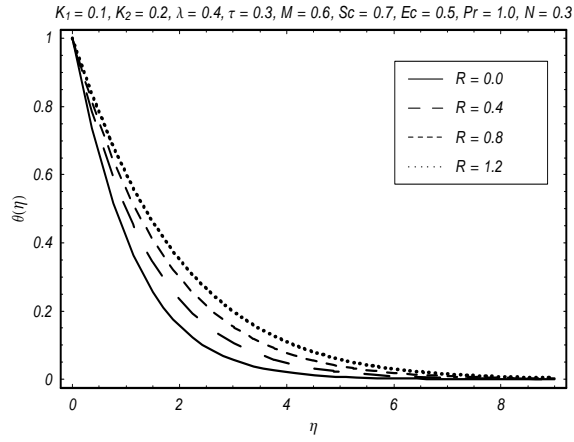


Fig. 2.15: Influence of  $R$  on  $\theta(\eta)$

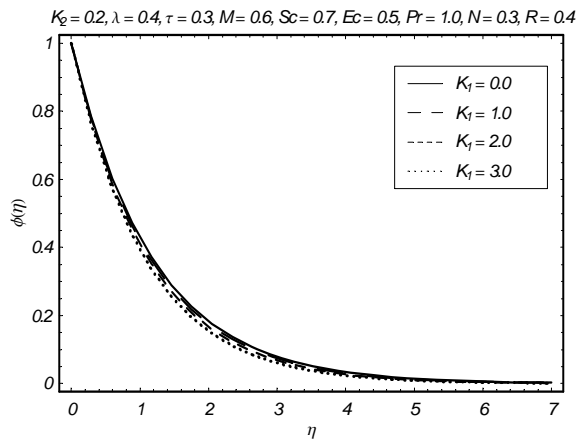


Fig. 2.16: Influence of  $K_1$  on  $\phi(\eta)$

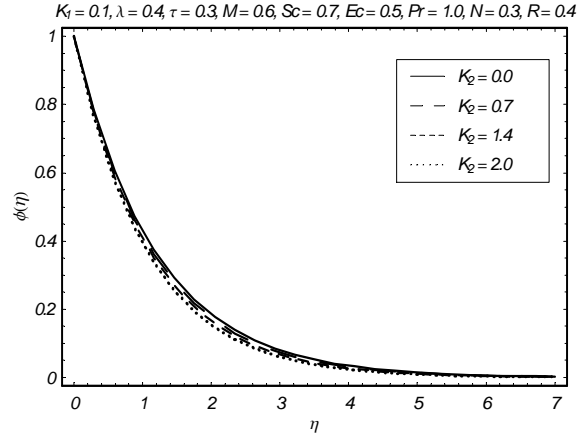


Fig. 2.17: Influence of  $K_2$  on  $\phi(\eta)$

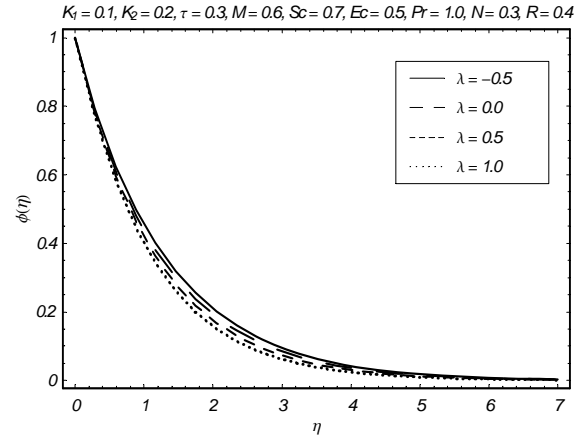


Fig. 2.18: Influence of  $\lambda$  on  $\phi(\eta)$

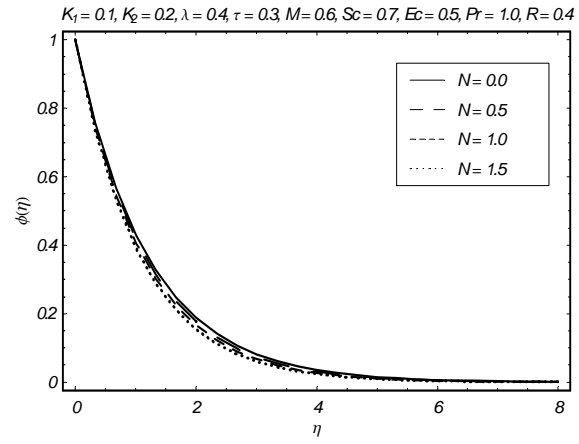


Fig. 2.19: Influence of  $N$  on  $\phi(\eta)$

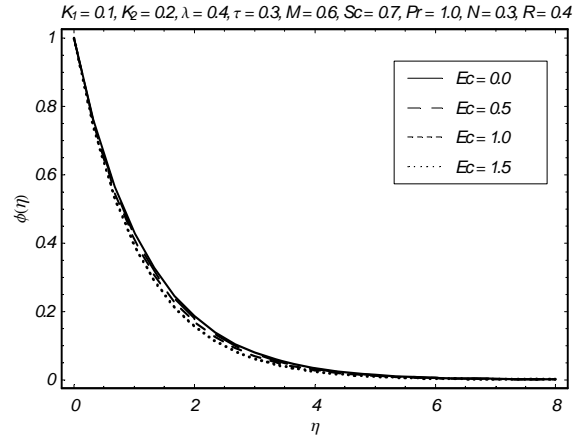


Fig. 2.20: Influence of  $Ec$  on  $\phi(\eta)$

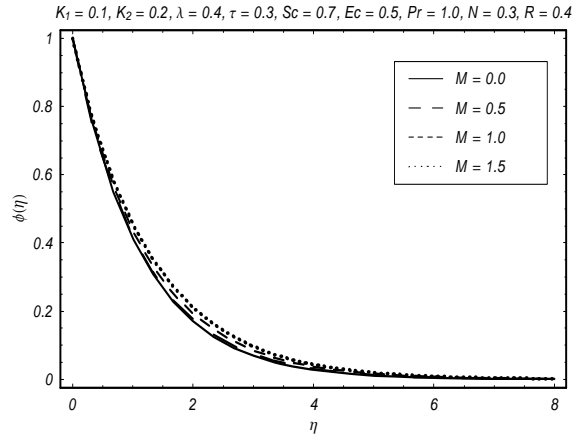


Fig. 2.21: Influence of  $M$  on  $\phi(\eta)$

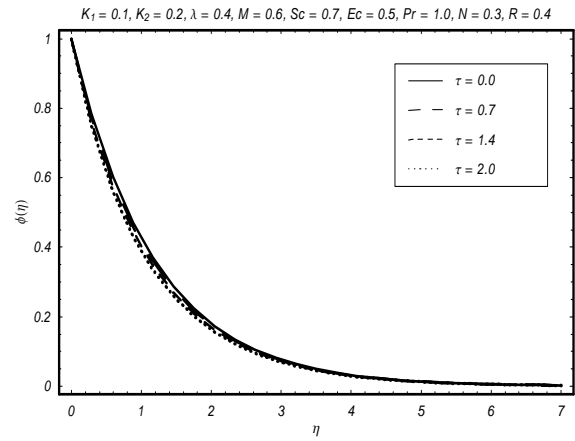


Fig. 2.22: Influence of  $\tau$  on  $\phi(\eta)$

Table 2.2 is made to find the numerical values of skin-friction coefficient for various values of  $K_1$ ,  $K_2$ ,  $M$ ,  $\lambda$  and  $\tau$  when the other parameters are fixed. We noted that the values of skin-friction coefficient are decreased by increasing  $K_1$ ,  $K_2$  and  $\lambda$ . However reverse situation is noted for  $M$  and  $\tau$ . Table 2. 3 analyzes the numerical values of local Nusselt number and local Sherwood number for different values of emerging parameters in viscous and non-Newtonian cases. We observed that the values of local Nusselt number and local Sherwood number is large in the case of non-Newtonian fluid when compared with the case of viscous fluid. Table 2.4 is computed for the comparison of  $f''(0)$  and  $\theta'(0)$  through different values of Prandtl number and local buoyancy parameter when all other parameters are zero. From this Table, it is analyzed that our series solutions have a good agreement with the numerical solutions in a limiting case.

**Table 2.2:** Numerical values of skin-friction coefficient for different values of  $K_1$ ,  $K_2$ ,  $M$ ,  $\lambda$  and  $\tau$  when  $N = 0.3$ ,  $R = 0.4$ ,  $Pr = 1.0$ ,  $Ec = 0.5$  and  $Sc = 0.7$ .

$K_1$	$K_2$	$M$	$\lambda$	$\tau$	$-Re_x^{1/2}C_f$
0.0	0.2	0.6	0.4	0.4	0.84799
0.3					0.79227
0.5					0.76088
0.2	0.0	0.6	0.4	0.4	0.84923
	0.3				0.79373
	0.5				0.76247
0.2	0.2	0.0	0.4	0.4	0.71906
		0.5			0.80959
		1.0			1.01672
0.2	0.2	0.5	0.0	0.4	0.95561
			0.4		0.76145
			0.8		0.56391
0.2	0.2	0.5	0.3	0.0	0.80923
				1.0	0.81003
				2.0	0.81106

**Table 2.3:** Numerical values of local Nusselt number and local Sherwood number for different

values of  $M$ ,  $Ec$ ,  $Pr$ ,  $N$  and  $R$  when  $\lambda = 0.3$  and  $\tau = 0.4$ .

$M$	$Sc$	$Ec$	$Pr$	$N$	$R$	$-\theta'(0)$	$-\phi'(0)$	$-\theta'(0)$	$-\phi'(0)$
						$K_1 = K_2 = 0.0$		$K_1 = K_2 = 0.2$	
0.0	0.7	0.5	1.0	0.3	0.4	0.67883	0.87335	0.69254	0.88088
0.5						0.58160	0.86284	0.60339	0.86671
1.0						0.29936	0.83862	0.36075	0.84058
0.5	0.5	0.5	1.0	0.3	0.4	0.58763	0.62245	0.60862	0.68707
	1.0					0.57572	1.10358	0.59829	1.10750
	1.5					0.57065	1.45081	0.59387	1.45463
0.5	0.7	0.3	1.0	0.3	0.4	0.66211	0.84754	0.67841	0.85318
		0.6				0.54179	0.87021	0.56632	0.87341
		0.8				0.46338	0.88469	0.49302	0.88618
0.5	0.7	0.5	0.5	0.3	0.4	0.41490	0.88107	0.42578	0.88426
			0.8			0.52313	0.86855	0.54006	0.87243
			1.3			0.65577	0.85452	0.68482	0.85721
0.5	0.7	0.5	1.0	0.0	0.4	0.55688	0.85559	0.58355	0.85988
				0.5		0.59650	0.86737	0.61561	0.87109
				1.0		0.62949	0.87800	0.64317	0.88142
0.5	0.7	0.5	1.0	0.3	0.0	0.70547	0.84788	0.73986	0.85133
					0.5	0.55912	0.86538	0.57908	0.86942
					1.0	0.47505	0.87469	0.48877	0.87958

**Table 2.4:** Comparison of  $f''(0)$  and  $\theta'(0)$  with Singh et al. [76] for different values of  $Pr$  and

$\lambda$ .

	Singh et al. [76]		Present solutions	
	$f''(0)$	$\theta'(0)$	$f''(0)$	$\theta'(0)$
$Pr = 0.7$ $\lambda = 0.0$	-1.00	-0.79366	-1.00000	-0.79373
$Pr = 0.7$ $\lambda = 1.0$	-0.50751	-0.89613	-0.50767	-0.89614
$Pr = 0.7$ $\lambda = 10.0$	2.57771	-1.17244	2.57789	-1.17287
$Pr = 10.0$ $\lambda = 0.0$	-1.00	-3.72067	-1.00000	-3.72033
$Pr = 10.0$ $\lambda = 1.0$	-0.82568	-3.74856	-0.82529	-3.74718
$Pr = 10.0$ $\lambda = 10.0$	0.61966	-3.95235	0.61940	-3.95266

## 2.4 Closing remarks

Effects of Joule heating, thermophoresis and thermal radiation in MHD flow of thixotropic fluid are analyzed. The main observations are listed below.

- The non-Newtonian parameters  $K_1$  and  $K_2$  have similar effects on the velocity in a qualitative sense.
- The effects of  $M$  and  $\lambda$  on the velocity field are quite opposite.
- The variations of  $K_1$  and  $K_2$  on temperature and concentration are opposite in comparison to velocity.
- An increase in Schmidt number corresponds to a smaller variation in concentration field.

## Chapter 3

# Three-dimensional mixed convection flow of viscoelastic fluid with thermal radiation and convective conditions

The objective of this chapter is to examine the thermal radiation effect in three-dimensional mixed convection flow of viscoelastic fluid. The resulting partial differential equations are reduced into a system of nonlinear ordinary differential equations using appropriate transformations. The series solutions are developed through a modern technique known as the homotopy analysis method. The convergent expressions of the velocity components and temperature are derived. The solutions obtained are dependent on seven sundry parameters including the viscoelastic parameter, mixed convection parameter, ratio parameter, temperature exponent, Prandtl number, Biot number and radiation parameter. Discussion to these parameters is made via plots.



### 3.1 Mathematical analysis

Let us consider three-dimensional mixed convection flow of second grade fluid due to an exponentially stretching surface. The surface coincides with the plane  $z = 0$  and the flow is confined in the region  $z > 0$ . The surface also possess the convective boundary condition. Influence of thermal radiation through Rosseland's approximation is taken into account. Flow configuration is given below.

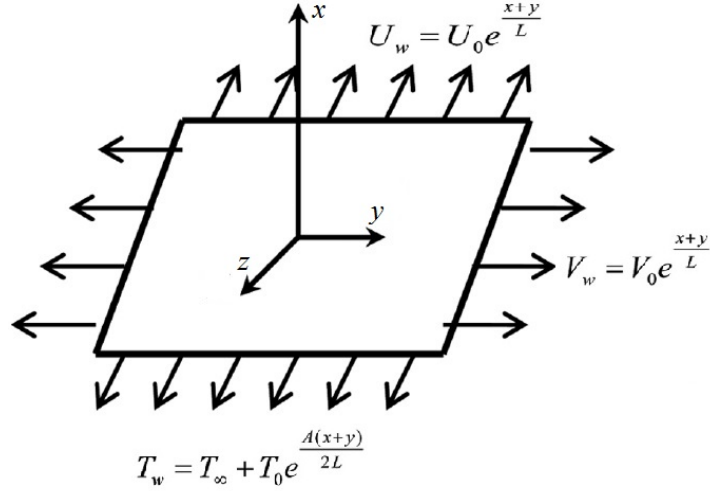


Fig. 3.1: Geometry of problem

The governing boundary layer equations for steady three-dimensional flow of viscoelastic fluid can be put into the forms:

$$\frac{\partial u}{\partial x} + \frac{\partial v}{\partial y} + \frac{\partial w}{\partial z} = 0, \quad (3.1)$$

$$\begin{aligned} u \frac{\partial u}{\partial x} + v \frac{\partial u}{\partial y} + w \frac{\partial u}{\partial z} = & \nu \frac{\partial^2 u}{\partial z^2} + \frac{\alpha_1}{\rho} \left( u \frac{\partial^3 u}{\partial x \partial z^2} + w \frac{\partial^3 u}{\partial z^3} - \left( \frac{\partial u}{\partial x} \frac{\partial^2 u}{\partial z^2} + \frac{\partial u}{\partial z} \frac{\partial^2 w}{\partial z^2} \right) \right) \\ & + g \beta_T (T - T_\infty), \end{aligned} \quad (3.2)$$

$$u \frac{\partial v}{\partial x} + v \frac{\partial v}{\partial y} + w \frac{\partial v}{\partial z} = \nu \frac{\partial^2 v}{\partial z^2} + \frac{\alpha_1}{\rho} \left( v \frac{\partial^3 v}{\partial y \partial z^2} + w \frac{\partial^3 v}{\partial z^3} - \left( \frac{\partial v}{\partial y} \frac{\partial^2 v}{\partial z^2} + \frac{\partial v}{\partial z} \frac{\partial^2 w}{\partial z^2} \right) \right), \quad (3.3)$$

$$u \frac{\partial T}{\partial x} + v \frac{\partial T}{\partial y} + w \frac{\partial T}{\partial z} = \frac{k}{\rho c_p} \frac{\partial^2 T}{\partial z^2} - \frac{1}{\rho c_p} \frac{\partial q_r}{\partial z}, \quad (3.4)$$

where  $u$ ,  $v$  and  $w$  are the velocity components in the  $x$ -,  $y$ - and  $z$ -directions respectively,  $\alpha_1$  is the material fluid parameter,  $\nu = (\mu/\rho)$  is the kinematic viscosity,  $\mu$  is the dynamic viscosity,  $\rho$  is the fluid density,  $T$  is the fluid temperature,  $g$  is the gravitational acceleration,  $\beta_T$  is thermal expansion coefficient of temperature,  $c_p$  is the specific heat,  $k$  is the thermal conductivity and  $q_r$  the radiative heat flux. By using the Rosseland approximation, the radiative heat flux  $q_r$  is given by

$$q_r = -\frac{4\sigma_s}{3k_e} \frac{\partial T^4}{\partial z} \quad (3.5)$$

where  $\sigma_s$  is the Stefan-Boltzmann constant and  $k_e$  the mean absorption coefficient. By using the Rosseland approximation, the present analysis is limited to optically thick fluids. If the temperature differences are sufficiently small then Eq. (3.5) can be linearized by expanding  $T^4$  into the Taylor series about  $T_\infty$ , which after neglecting higher order terms takes the form:

$$T^4 = 4T_\infty^3 T - 3T_\infty^4. \quad (3.6)$$

By using Eqs. (3.5) and (3.6), Eq. (3.4) reduces to

$$u \frac{\partial T}{\partial x} + v \frac{\partial T}{\partial y} + w \frac{\partial T}{\partial z} = \frac{k}{\rho c_p} \frac{\partial^2 T}{\partial z^2} - \frac{16\sigma_s T_\infty^3}{3k_e \rho c_p} \frac{\partial^2 T}{\partial z^2}.$$

The boundary conditions can be expressed as follows:

$$u = U_w, \quad v = V_w, \quad w = 0, \quad -k \frac{\partial T}{\partial z} = h(T_f - T), \quad \text{at } z = 0, \quad (3.7)$$

$$u \rightarrow 0, \quad v \rightarrow 0, \quad T \rightarrow T_\infty \quad \text{as } z \rightarrow \infty, \quad (3.8)$$

where subscript  $w$  corresponds to the wall condition,  $k$  is the thermal conductivity,  $T_f$  is the hot fluid temperature,  $h$  is the heat transfer coefficient and  $T_\infty$  is the free stream temperature.

The velocities and temperature are taken in the following forms:

$$U_w = U_0 e^{\frac{x+y}{L}}, \quad V_w = V_0 e^{\frac{x+y}{L}}, \quad T_w = T_f = T_\infty + T_0 e^{\frac{A(x+y)}{2L}} \quad (3.9)$$

in which  $U_0$ ,  $V_0$  are the constants,  $L$  is the reference length and  $A$  is the temperature exponent.

The mathematical analysis of the problem is simplified by using the transformations [25]:

$$\begin{aligned} u &= U_0 e^{\frac{x+y}{L}} f'(\eta), \quad v = U_0 e^{\frac{x+y}{L}} g'(\eta), \quad w = - \left( \frac{\nu U_0}{2L} \right)^{1/2} e^{\frac{x+y}{2L}} (f + \eta f' + g + \eta g'), \\ T &= T_\infty + T_0 e^{\frac{A(x+y)}{2L}} \theta(\eta), \quad \eta = \left( \frac{U_0}{2\nu L} \right)^{1/2} e^{\frac{x+y}{2L}} z. \end{aligned} \quad (3.10)$$

Incompressibility condition is now clearly satisfied whereas Eqs. (3.2) – (3.8) give

$$f''' + (f + g)f'' - 2(f' + g')f' + K \begin{pmatrix} 6f'''f' + (3g'' - 3f'' + \eta g''')f'' \\ + (4g' + 2\eta g'')f''' - (f + g + \eta g')f''' \end{pmatrix} + 2\lambda\theta = 0, \quad (3.11)$$

$$g''' + (f + g)g'' - 2(f' + g')g' + K \begin{pmatrix} 6g'''g' + (3f'' - 3g'' + \eta f''')g'' \\ + (4f' + 2\eta f'')g''' - (f + g + \eta f')g''' \end{pmatrix} = 0, \quad (3.12)$$

$$(1 + \frac{4}{3}R)\theta'' + Pr(f + g)\theta' - Pr A(f' + g')\theta = 0, \quad (3.13)$$

$$f = 0, \quad g = 0, \quad f' = 1, \quad g' = \beta, \quad \theta' = -\gamma_1(1 - \theta(0)) \quad \text{at } \eta = 0, \quad (3.14)$$

$$f' \rightarrow 0, \quad g' \rightarrow 0, \quad \theta \rightarrow 0 \quad \text{as } \eta \rightarrow \infty \quad (3.15)$$

in which  $K$  is the viscoelastic parameter,  $\beta$  is the ratio parameter,  $Pr$  is the Prandtl number,  $Gr_x$  is the local Grashof number,  $R$  is the radiation parameter,  $A$  is the temperature exponent,  $\gamma_1$  is the Biot number,  $Re_x$  is the local Reynold number,  $\lambda$  is the mixed convection parameter and prime denotes the differentiation with respect to  $\eta$ . These can be defined as

$$\begin{aligned} K &= \frac{\alpha_1 U_w}{2\mu L}, \quad \beta = \frac{V_0}{U_0}, \quad Pr = \frac{\mu c_p}{k}, \quad R = \left( \frac{4\sigma^* T_\infty^3}{k_e k} \right), \quad \gamma_1 = \frac{h}{k} \sqrt{\frac{2\nu L}{U_w}}, \\ Re_x &= \frac{U_0 L}{\nu} e^{\frac{x+y}{L}}, \quad \lambda = \frac{Gr_x}{Re_x^2}, \quad Gr_x = \frac{g\beta_T(T_f - T_\infty)x^3}{\nu^2}. \end{aligned} \quad (3.16)$$

The skin-friction coefficients in the  $x$  and  $y$  directions are given by

$$C_{fx} = \frac{\tau_{wx}}{1/2\rho U_w^2}, \quad (3.17)$$

$$C_{fy} = \frac{\tau_{wy}}{1/2\rho U_w^2}, \quad (3.18)$$

where

$$\begin{aligned} \tau_{wx}|_{z=0} &= \left( \mu \frac{\partial u}{\partial z} + k_0 \left[ u \frac{\partial^2 u}{\partial x \partial z} + v \frac{\partial^2 u}{\partial y \partial z} + w \frac{\partial^2 u}{\partial z^2} + \frac{\partial u}{\partial z} \frac{\partial u}{\partial x} \right. \right. \\ &\quad \left. \left. + \frac{\partial v}{\partial z} \frac{\partial v}{\partial x} + 2 \frac{\partial w}{\partial z} \frac{\partial w}{\partial x} - \frac{\partial w}{\partial z} \frac{\partial u}{\partial z} \right] \right)_{z=0}, \\ \tau_{wy}|_{z=0} &= \left( \mu \frac{\partial v}{\partial z} + k_0 \left[ u \frac{\partial^2 v}{\partial x \partial z} + v \frac{\partial^2 v}{\partial y \partial z} + w \frac{\partial^2 v}{\partial z^2} + \frac{\partial u}{\partial z} \frac{\partial v}{\partial y} \right. \right. \\ &\quad \left. \left. + \frac{\partial v}{\partial z} \frac{\partial v}{\partial y} + 2 \frac{\partial w}{\partial z} \frac{\partial w}{\partial y} - \frac{\partial w}{\partial z} \frac{\partial v}{\partial z} \right] \right)_{z=0}. \end{aligned} \quad (3.19)$$

By using Eq. (3.19) in Eqs. (3.17) and (3.18), the non-dimensional forms of skin friction coefficients are as follows:

$$C_{fx} = \left( \frac{\text{Re}}{2} \right)^{-1/2} [f'' + K(-(f+g)f''' + 5(f'+g')f'' + 2f'f'' + 2g'g'')]_{\eta=0}, \quad (3.20)$$

$$C_{fy} = \left( \frac{\text{Re}}{2} \right)^{-1/2} [g'' + K(-(f+g)g''' + 5(f'+g')g'' + 2f'f'' + 2g'g'')]_{\eta=0}. \quad (3.21)$$

Further the local Nusselt number has the form

$$Nu = \frac{-\left(\frac{16\sigma_s T_\infty^3}{3k_e} + k\right) \frac{\partial T}{\partial z}}{k(T_w - T_\infty)/x} = -\frac{x}{L} \left( \frac{\text{Re}}{2} \right)^{1/2} \left( 1 + \frac{4}{3}R \right) \theta'(0). \quad (3.22)$$

### 3.2 Solutions development

The initial guesses and auxiliary linear operators in the desired HAM solutions are

$$f_0(\eta) = (1 - e^{-\eta}), \quad g_0(\eta) = \beta(1 - e^{-\eta}), \quad \theta_0(\eta) = \frac{\gamma_1 \exp(-\eta)}{1 + \gamma_1}, \quad (3.23)$$

$$\mathcal{L}_f = f''' - f', \quad \mathcal{L}_g = g''' - g', \quad \mathcal{L}_\theta = \theta'' - \theta, \quad (3.24)$$

subject to the properties

$$\begin{aligned}\mathcal{L}_f(C_1 + C_2 e^\eta + C_3 e^{-\eta}) &= 0, \quad \mathcal{L}_g(C_4 + C_5 e^\eta + C_6 e^{-\eta}) = 0, \\ \mathcal{L}_\theta(C_7 e^\eta + C_8 e^{-\eta}) &= 0.\end{aligned}\tag{3.25}$$

in which  $C_i$  ( $i = 1 - 8$ ) are the arbitrary constants,  $\mathcal{L}_f, \mathcal{L}_g$  and  $\mathcal{L}_\theta$  are the linear operators and  $f_0(\eta), g_0(\eta)$  and  $\theta_0(\eta)$  are the initial guesses.

Following the idea in ref. [78] the zeroth order deformation problems are

$$(1 - p) \mathcal{L}_f [\hat{f}(\eta; p) - f_0(\eta)] = p \hbar_f \mathcal{N}_f [\hat{f}(\eta; p), \hat{g}(\eta; p)], \tag{3.26}$$

$$(1 - p) \mathcal{L}_g [\hat{g}(\eta; p) - g_0(\eta)] = p \hbar_g \mathcal{N}_g [\hat{f}(\eta; p), \hat{g}(\eta; p)], \tag{3.27}$$

$$(1 - p) \mathcal{L}_\theta [\hat{\theta}(\eta; p) - \theta_0(\eta)] = p \hbar_\theta \mathcal{N}_\theta [\hat{f}(\eta; p), \hat{g}(\eta; p), \hat{\theta}(\eta; p)], \tag{3.28}$$

$$\hat{f}(0; p) = 0, \quad \hat{f}'(0; p) = 1, \quad \hat{f}'(\infty; p) = 0, \quad \hat{g}(0; p) = 0, \tag{3.29}$$

$$\hat{g}'(0; p) = \alpha, \quad \hat{g}'(\infty; p) = 0, \quad \hat{\theta}'(0, p) = -\gamma_1[1 - \theta(0, p)], \quad \hat{\theta}(\infty, p) = 0. \tag{3.30}$$

For  $p = 0$  and  $p = 1$  one has

$$\begin{aligned}\hat{f}(\eta; 0) &= f_0(\eta), \quad \hat{g}(\eta; 0) = g_0(\eta), \quad \hat{\theta}(\eta, 0) = \theta_0(\eta), \quad \text{and} \quad \hat{f}(\eta; 1) = f(\eta), \\ \hat{g}(\eta; 1) &= g(\eta), \quad \hat{\theta}(\eta, 1) = \theta(\eta).\end{aligned}\tag{3.31}$$

Note that when  $p$  increases from 0 to 1 then  $f(\eta, p), g(\eta, p)$  and  $\theta(\eta, p)$  vary from  $f_0(\eta), g_0(\eta)$  and  $\theta_0(\eta)$  to  $f(\eta), g(\eta)$  and  $\theta(\eta)$ . So as the embedding parameter  $p \in [0, 1]$  increases from 0 to 1, the solutions  $\hat{f}(\eta; p), \hat{g}(\eta; p)$  and  $\hat{\theta}(\eta; p)$  of the zeroth order deformation equations deform from the initial guesses  $f_0(\eta), g_0(\eta)$  and  $\theta_0(\eta)$  to the exact solutions  $f(\eta), g(\eta)$  and  $\theta(\eta)$  of the original nonlinear differential equations. Such kind of continuous variation is called deformation in topology and that is why the Eqs. (3.26-3.28) are called the zeroth order deformation equations.

The values of the nonlinear operators are given below:

$$\begin{aligned}
\mathcal{N}_f[\hat{f}(\eta, p), \hat{g}(\eta, p)] &= \frac{\partial^3 \hat{f}(\eta, p)}{\partial \eta^3} - 2 \left( \frac{\partial \hat{f}(\eta, p)}{\partial \eta} + \frac{\partial \hat{g}(\eta, p)}{\partial \eta} \right) \frac{\partial \hat{f}(\eta, p)}{\partial \eta} + \left( \hat{f}(\eta, p) + \hat{g}(\eta, p) \right) \frac{\partial^2 \hat{f}(\eta, p)}{\partial \eta^2} \\
&+ K \left( \begin{aligned} &6 \frac{\partial \hat{f}(\eta, p)}{\partial \eta} \frac{\partial^3 \hat{f}(\eta, p)}{\partial \eta^3} + \left( 3 \frac{\partial^2 \hat{g}(\eta, p)}{\partial \eta^2} - 3 \frac{\partial^2 \hat{f}(\eta, p)}{\partial \eta^2} + \eta \frac{\partial^3 \hat{g}(\eta, p)}{\partial \eta^3} \right) \\ &\frac{\partial^2 \hat{f}(\eta, p)}{\partial \eta^2} + \left( 4 \frac{\partial \hat{g}(\eta, p)}{\partial \eta} + 2 \eta \frac{\partial^2 \hat{g}(\eta, p)}{\partial \eta^2} \right) \frac{\partial^3 \hat{f}(\eta, p)}{\partial \eta^3} \\ &- \left( \hat{f}(\eta, p) + \hat{g}(\eta, p) + \eta \frac{\partial \hat{g}(\eta, p)}{\partial \eta} \right) \frac{\partial^4 \hat{f}(\eta, p)}{\partial \eta^4} \end{aligned} \right) \\
&+ 2\lambda \hat{\theta}(\eta, p), \tag{3.32}
\end{aligned}$$

$$\begin{aligned}
\mathcal{N}_g[\hat{g}(\eta, p), \hat{f}(\eta, p)] &= \frac{\partial^3 \hat{g}(\eta, p)}{\partial \eta^3} - 2 \left( \begin{aligned} &\frac{\partial \hat{f}(\eta, p)}{\partial \eta} \\ &+ \frac{\partial \hat{g}(\eta, p)}{\partial \eta} \end{aligned} \right) \frac{\partial \hat{g}(\eta, p)}{\partial \eta} + \left( \begin{aligned} &\hat{f}(\eta, p) \\ &+ \hat{g}(\eta, p) \end{aligned} \right) \frac{\partial^2 \hat{g}(\eta, p)}{\partial \eta^2} \\
&+ K \left( \begin{aligned} &6 \frac{\partial \hat{g}(\eta, p)}{\partial \eta} \frac{\partial^3 \hat{g}(\eta, p)}{\partial \eta^3} + \left( 3 \frac{\partial^2 \hat{f}(\eta, p)}{\partial \eta^2} - 3 \frac{\partial^2 \hat{g}(\eta, p)}{\partial \eta^2} + \eta \frac{\partial^3 \hat{f}(\eta, p)}{\partial \eta^3} \right) \\ &\frac{\partial^2 \hat{g}(\eta, p)}{\partial \eta^2} + \left( 4 \frac{\partial \hat{f}(\eta, p)}{\partial \eta} + 2 \eta \frac{\partial^2 \hat{f}(\eta, p)}{\partial \eta^2} \right) \frac{\partial^3 \hat{g}(\eta, p)}{\partial \eta^3} \\ &- \left( \hat{f}(\eta, p) + \hat{g}(\eta, p) + \eta \frac{\partial \hat{f}(\eta, p)}{\partial \eta} \right) \frac{\partial^4 \hat{g}(\eta, p)}{\partial \eta^4} \end{aligned} \right) \tag{3.33}
\end{aligned}$$

$$\begin{aligned}
\mathcal{N}_\theta[\hat{\theta}(\eta, p), \hat{f}(\eta, p), \hat{g}(\eta, p)] &= \left( 1 + \frac{4}{3} R \right) \frac{\partial^2 \hat{\theta}(\eta, p)}{\partial \eta^2} + \text{Pr}(\hat{f}(\eta, p) + \hat{g}(\eta, p)) \frac{\partial \hat{\theta}(\eta, p)}{\partial \eta} \\
&- \text{Pr} A \left( \frac{\partial \hat{f}(\eta, p)}{\partial \eta} + \frac{\partial \hat{g}(\eta, p)}{\partial \eta} \right) \hat{\theta}(\eta, p). \tag{3.34}
\end{aligned}$$

Here  $\hbar_f$ ,  $\hbar_g$  and  $\hbar_\theta$  are the non-zero auxiliary parameters and  $\mathcal{N}_f$ ,  $\mathcal{N}_g$  and  $\mathcal{N}_\theta$  the nonlinear operators. Taylor series expansion gives

$$f(\eta, p) = f_0(\eta) + \sum_{m=1}^{\infty} f_m(\eta) p^m, \quad f_m(\eta) = \frac{1}{m!} \left. \frac{\partial^m f(\eta; p)}{\partial p^m} \right|_{p=0}, \tag{3.35}$$

$$g(\eta, p) = g_0(\eta) + \sum_{m=1}^{\infty} g_m(\eta) p^m, \quad g_m(\eta) = \frac{1}{m!} \left. \frac{\partial^m g(\eta; p)}{\partial p^m} \right|_{p=0}, \tag{3.36}$$

$$\theta(\eta, p) = \theta_0(\eta) + \sum_{m=1}^{\infty} \theta_m(\eta) p^m, \quad \theta_m(\eta) = \frac{1}{m!} \left. \frac{\partial^m \theta(\eta; p)}{\partial p^m} \right|_{p=0}, \tag{3.37}$$

where the convergence of above series strongly depends upon  $\hbar_f$ ,  $\hbar_g$  and  $\hbar_\theta$ . Considering that

$\hbar_f$ ,  $\hbar_g$  and  $\hbar_\theta$  are chosen in such a manner that Eqs. (3.35) – (3.37) converge at  $p = 1$  then

$$f(\eta) = f_0(\eta) + \sum_{m=1}^{\infty} f_m(\eta), \quad (3.38)$$

$$g(\eta) = g_0(\eta) + \sum_{m=1}^{\infty} g_m(\eta), \quad (3.39)$$

$$\theta(\eta) = \theta_0(\eta) + \sum_{m=1}^{\infty} \theta_m(\eta). \quad (3.40)$$

The corresponding problems at mth order deformations satisfy

$$\mathcal{L}_f[f_m(\eta) - \chi_m f_{m-1}(\eta)] = \hbar_f \mathcal{R}_f^m(\eta), \quad (3.41)$$

$$\mathcal{L}_g[g_m(\eta) - \chi_m g_{m-1}(\eta)] = \hbar_g \mathcal{R}_g^m(\eta), \quad (3.42)$$

$$\mathcal{L}_\theta[\theta_m(\eta) - \chi_m \theta_{m-1}(\eta)] = \hbar_\theta \mathcal{R}_\theta^m(\eta). \quad (3.43)$$

$$\begin{aligned} f_m(0) &= f'_m(0) = f'_m(\infty) = 0, \quad g_m(0) = g'_m(0) = g'_m(\infty) = 0, \\ \theta'_m(0) - \gamma_1 \theta_m(0) &= \theta_m(\infty) = 0, \end{aligned} \quad (3.44)$$

$$\begin{aligned} \mathcal{R}_f^m(\eta) &= f'''_{m-1}(\eta) - 2 \sum_{k=0}^{m-1} f'_{m-1-k} f'_k - 2 \sum_{k=0}^{m-1} g'_{m-1-k} f'_k + \sum_{k=0}^{m-1} (f_{m-1-k} f''_k + g_{m-1-k} f''_k) \\ &+ K \left( \begin{aligned} &6 \sum_{k=0}^{m-1} f'_{m-1-k} f'''_k + 3 \sum_{k=0}^{m-1} g''_{m-1-k} f''_k - 3 \sum_{k=0}^{m-1} f''_{m-1-k} f''_k \\ &+ \sum_{k=0}^{m-1} \eta g'''_{m-1-k} f''_k + 4 \sum_{k=0}^{m-1} g'_{m-1-k} f'''_k + 2 \sum_{k=0}^{m-1} \eta g''_{m-1-k} f'''_k \\ &- \sum_{k=0}^{m-1} f_{m-1-k} f'''_k - \sum_{k=0}^{m-1} g_{m-1-k} f'''_k - \sum_{k=0}^{m-1} \eta g'_{m-1-k} f'''_k \end{aligned} \right) \\ &+ 2\lambda\theta, \end{aligned} \quad (3.45)$$

$$\begin{aligned}
\mathcal{R}_g^m(\eta) = & g_{m-1}'''(\eta) - 2 \sum_{k=0}^{m-1} g'_{m-1-k} g'_k - 2 \sum_{k=0}^{m-1} g'_{m-1-k} f'_k + \sum_{k=0}^{m-1} (f_{m-1-k} g''_k + g_{m-1-k} g''_k) \\
& + K \left( \begin{aligned} & 6 \sum_{k=0}^{m-1} g'_{m-1-k} g'''_k + 3 \sum_{k=0}^{m-1} f''_{m-1-k} g''_k - 3 \sum_{k=0}^{m-1} g''_{m-1-k} g''_k \\ & + \sum_{k=0}^{m-1} \eta f'''_{m-1-k} g''_k + 4 \sum_{k=0}^{m-1} f'_{m-1-k} g'''_k + 2 \sum_{k=0}^{m-1} \eta f''_{m-1-k} g'''_k \\ & - \sum_{k=0}^{m-1} g_{m-1-k} g''''_k - \sum_{k=0}^{m-1} f_{m-1-k} g''''_k - \sum_{k=0}^{m-1} \eta f'_{m-1-k} g''''_k \end{aligned} \right), \quad (3.46)
\end{aligned}$$

$$\begin{aligned}
\mathcal{R}_\theta^m(\eta) = & (1 + \frac{4}{3}R)\theta''_{m-1} + \Pr \sum_{k=0}^{m-1} (\theta'_{m-1-k} f_k + \theta'_{m-1-k} g_k) \\
& - \Pr A \sum_{k=0}^{m-1} (f'_{m-1-k} \theta_k + g'_{m-1-k} \theta_k), \quad (3.47)
\end{aligned}$$

$$\chi_m = \begin{cases} 0, & m \leq 1, \\ 1, & m > 1. \end{cases} \quad (3.48)$$

The  $m$ th order deformation problems have the solutions

$$f_m(\eta) = f_m^*(\eta) + C_1 + C_2 e^\eta + C_3 e^{-\eta}, \quad (3.49)$$

$$g_m(\eta) = g_m^*(\eta) + C_4 + C_5 e^\eta + C_6 e^{-\eta}, \quad (3.50)$$

$$\theta_m(\eta) = \theta_m^*(\eta) + C_7 e^\eta + C_8 e^{-\eta}, \quad (3.51)$$

where the special solutions are  $f_m^*$ ,  $g_m^*$  and  $\theta_m^*$ .

### 3.3 Convergence analysis

We recall that the series (3.38) – (3.40) contain the auxiliary parameters  $\hbar_f$ ,  $\hbar_g$  and  $\hbar_\theta$ . These parameters are useful to adjust and control the convergence of homotopic solutions. Hence the  $\hbar$ -curves are sketched at 15<sup>th</sup> order of approximations in order to determine the suitable ranges for  $\hbar_f$ ,  $\hbar_g$  and  $\hbar_\theta$ . Fig. 3.2 denotes that the ranges of admissible values of  $\hbar_f$ ,  $\hbar_g$  and  $\hbar_\theta$  are  $-0.7 \leq \hbar_f \leq -0.2$ ,  $-0.7 \leq \hbar_g \leq -0.1$  and  $-0.8 \leq \hbar_\theta \leq -0.2$ . Table 3.1 presents the numerical values of  $-f''(0)$ ,  $-g''(0)$  and  $-\theta'(0)$  for different order of approximations when  $\hbar_f = -0.5$ ,  $\hbar_g =$



$-0.6$  and  $\hbar_\theta = -0.7$ . It is seen that the values of  $-f''(0)$  and  $-g''(0)$  converge from 20th order of deformations whereas the values of  $-\theta'(0)$  converge from 25th order approximations. Further, it is observed that we have to compute less deformations for the velocities in comparison to temperature for convergent series solutions.

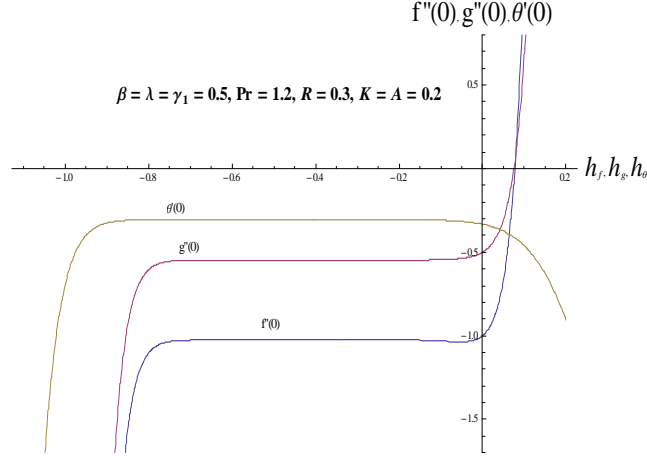


Fig. 3.2:  $\hbar$ -curves for the functions  $f$ ,  $g$  and  $\theta$

**Table 3.1:** Convergence of series solutions for different order of approximations when  $K = 0.1$ ,  $A = 0.2$ ,  $\text{Pr} = 1.2$ ,  $\gamma_1 = 0.6$ ,  $\beta = 0.2$ ,  $\hbar_f = -0.5$ ,  $\hbar_g = -0.6$  and  $\hbar_\theta = -0.7$ .

order of approximations	1	5	10	15	20	25
$-f''(0)$	1.06111	1.02482	1.02609	1.02623	1.02618	1.02618
$-g''(0)$	0.544444	0.548057	0.548092	0.548043	0.548053	0.548053
$-\theta'(0)$	0.317778	0.305581	0.305729	0.305744	0.305738	0.305738

### 3.4 Discussion of results

The effects of ratio parameter  $\beta$ , viscoelastic parameter  $K$ , mixed convection parameter  $\lambda$ , Biot number  $\gamma_1$  and radiation parameter  $R$  on the velocity component  $f'(\eta)$  are shown in the Figs. 3.3-3.5. It is observed from Fig. 3.3 that velocity component  $f'(\eta)$  and thermal boundary layer thickness are decreasing functions of ratio parameter  $\beta$ . This is due to the fact that with the increase of ratio parameter  $\beta$ , the  $x$ -component of velocity coefficient decreases which leads to a decrease in both the momentum boundary layer and velocity component  $f'(\eta)$ . Fig. 3.4

illustrates the influence of viscoelastic parameter  $K$  on the velocity component  $f'(\eta)$ . It is clear that both the boundary layer and velocity component  $f'(\eta)$  increase when the viscoelastic parameter increases. Influence of mixed convection parameter  $\lambda$  on the velocity component  $f'(\eta)$  is analyzed in Fig. 3.5. Increase in mixed convection parameter  $\lambda$  shows an increase in velocity component  $f'(\eta)$ . This is due to the fact that the buoyancy forces are much more effective rather than the viscous forces. Figs. 3.6 and 3.7 illustrate the variations of ratio parameter  $\beta$  and viscoelastic parameter  $K$  on the velocity component  $g'(\eta)$ . Variation of ratio parameter  $\beta$  is analyzed in Fig. 3.6. Through comparative study with Fig. 3.3 it is noted that  $f'(\eta)$  decreases while  $g'(\eta)$  increases when  $\beta$  increases. Physically, when  $\beta$  increases from zero, the lateral surface starts moving in  $y$ -direction and thus the velocity component  $g'(\eta)$  increases and the velocity component  $f'(\eta)$  decreases. Fig. 3.7 is plotted to see the variation of viscoelastic parameter  $K$  on the velocity component  $g'(\eta)$ . It is found that both the velocity component  $g'(\eta)$  and momentum boundary layer thicknesses are increasing functions of  $K$ . It is revealed from Figs. 3.4 and 3.7 that the effect of  $K$  on both the velocities are qualitatively similar.

Figs. 3.8-3.14 are sketched to see the effects of ratio parameter  $\beta$ , viscoelastic parameter  $K$ , the temperature exponent  $A$ , Biot number  $\gamma_1$ , mixed convection parameter  $\lambda$ , Radiation parameter  $R$  and Prandtl number  $Pr$  on the temperature  $\theta(\eta)$ . Fig. 3.8 is drawn to see the impact of ratio parameter  $\beta$  on the temperature  $\theta(\eta)$ . It is noted that the temperature  $\theta(\eta)$  and also the thermal boundary layer thickness decrease with increasing  $\beta$ . Variation of the viscoelastic parameter  $K$  on the temperature  $\theta(\eta)$  is shown in Fig. 3.9. Here both the temperature and thermal boundary layer thickness are decreasing functions of  $K$ . Variation of mixed convection parameter  $\lambda$  is analyzed in Fig. 3.10. It is seen that both the temperature  $\theta(\eta)$  and thermal boundary layer thickness are decreasing functions of mixed convection parameter  $\lambda$ . Fig. 3.11 presents the plots for the variation of Biot number  $\gamma_1$ . Note that  $\theta(\eta)$  increases when  $\gamma_1$  increases. The thermal boundary layer thickness is also increasing function of  $\gamma_1$ . It is also noted that the fluid temperature is zero when the Biot number vanishes. Influence of temperature exponent  $A$  is displayed in Fig. 3.12. It is found that both the temperature  $\theta(\eta)$  and thermal boundary layer thickness decrease when  $A$  is increased. Also both the temperature  $\theta(\eta)$  and thermal boundary layer thickness are increasing functions of thermal radiation parameter  $R$ .

( see Fig. 3.13). It is observed that an increase in  $R$  has the ability to increase the thermal boundary layer. It is due to the fact that when the thermal radiation parameter increases, the mean absorption coefficient  $k_e$  will be decreased which in turn increases the divergence of the radiative heat flux. Hence the rate of radiative heat transfer to the fluid is increased and consequently the fluid temperature increases. Fig. 3.14 is plotted to see the effects of  $Pr$  on  $\theta(\eta)$ . It is noticed that both the temperature profile and thermal boundary layer thickness are decreasing functions of  $Pr$ . In fact when  $Pr$  increases then thermal diffusivity decreases. This indicates reduction in energy transfer ability and ultimate it results in the decrease of thermal boundary layer.

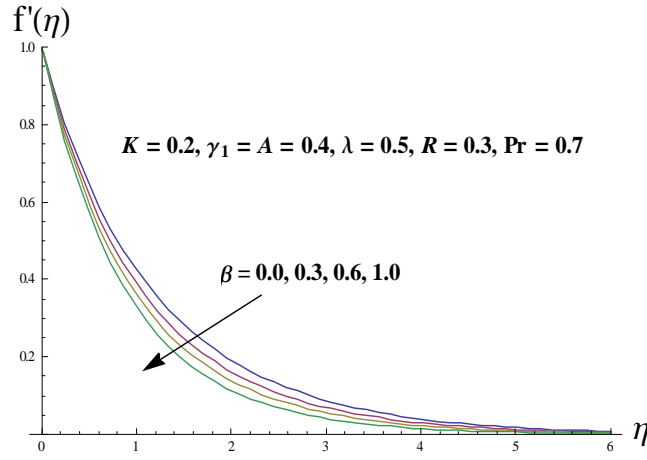


Fig. 3.3: Influence of  $\beta$  on the velocity  $f'(\eta)$ .

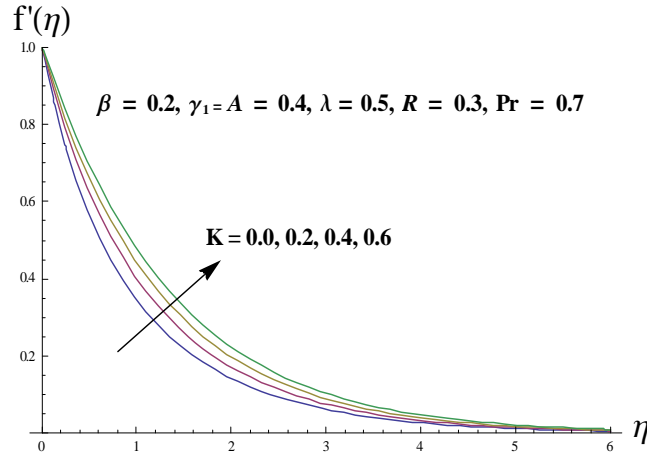


Fig. 3.4: Influence of  $K$  on the velocity  $f'(\eta)$ .

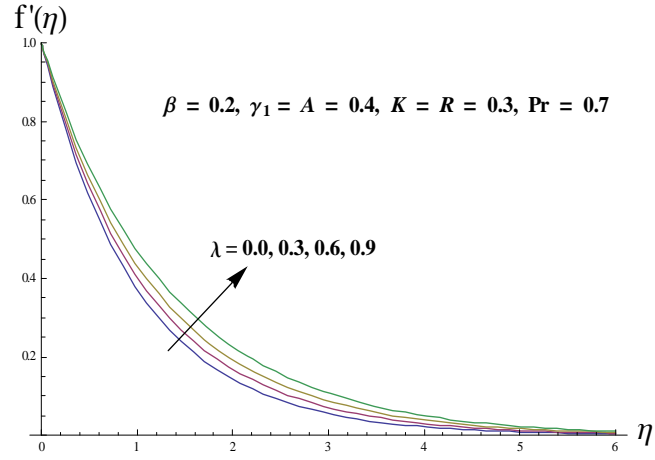


Fig. 3.5: Influence of  $\lambda$  on the velocity  $f'(\eta)$ .

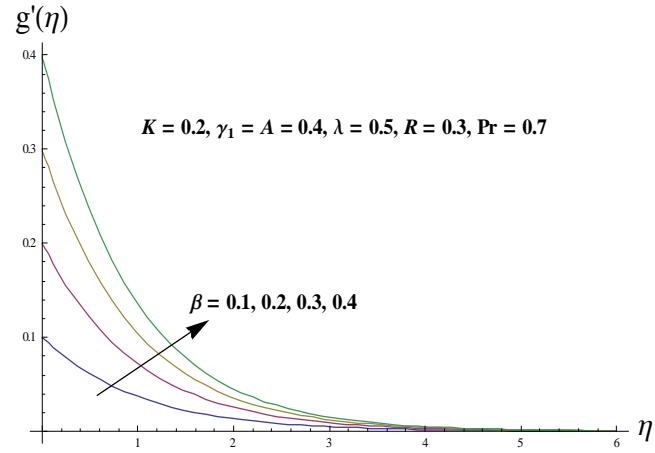


Fig. 3.6: Influence of  $\beta$  on the velocity  $g'(\eta)$ .

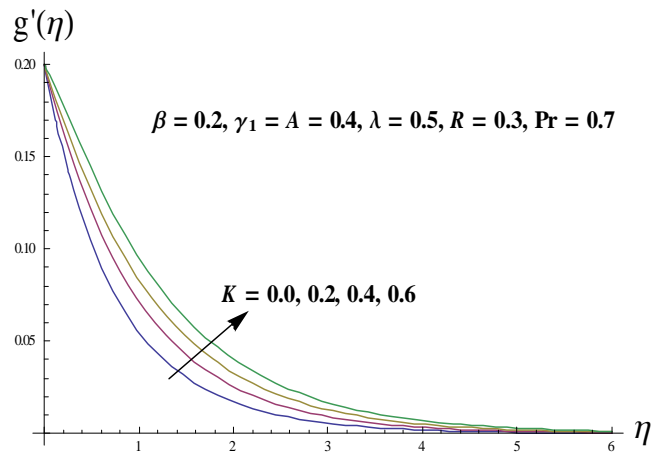


Fig. 3.7: Influence of  $K$  on the velocity  $g'(\eta)$ .

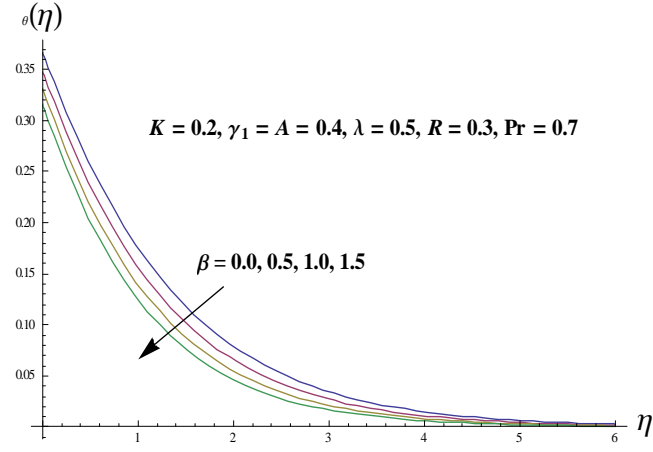


Fig. 3.8: Influence of  $\beta$  on the temperature  $\theta(\eta)$ .

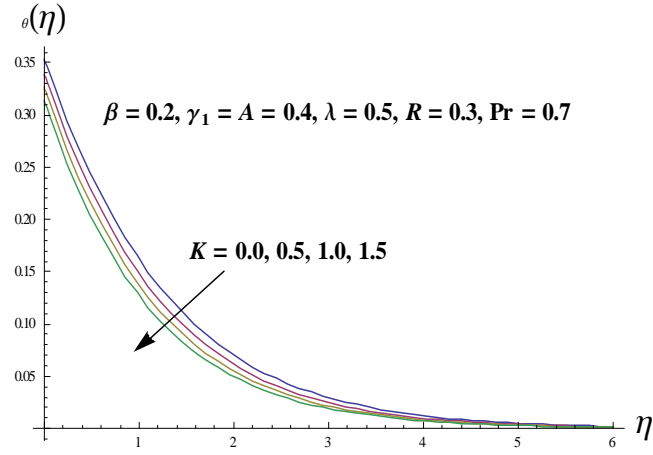


Fig. 3.9: Influence of  $K$  on the temperature  $\theta(\eta)$ .

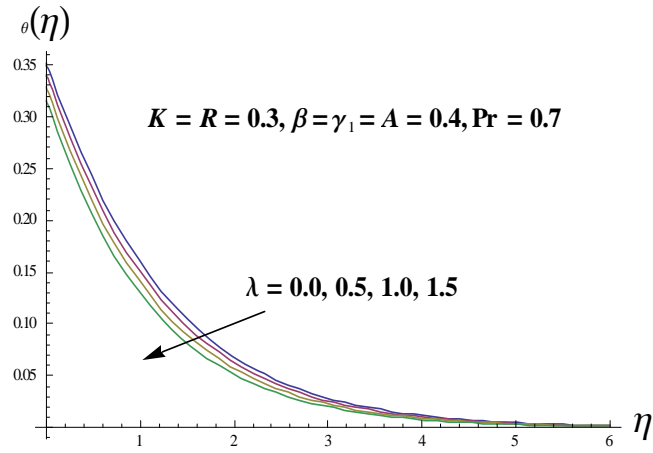


Fig. 3.10: Influence of  $\lambda$  on the temperature  $\theta(\eta)$ .

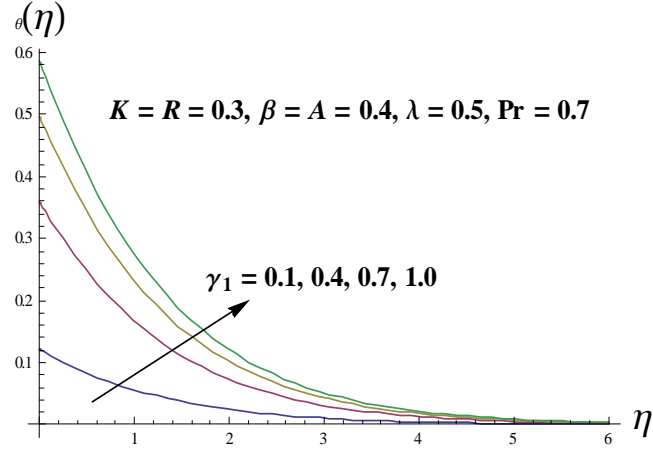


Fig. 3.11: Influence of  $\gamma_1$  on the temperature  $\theta(\eta)$ .

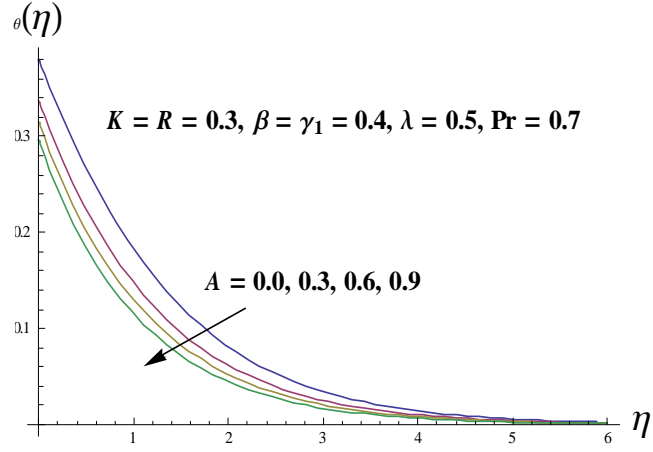


Fig. 3.12: Influence of  $A$  on the temperature  $\theta(\eta)$ .

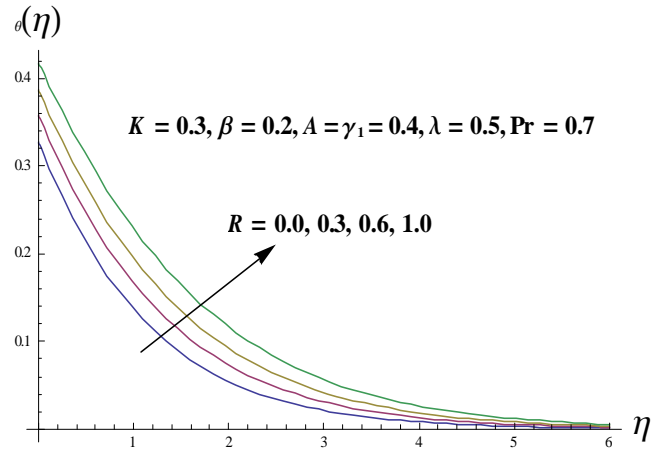


Fig. 3.13: Influence of  $R$  on the temperature  $\theta(\eta)$ .

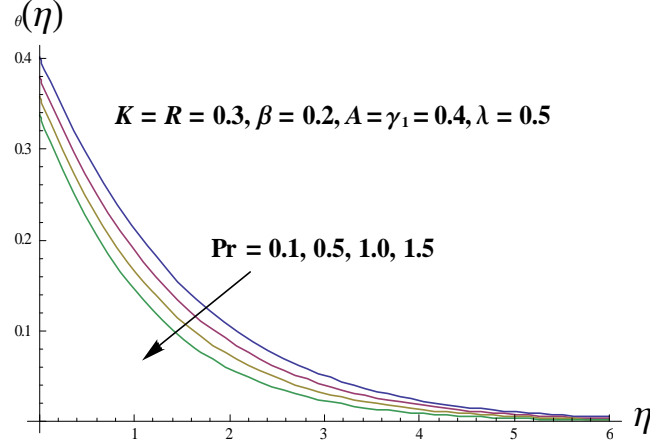


Fig. 3.14: Influence of  $Pr$  on the temperature  $\theta(\eta)$ .

Table 3.2 includes the values for comparison of existing solutions with the previous available solutions in a limiting case when  $K = \lambda = \gamma_1 = R = 0$  and  $\beta$  varies. This Table presents an excellent agreement with the previous available solutions. Table 3.3 is computed to see the influences of viscoelastic parameter  $K$  and ratio parameter  $\beta$  on skin friction coefficients in the  $x$  and  $y$  directions. It is noted that  $K$  has quite opposite effect on skin friction coefficients while quite similar effect is seen within the increase of ratio parameter  $\beta$ . Table 3.4 examines the impact of viscoelastic parameter  $K$ , mixed convection parameter  $\lambda$ , ratio parameter  $\beta$ , Biot number  $\gamma_1$ , radiation parameter  $R$ , Prandtl number  $Pr$  and temperature exponent  $A$  on the local Nusselt number (rate of heat transfer at the wall). It is noted that the value of rate of heat transfer increases for larger viscoelastic parameter  $K$ , mixed convection parameter  $\lambda$ , ratio parameter  $\beta$ , Biot number  $\gamma_1$ , Prandtl number  $Pr$  and temperature exponent  $A$  while it decreases through an increase in radiation parameter  $R$ .

**Table 3.2:** Comparative values of  $-f''(0)$ ,  $-g''(0)$  and  $f(\infty) + g(\infty)$  for different values  $\beta$  when  $K = \lambda = \gamma_1 = R = 0$ .

$\alpha$	Liu et al. [25]			Present results		
	$-f''(0)$	$-g''(0)$	$f(\infty) + g(\infty)$	$-f''(0)$	$-g''(0)$	$f(\infty) + g(\infty)$
0.0	1.28180856	0	0.90564383	1.28181	0	0.90564
0.50	1.56988846	0.78494423	1.10918263	1.56989	0.78494	1.10918
1.00	1.81275105	1.81275105	1.28077378	1.81275	1.81275	1.28077

**Table 3.3:** Values of skin friction coefficients for different values of  $K$  and  $\beta$  when  $\lambda = \gamma_1 = 0.5$ ,  $R = 0.3$ ,  $\text{Pr} = 1.2$  and  $A = 0.2$ .

$K$	$\alpha$	$-\left(\frac{\text{Re}}{2}\right)^{1/2} C_{fx}$	$-\left(\frac{\text{Re}}{2}\right)^{1/2} C_{fy}$
0.0	0.5	4.95289	4.37363
0.2		5.16586	3.97055
0.3		5.42622	3.96130
0.3	0.0	3.72170	1.65409
	0.2	4.30247	2.34617
	0.5	5.42622	3.96130

**Table 3.4:** Values of local Nusselt number  $-(1 + \frac{4}{3}R)\theta'(0)$  for different values of the parameters  $K$ ,  $\beta$ ,  $\lambda$ ,  $R$ ,  $A$ ,  $\text{Pr}$  and  $\gamma_1$ .



$K$	$\lambda$	$\beta$	$\gamma_1$	$R$	Pr	$A$	$-(1 + \frac{4}{3}R)\theta'(0)$
0.0	0.5	0.5	0.5	0.3	1.2	0.2	0.297492
0.3							0.308234
0.5							0.311853
0.2	0.0						0.303062
	0.3						0.304775
	0.5						0.305738
0.2	0.5	0.0					0.282007
		0.3					0.297135
		0.5					0.305738
			0.1				0.0885730
			0.3				0.216850
			0.5				0.305738
0.2	0.5	0.5	0.5	0.0			0.329701
				0.3			0.305738
				0.5			0.292750
0.2	0.5	0.5	0.5	0.3	1.0		0.292152
					1.2		0.305738
					1.5		0.321826
0.2	0.5	0.5	0.5	0.3	1.2	0.0	0.288530
						0.2	0.305738
						0.5	0.325492

### 3.5 Conclusions

Three-dimensional mixed convection flow of viscoelastic fluid over an exponentially stretching surface is analyzed. The analysis is carried out in the presence of thermal radiation and convective boundary conditions. The main observations can be summarized as follows.

- Influence of ratio parameter  $\beta$  on the velocities  $f'(\eta)$  and  $g'(\eta)$  is quite opposite. However the effect of viscoelastic parameter  $K$  on the velocities  $f'(\eta)$  and  $g'(\eta)$  is qualitatively

similar.

- Momentum boundary layer thickness increases for  $g'(\eta)$  when ratio parameter  $\beta$  is large. Effect of  $\beta$  on  $f'(\eta)$  is opposite to that of  $g'(\eta)$ .
- Velocity component  $f'(\eta)$  is increasing function of mixed convection parameter  $\lambda$ . However  $\theta(\eta)$  decreases with an increase of mixed convection parameter  $\lambda$ . The impacts of Biot number  $\gamma_1$  and radiation parameter  $R$  on  $f'(\eta)$  and  $\theta(\eta)$  are qualitatively similar.
- Momentum boundary layer is an increasing function of mixed convection parameter  $\lambda$  while thermal boundary layer is decreasing function of mixed convection parameter  $\lambda$ .
- Increase in Prandtl number decreases the temperature  $\theta(\eta)$ .
- Thermal boundary layer thickness decreases when ratio parameter  $\beta$ , viscoelastic parameter  $K$ , mixed convection parameter  $\lambda$ , Prandtl number  $Pr$  and temperature exponent  $A$  are increased.
- Influence of viscoelastic parameter  $K$  on the  $x$  and  $y$  directions of skin friction coefficients is opposite.
- Both components of skin friction coefficient increase through an increase in ratio parameter  $\beta$ .
- Local Nusselt number is an increasing function of Prandtl number  $Pr$ , ratio parameter  $\beta$ , viscoelastic parameter  $K$ , mixed convection parameter  $\lambda$ , Biot number  $\gamma_1$  and temperature exponent  $A$  while it decreases for radiation parameter  $R$ .

## Chapter 4

# Convective heat and mass transfer in three-dimensional mixed convection flow of viscoelastic fluid with chemical reaction and heat source/sink

This chapter investigates the heat and mass transfer effects in three-dimensional mixed convection flow of viscoelastic fluid with internal heat source/sink and chemical reaction. An exponential stretching surface induces the flow. Magnetic field normal to the direction of flow is applied. Convective conditions at boundary surface are also encountered. Appropriate similarity transformations are utilized to reduce the boundary layer partial differential equations into ordinary differential equations. Analytical solutions of the resulting systems are obtained. Convergence of the obtained solutions is discussed explicitly. The local Nusselt and Sherwood numbers are sketched and examined.

## 4.1 Mathematical modeling

We consider the three-dimensional mixed convection boundary layer flow of viscoelastic fluid past an exponentially stretching surface. Mathematical analysis has been carried out in presence of internal heat source/sink and generative/destructive chemical reaction. Magnetic field is applied to the normal direction of flow. The surface coincides with the plane at  $z = 0$  and the flow is confined in the region  $z > 0$ . Convective boundary conditions for both heat and mass transfer on the sheet are taken into account. The governing equations for three-dimensional flow are expressed as follows:

$$u \frac{\partial u}{\partial x} + v \frac{\partial u}{\partial y} + w \frac{\partial u}{\partial z} = 0, \quad (4.1)$$

$$\begin{aligned} u \frac{\partial u}{\partial x} + v \frac{\partial u}{\partial y} + w \frac{\partial u}{\partial z} = & \nu \frac{\partial^2 u}{\partial z^2} + \frac{\alpha_1}{\rho} \left( u \frac{\partial^3 u}{\partial x \partial z^2} + w \frac{\partial^3 u}{\partial z^3} - \left( \frac{\partial u}{\partial x} \frac{\partial^2 u}{\partial z^2} + \frac{\partial u}{\partial z} \frac{\partial^2 w}{\partial z^2} \right) \right. \\ & \left. + 2 \frac{\partial u}{\partial z} \frac{\partial^2 u}{\partial x \partial z} + 2 \frac{\partial w}{\partial z} \frac{\partial^2 u}{\partial z^2} \right) \\ & + g\beta_T(T - T_\infty) + g\beta_C(C - C_\infty) - \frac{\sigma^* B_0^2}{\rho} u, \end{aligned} \quad (4.2)$$

$$\begin{aligned} u \frac{\partial v}{\partial x} + v \frac{\partial v}{\partial y} + w \frac{\partial v}{\partial z} = & \nu \frac{\partial^2 v}{\partial z^2} + \frac{\alpha_1}{\rho} \left( v \frac{\partial^3 v}{\partial y \partial z^2} + w \frac{\partial^3 v}{\partial z^3} - \left( \frac{\partial v}{\partial y} \frac{\partial^2 v}{\partial z^2} + \frac{\partial v}{\partial z} \frac{\partial^2 w}{\partial z^2} \right) \right. \\ & \left. + 2 \frac{\partial v}{\partial z} \frac{\partial^2 v}{\partial y \partial z} + 2 \frac{\partial w}{\partial z} \frac{\partial^2 v}{\partial z^2} \right) \\ & - \frac{\sigma^* B_0^2}{\rho} v, \end{aligned} \quad (4.3)$$

$$u \frac{\partial T}{\partial x} + v \frac{\partial T}{\partial y} + w \frac{\partial T}{\partial z} = \sigma \frac{\partial^2 T}{\partial z^2} + \frac{Q}{\rho c_p} (T - T_\infty), \quad (4.4)$$

$$u \frac{\partial C}{\partial x} + v \frac{\partial C}{\partial y} + w \frac{\partial C}{\partial z} = D_B \frac{\partial^2 C}{\partial z^2} - k_1 (C - C_\infty). \quad (4.5)$$

In the above equations,  $u$ ,  $v$  and  $w$  are the velocity components in the  $x$ -,  $y$ - and  $z$ -directions respectively,  $\alpha_1$  the material fluid parameter,  $\beta_T$  the thermal expansion coefficient,  $\beta_C$  the concentration expansion coefficient,  $\sigma^*$  the electrical conductivity,  $B_0$  the magnitude of applied magnetic field,  $\rho$  the density of fluid,  $g$  the gravitational acceleration,  $\nu = (\mu/\rho)$  the kinematic viscosity,  $\mu$  the dynamic viscosity,  $\sigma$  the thermal diffusivity,  $T$  the fluid temperature,  $c_p$  the specific heat of the fluid,  $Q$  the uniform volumetric heat generation/absorption,  $C$  the con-

centration field,  $D$  the mass diffusivity and prime denotes the differentiation with respect to  $\eta$ .

The boundary conditions are given by

$$u = U_w, \quad v = V_w, \quad w = 0, \quad -k \frac{\partial T}{\partial z} = h(T_f - T), \quad -D \frac{\partial C}{\partial z} = h^*(C_f - C) \quad \text{at } z = 0, \quad (4.6)$$

$$u \rightarrow 0, \quad v \rightarrow 0, \quad T \rightarrow T_\infty, \quad C \rightarrow C_\infty \quad \text{as } z \rightarrow \infty, \quad (4.7)$$

where subscript  $w$  corresponds to the wall condition,  $h$  is the heat transfer coefficient,  $h^*$  is the concentration transfer coefficient,  $T_f$  is the ambient fluid temperature and  $C_f$  is the ambient fluid concentration.

At wall the velocities, temperature and concentration distributions are defined as:

$$U_w = U_0 e^{\frac{x+y}{L}}, \quad V_w = V_0 e^{\frac{x+y}{L}}, \quad T_w = T_\infty + T_0 e^{\frac{A(x+y)}{2L}}, \quad C_w = C_\infty + C_0 e^{\frac{B(x+y)}{2L}}, \quad (4.8)$$

where  $U_0, V_0, W_0$  are the constants,  $L$  is the reference length,  $T_\infty$  is the ambient temperature,  $C_\infty$  is the ambient concentration,  $A$  is the temperature exponent and  $B$  is the concentration exponent. By using similarity transformations [25]:

$$\begin{aligned} u &= U_0 e^{\frac{x+y}{L}} f'(\eta), \quad v = U_0 e^{\frac{x+y}{L}} g'(\eta), \quad w = -\left(\frac{\nu U_0}{2L}\right)^{1/2} e^{\frac{x+y}{2L}} (f + \eta f' + g + \eta g'), \\ T &= T_\infty + T_0 e^{\frac{A(x+y)}{2L}} \theta(\eta), \quad C = C_\infty + C_0 e^{\frac{B(x+y)}{2L}} \phi(\eta), \quad \eta = \left(\frac{U_0}{2\nu L}\right)^{1/2} e^{\frac{x+y}{2L}} z, \end{aligned} \quad (4.9)$$

equation (4.1) is identically satisfied and Eqs. (4.2) – (4.9) give:

$$f''' + (f+g)f'' - 2(f'+g')f' + K \left( \begin{array}{c} 6f'''f' + (3g'' - 3f'' + \eta g''')f'' \\ + ((4g' + 2\eta g'')f''' - (f+g+\eta g')f'''' \end{array} \right) + 2\lambda(\theta + N\phi) - Mf' = 0, \quad (4.10)$$

$$g''' + (f+g)g'' - 2(f'+g')g' + K \left( \begin{array}{c} 6g'''g' + (3f'' - 3g'' + \eta f''')g'' \\ + (4f' + 2\eta f'')g''' - (f+g+\eta f')g'''' \end{array} \right) - Mg' = 0, \quad (4.11)$$

$$\theta'' + Pr(f+g)\theta' - Pr A(f'+g')\theta + Pr \beta^* \theta = 0, \quad (4.12)$$

$$\phi'' + Sc(f+g)\phi' - Sc B(f'+g')\phi - Sc k^* \phi = 0, \quad (4.13)$$

$$f = 0, \quad g = 0, \quad f' = 1, \quad g' = \beta, \quad \theta' = -\gamma_1(1 - \theta(0)), \quad \phi' = -\gamma_2(1 - \phi(0)), \quad \text{at } \eta = 0, \quad (4.14)$$

$$f' \rightarrow 0, \quad g' \rightarrow 0, \quad \theta \rightarrow 0, \quad \phi \rightarrow 0 \quad \text{as } \eta \rightarrow \infty, \quad (4.15)$$

where  $K$  is the viscoelastic parameter,  $\lambda$  is the mixed convection parameter,  $Gr_x$  is the local Grashof number,  $N$  is the concentration buoyancy parameter,  $M$  is the Hartman number,  $Pr$  is the Prandtl number,  $\beta^*$  is the heat source/sink parameter,  $k^*$  is the chemical reaction parameter,  $Sc$  is the Schmidt number,  $\beta$  is the ratio parameter,  $\gamma_1$  is the heat transfer Biot number and  $\gamma_2$  is the mass transfer Biot number. The definitions of these variables are

$$\begin{aligned} K &= \frac{\alpha_1 U_w}{2\nu L}, \lambda = \frac{Gr_x}{Re_x^2}, Gr_x = \frac{g\beta_T(T_f - T_\infty)x^3}{\nu^2}, N = \frac{\beta_C(C_w - C_\infty)}{\beta_T(T_f - T_\infty)}, M = \frac{\sigma^* B_0^2}{\rho}, \\ Pr &= \frac{\nu}{\sigma}, \beta^* = \frac{Q}{\rho c_p}, k^* = \frac{k_1}{U_0}, Sc = \frac{\nu}{D}, \beta = \frac{V_0}{U_0}, \gamma_1 = \frac{h}{k}\sqrt{\frac{\nu}{a}}, \gamma_2 = \frac{h^*}{D}\sqrt{\frac{\nu}{a}}. \end{aligned} \quad (4.16)$$

The local Nusselt and Sherwood numbers in dimensionless forms are

$$Nu/Re_x^{1/2} = -\frac{x}{2L}\theta'(0), \quad (4.17)$$

$$Sh/Re_x^{1/2} = -\frac{x}{2L}\phi'(0), \quad (4.18)$$

in which  $Re_x = \frac{U_0 L}{\nu} e^{\frac{x+y}{L}}$  is the local Reynolds number.

## 4.2 Series solutions

For homotopic solutions, the initial guesses and auxiliary linear operators are chosen as follows:

$$f_0(\eta) = (1 - e^{-\eta}), \quad g_0(\eta) = \beta(1 - e^{-\eta}), \quad \theta_0(\eta) = \frac{\gamma_1 \exp(-\eta)}{1 + \gamma_1}, \quad \phi_0(\eta) = \frac{\gamma_2 \exp(-\eta)}{1 + \gamma_2}, \quad (4.19)$$

$$\mathcal{L}_f = f''' - f', \quad \mathcal{L}_g = g''' - g', \quad \mathcal{L}_\theta = \theta'' - \theta, \quad \mathcal{L}_\phi = \phi'' - \phi. \quad (4.20)$$

The above operators satisfy the following properties

$$\begin{aligned}\mathcal{L}_f(C_1 + C_2 e^\eta + C_3 e^{-\eta}) &= 0, \quad \mathcal{L}_g(C_4 + C_5 e^\eta + C_6 e^{-\eta}) = 0, \\ \mathcal{L}_\theta(C_7 e^\eta + C_8 e^{-\eta}) &= 0, \quad \mathcal{L}_\phi(C_9 e^\eta + C_{10} e^{-\eta}) = 0,\end{aligned}\tag{4.21}$$

where  $C_i$  ( $i = 1 - 10$ ) are the arbitrary constants.

The problems corresponding to zeroth order are

$$(1 - p) \mathcal{L}_f [\hat{f}(\eta; p) - f_0(\eta)] = p \hbar_f \mathcal{N}_f [\hat{f}(\eta; p), \hat{g}(\eta; p), \hat{\theta}(\eta; p), \hat{\phi}(\eta; p)], \tag{4.22}$$

$$(1 - p) \mathcal{L}_g [\hat{g}(\eta; p) - g_0(\eta)] = p \hbar_g \mathcal{N}_g [\hat{f}(\eta; p), \hat{g}(\eta; p)], \tag{4.23}$$

$$(1 - p) \mathcal{L}_\theta [\hat{\theta}(\eta; p) - \theta_0(\eta)] = p \hbar_\theta \mathcal{N}_\theta [\hat{f}(\eta; p), \hat{g}(\eta; p), \hat{\theta}(\eta; p), \hat{\phi}(\eta; p)], \tag{4.24}$$

$$(1 - p) \mathcal{L}_\phi [\hat{\phi}(\eta; p) - \phi_0(\eta)] = p \hbar_\phi \mathcal{N}_\phi [\hat{f}(\eta; p), \hat{g}(\eta; p), \hat{\theta}(\eta; p), \hat{\phi}(\eta; p)], \tag{4.25}$$

$$\hat{f}(0; p) = 0, \quad \hat{f}'(0; p) = 1, \quad \hat{f}'(\infty; p) = 0, \quad \hat{g}(0; p) = 0, \tag{4.26}$$

$$\hat{g}'(0; p) = \alpha, \quad \hat{g}'(\infty; p) = 0, \quad \hat{\theta}'(0, p) = -\gamma_1[1 - \theta(0, p)], \tag{4.27}$$

$$\hat{\theta}(\infty, p) = 0, \quad \hat{\phi}'(0, p) = -\gamma_2[1 - \hat{\phi}(0, p)], \quad \hat{\phi}(\infty, p) = 0, \tag{4.28}$$

$$\begin{aligned}\mathcal{N}_f[\hat{f}(\eta; p), \hat{g}(\eta; p), \hat{\theta}(\eta; p), \hat{\phi}(\eta; p)] &= \frac{\partial^3 \hat{f}(\eta, p)}{\partial \eta^3} - 2 \left( \frac{\partial \hat{f}(\eta, p)}{\partial \eta} + \frac{\partial \hat{g}(\eta, p)}{\partial \eta} \right) \frac{\partial \hat{f}(\eta, p)}{\partial \eta} \\ &+ \left( \begin{array}{c} \hat{f}(\eta, p) \\ + \hat{g}(\eta, p) \end{array} \right) \frac{\partial^2 \hat{f}(\eta, p)}{\partial \eta^2} + 2\lambda \left( \begin{array}{c} \hat{\theta}(\eta, p) \\ + N \hat{\phi}(\eta; p) \end{array} \right) - M \frac{\partial \hat{f}(\eta, p)}{\partial \eta} \\ &+ K \left( \begin{array}{c} 6 \frac{\partial \hat{f}(\eta, p)}{\partial \eta} \frac{\partial^3 \hat{f}(\eta, p)}{\partial \eta^3} + \left( \begin{array}{c} 3 \frac{\partial^2 \hat{g}(\eta, p)}{\partial \eta^2} \\ - 3 \frac{\partial^2 \hat{f}(\eta, p)}{\partial \eta^2} + \eta \frac{\partial^3 \hat{g}(\eta, p)}{\partial \eta^3} \end{array} \right) \\ \frac{\partial^2 \hat{f}(\eta, p)}{\partial \eta^2} + \left( \begin{array}{c} 4 \frac{\partial \hat{g}(\eta, p)}{\partial \eta} \\ + 2 \eta \frac{\partial^2 \hat{g}(\eta, p)}{\partial \eta^2} \end{array} \right) \frac{\partial^3 \hat{f}(\eta, p)}{\partial \eta^3} \\ - \left( \begin{array}{c} \hat{f}(\eta, p) + \hat{g}(\eta, p) \\ + \eta \frac{\partial \hat{g}(\eta, p)}{\partial \eta} \end{array} \right) \frac{\partial^4 \hat{f}(\eta, p)}{\partial \eta^4} \end{array} \right), \end{aligned} \tag{4.29}$$

$$\begin{aligned}
\mathcal{N}_g[\hat{f}(\eta; p), \hat{g}(\eta; p), \hat{\theta}(\eta; p), \hat{\phi}(\eta; p)] &= \frac{\partial^3 \hat{g}(\eta, p)}{\partial \eta^3} - 2 \left( \frac{\frac{\partial \hat{f}(\eta, p)}{\partial \eta}}{+\frac{\partial \hat{g}(\eta, p)}{\partial \eta}} \right) \frac{\partial \hat{g}(\eta, p)}{\partial \eta} + \left( \frac{\hat{f}(\eta, p)}{+\hat{g}(\eta, p)} \right) \frac{\partial^2 \hat{g}(\eta, p)}{\partial \eta^2} \\
&+ K \left( \begin{aligned} &6 \frac{\partial \hat{g}(\eta, p)}{\partial \eta} \frac{\partial^3 \hat{g}(\eta, p)}{\partial \eta^3} \\ &+ \left( \frac{3 \frac{\partial^2 \hat{f}(\eta, p)}{\partial \eta^2} -}{3 \frac{\partial^2 \hat{g}(\eta, p)}{\partial \eta^2} + \eta \frac{\partial^3 \hat{f}(\eta, p)}{\partial \eta^3}} \right) \end{aligned} \right) \\
&+ K \left( \begin{aligned} &\frac{\partial^2 \hat{g}(\eta, p)}{\partial \eta^2} + \left( \frac{4 \frac{\partial \hat{f}(\eta, p)}{\partial \eta}}{+2\eta \frac{\partial^2 \hat{f}(\eta, p)}{\partial \eta^2}} \right) \frac{\partial^3 \hat{g}(\eta, p)}{\partial \eta^3} \\ &- \left( \frac{\hat{f}(\eta, p) + \hat{g}(\eta, p)}{+\eta \frac{\partial \hat{f}(\eta, p)}{\partial \eta}} \right) \frac{\partial^4 \hat{g}(\eta, p)}{\partial \eta^4} \end{aligned} \right) \\
&- M \frac{\partial \hat{g}(\eta, p)}{\partial \eta}, \tag{4.30}
\end{aligned}$$

$$\begin{aligned}
\mathcal{N}_\theta[\hat{f}(\eta; p), \hat{g}(\eta; p), \hat{\theta}(\eta; p), \hat{\phi}(\eta; p)] &= \frac{\partial^2 \hat{\theta}(\eta, p)}{\partial \eta^2} + \text{Pr} \left( \frac{\hat{f}(\eta, p)}{+\hat{g}(\eta, p)} \right) \frac{\partial \hat{\theta}(\eta, p)}{\partial \eta} + \text{Pr} \beta^* \hat{\theta}(\eta, p) \\
&- \text{Pr} A \left( \frac{\partial \hat{f}(\eta, p)}{\partial \eta} + \frac{\partial \hat{g}(\eta, p)}{\partial \eta} \right) \hat{\theta}(\eta, p), \tag{4.31}
\end{aligned}$$

$$\begin{aligned}
\mathcal{N}_\phi[\hat{f}(\eta; p), \hat{g}(\eta; p), \hat{\theta}(\eta; p), \hat{\phi}(\eta; p)] &= \frac{\partial^2 \hat{\phi}(\eta; p)}{\partial \eta^2} + Sc \left( \frac{\hat{f}(\eta, p)}{+\hat{g}(\eta, p)} \right) \frac{\partial \hat{\phi}(\eta; p)}{\partial \eta} - Sck^* \hat{\phi}(\eta; p) \\
&- ScB \left( \frac{\partial \hat{f}(\eta, p)}{\partial \eta} + \frac{\partial \hat{g}(\eta, p)}{\partial \eta} \right) \hat{\phi}(\eta; p). \tag{4.32}
\end{aligned}$$

Here  $p$  is an embedding parameter, the non-zero auxiliary parameters are  $\hbar_f$ ,  $\hbar_g$ ,  $\hbar_\theta$  and  $\hbar_\phi$  and the nonlinear operators are  $\mathcal{N}_f$ ,  $\mathcal{N}_g$ ,  $\mathcal{N}_\theta$  and  $\mathcal{N}_\phi$ . Taking  $p = 0$  and  $p = 1$  we get

$$\begin{aligned}
\hat{f}(\eta; 0) &= f_0(\eta), \quad \hat{g}(\eta; 0) = g_0(\eta), \quad \hat{\theta}(\eta, 0) = \theta_0(\eta), \quad \hat{\phi}(\eta; 0) = \phi_0(\eta) \text{ and } \hat{f}(\eta; 1) = f(\eta), \\
\hat{g}(\eta; 1) &= g(\eta), \quad \hat{\theta}(\eta, 1) = \theta(\eta), \quad \hat{\phi}(\eta; 1) = \phi(\eta). \tag{4.33}
\end{aligned}$$

As  $p$  enhances from 0 to 1 then  $f(\eta, p)$ ,  $g(\eta, p)$ ,  $\theta(\eta, p)$  and  $\phi(\eta, p)$  differ from  $f_0(\eta)$ ,  $g_0(\eta)$ ,  $\theta_0(\eta)$



and  $\phi_0(\eta)$  to  $f(\eta)$ ,  $g(\eta)$ ,  $\theta(\eta)$  and  $\phi(\eta)$ . Applying Taylor's expansion we have

$$f(\eta, p) = f_0(\eta) + \sum_{m=1}^{\infty} f_m(\eta) p^m, \quad f_m(\eta) = \frac{1}{m!} \left. \frac{\partial^m f(\eta; p)}{\partial p^m} \right|_{p=0}, \quad (4.34)$$

$$g(\eta, p) = g_0(\eta) + \sum_{m=1}^{\infty} g_m(\eta) p^m, \quad g_m(\eta) = \frac{1}{m!} \left. \frac{\partial^m g(\eta; p)}{\partial p^m} \right|_{p=0}, \quad (4.35)$$

$$\theta(\eta, p) = \theta_0(\eta) + \sum_{m=1}^{\infty} \theta_m(\eta) p^m, \quad \theta_m(\eta) = \frac{1}{m!} \left. \frac{\partial^m \theta(\eta; p)}{\partial p^m} \right|_{p=0}, \quad (4.36)$$

$$\phi(\eta, p) = \phi_0(\eta) + \sum_{m=1}^{\infty} \phi_m(\eta) p^m, \quad \phi_m(\eta) = \frac{1}{m!} \left. \frac{\partial^m \phi(\eta; p)}{\partial p^m} \right|_{p=0}. \quad (4.37)$$

The convergence of above series strongly depends upon  $\hbar_f$ ,  $\hbar_g$ ,  $\hbar_\theta$  and  $\hbar_\phi$ . Considering that  $\hbar_f$ ,  $\hbar_g$ ,  $\hbar_\theta$  and  $\hbar_\phi$  are selected properly so that Eqs. (4.34) – (4.37) converge at  $p = 1$ . Therefore

$$f(\eta) = f_0(\eta) + \sum_{m=1}^{\infty} f_m(\eta), \quad (4.38)$$

$$g(\eta) = g_0(\eta) + \sum_{m=1}^{\infty} g_m(\eta), \quad (4.39)$$

$$\theta(\eta) = \theta_0(\eta) + \sum_{m=1}^{\infty} \theta_m(\eta), \quad (4.40)$$

$$\phi(\eta) = \phi_0(\eta) + \sum_{m=1}^{\infty} \phi_m(\eta). \quad (4.41)$$

The general solution expressions can be written as

$$f_m(\eta) = f_m^*(\eta) + C_1 + C_2 e^\eta + C_3 e^{-\eta}, \quad (4.42)$$

$$g_m(\eta) = g_m^*(\eta) + C_4 + C_5 e^\eta + C_6 e^{-\eta}, \quad (4.43)$$

$$\theta_m(\eta) = \theta_m^*(\eta) + C_7 e^\eta + C_8 e^{-\eta}, \quad (4.44)$$

$$\phi_m(\eta) = \phi_m^*(\eta) + C_9 e^\eta + C_{10} e^{-\eta}, \quad (4.45)$$

where the special solutions are  $f_m^*$ ,  $g_m^*$ ,  $\theta_m^*$  and  $\phi_m^*$ .

### 4.3 Convergence analysis and discussion

Homotopic solutions (4.38) – (4.41) obviously depend on the auxiliary parameters  $\hbar_f$ ,  $\hbar_g$ ,  $\hbar_\theta$  and  $\hbar_\phi$ . In order to control the convergence of series solutions' these auxiliary parameters play a central role. To obtain the convergence region, the  $\hbar$ -curves have been plotted at 14<sup>th</sup> order of approximations in Fig. 4.1. This Fig. clearly shows that the acceptable values of  $\hbar_f$ ,  $\hbar_g$ ,  $\hbar_\theta$  and  $\hbar_\phi$  are  $-1.0 \leq \hbar_f \leq -0.4$ ,  $-1.0 \leq \hbar_g \leq -0.2$ ,  $-1.2 \leq \hbar_\theta \leq -0.1$  and  $-1.2 \leq \hbar_\phi \leq -0.1$ . Table 4.1 ensures that the series solutions converge in the whole region of  $\eta$  when  $\hbar_f = \hbar_g = \hbar_\theta = \hbar_\phi = -0.5$ .

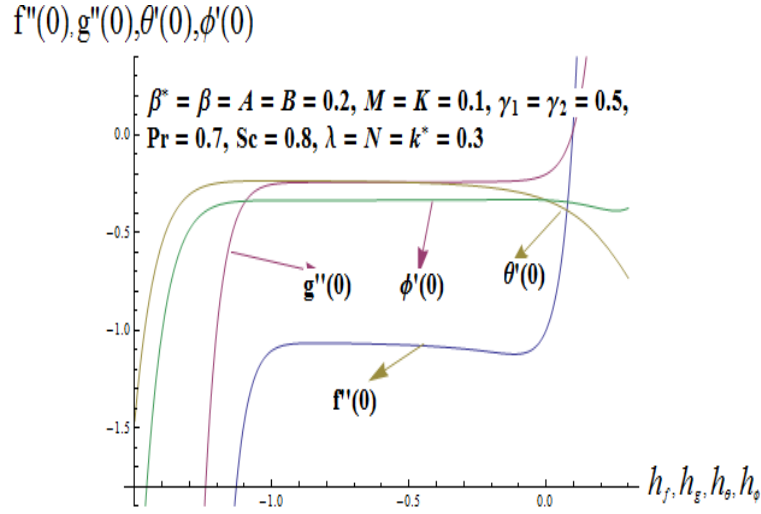


Fig. 4.1:  $\hbar$ -curves for the functions  $f$ ,  $g$ ,  $\theta$  and  $\phi$ .

**Table 4.1:** Convergence of series solutions for different order of approximations when  $K = M = 0.1$ ,  $A = B = \beta^* = \beta = 0.2$ ,  $\lambda = N = k^* = 0.3$ ,  $\gamma_1 = \gamma_2 = 0.5$ ,  $\text{Pr} = 0.7$ ,  $\text{Sc} = 0.8$  and  $\hbar_f = \hbar_g = \hbar_\theta = \hbar_\phi = -0.6$ .

order of approximations	1	5	10	15	20	25	30	35
$-f''(0)$	1.155	1.104	1.078	1.068	1.065	1.064	1.064	1.064
$-g''(0)$	0.2359	0.2395	0.2414	0.2420	0.2422	0.2422	0.2422	0.2422
$-\theta'(0)$	0.3084	0.2620	0.2437	0.2373	0.2349	0.2341	0.2340	0.2340
$-\phi'(0)$	0.3300	0.3318	0.3336	0.3340	0.3341	0.3341	0.3341	0.3341

Figs. 4.2 and 4.3 are plotted to see the effects of Hartman number  $M$  on the velocity profile  $f'(\eta)$  and  $g'(\eta)$ . The velocity profiles  $f'(\eta)$  and  $g'(\eta)$  are decreased when we increase the values of  $M$ . Also the momentum boundary layer thicknesses are decreasing functions of  $M$ . Fig. 4.4 is drawn to see the influence of internal heat source/ sink parameter  $\beta^*$  on the velocity profile  $f'(\eta)$ . Clearly in case of heat sink parameter  $\beta^* < 0$  both momentum boundary layer thickness and  $f'(\eta)$  decrease while in case of heat source parameter  $\beta^* > 0$  kinetic energy of the fluid particles increases due to which the velocity profile  $f'(\eta)$  increases. Outcome of mixed convection parameter  $\lambda$  on the velocity profile  $f'(\eta)$  in both assisting and opposing flows is seen in Fig. 4.5. In case of assisting flow  $\lambda > 0$  both  $f'(\eta)$  and momentum boundary layer thickness are enhanced while reverse effect is observed for opposing flow  $\lambda < 0$ . Fig. 4.6 exhibits the variation of concentration buoyancy parameter  $N$  on the velocity profile  $f'(\eta)$ . It is examined that an enhancement in  $N$  gives rise to the velocity profile  $f'(\eta)$ .

Fig. 4.7 depicts the influence of internal heat source/sink parameter  $\beta^*$  on the temperature  $\theta(\eta)$ . With an increase in internal heat source  $\beta^* > 0$  both the thermal boundary layer thickness and  $\theta(\eta)$  increase while in case of heat sink parameter  $\beta^* < 0$  both the thermal boundary layer thickness and  $\theta(\eta)$  decrease.

Figs. 4.8-4.10 are sketched to see the variations of chemical reaction parameter  $k^*$ , concentration exponent  $B$  and mass transfer Biot number  $\gamma_2$  on the concentration profile  $\phi(\eta)$ . Fig. 4.8 is presented to analyze the variation of chemical reaction parameter  $k^*$  on the concentration profile  $\phi(\eta)$ . It is noted that the associated boundary layer thickness and concentration profile  $\phi(\eta)$  decrease for generative chemical reaction  $k^* > 0$  while reverse phenomena is noted for destructive chemical reaction  $k^* < 0$ . With an enhancement in concentration exponent  $B$  both the concentration profile  $\phi(\eta)$  and the boundary layer thickness decrease (see Fig. 4.9). Variation of mass transfer Biot number  $\gamma_2$  on the concentration profile  $\phi(\eta)$  is displayed in Fig. 4.10. Here we examined that the effect of  $\gamma_2$  on the concentration profile  $\phi(\eta)$  and associated boundary layer thickness are increasing.

Figs. 4.11-4.13 are displayed to see the impacts of mixed convection parameter  $\lambda$ , concentration buoyancy parameter  $N$ , ratio parameter  $\beta$ , Hartman number  $M$ , internal heat source/sink  $\beta^*$  and heat transfer Biot number  $\gamma_1$  on the local Nusselt number  $-\theta'(0)$ . Fig. 4.11 shows that the heat transfer rate at the wall increases for assisting flow  $\lambda > 0$  while it decreases for op-

posing flow  $\lambda < 0$ . It is also examined that the heat transfer rate at wall is increasing function of concentration buoyancy parameter  $N$ . Fig. 4.12 exhibited that the larger values of ratio parameter  $\beta$  corresponds to a higher heat transfer rate  $-\theta'(0)$ . Also it is to be noted that with an increase in Hartman number heat transfer rate decreases. Fig. 4.13 depicts that the heat transfer rate at the wall  $-\theta'(0)$  decreases with internal heat source  $\beta^* > 0$  while increases with internal heat sink  $\beta^* < 0$ .

Variations of mixed convection parameter  $\lambda$ , concentration buoyancy parameter  $N$ , ratio parameter  $\beta$ , Hartman number  $M$ , chemical reaction  $k^*$  and mass transfer Biot number  $\gamma_2$  on Sherwood number  $-\phi'(0)$  are plotted in the Figs. 4.14-4.16. Fig. 4.14 is drawn to see the influences of mixed convection parameter  $\lambda$  and concentration buoyancy parameter  $N$  on the Sherwood number  $-\phi'(0)$ . It is seen that the Sherwood number  $-\phi'(0)$  is increasing function of  $\lambda$  and  $N$  in case of assisting flow  $\lambda > 0$  while decreasing function for opposing flow case. Fig. 4.15 depicts that the Sherwood number  $-\phi'(0)$  decreases with an enhancement in Hartman number  $M$  while it increases with an increase in ratio parameter  $\beta$ . Fig. 4.16 exhibits that the mass transfer at the wall  $-\phi'(0)$  enhances with generative chemical reaction  $k^* > 0$  while it reduces with destructive chemical reaction  $k^* < 0$ . It is also observed that the mass transfer at the wall  $-\phi'(0)$  is an increasing function of mass transfer Biot number  $\gamma_2$ . Table 4.2 ensures the validity of present results with Liu et al. [25] in the limiting sense.

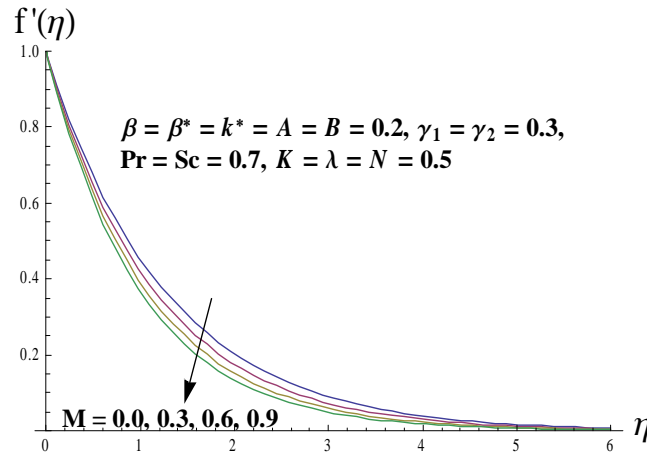


Fig. 4.2: Influence of  $M$  on velocity  $f'(\eta)$ .

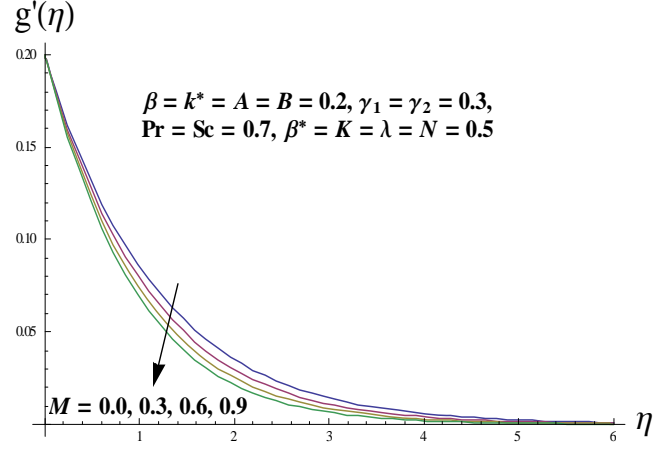


Fig. 4.3: Influence of  $M$  on velocity  $g'(\eta)$ .

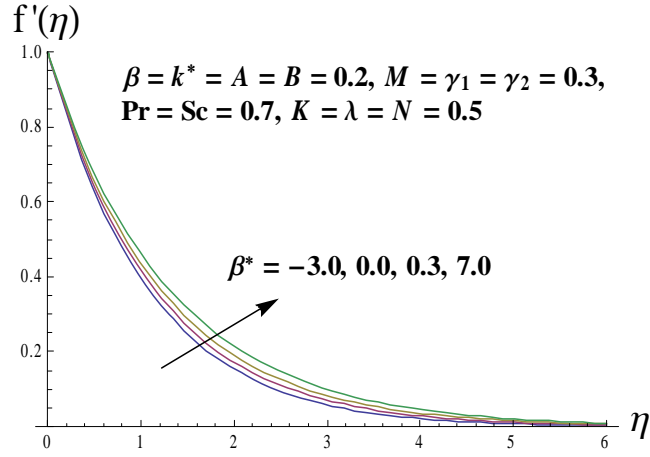


Fig. 4.4: Influence of  $\beta^*$  on velocity  $f'(\eta)$ .

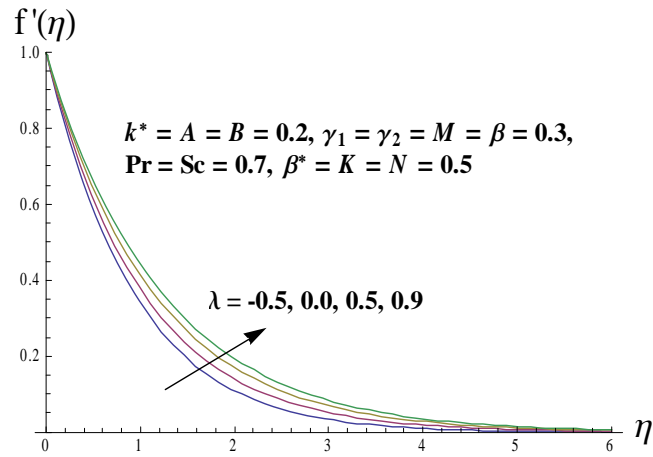


Fig. 4.5: Influence of  $\lambda$  on velocity  $f'(\eta)$ .

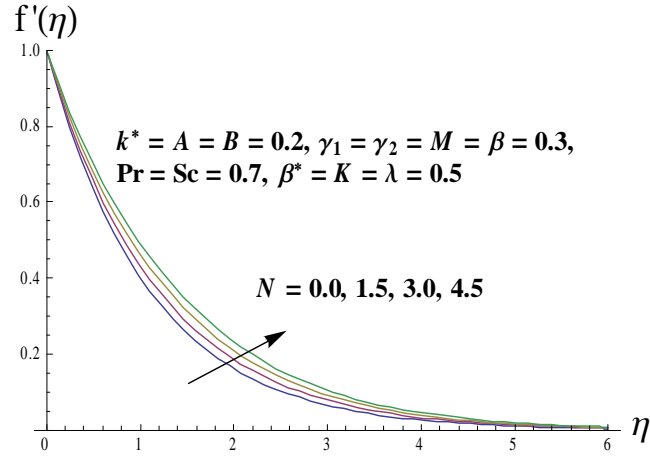


Fig. 4.6: Influence of  $N$  on velocity  $f'(\eta)$ .

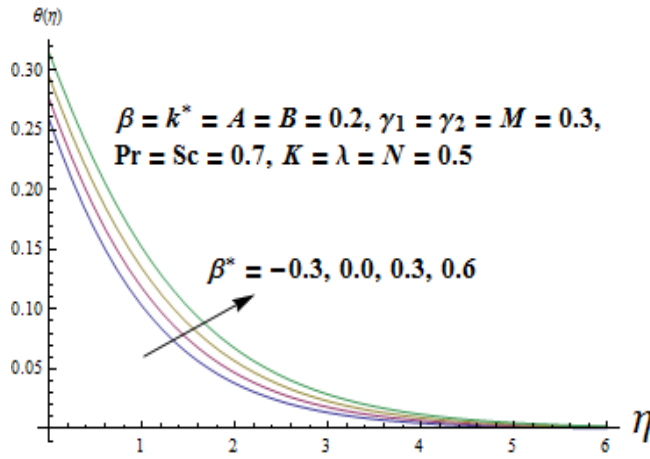


Fig. 4.7: Influence of  $\beta^*$  on temperature  $\theta(\eta)$ .

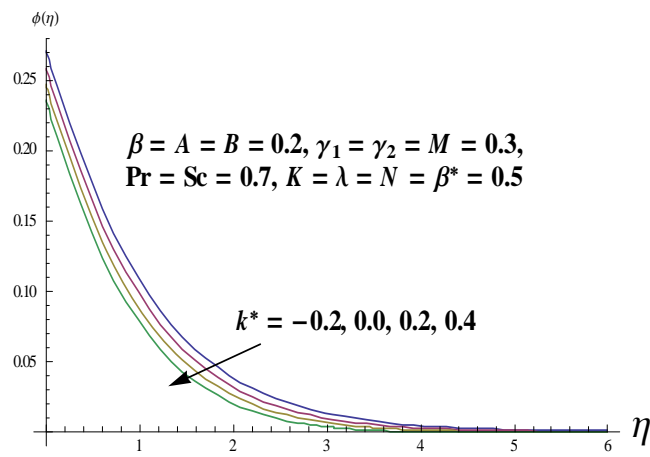


Fig. 4.8: Influence of  $k^*$  on  $\phi(\eta)$ .

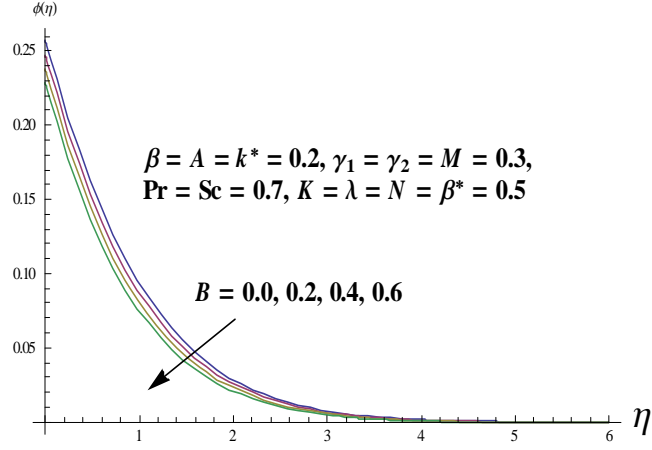


Fig. 4.9: Influence of  $B$  on concentration  $\phi(\eta)$ .

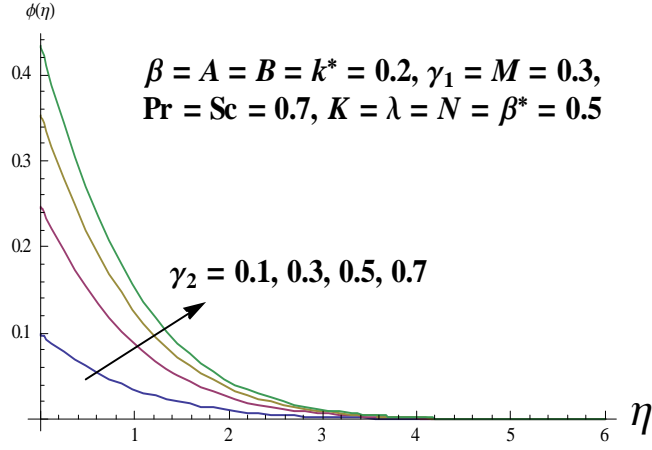


Fig. 4.10: Influence of  $\gamma_2$  on  $\phi(\eta)$ .

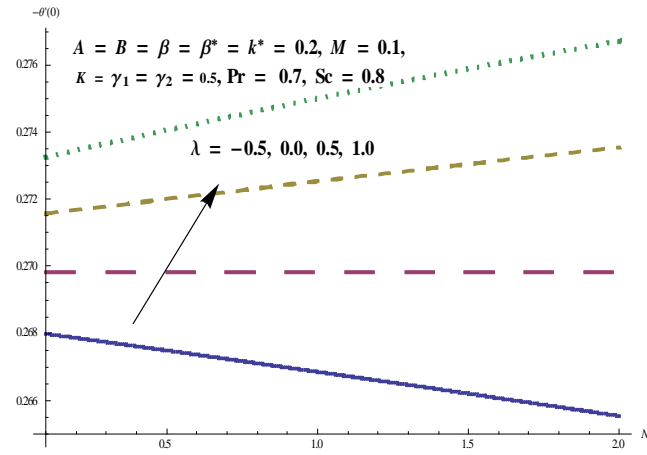


Fig. 4.11: Influence of  $\lambda$  and  $N$  on  $-\theta'(0)$ .

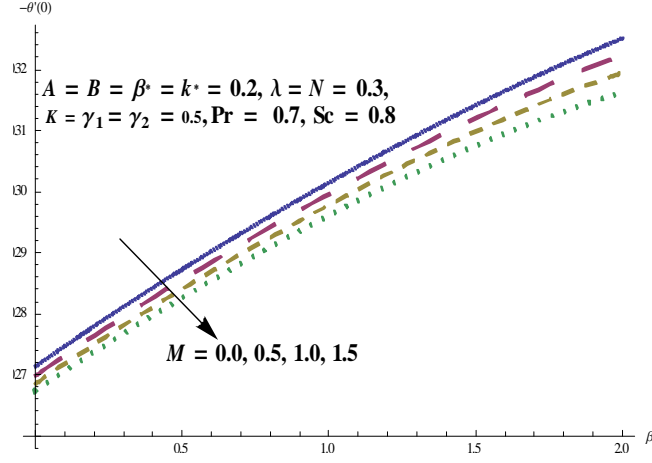


Fig. 4.11: Influence of  $M$  and  $\beta$  on  $-\theta'(0)$ .

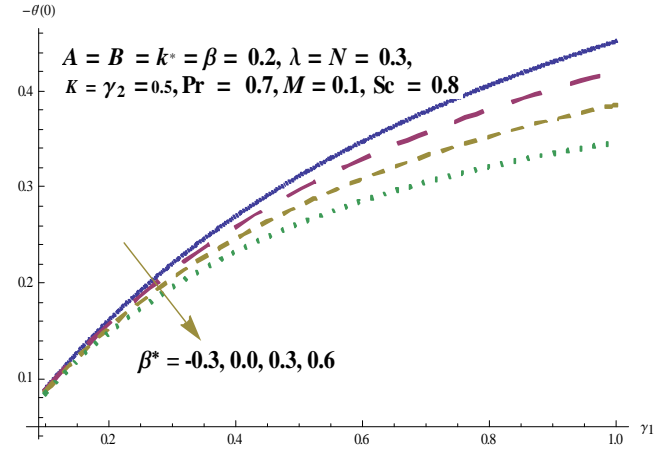


Fig. 4.13: Influence of  $\beta^*$  and  $\gamma_1$  on  $-\theta'(0)$ .

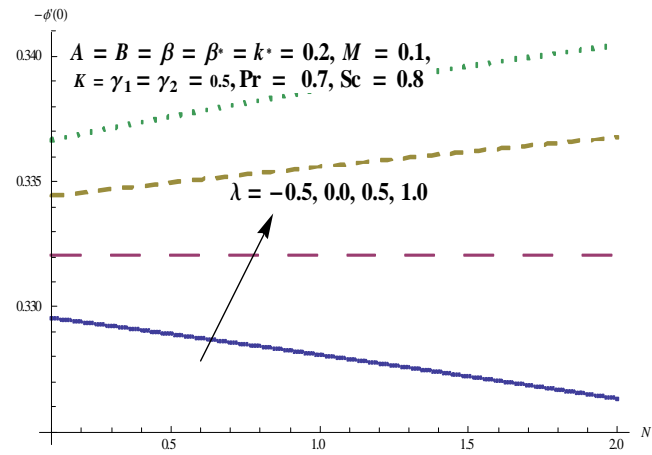


Fig. 4.14: Influence of  $\lambda$  and  $N$  on  $-\phi'(0)$ .



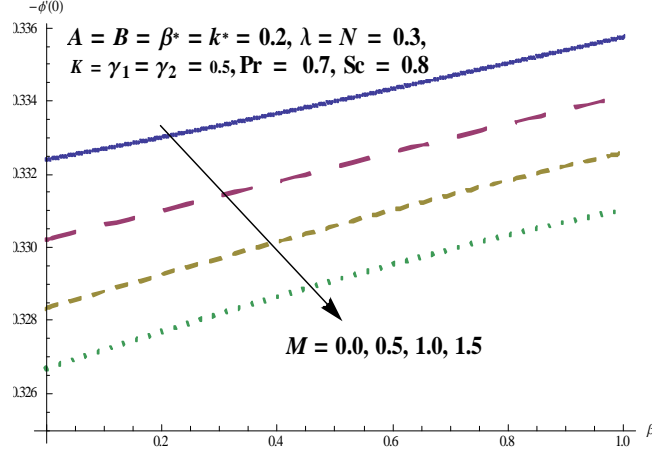


Fig. 4.15: Influence of  $M$  and  $\beta$  on  $-\phi'(0)$ .

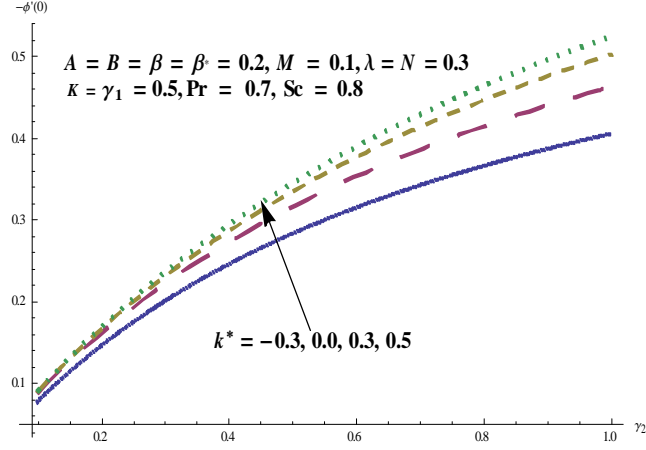


Fig. 4.16: Influence of  $k^*$  and  $\gamma_2$  on  $-\phi'(0)$ .

**Table 4.2:** Comparative values of  $-f''(0)$ ,  $-g''(0)$  and  $f(\infty) + g(\infty)$  for different values of  $\beta$  when  $K = \lambda = N = \gamma_1 = \gamma_2 = \beta^* = k^* = 0$ .

$\beta$	Liu et al. [25]			Present results		
	$-f''(0)$	$-g''(0)$	$f(\infty) + g(\infty)$	$-f''(0)$	$-g''(0)$	$f(\infty) + g(\infty)$
0.0	1.28180856	0	0.90564383	1.28181	0	0.90564
0.50	1.56988846	0.78494423	1.10918263	1.56989	0.78494	1.10918
1.00	1.81275105	1.81275105	1.28077378	1.81275	1.81275	1.28077

## 4.4 Closing remarks

The present chapter deals with the three-dimensional mixed convection flow of MHD viscoelastic fluid over an exponentially stretching surface in presence of heat source/sink and generative/destructive chemical reaction. The main outcomes are as follows.

- Velocity profiles  $f'(\eta)$  and  $g'(\eta)$  reduce with an increase in Hartman number  $M$ .
- Momentum boundary layer thickness decreases with an increase in ratio parameter  $\beta$ .
- Both the velocity profile  $f'(\eta)$  and momentum boundary layer thicknesses are increasing functions of internal heat source parameter  $\beta^* > 0$ , assisting flow case  $\lambda > 0$  and concentration buoyancy parameter  $N$  while decreasing functions of internal heat sink parameter  $\beta^* < 0$  and opposing flow case  $\lambda < 0$ .
- Thermal boundary layer thickness and temperature  $\theta(\eta)$  decrease with an increase in internal heat sink  $\beta^* < 0$  while thermal boundary layer thickness and temperature  $\theta(\eta)$  increase with an increase in internal heat source  $\beta^* > 0$ .
- With an enhancement in generative chemical reaction  $k^* > 0$ , concentration exponent  $B$  and Schmidt number  $Sc$  decreases the concentration profile  $\phi(\eta)$ . The concentration boundary layer thickness increases for larger mass transfer Biot number  $\gamma_2$  and destructive chemical reaction  $k^* < 0$ .
- Heat transfer rate  $-\theta'(0)$  boosts up in case of assisting flow  $\lambda > 0$ , concentration buoyancy parameter  $N$ , ratio parameter  $\beta$ , heat transfer Biot number  $\gamma_1$  and internal heat sink parameter  $\beta^* < 0$  while heat transfer rate  $-\theta'(0)$  reduces with opposing flow  $\lambda < 0$ , Hartman number  $M$  and internal heat source  $\beta^* > 0$ .
- With an increase in assisting flow  $\lambda > 0$ , concentration buoyancy parameter  $N$ , ratio parameter  $\beta$ , mass transfer Biot number  $\gamma_2$  and generative chemical reaction parameter  $k^* > 0$ , the Sherwood number  $-\phi'(0)$  enhances while reverse behavior is noted in case of opposing flow  $\lambda < 0$ , Hartman number  $M$  and destructive chemical reaction parameter  $k^* < 0$ .

## Chapter 5

# Thermophoresis and MHD mixed convection flow with Soret and Dufour effects

This chapter investigates the heat and mass transfer effects in three-dimensional mixed convection flow of viscoelastic fluid over a stretching surface with convective boundary conditions. The fluid is electrically conducting in the presence of constant applied magnetic field. Conservation laws of energy and concentration are based upon the Soret and Dufour effects. First order chemical reaction effects are also taken into account. Dimensionless velocity, temperature and concentration distributions are shown graphically for different values of involved parameters. Numerical values of local Nusselt and Sherwood numbers are computed and analyzed.

### 5.1 Mathematical analysis

We consider the steady three-dimensional magnetohydrodynamic mixed convection flow of an incompressible viscoelastic fluid over a stretching surface at  $z = 0$ . The flow takes place in the domain  $z > 0$ . Heat and mass transfer characteristics are taken into account in the presence of Soret and Dufour and thermophoresis effects. The ambient fluid temperature is taken as  $T_\infty$  while the surface temperature is maintained by convective heat transfer at a certain value  $T_f$ . A constant magnetic field  $B_0$  is applied in the  $z$ -direction. Induced magnetic field is not

considered due to small Reynolds number. In addition the effects of first order chemical reaction in mass transfer are taken into account. The governing boundary layer equations for the flow under consideration are

$$\frac{\partial u}{\partial x} + \frac{\partial v}{\partial y} + \frac{\partial w}{\partial z} = 0, \quad (5.1)$$

$$\begin{aligned} u \frac{\partial u}{\partial x} + v \frac{\partial u}{\partial y} + w \frac{\partial u}{\partial z} = & \nu \frac{\partial^2 u}{\partial z^2} + \frac{\alpha_1}{\rho} \left( u \frac{\partial^3 u}{\partial x \partial z^2} + w \frac{\partial^3 u}{\partial z^3} - \left( \frac{\partial u}{\partial x} \frac{\partial^2 u}{\partial z^2} + \frac{\partial u}{\partial z} \frac{\partial^2 w}{\partial z^2} \right) \right. \\ & \left. + 2 \frac{\partial u}{\partial z} \frac{\partial^2 u}{\partial x \partial z} + 2 \frac{\partial w}{\partial z} \frac{\partial^2 u}{\partial z^2} \right) \\ & + g\beta_T(T - T_\infty) + g\beta_C(C - C_\infty) - \frac{\sigma^* B_0^2}{\rho} u, \end{aligned} \quad (5.2)$$

$$\begin{aligned} u \frac{\partial v}{\partial x} + v \frac{\partial v}{\partial y} + w \frac{\partial v}{\partial z} = & \nu \frac{\partial^2 v}{\partial z^2} + \frac{\alpha_1}{\rho} \left( v \frac{\partial^3 v}{\partial y \partial z^2} + w \frac{\partial^3 v}{\partial z^3} - \left( \frac{\partial v}{\partial y} \frac{\partial^2 v}{\partial z^2} + \frac{\partial v}{\partial z} \frac{\partial^2 w}{\partial z^2} \right) \right. \\ & \left. + 2 \frac{\partial v}{\partial z} \frac{\partial^2 v}{\partial y \partial z} + 2 \frac{\partial w}{\partial z} \frac{\partial^2 v}{\partial z^2} \right) \\ & - \frac{\sigma^* B_0^2}{\rho} v, \end{aligned} \quad (5.3)$$

$$u \frac{\partial T}{\partial x} + v \frac{\partial T}{\partial y} + w \frac{\partial T}{\partial z} = \sigma \frac{\partial^2 T}{\partial z^2} + \frac{D_e k_T}{C_s C_p} \frac{\partial^2 C}{\partial z^2}, \quad (5.4)$$

$$u \frac{\partial C}{\partial x} + v \frac{\partial C}{\partial y} + w \frac{\partial C}{\partial z} = D_e \frac{\partial^2 C}{\partial z^2} + \frac{D_e k_T}{T_m} \frac{\partial^2 T}{\partial z^2} - k_1(C - C_\infty) - \frac{\partial}{\partial z}(V_T(C - C_\infty)). \quad (5.5)$$

In Eqs. (5.1) – (5.5) the respective velocity components in the  $x$ –,  $y$ – and  $z$ –directions are denoted by  $u$ ,  $v$  and  $w$ ,  $\alpha_1$  the viscoelastic parameter,  $\sigma^*$  the electrical conductivity,  $B_0$  is the magnitude of applied magnetic field,  $\rho$  the density of fluid,  $g$  the gravitational acceleration,  $\beta_T$  the thermal expansion coefficient,  $\beta_C$  the concentration expansion coefficient,  $T$  the fluid temperature,  $\sigma$  the thermal diffusivity of fluid,  $\nu$  the kinematic viscosity,  $\mu$  the dynamic viscosity of fluid,  $C$  the concentration field,  $D_e$  the mass diffusivity,  $k_T$  the thermal diffusion ratio,  $c_p$  the specific heat,  $C_s$  the concentration susceptibility and  $V_T$  the thermophoretic velocity.

In Eq. (5.5) the thermophoretic term  $V_T$  can be defined as

$$V_T = -k_2 \frac{\nu}{T_r} \frac{\partial T}{\partial z} \quad (5.6)$$

where  $k_2$  is the thermophoretic coefficient and  $T_r$  is the reference temperature. A thermophoretic

parameter  $\tau$  is defined as

$$\tau = -\frac{k_2(T_f - T_\infty)}{T_r} \quad (5.7)$$

The boundary conditions appropriate to the flow under consideration are given by

$$\begin{aligned} u = u_e = ax, \quad v = by, \quad w = 0, \quad -k \frac{\partial T}{\partial z} = h(T_f - T), \quad C = C_w \text{ at } z = 0, \\ u \rightarrow 0, \quad v \rightarrow 0, \quad T \rightarrow T_\infty, \quad C \rightarrow C_\infty \text{ as } z \rightarrow \infty, \end{aligned} \quad (5.8)$$

where  $k$  indicates the thermal conductivity of fluid,  $T_f$  is the hot fluid temperature,  $C_\infty$  the ambient concentration and  $a$  and  $b$  have dimension inverse of time.

We now define

$$\begin{aligned} u &= axf'(\eta), \quad v = ayg'(\eta), \quad w = -\sqrt{a\nu}(f(\eta) + g(\eta)), \\ \theta(\eta) &= \frac{T - T_\infty}{T_f - T_\infty}, \quad \eta = z\sqrt{\frac{a}{\nu}}, \quad \phi(\eta) = \frac{C - C_\infty}{C_w - C_\infty}. \end{aligned} \quad (5.9)$$

Now the use of above variables satisfy Eq. (5.1) automatically while Eqs. (5.2)-(5.8) are reduced as follows:

$$\begin{aligned} f''' + (f + g)f'' - f'^2 - K((f + g)f'''' + (f'' - g'')f'' - 2(f' + g')f''') \\ - M^2 f' + \lambda(\theta + N\phi) = 0, \end{aligned} \quad (5.10)$$

$$g''' + (f + g)g'' - g'^2 - K((f + g)g'''' + (f'' - g'')g'' - 2(f' + g')g''') - M^2 g' = 0, \quad (5.11)$$

$$\theta'' + Pr(f + g)\theta' + Pr D_f \phi'' = 0, \quad (5.12)$$

$$\phi'' + Sc(f + g)\phi' - Sck^*\phi + ScSr\theta'' - Sc\tau(\phi'\theta' - \phi\theta'') = 0,$$

$$f = 0, \quad g = 0, \quad f' = 1, \quad g' = \beta, \quad \theta' = -\gamma_1(1 - \theta(0)), \quad \phi = 1 \quad \text{at } \eta = 0, \quad (5.13)$$

$$f' \rightarrow 0, \quad g' \rightarrow 0, \quad \theta \rightarrow 0, \quad \phi \rightarrow 0 \quad \text{as } \eta \rightarrow \infty, \quad (5.14)$$

where  $K$  is the dimensionless viscoelastic parameter,  $M$  is the Hartman number,  $\lambda$  is the local buoyancy parameter,  $Gr_x$  is the local Grashof number,  $N$  is the constant dimensionless

concentration buoyancy parameter,  $Pr$  is the Prandtl number,  $D_f$  is the Dufour number,  $Sc$  is the Schmidt number,  $Sr$  is the Soret number,  $k^*$  is the chemical reaction parameter,  $\tau$  is the thermophoretic parameter,  $\beta$  is ratio of rates parameters,  $\gamma_1$  is the Biot number and prime shows the differentiation with respect to  $\eta$ . These are given by

$$\begin{aligned} K &= \frac{\alpha_1 a}{\nu}, \quad M = \frac{\sigma^* B_0^2}{\rho}, \quad \lambda = \frac{Gr_x}{Re_x^2}, \quad Gr_x = \frac{g\beta_T(T_f - T_\infty)x^3}{\nu^2}, \quad N = \frac{\beta_C(C_w - C_\infty)}{\beta_T(T_f - T_\infty)} \\ Pr &= \frac{\nu}{\sigma}, \quad D_f = \frac{D_e k_T}{C_s C_p} \frac{(C_w - C_\infty)}{(T_f - T_\infty)\nu}, \quad Sc = \frac{\nu}{D}, \quad Sr = \frac{D_e k_T}{T_m \nu} \frac{(T_f - T_\infty)}{(C_w - C_\infty)}, \quad k^* = \frac{k_1}{a}, \quad \tau = -\frac{k_2(T_f - T_\infty)}{T_r}, \\ \beta &= \frac{b}{a}, \quad \gamma_1 = \frac{h}{k} \sqrt{\frac{\nu}{a}}. \end{aligned}$$

Local Nusselt and Sherwood numbers in dimensionless forms are given by

$$Nu/Re_x^{1/2} = -\theta'(0), \quad (5.15)$$

$$Sh/Re_x^{1/2} = -\phi'(0), \quad (5.16)$$

in which  $Re_x = u_e x / \nu$  is the local Reynolds number.

## 5.2 Construction of solutions

The initial approximations and auxiliary linear operators required for homotopy analysis solutions are presented below i.e.

$$f_0(\eta) = (1 - e^{-\eta}), \quad g_0(\eta) = \beta(1 - e^{-\eta}), \quad \theta_0(\eta) = \frac{\gamma_1 \exp(-\eta)}{1 + \gamma_1}, \quad \phi_0(\eta) = \exp(-\eta) \quad (5.17)$$

$$\mathcal{L}_f = f''' - f', \quad \mathcal{L}_g = g''' - g', \quad \mathcal{L}_\theta = \theta'' - \theta, \quad \mathcal{L}_\phi = \phi'' - \phi, \quad (5.18)$$

with the following properties of the defined operators in Eq. (5.18) i.e.

$$\begin{aligned} \mathcal{L}_f(C_1 + C_2 e^\eta + C_3 e^{-\eta}) &= 0, \quad \mathcal{L}_g(C_4 + C_5 e^\eta + C_6 e^{-\eta}) = 0, \\ \mathcal{L}_\theta(C_7 e^\eta + C_8 e^{-\eta}) &= 0, \quad \mathcal{L}_\phi(C_9 e^\eta + C_{10} e^{-\eta}) = 0 \end{aligned} \quad (5.19)$$

where  $C_i$  ( $i = 1 - 10$ ) indicate the arbitrary constants.

The corresponding problems at the zeroth order are given in the following forms:

$$(1-p) \mathcal{L}_f [\hat{f}(\eta; p) - f_0(\eta)] = p \hbar_f \mathcal{N}_f [\hat{f}(\eta; p), \hat{g}(\eta; p)], \quad (5.20)$$

$$(1-p) \mathcal{L}_g [\hat{g}(\eta; p) - g_0(\eta)] = p \hbar_g \mathcal{N}_g [\hat{f}(\eta; p), \hat{g}(\eta; p)], \quad (5.21)$$

$$(1-p) \mathcal{L}_\theta [\hat{\theta}(\eta; p) - \theta_0(\eta)] = p \hbar_\theta \mathcal{N}_\theta [\hat{f}(\eta; p), \hat{g}(\eta; p), \hat{\theta}(\eta; p), \hat{\phi}(\eta; p)], \quad (5.22)$$

$$(1-p) \mathcal{L}_\phi [\hat{\phi}(\eta; p) - \phi_0(\eta)] = p \hbar_\phi \mathcal{N}_\phi [\hat{f}(\eta; p), \hat{g}(\eta; p), \hat{\theta}(\eta; p), \hat{\phi}(\eta; p)], \quad (5.23)$$

$$\begin{aligned} \hat{f}(0; p) &= 0, \quad \hat{f}'(0; p) = 1, \quad \hat{f}'(\infty; p) = 0, \quad \hat{g}(0; p) = 0, \quad \hat{g}'(0; p) = \beta, \quad \hat{g}'(\infty; p) = 0, \\ \hat{\theta}'(0, p) &= -\gamma_1[1 - \theta(0, p)], \quad \hat{\theta}(\infty, p) = 0, \quad \hat{\phi}(0, p) = 1, \quad \hat{\phi}(\infty, p) = 0 \end{aligned} \quad (5.24)$$

$$\begin{aligned} \mathcal{N}_f[\hat{f}(\eta, p), \hat{g}(\eta, p), \hat{\theta}(\eta, p), \hat{\phi}(\eta, p)] &= \frac{\partial^3 \hat{f}(\eta, p)}{\partial \eta^3} - \left( \frac{\partial \hat{f}(\eta, p)}{\partial \eta} \right)^2 + (\hat{f}(\eta, p) + \hat{g}(\eta, p)) \frac{\partial^2 \hat{f}(\eta, p)}{\partial \eta^2} \\ &\quad - K \left( \begin{aligned} &(\hat{f}(\eta, p) + \hat{g}(\eta, p)) \frac{\partial^4 \hat{f}(\eta, p)}{\partial \eta^4} \\ &+ \left( \frac{\partial^2 \hat{f}(\eta, p)}{\partial \eta^2} - \frac{\partial^2 \hat{g}(\eta, p)}{\partial \eta^2} \right) \frac{\partial^2 \hat{f}(\eta, p)}{\partial \eta^2} \\ &- 2 \left( \frac{\partial \hat{f}(\eta, p)}{\partial \eta} + \frac{\partial \hat{g}(\eta, p)}{\partial \eta} \right) \frac{\partial^3 \hat{f}(\eta, p)}{\partial \eta^3} \end{aligned} \right) \\ &\quad - M^2 \frac{\partial \hat{f}(\eta, p)}{\partial \eta} + \lambda \hat{\theta}(\eta, p) + \lambda N \hat{\phi}(\eta, p), \end{aligned} \quad (5.25)$$

$$\begin{aligned} \mathcal{N}_g[\hat{g}(\eta, p), \hat{f}(\eta, p), \hat{\theta}(\eta, p), \hat{\phi}(\eta, p)] &= \frac{\partial^3 \hat{g}(\eta, p)}{\partial \eta^3} - \left( \frac{\partial \hat{g}(\eta, p)}{\partial \eta} \right)^2 + (\hat{f}(\eta, p) + \hat{g}(\eta, p)) \frac{\partial^2 \hat{g}(\eta, p)}{\partial \eta^2} \\ &\quad + K \left( \begin{aligned} &(\hat{f}(\eta, p) + \hat{g}(\eta, p)) \frac{\partial^4 \hat{g}(\eta, p)}{\partial \eta^4} \\ &+ \left( \frac{\partial^2 \hat{f}(\eta, p)}{\partial \eta^2} - \frac{\partial^2 \hat{g}(\eta, p)}{\partial \eta^2} \right) \frac{\partial^2 \hat{g}(\eta, p)}{\partial \eta^2} \\ &- 2 \left( \frac{\partial \hat{f}(\eta, p)}{\partial \eta} + \frac{\partial \hat{g}(\eta, p)}{\partial \eta} \right) \frac{\partial^3 \hat{g}(\eta, p)}{\partial \eta^3} \end{aligned} \right) \\ &\quad - M^2 \frac{\partial \hat{g}(\eta, p)}{\partial \eta}, \end{aligned} \quad (5.26)$$

$$\begin{aligned}\mathcal{N}_\theta[\hat{\theta}(\eta, p), \hat{\phi}(\eta, p), \hat{f}(\eta, p), \hat{g}(\eta, p)] &= \frac{\partial^2 \hat{\theta}(\eta, p)}{\partial \eta^2} + \text{Pr}(\hat{f}(\eta, p) + \hat{g}(\eta, p)) \frac{\partial \hat{\theta}(\eta, p)}{\partial \eta} \\ &+ \text{Pr} D_f \frac{\partial^2 \hat{\phi}(\eta, p)}{\partial \eta^2}.\end{aligned}\quad (5.27)$$

$$\begin{aligned}\mathcal{N}_\phi[\hat{\phi}(\eta, p), \hat{\theta}(\eta, p), \hat{f}(\eta, p), \hat{g}(\eta, p)] &= \frac{\partial^2 \hat{\phi}(\eta, p)}{\partial \eta^2} + Sc(f(\eta, p) + g(\eta, p)) \frac{\partial \hat{\phi}(\eta, p)}{\partial \eta} \\ &- Sck^* \hat{\phi}(\eta, p) + ScSr \frac{\partial^2 \hat{\theta}(\eta, p)}{\partial \eta^2} - Sc\tau \left( \frac{\partial \hat{\phi}(\eta, p)}{\partial \eta} \frac{\partial \hat{\theta}(\eta, p)}{\partial \eta} \right. \\ &\left. - \hat{\phi}(\eta, p) \frac{\partial^2 \hat{\theta}(\eta, p)}{\partial \eta^2} \right).\end{aligned}\quad (5.28)$$

Here  $p$  is an embedding parameter,  $\hbar_f$ ,  $\hbar_g$ ,  $\hbar_\theta$  and  $\hbar_\phi$  are the non-zero auxiliary parameters and  $\mathcal{N}_f$ ,  $\mathcal{N}_g$ ,  $\mathcal{N}_\theta$  and  $\mathcal{N}_\phi$  indicate the nonlinear operators. When  $p = 0$  and  $p = 1$  one has

$$\begin{aligned}\hat{f}(\eta; 0) &= f_0(\eta), \quad \hat{\theta}(\eta, 0) = \theta_0(\eta), \quad \hat{\phi}(\eta, 0) = \phi_0(\eta) \\ \hat{f}(\eta; 1) &= f(\eta), \quad \hat{\theta}(\eta, 1) = \theta(\eta), \quad \hat{\phi}(\eta, 1) = \phi(\eta).\end{aligned}\quad (5.29)$$

Clearly when  $p$  is increased from 0 to 1 then  $f(\eta, p)$ ,  $g(\eta, p)$ ,  $\theta(\eta, p)$  and  $\phi(\eta, p)$  vary from  $f_0(\eta)$ ,  $g_0(\eta)$ ,  $\theta_0(\eta)$  and  $\phi_0(\eta)$  to  $f(\eta)$ ,  $g(\eta)$ ,  $\theta(\eta)$  and  $\phi(\eta)$ . By Taylor's expansion we have

$$f(\eta, p) = f_0(\eta) + \sum_{m=1}^{\infty} f_m(\eta) p^m, \quad f_m(\eta) = \frac{1}{m!} \left. \frac{\partial^m f(\eta; p)}{\partial p^m} \right|_{p=0}, \quad (5.30)$$

$$g(\eta, p) = g_0(\eta) + \sum_{m=1}^{\infty} g_m(\eta) p^m, \quad g_m(\eta) = \frac{1}{m!} \left. \frac{\partial^m g(\eta; p)}{\partial p^m} \right|_{p=0}, \quad (5.31)$$

$$\theta(\eta, p) = \theta_0(\eta) + \sum_{m=1}^{\infty} \theta_m(\eta) p^m, \quad \theta_m(\eta) = \frac{1}{m!} \left. \frac{\partial^m \theta(\eta; p)}{\partial p^m} \right|_{p=0}, \quad (5.32)$$

$$\phi(\eta, p) = \phi_0(\eta) + \sum_{m=1}^{\infty} \phi_m(\eta) p^m, \quad \phi_m(\eta) = \frac{1}{m!} \left. \frac{\partial^m \phi(\eta; p)}{\partial p^m} \right|_{p=0}, \quad (5.33)$$

where the convergence of above series strongly depends upon  $\hbar_f$ ,  $\hbar_g$ ,  $\hbar_\theta$  and  $\hbar_\phi$ . Considering that  $\hbar_f$ ,  $\hbar_g$ ,  $\hbar_\theta$  and  $\hbar_\phi$  are selected properly so that Eqs. (5.30) – (5.33) converge at  $p = 1$  then we can write

$$f(\eta) = f_0(\eta) + \sum_{m=1}^{\infty} f_m(\eta), \quad (5.34)$$



$$g(\eta) = g_0(\eta) + \sum_{m=1}^{\infty} g_m(\eta), \quad (5.35)$$

$$\theta(\eta) = \theta_0(\eta) + \sum_{m=1}^{\infty} \theta_m(\eta), \quad (5.36)$$

$$\phi(\eta) = \phi_0(\eta) + \sum_{m=1}^{\infty} \phi_m(\eta). \quad (5.37)$$

The resulting problems at  $m$ th order deformation can be constructed as follows:

$$\mathcal{L}_f[f_m(\eta) - \chi_m f_{m-1}(\eta)] = \hbar_f \mathcal{R}_f^m(\eta), \quad (5.38)$$

$$\mathcal{L}_g[g_m(\eta) - \chi_m g_{m-1}(\eta)] = \hbar_g \mathcal{R}_g^m(\eta), \quad (5.39)$$

$$\mathcal{L}_\theta[\theta_m(\eta) - \chi_m \theta_{m-1}(\eta)] = \hbar_\theta \mathcal{R}_\theta^m(\eta), \quad (5.40)$$

$$\mathcal{L}_\phi[\phi_m(\eta) - \chi_m \phi_{m-1}(\eta)] = \hbar_\phi \mathcal{R}_\phi^m(\eta). \quad (5.41)$$

$$f_m(0) = f'_m(0) = f'_m(\infty) = 0, \quad (5.42)$$

$$g_m(0) = g'_m(0) = g'_m(\infty) = 0, \quad (5.43)$$

$$\theta'_m(0) - \gamma_1 \theta_m(0) = \theta_m(\infty) = 0, \phi_m(0) = \phi_m(\infty) = 0. \quad (5.44)$$

$$\begin{aligned} \mathcal{R}_f^m(\eta) = & f'''_{m-1}(\eta) - \sum_{k=0}^{m-1} f'_{m-1-k} f'_k + \sum_{k=0}^{m-1} (f_{m-1-k} f''_k + g_{m-1-k} f''_k) \\ & - K \left( \begin{aligned} & \sum_{k=0}^{m-1} f_{m-1-k} f'''_k + \sum_{k=0}^{m-1} g_{m-1-k} f'''_k \\ & + \sum_{k=0}^{m-1} f''_{m-1-k} f''_k - \sum_{k=0}^{m-1} g''_{m-1-k} f''_k \\ & - 2 \sum_{k=0}^{m-1} f'_{m-1-k} f'''_k - 2 \sum_{k=0}^{m-1} g'_{m-1-k} f'''_k \end{aligned} \right) \\ & - M^2 f'_{m-1} + \lambda \theta + \lambda N \phi, \end{aligned} \quad (5.45)$$

$$\begin{aligned}\mathcal{R}_g^m(\eta) = & g_{m-1}'''(\eta) - \sum_{k=0}^{m-1} g'_{m-1-k}g'_k + \sum_{k=0}^{m-1} (f_{m-1-k}g''_k + g_{m-1-k}g''_k) \\ & - K \left( \begin{aligned} & \sum_{k=0}^{m-1} f_{m-1-k}g_k'''' + \sum_{k=0}^{m-1} g_{m-1-k}g_k'''' \\ & + \sum_{k=0}^{m-1} f''_{m-1-k}g''_k - \sum_{k=0}^{m-1} g''_{m-1-k}g''_k \\ & - 2 \sum_{k=0}^{m-1} f'_{m-1-k}g_k''' - 2 \sum_{k=0}^{m-1} g'_{m-1-k}g_k''' \end{aligned} \right) - M^2 g'_{m-1}, \quad (5.46)\end{aligned}$$

$$\mathcal{R}_\theta^m(\eta) = \theta''_{m-1} + Pr \sum_{k=0}^{m-1} (\theta'_{m-1-k}f_k + \theta'_{m-1-k}g_k) + Pr D_f \phi''_{m-1}, \quad (5.47)$$

$$\begin{aligned}\mathcal{R}_\phi^m(\eta) = & \phi''_{m-1} + Sc \sum_{k=0}^{m-1} (\phi'_{m-1-k}f_k + \phi'_{m-1-k}g_k) - Sc k^* \phi + Sc Sr \theta''_{m-1} \\ & - Sc \tau \sum_{k=0}^{m-1} (\phi'_{m-1-k}\theta'_k - \phi_{m-1-k}\theta''_k), \quad (5.48)\end{aligned}$$

$$\chi_m = \begin{cases} 0, & m \leq 1, \\ 1, & m > 1. \end{cases} \quad (5.49)$$

Solving the above mth order deformation problems we have

$$f_m(\eta) = f_m^*(\eta) + C_1 + C_2 e^\eta + C_3 e^{-\eta}, \quad (5.50)$$

$$g_m(\eta) = g_m^*(\eta) + C_4 + C_5 e^\eta + C_6 e^{-\eta}, \quad (5.51)$$

$$\theta_m(\eta) = \theta_m^*(\eta) + C_7 e^\eta + C_8 e^{-\eta}, \quad (5.52)$$

$$\phi_m(\eta) = \phi_m^*(\eta) + C_9 e^\eta + C_{10} e^{-\eta}, \quad (5.53)$$

in which the  $f_m^*$ ,  $g_m^*$ ,  $\theta_m^*$  and  $\phi_m^*$  indicate the special solutions.

### 5.3 Analysis

Obviously the series solutions (5.34) – (5.37) contain the auxiliary parameters  $\hbar_f$ ,  $\hbar_g$ ,  $\hbar_\theta$  and  $\hbar_\phi$ . These parameters are very important in adjusting and controlling the convergence of homotopic solutions. Hence the  $\hbar$ –curves are plotted at  $10^{th}$  order of approximations in order to find the

suitable ranges of  $\hbar_f$ ,  $\hbar_g$ ,  $\hbar_\theta$  and  $\hbar_\phi$ . Fig. 5.1 indicate that the admissible values of  $\hbar_f$ ,  $\hbar_g$ ,  $\hbar_\theta$  and  $\hbar_\phi$  here are  $-1.5 \leq \hbar_f \leq -0.40$ ,  $-1.4 \leq \hbar_g \leq -0.30$ ,  $-1.40 \leq \hbar_\theta \leq -0.25$  and  $-1.40 \leq \hbar_\phi \leq -0.20$ . Table 5.1 presents the convergence of homotopic solutions. It is noted that computations are sufficient for 45<sup>th</sup> order iterations of velocity and 35<sup>th</sup> order iterations of the temperature and concentration profiles for the convergent series solutions.

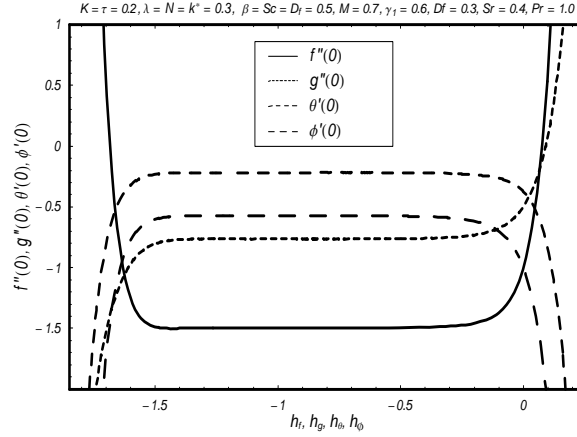


Fig. 5.1:  $\hbar$ -curves for the functions  $f$ ,  $g$ ,  $\theta$  and  $\phi$ .

**Table 5.1:** Convergence of series solutions for different order of approximations when  $K = \tau = 0.2$ ,  $\beta = D_f = Sc = 0.5$ ,  $Pr = 1.0$ ,  $Sr = 0.4$ ,  $M = 0.7$ ,  $\lambda = N = k^* = 0.3$ ,  $\gamma_1 = 0.6$  and  $\hbar_f = \hbar_g = \hbar_\theta = \hbar_\phi = -0.7$ .

order of approximations	$-f''(0)$	$-g''(0)$	$-\theta'(0)$	$-\phi'(0)$
1	1.31063	0.632417	0.284766	0.763750
5	1.47588	0.746614	0.230340	0.599613
10	1.49331	0.762859	0.221636	0.578386
15	1.49592	0.764867	0.220665	0.575416
20	1.49650	0.765053	0.220797	0.574753
25	1.49664	0.765041	0.220916	0.574545
30	1.49667	0.765030	0.220950	0.574483
35	1.49667	0.765027	0.220953	0.574471
40	1.49667	0.765027	0.220953	0.574471

Figs. 5.2 – 5.5 depict the behaviors of mixed convection parameter  $\lambda$  and concentration

buoyancy parameter  $N$  on  $f'(\eta)$  and  $g'(\eta)$ . Figs. 5.2 and 5.3 are drawn to analyze the effects of mixed convection parameter  $\lambda$  on the velocity components  $f'(\eta)$  and  $g'(\eta)$ . It is shown that  $f'(\eta)$  and  $g'(\eta)$  increase with an increase in  $\lambda$ . Effect of concentration buoyancy parameter  $N$  on the velocity components  $f'(\eta)$  and  $g'(\eta)$  are shown in the Figs. 5.4 and 5.5. It is examined that the concentration buoyancy parameter  $N$  shows the similar effects on momentum boundary layer thicknesses and velocity components  $f'(\eta)$  and  $g'(\eta)$  as we observed for mixed convection parameter  $\lambda$ .

Figs. 5.6 – 5.9 examine the variation of Dufour number  $D_f$  and Soret number  $Sr$  on the temperature  $\theta(\eta)$  and concentration  $\phi(\eta)$ . Variations of  $D_f$  on temperature  $\theta(\eta)$  and concentration  $\phi(\eta)$  are analyzed in the Figs. 5.6 and 5.7. It is noted from these Figs. that  $D_f$  has reverse effects on temperature  $\theta(\eta)$  and concentration  $\phi(\eta)$ . Figs. 5.8 and 5.9 are displayed to see the variation of  $Sr$  on the temperature  $\theta(\eta)$  and concentration profiles  $\phi(\eta)$ . We noticed that the temperature  $\theta(\eta)$  and thermal boundary layer are reduced for an increase in  $Sr$ . The concentration profile  $\phi(\eta)$  increases when  $Sr$  is increased. To analyze the effect of thermophoretic parameter  $\tau$  on the concentration  $\phi(\eta)$  profile we have sketched Fig. 5.10. It is found that an increase in thermophoretic parameter  $\tau$  leads to a decrease in both concentration profile  $\phi(\eta)$  and concentration boundary layer thickness.

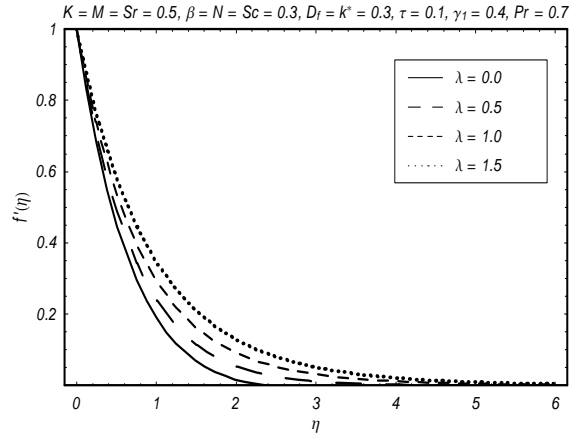


Fig. 5.2: Influence of  $\lambda$  on  $f'(\eta)$ .

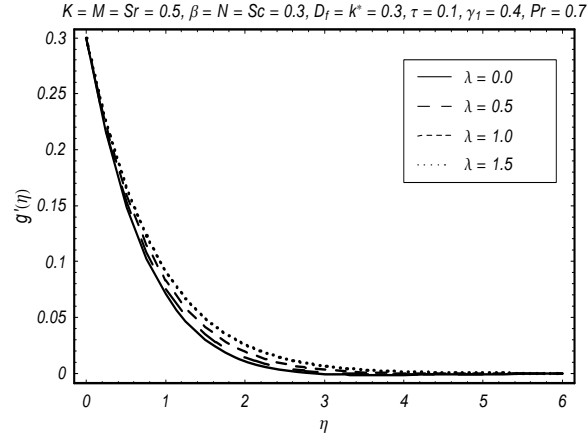


Fig. 5.3: Influence of  $\lambda$  on  $g'(\eta)$ .

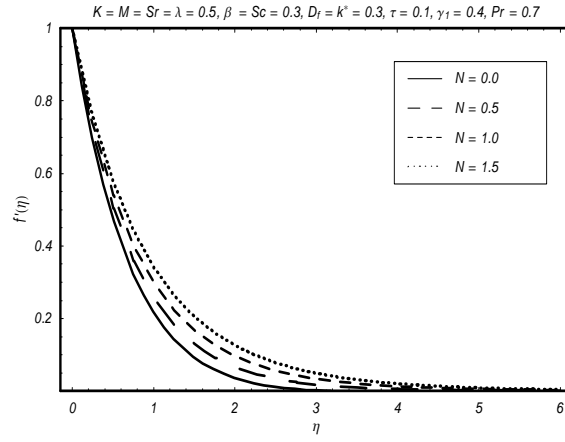


Fig. 5.4: Influence of  $N$  on  $f'(\eta)$ .

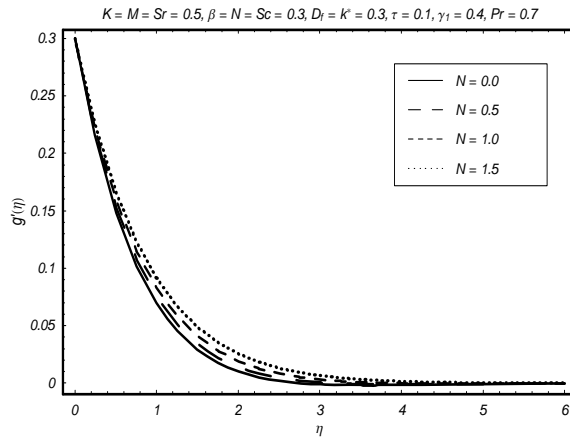


Fig. 5.5: Influence of  $N$  on  $g'(\eta)$ .

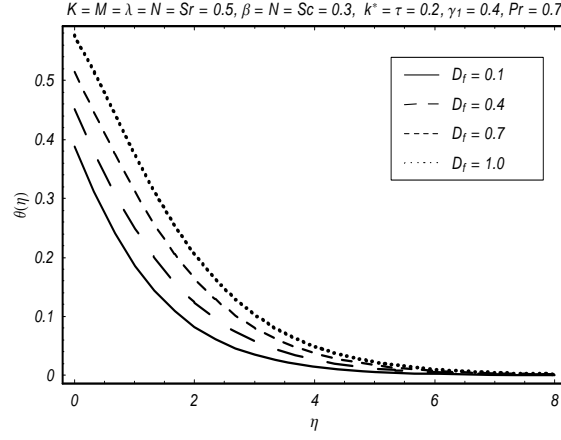


Fig. 5.6: Influence of  $D_f$  on  $\theta(\eta)$ .

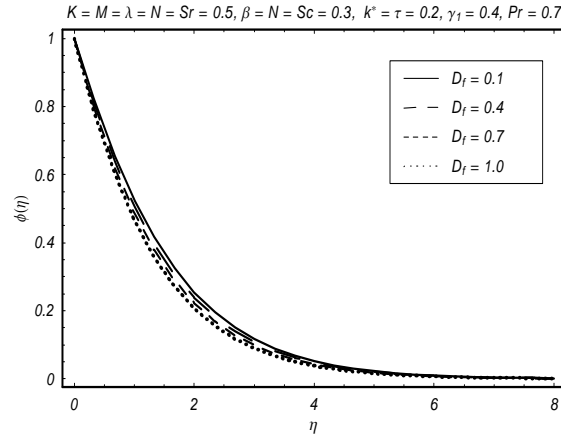


Fig. 5.7: Influence of  $D_f$  on  $\phi(\eta)$ .

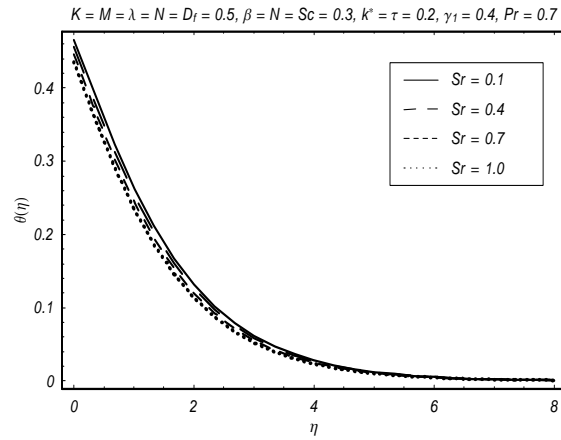


Fig. 5.8: Influence of  $Sr$  on  $\theta(\eta)$ .

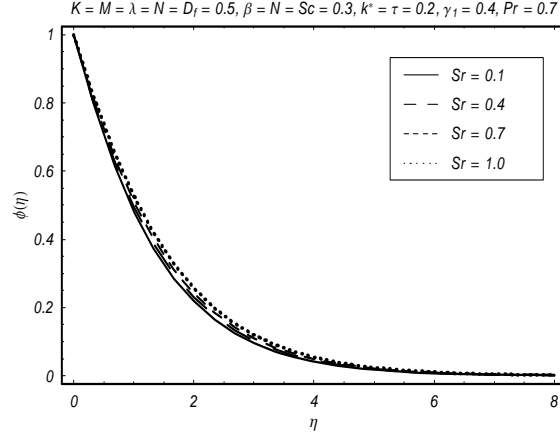


Fig. 5.9: Influence of  $Sr$  on  $\phi(\eta)$ .

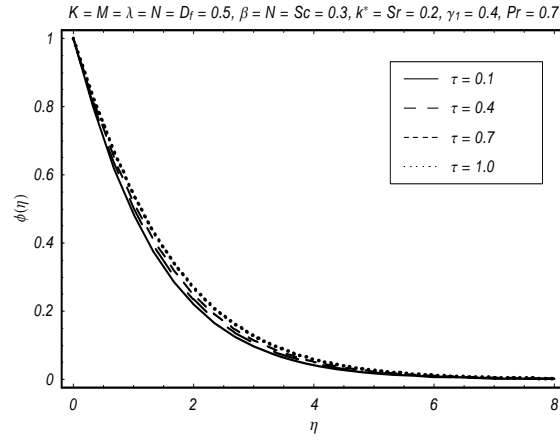


Fig. 5.10: Influence of  $\tau$  on  $\phi(\eta)$ .

Table 5.2 is prepared to analyze numerical values of local Nusselt and Sherwood numbers. The values of  $-\theta'(0)$  and  $-\phi'(0)$  decrease by increasing Deborah number. Here  $-\theta'(0)$  increases by increasing Prandtl and Biot numbers while reverse is the case of  $-\phi'(0)$ . Table 5.3 shows that local Nusselt  $-\theta'(0)$  and Sherwood numbers  $-\phi'(0)$  decrease with the increase in Hartman and Soret numbers. Values of local Nusselt  $-\theta'(0)$  and Sherwood numbers  $-\phi'(0)$  are opposite for Schmidt, Dufour, thermophoretic and chemical reaction parameters.

**Table 5.2:** Values of local Nusselt  $-\theta'(0)$  and Sherwood numbers  $-\phi'(0)$  for different values of the parameters  $K$ ,  $\beta$ ,  $\lambda$ ,  $N$ ,  $Pr$ , and  $\gamma_1$  when  $Sc = D_f = 0.5$ ,  $Sr = 0.4$ ,  $\tau = 0.2$ ,  $k^* = 0.3$

and  $M = 0.5$ .

$K$	$\beta$	$\lambda$	$N$	$Pr$	$\gamma_1$	$-\theta'(0)$	$-\phi'(0)$
0.0	0.5	0.5	0.3	1.0	0.6	0.24700	0.61363
0.2						0.23486	0.59297
0.4						0.18422	0.51482
0.2	0.0					0.21393	0.55535
	0.2					0.22444	0.57294
	0.4					0.23200	0.58714
0.2	0.2	0.0				0.19606	0.54490
		0.3				0.21647	0.56327
		0.5				0.22444	0.57295
0.2	0.2	0.5	0.0			0.21880	0.56592
			0.3			0.22446	0.57285
			0.5			0.22772	0.57750
0.2	0.2	0.5	0.3	1.0		0.22443	0.57291
				1.5		0.24490	0.56585
				2.0		0.25725	0.56080
0.2	0.2	0.5	0.3	1.0	0.2	0.10779	0.58240
					0.5	0.20254	0.57481
					0.7	0.24341	0.57118

**Table 5.3:** Values of local Nusselt  $-\theta'(0)$  and Sherwood numbers  $-\phi'(0)$  for different values of the parameters  $Sc$ ,  $Sr$ ,  $\tau$ ,  $D_f$ ,  $k^*$  and  $M$  when  $\alpha = \beta = 0.2$ ,  $\lambda = 0.5$ ,  $N_1 = 0.3$ ,  $Pr = 1$  and  $\gamma = 0.6$ .



$Sc$	$Sr$	$Df$	$\tau$	$k^*$	$M$	$-\theta'(0)$	$-\phi'(0)$
0.2	0.4	0.5	0.2	0.3	0.5	0.26950	0.32824
0.5						0.22446	0.57285
0.7						0.19729	0.71482
0.5	0.2					0.22285	0.58265
	0.5					0.22530	0.56786
	0.7					0.22690	0.55779
0.5	0.4	0.2				0.27834	0.52746
		0.5				0.22695	0.55765
		0.7				0.18905	0.57984
0.5	0.4	0.5	0.4			0.22160	0.58610
			0.7			0.21705	0.60820
			1.0			0.21164	0.63434
0.5	0.4	0.5	0.2	0.5		0.20529	0.67118
				0.7		0.18854	0.75605
				1.0		0.16638	0.86737
0.5	0.4	0.5	0.2	0.3	0.6	0.22122	0.56859
					0.8	0.21345	0.55880
					1.0	0.20402	0.54895

## 5.4 Conclusions

MHD three-dimensional flow of viscoelastic fluid over a stretching surface is analyzed in the presence of thermophoresis and convective condition. Effects of chemical reaction and Soret and Dufour are analyzed. The main observations are listed below.

- Effects of mixed convection parameter  $\lambda$  and buoyancy concentration parameter  $N$  on the velocity profiles and momentum boundary layer thickness are similar.
- Effects of  $Sr$  and  $Df$  on  $\theta(\eta)$  and  $\phi(\eta)$  are opposite.
- Thermal boundary layer thickness and temperature field increase when  $Df$  increases.

- Concentration  $\phi(\eta)$  and associated boundary layer thickness are decreasing functions of thermophoretic parameter  $\tau$ .
- There are opposite effects of local Nusselt number and local Sherwood number when  $\gamma_1$ ,  $Pr$ ,  $Sc$ ,  $Df$ ,  $k^*$ ,  $\tau$  and  $Sr$  increase.
- Qualitative effects of local Nusselt number and local Sherwood number are similar when  $\lambda$ ,  $N$ ,  $M$  and  $K$  increase.

## Chapter 6

# Three-dimensional flow of Maxwell fluid over a stretching surface with heat source and convective conditions

Heat and mass transfer effects in three-dimensional flow of Maxwell fluid over a stretching surface are addressed in this chapter. Analysis has been performed in presence of internal heat generation/absorption. Concentration and thermal buoyancy effects are accounted. Convective boundary conditions for heat and mass transfer analysis are explored. Series solutions of the resulting problems are developed. Effects of mixed convection, internal heat generation/absorption parameter and Biot numbers on the dimensionless velocity, temperature and concentration distributions are illustrated graphically. Numerical values of local Nusselt and Sherwood numbers are obtained and analyzed for all the physical parameters.

### 6.1 Governing problems

Here we consider the steady three-dimensional flow of an incompressible Maxwell fluid over a stretching surface at  $z = 0$ . The flow takes place in the domain  $z > 0$ . Heat and mass transfer

characteristics are taken into account in the presence of internal heat generation/absorption and mixed convection. Convective heat and mass boundary conditions are considered. The ambient fluid temperature and concentration are taken as  $T_\infty$  and  $C_\infty$  while the surface temperature and concentration are maintained by convective heat and mass transfer at certain value  $T_f$  and  $C_f$ . The governing partial differential equations subject to boundary layer flow are

$$\frac{\partial u}{\partial x} + \frac{\partial v}{\partial y} + \frac{\partial w}{\partial z} = 0, \quad (6.1)$$

$$\begin{aligned} u \frac{\partial u}{\partial x} + v \frac{\partial u}{\partial y} + w \frac{\partial u}{\partial z} = & \nu \frac{\partial^2 u}{\partial z^2} - \lambda_1 \left( u^2 \frac{\partial^2 u}{\partial x^2} + v^2 \frac{\partial^2 u}{\partial y^2} + w^2 \frac{\partial^2 u}{\partial z^2} + 2uv \frac{\partial^2 u}{\partial x \partial y} \right. \\ & \left. + 2vw \frac{\partial^2 u}{\partial y \partial z} + 2uw \frac{\partial^2 u}{\partial x \partial z} \right) \\ & + g(\beta_T(T - T_\infty) + \beta_C(C - C_\infty)), \end{aligned} \quad (6.2)$$

$$u \frac{\partial v}{\partial x} + v \frac{\partial v}{\partial y} + w \frac{\partial v}{\partial z} = \nu \frac{\partial^2 v}{\partial z^2} - \lambda_1 \left( u^2 \frac{\partial^2 v}{\partial x^2} + v^2 \frac{\partial^2 v}{\partial y^2} + w^2 \frac{\partial^2 v}{\partial z^2} + 2uv \frac{\partial^2 v}{\partial x \partial y} + \right. \\ \left. 2vw \frac{\partial^2 v}{\partial y \partial z} + 2uw \frac{\partial^2 v}{\partial x \partial z} \right), \quad (6.3)$$

$$\rho c_p \left( u \frac{\partial T}{\partial x} + v \frac{\partial T}{\partial y} + w \frac{\partial T}{\partial z} \right) = k \frac{\partial^2 T}{\partial z^2} + Q(T - T_\infty), \quad (6.4)$$

$$u \frac{\partial C}{\partial x} + v \frac{\partial C}{\partial y} + w \frac{\partial C}{\partial z} = D \frac{\partial^2 C}{\partial z^2}. \quad (6.5)$$

In Eqs. (6.1) – (6.5) the respective velocity components in the  $x$ -,  $y$ - and  $z$ -directions are denoted by  $u$ ,  $v$  and  $w$ ,  $\lambda_1$  shows the relaxation time,  $\sigma^*$  is the electrical conductivity,  $\rho$  is the density of fluid,  $g$  is the gravitational acceleration,  $\beta_T$  and  $\beta_C$  are the thermal and concentration expansion coefficients respectively,  $T$  is the fluid temperature,  $\nu = (\mu/\rho)$  is the kinematic viscosity,  $\mu$  is the dynamic viscosity of fluid,  $c_p$  is the specific heat,  $k$  is the thermal conductivity,  $Q$  is the uniform volumetric heat generation/absorption,  $C$  is the concentration field and  $D$  is the mass diffusivity.

The subjected boundary conditions are given by

$$u = u_e = ax, \quad v = by, \quad w = 0, \quad -k \frac{\partial T}{\partial z} = h(T_f - T), \quad -D \frac{\partial C}{\partial z} = h^*(C_f - C) \quad \text{at } z = 0, \quad (6.6)$$

$$u \rightarrow 0, \quad v \rightarrow 0, \quad T \rightarrow T_\infty, \quad C \rightarrow C_\infty \quad \text{as } z \rightarrow \infty, \quad (6.7)$$

where  $h$  is the heat transfer coefficient,  $h^*$  is the concentration transfer coefficient and  $a$  and  $b$  are constants and have dimension  $(time)^{-1}$ .

We now define

$$\begin{aligned} u &= axf'(\eta), \quad v = ayg'(\eta), \quad w = -\sqrt{a\nu}(f(\eta) + g(\eta)), \\ \theta(\eta) &= \frac{T - T_\infty}{T_f - T_\infty}, \quad \eta = z\sqrt{\frac{a}{\nu}}, \quad \phi(\eta) = \frac{C - C_\infty}{C_w - C_\infty}. \end{aligned} \quad (6.8)$$

The above variables satisfy Eq. (6.1) automatically while Eqs. (6.2)-(6.7) are converted to the following forms:

$$f''' + (f + g)f'' - f'^2 + \beta_1[2(f + g)f'f'' - (f + g)^2f'''] + \lambda(\theta + N\phi) = 0, \quad (6.9)$$

$$g''' + (f + g)g'' - g'^2 + \beta_1[2(f + g)g'g'' - (f + g)^2g'''] = 0, \quad (6.10)$$

$$\theta'' + Pr(f + g)\theta' + \beta^*\theta = 0, \quad (6.11)$$

$$\phi'' + Sc(f + g)\phi' = 0, \quad (6.12)$$

$$f = 0, \quad g = 0, \quad f' = 1, \quad g' = \beta, \quad \theta' = -\gamma_1(1 - \theta(0)), \quad \phi' = -\gamma_2(1 - \phi(0)), \quad \text{at } \eta = 0, \quad (6.13)$$

$$f' \rightarrow 0, \quad g' \rightarrow 0, \quad \theta \rightarrow 0, \quad \phi \rightarrow 0 \quad \text{as } \eta \rightarrow \infty, \quad (6.14)$$

where  $\beta_1$  is the dimensionless Deborah number,  $\lambda$  is the local buoyancy parameter,  $Gr_x$  is the local Grashof number,  $N$  is the concentration buoyancy parameter,  $Pr$  is the Prandtl number,  $\beta^*$  is the heat generation/absorption parameter,  $Sc$  is the Schmidt number,  $\beta$  is ratio of rates parameters,  $\gamma_1$  and  $\gamma_2$  are the Biot numbers and prime shows the differentiation with respect to  $\eta$ . These are given by

$$\begin{aligned} \beta_1 &= \lambda_1 a, \quad \lambda = \frac{Gr_x}{Re_x^2}, \quad Gr_x = \frac{g\beta_T(T_f - T_\infty)x^3}{\nu^2}, \quad N = \frac{\beta_C(C_w - C_\infty)}{\beta_T(T_f - T_\infty)} \\ Pr &= \frac{\nu}{\sigma}, \quad \beta^* = \frac{Q}{\rho c_p}, \quad Sc = \frac{\nu}{D}, \quad \beta = \frac{b}{a}, \quad \gamma_1 = \frac{h}{k}\sqrt{\frac{\nu}{a}}, \quad \gamma_2 = \frac{h^*}{D}\sqrt{\frac{\nu}{a}}. \end{aligned} \quad (6.15)$$

In dimensionless form the local Nusselt and local Sherwood numbers are given by

$$Nu/Re_x^{1/2} = -\theta'(0), \quad (6.16)$$

$$Sh/Re_x^{1/2} = -\phi'(0), \quad (6.17)$$

where  $Re_x = u_e x / \nu$  is the local Reynolds number.

## 6.2 Series solutions

The initial approximations and auxiliary linear operators are required to develop homotopic solutions. We select the following initial guesses and linear operators for the present flow analysis:

$$f_0(\eta) = (1 - e^{-\eta}), \quad g_0(\eta) = \beta(1 - e^{-\eta}), \quad \theta_0(\eta) = \frac{\gamma_1 \exp(-\eta)}{1 + \gamma_1}, \quad \phi_0(\eta) = \frac{\gamma_2 \exp(-\eta)}{1 + \gamma_2}, \quad (6.18)$$

$$\mathcal{L}_f = f''' - f', \quad \mathcal{L}_g = g''' - g', \quad \mathcal{L}_\theta = \theta'' - \theta, \quad \mathcal{L}_\phi = \phi'' - \phi, \quad (6.19)$$

with the following properties of the defined operators in Eq. (6.19) i.e.

$$\begin{aligned} \mathcal{L}_f(C_1 + C_2 e^\eta + C_3 e^{-\eta}) &= 0, \quad \mathcal{L}_g(C_4 + C_5 e^\eta + C_6 e^{-\eta}) = 0, \\ \mathcal{L}_\theta(C_7 e^\eta + C_8 e^{-\eta}) &= 0, \quad \mathcal{L}_\phi(C_9 e^\eta + C_{10} e^{-\eta}) = 0, \end{aligned} \quad (6.20)$$

where  $C_i$  ( $i = 1 - 10$ ) are the arbitrary constants.

The corresponding problems at the zeroth order deformations are given in the following forms:

$$(1 - p) \mathcal{L}_f [\hat{f}(\eta; p) - f_0(\eta)] = p \hbar_f \mathcal{N}_f [\hat{f}(\eta; p), \hat{g}(\eta; p), \hat{\theta}(\eta, p), \hat{\phi}(\eta, p)], \quad (6.21)$$

$$(1 - p) \mathcal{L}_g [\hat{g}(\eta; p) - g_0(\eta)] = p \hbar_g \mathcal{N}_g [\hat{f}(\eta; p), \hat{g}(\eta; p), \hat{\theta}(\eta, p), \hat{\phi}(\eta, p)], \quad (6.22)$$

$$(1 - p) \mathcal{L}_\theta [\hat{\theta}(\eta; p) - \theta_0(\eta)] = p \hbar_\theta \mathcal{N}_\theta [\hat{f}(\eta; p), \hat{g}(\eta; p), \hat{\theta}(\eta, p), \hat{\phi}(\eta, p)], \quad (6.23)$$

$$(1 - p) \mathcal{L}_\phi [\hat{\phi}(\eta; p) - \phi_0(\eta)] = p \hbar_\phi \mathcal{N}_\phi [\hat{f}(\eta; p), \hat{g}(\eta; p), \hat{\theta}(\eta, p), \hat{\phi}(\eta, p)], \quad (6.24)$$

$$\begin{aligned}
\hat{f}(0; p) &= 0, \quad \hat{f}'(0; p) = 1, \quad \hat{f}'(\infty; p) = 0, \\
\hat{g}(0; p) &= 0, \quad \hat{g}'(0; p) = \beta, \quad \hat{g}'(\infty; p) = 0, \quad \hat{\theta}'(0, p) = -\gamma_1[1 - \theta(0, p)], \\
\hat{\theta}(\infty, p) &= 0, \quad \hat{\phi}'(0, p) = -\gamma_2[1 - \hat{\phi}(0, p)], \quad \hat{\phi}(\infty, p) = 0
\end{aligned} \tag{6.25}$$

$$\begin{aligned}
\mathcal{N}_f[\hat{f}(\eta, p), \hat{g}(\eta, p), \hat{\theta}(\eta, p), \hat{\phi}(\eta, p)] &= \frac{\partial^3 \hat{f}(\eta, p)}{\partial \eta^3} - \left( \frac{\partial \hat{f}(\eta, p)}{\partial \eta} \right)^2 + (\hat{f}(\eta, p) + \hat{g}(\eta, p)) \frac{\partial^2 \hat{f}(\eta, p)}{\partial \eta^2} \\
&\quad + \beta_1 \left[ \begin{array}{c} 2(\hat{f}(\eta, p) + \hat{g}(\eta, p)) \\ \frac{\partial \hat{f}(\eta, p)}{\partial \eta} \frac{\partial^2 \hat{f}(\eta, p)}{\partial \eta^2} \\ -(\hat{f}(\eta, p) + \hat{g}(\eta, p))^2 \frac{\partial^3 \hat{f}(\eta, p)}{\partial \eta^3} \end{array} \right] \\
&\quad + \lambda[\hat{\theta}(\eta, p) + N_1 \hat{\phi}(\eta, p)],
\end{aligned} \tag{6.26}$$

$$\begin{aligned}
\mathcal{N}_g[\hat{g}(\eta, p), \hat{f}(\eta, p), \hat{\theta}(\eta, p), \hat{\phi}(\eta, p)] &= \frac{\partial^3 \hat{g}(\eta, p)}{\partial \eta^3} - \left( \frac{\partial \hat{g}(\eta, p)}{\partial \eta} \right)^2 + (\hat{f}(\eta, p) + \hat{g}(\eta, p)) \frac{\partial^2 \hat{g}(\eta, p)}{\partial \eta^2} \\
&\quad + \beta_1 \left[ \begin{array}{c} 2(\hat{f}(\eta, p) + \hat{g}(\eta, p)) \\ \frac{\partial \hat{g}(\eta, p)}{\partial \eta} \frac{\partial^2 \hat{g}(\eta, p)}{\partial \eta^2} \\ -(\hat{f}(\eta, p) + \hat{g}(\eta, p))^2 \frac{\partial^3 \hat{g}(\eta, p)}{\partial \eta^3} \end{array} \right],
\end{aligned} \tag{6.27}$$

$$\mathcal{N}_\theta[\hat{\theta}(\eta, p), \hat{\phi}(\eta, p), \hat{f}(\eta, p), \hat{g}(\eta, p)] = \frac{\partial^2 \hat{\theta}(\eta, p)}{\partial \eta^2} + \text{Pr}(\hat{f}(\eta, p) + \hat{g}(\eta, p)) \frac{\partial \hat{\theta}(\eta, p)}{\partial \eta} + \beta^* \hat{\theta}(\eta, p), \tag{6.28}$$

$$\mathcal{N}_\phi[\hat{\phi}(\eta, p), \hat{\theta}(\eta, p), \hat{f}(\eta, p), \hat{g}(\eta, p)] = \frac{\partial^2 \hat{\phi}(\eta, p)}{\partial \eta^2} + Sc(\hat{f}(\eta, p) + \hat{g}(\eta, p)) \frac{\partial \hat{\phi}(\eta, p)}{\partial \eta}. \tag{6.29}$$

Here  $p$  is an embedding parameter, the non-zero auxiliary parameters are  $\hbar_f$ ,  $\hbar_g$ ,  $\hbar_\theta$  and  $\hbar_\phi$  and the nonlinear operators are  $\mathcal{N}_f$ ,  $\mathcal{N}_g$ ,  $\mathcal{N}_\theta$  and  $\mathcal{N}_\phi$ . When  $p = 0$  and  $p = 1$  one has

$$\begin{aligned}
\hat{f}(\eta; 0) &= f_0(\eta), \quad \hat{g}(\eta, 0) = g_0(\eta), \quad \hat{\theta}(\eta, 0) = \theta_0(\eta), \quad \hat{\phi}(\eta, 0) = \phi_0(\eta), \\
\hat{f}(\eta; 1) &= f(\eta), \quad \hat{g}(\eta, 1) = g(\eta), \quad \hat{\theta}(\eta, 1) = \theta(\eta), \quad \hat{\phi}(\eta, 1) = \phi(\eta).
\end{aligned} \tag{6.30}$$

Clearly when  $p$  is increased from 0 to 1 then  $f(\eta, p)$ ,  $g(\eta, p)$ ,  $\theta(\eta, p)$  and  $\phi(\eta, p)$  vary from  $f_0(\eta)$ ,

$g_0(\eta)$ ,  $\theta_0(\eta)$  and  $\phi_0(\eta)$  to  $f(\eta)$ ,  $g(\eta)$ ,  $\theta(\eta)$  and  $\phi(\eta)$ . By Taylor's expansion we have

$$f(\eta, p) = f_0(\eta) + \sum_{m=1}^{\infty} f_m(\eta) p^m, \quad f_m(\eta) = \frac{1}{m!} \left. \frac{\partial^m f(\eta; p)}{\partial p^m} \right|_{p=0}, \quad (6.31)$$

$$g(\eta, p) = g_0(\eta) + \sum_{m=1}^{\infty} g_m(\eta) p^m, \quad g_m(\eta) = \frac{1}{m!} \left. \frac{\partial^m g(\eta; p)}{\partial p^m} \right|_{p=0}, \quad (6.32)$$

$$\theta(\eta, p) = \theta_0(\eta) + \sum_{m=1}^{\infty} \theta_m(\eta) p^m, \quad \theta_m(\eta) = \frac{1}{m!} \left. \frac{\partial^m \theta(\eta; p)}{\partial p^m} \right|_{p=0}, \quad (6.33)$$

$$\phi(\eta, p) = \phi_0(\eta) + \sum_{m=1}^{\infty} \phi_m(\eta) p^m, \quad \phi_m(\eta) = \frac{1}{m!} \left. \frac{\partial^m \phi(\eta; p)}{\partial p^m} \right|_{p=0}, \quad (6.34)$$

where the convergence of above series strongly depends upon  $\hbar_f$ ,  $\hbar_g$ ,  $\hbar_\theta$  and  $\hbar_\phi$ . Considering that  $\hbar_f$ ,  $\hbar_g$ ,  $\hbar_\theta$  and  $\hbar_\phi$  are selected properly so that Eqs. (6.31) – (6.34) converge at  $p = 1$  then we have

$$f(\eta) = f_0(\eta) + \sum_{m=1}^{\infty} f_m(\eta), \quad (6.35)$$

$$g(\eta) = g_0(\eta) + \sum_{m=1}^{\infty} g_m(\eta), \quad (6.36)$$

$$\theta(\eta) = \theta_0(\eta) + \sum_{m=1}^{\infty} \theta_m(\eta), \quad (6.37)$$

$$\phi(\eta) = \phi_0(\eta) + \sum_{m=1}^{\infty} \phi_m(\eta). \quad (6.38)$$

The general solutions can be expressed below:

$$f_m(\eta) = f_m^*(\eta) + C_1 + C_2 e^\eta + C_3 e^{-\eta}, \quad (6.39)$$

$$g_m(\eta) = g_m^*(\eta) + C_4 + C_5 e^\eta + C_6 e^{-\eta}, \quad (6.40)$$

$$\theta_m(\eta) = \theta_m^*(\eta) + C_7 e^\eta + C_8 e^{-\eta}, \quad (6.41)$$

$$\phi_m(\eta) = \phi_m^*(\eta) + C_9 e^\eta + C_{10} e^{-\eta}, \quad (6.42)$$

in which the  $f_m^*$ ,  $g_m^*$ ,  $\theta_m^*$  and  $\phi_m^*$  indicate the special solutions.



### 6.3 Convergence analysis and discussion

Clearly the homotopic series solutions (6.35) – (6.38) depend on the auxiliary parameters  $\hbar_f$ ,  $\hbar_g$ ,  $\hbar_\theta$  and  $\hbar_\phi$ . These parameters have important role in the convergence of series solutions. For this purpose, the  $\hbar$ –curves are drawn at 15<sup>th</sup> order of approximations to determine the suitable ranges of these auxiliary parameters. Fig. 6.1 shows that the acceptable values of  $\hbar_f$ ,  $\hbar_g$ ,  $\hbar_\theta$  and  $\hbar_\phi$  are  $-1.4 \leq \hbar_f \leq -0.20$ ,  $-1.6 \leq \hbar_g \leq -0.40$  and  $-1.50 \leq \hbar_\theta, \hbar_\phi \leq -0.30$ . Table 6.1 ensures the convergence of homotopic series solutions in the whole region of  $\eta$  when  $\hbar_f = \hbar_g = \hbar_\theta = \hbar_\phi = -0.5$ .

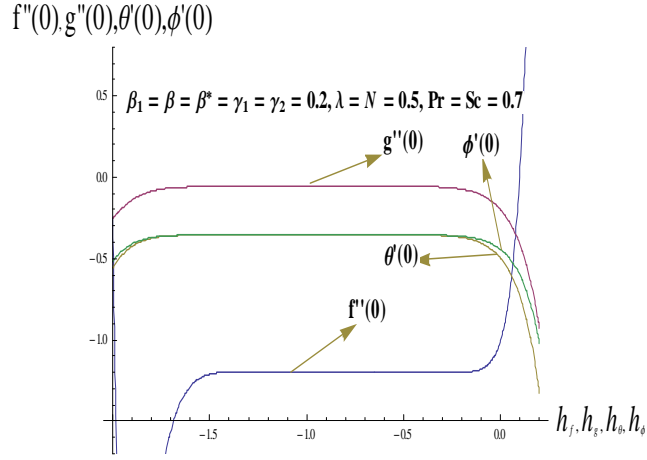


Fig. 6.1:  $\hbar$ –curves for the functions  $f$ ,  $g$ ,  $\theta$  and  $\phi$ .

**Table 6.1:** Convergence of series solutions for different order of approximations when  $\beta = \beta_1 = \beta^* = 0.2$ ,  $\gamma_2 = \lambda = N = 0.3$ ,  $\gamma_1 = 0.5$ ,  $Sc = 1.0$ ,  $Pr = 1.2$  and  $\hbar_f = \hbar_g = \hbar_\theta = \hbar_\phi = -0.5$ .

order of approximations	$-f''(0)$	$-g''(0)$	$-\theta'(0)$	$-\phi'(0)$
1	1.018	0.1497	0.3133	0.2228
5	1.029	0.06217	0.2782	0.2095
10	1.028	0.03940	0.2703	0.2067
15	1.029	0.03866	0.2702	0.2066
20	1.029	0.03982	0.2705	0.2066
25	1.029	0.03993	0.2705	0.2066
30	1.029	0.03993	0.2705	0.2066

Figs. 6.2-6.7 show the effects of Deborah number  $\beta_1$ , mixed convection parameter  $\lambda$ , con-

centration buoyancy parameter  $N$  and internal heat source/sink parameter  $\beta^*$  on the velocity profiles  $f'(\eta)$  and  $g'(\eta)$ . Figs. 6.2 and 6.3 are drawn to see the behavior of Deborah number  $\beta_1$  on the velocity profiles  $f'(\eta)$  and  $g'(\eta)$ . It is found that both the velocity profiles  $f'(\eta)$  and  $g'(\eta)$  decrease with an enhancement in  $\beta_1$ . It is also examined from these Figs. that associated boundary layer thicknesses are decreasing functions of  $\beta_1$ . This is due to the fact that  $\beta_1$  depends on relaxation time. Larger relaxation time offers more resistance to the flow due to which the velocities are decreased. Figs. 6.4 and 6.5 are displayed to see the impact of mixed convection parameter  $\lambda$  on the velocity profiles  $f'(\eta)$  and  $g'(\eta)$ . It is seen that both the velocity profiles  $f'(\eta)$  and  $g'(\eta)$  increase with an enhancement in  $\lambda$ . Also momentum boundary layer thicknesses are increased with an increase in  $\lambda$ . In fact an increase in  $\lambda$  enhances the buoyancy forces which are more dominant to viscous forces. Variations of concentration buoyancy parameter  $N$  on the velocity profiles  $f'(\eta)$  and  $g'(\eta)$  are displayed in the Figs. 6.6 and 6.7. Similar behavior of  $N$  is noted on the velocity profiles  $f'(\eta)$  and  $g'(\eta)$ .

Figs. 6.8 and 6.9 are plotted to see the variations of internal heat source/sink parameter  $\beta^*$  and heat transfer Biot number  $\gamma_1$  on the temperature  $\theta(\eta)$ . Fig. 6.8 depicts that the thermal boundary layer thickness and temperature  $\theta(\eta)$  are increasing functions of internal heat source parameter  $\beta^* > 0$  and decreasing functions of internal heat sink  $\beta^* < 0$ . With an increase in heat transfer Biot number  $\gamma_1$ , both the thermal boundary layer thickness and temperature  $\theta(\eta)$  are enhanced (see Fig. 6.9). The reason is that as  $\gamma_1$  depends on heat transfer coefficient  $h$  which leads to an increase in temperature  $\theta(\eta)$ .

Figs. 6.10 is displayed to analyze the behavior of concentration  $\phi(\eta)$  for different values of mass transfer Biot number  $\gamma_2$ . It is observed that as  $\gamma_2$  increases the associated boundary layer thickness and concentration profile  $\phi(\eta)$  grow. As mass transfer Biot number  $\gamma_2$  depends on mass transfer coefficient  $h^*$  so with an enhancement in  $\gamma_2$  the mass transfer coefficient increases which leads to an increase in concentration profile  $\phi(\eta)$ .

Impacts of mixed convection parameter  $\lambda$ , concentration buoyancy parameter  $N$ , Deborah number  $\beta_1$  and internal heat source/sink parameter  $\beta^*$  on the local Nusselt number  $(-\theta'(0))$  are displayed in the Figs. 6.11 and 6.12. It is found that local Nusselt number  $(-\theta'(0))$  enhances with an increase in  $\lambda$  and  $N$  (see Fig.6.11). Local Nusselt number  $(-\theta'(0))$  reduces with internal heat source parameter  $\beta^* > 0$  while it increases with internal heat sink parameter  $\beta^* < 0$  (see

Fig. 6.12). It is also noticed from Fig. 6.12 that local Nusselt number  $(-\theta'(0))$  decreases with an increase in  $\beta_1$ .

Figs. 6.13 and 6.14 are sketched to see the variations of mixed convection parameter  $\lambda$ , concentration buoyancy parameter  $N$ , Deborah number  $\beta_1$  and internal heat source/sink parameter  $\beta^*$  on the Sherwood number  $(-\phi'(0))$ . Fig. 6.13 shows that the Sherwood number  $(-\phi'(0))$  increases with an increase in  $\lambda$  and  $N$ . Fig. 6.14 indicates that the Sherwood number  $(-\phi'(0))$  increases by increasing internal heat source  $\beta^* > 0$  while reverse effect is examined with an increase in Deborah number  $\beta_1$ .

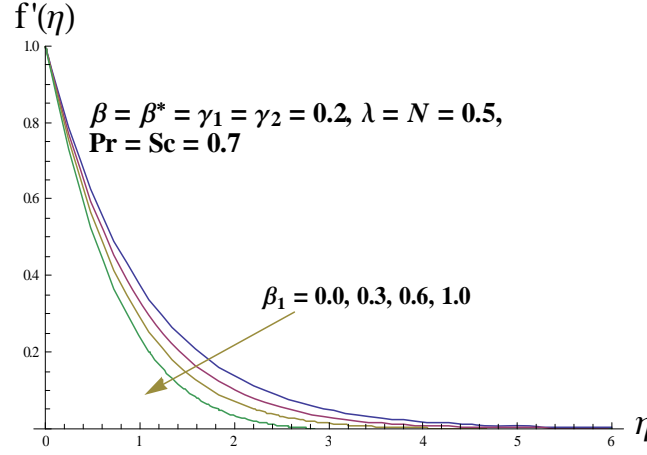


Fig. 6.2: Variation of  $\beta_1$  on  $f'(\eta)$ .

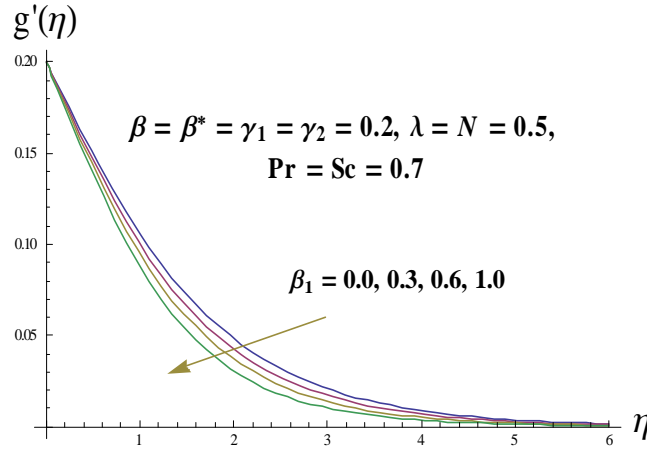


Fig. 6.3: Variation of  $\beta_1$  on  $g'(\eta)$ .

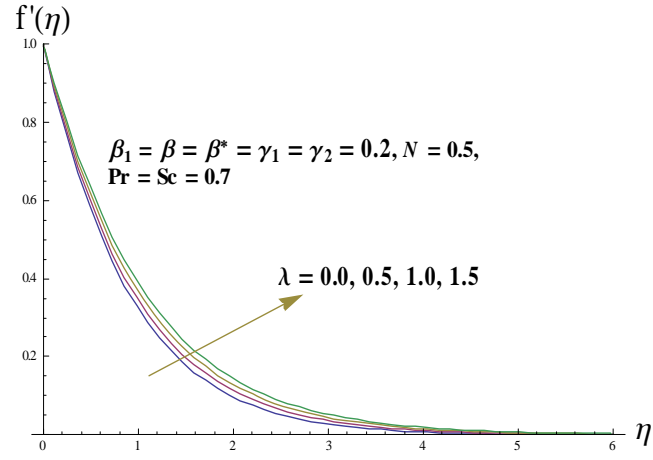


Fig. 6.4: Variation of  $\lambda$  on  $f'(\eta)$ .

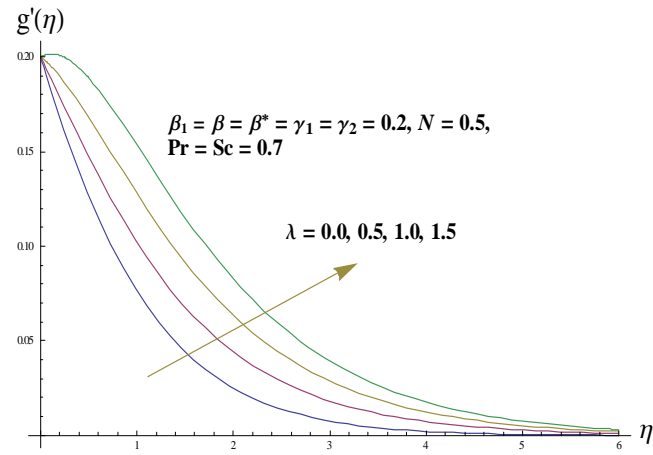


Fig. 6.5: Variation of  $\lambda$  on  $g'(\eta)$ .

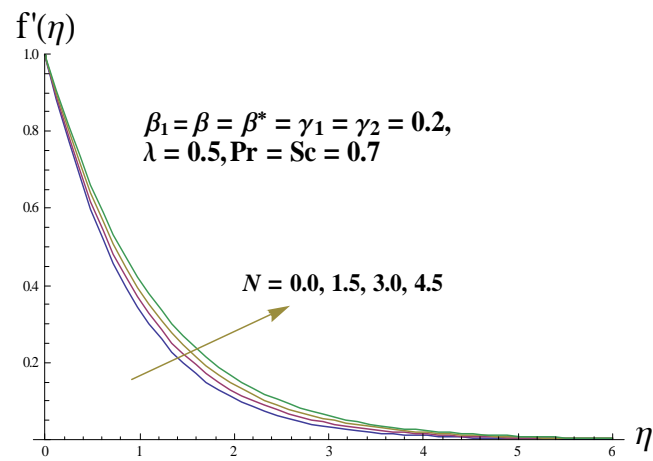


Fig. 6.6: Variation of  $N$  on  $f'(\eta)$ .

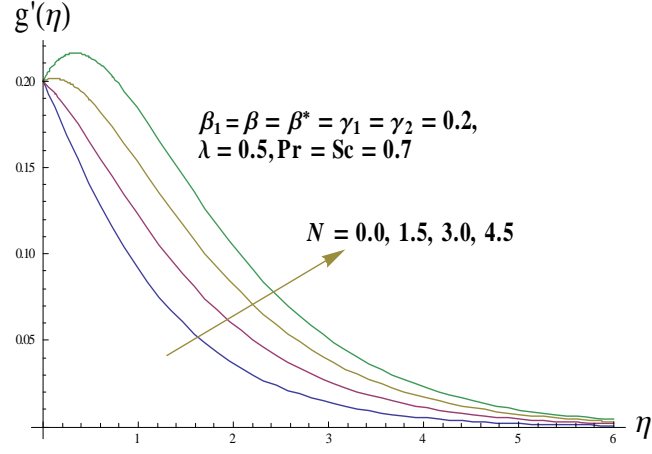


Fig. 6.7: Variation of  $N$  on  $g'(\eta)$ .

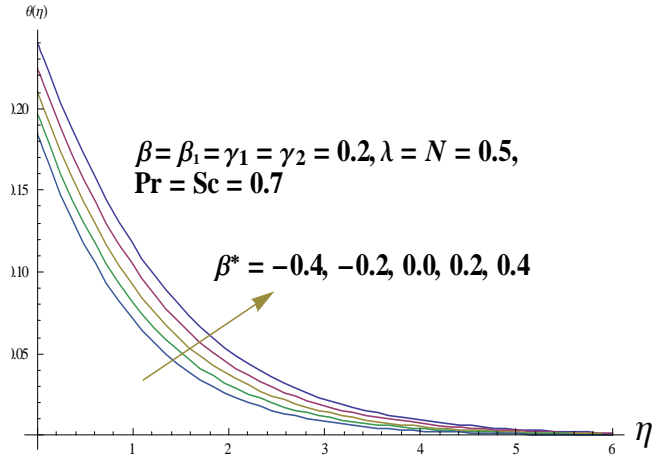


Fig. 6.8: Variation of  $\beta^*$  on  $\theta(\eta)$ .

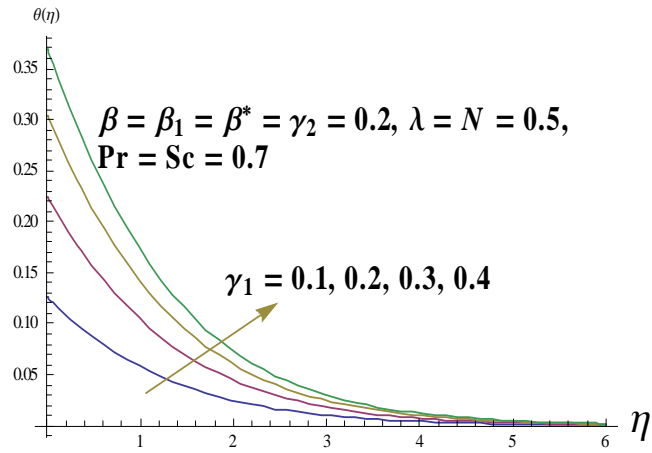


Fig. 6.9: Variation of  $\gamma_1$  on  $\theta(\eta)$ .

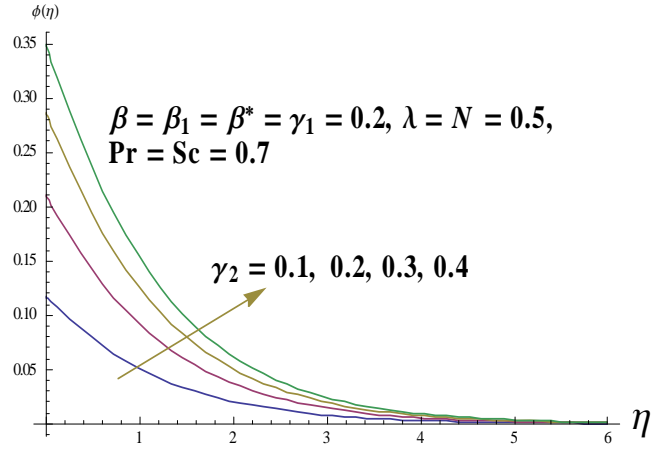


Fig. 6.10: Variation of  $\gamma_2$  on  $\phi(\eta)$ .

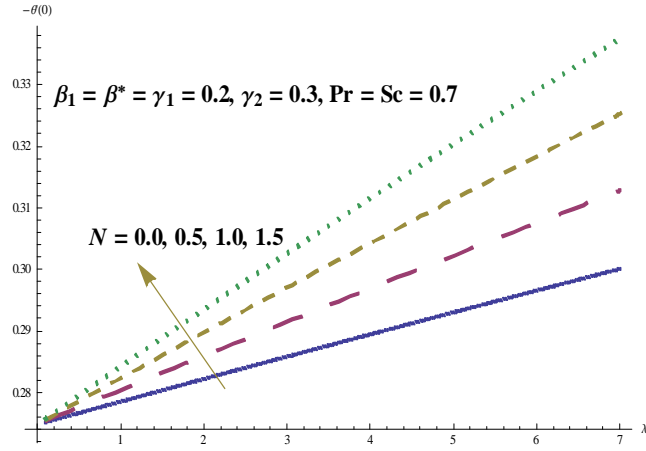


Fig. 6.11: Variations of  $\lambda$  and  $N$  on  $-\theta'(0)$ .

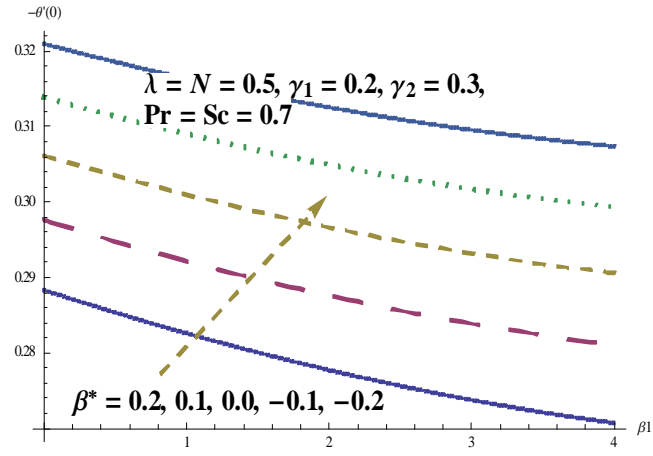


Fig. 6.12: Variations of  $\beta^*$  and  $\beta_1$  on  $-\theta'(0)$ .

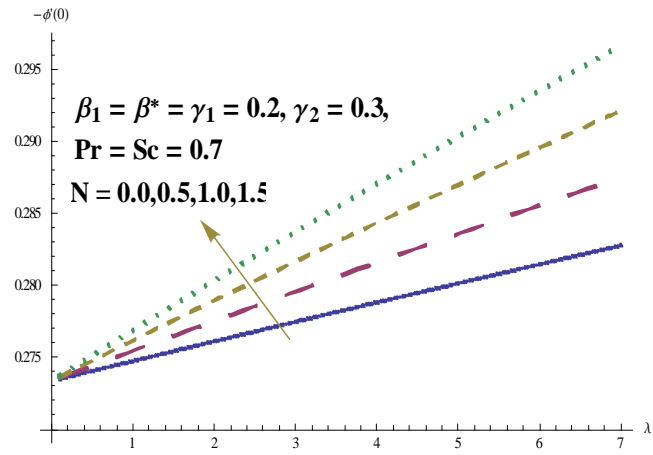


Fig. 6.13: Variations of  $\lambda$  and  $N$  on  $-\phi'(0)$ .

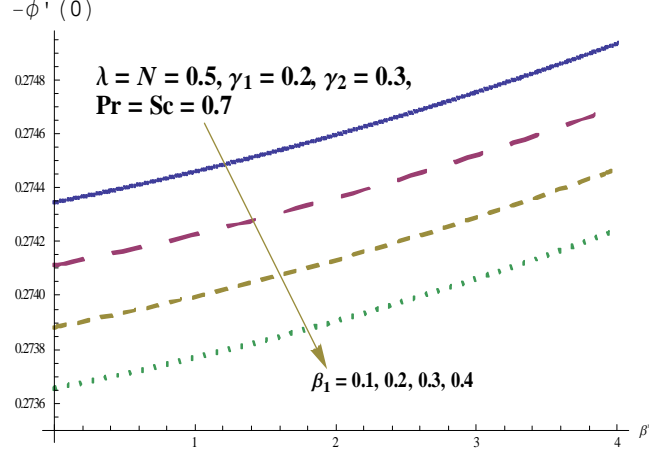


Fig. 6.14: Variations of  $\beta_1$  and  $\beta^*$  on  $-\theta'(0)$ .

### 6.3.1 Conclusions

Three-dimensional mixed convection flow of Maxwell fluid over a stretching sheet with internal heat generation/absorption is analyzed. Convective boundary conditions for both heat and mass transfer are considered. The main observations are mentioned below.

- Variations of mixed convection parameter  $\lambda$  and concentration buoyancy parameter  $N$  enhance the velocity profiles and associated boundary layer thicknesses.
- Velocity profiles and temperature increase in case of internal heat source  $\beta^* > 0$  while these reduce for heat sink  $\beta^* < 0$ .
- Heat transfer Biot number  $\gamma_1$  increases the thermal boundary layer thickness and temperature. Also concentration and its associated boundary layer are enhanced with an increase in mass transfer Biot number  $\gamma_2$ .
- The local Nusselt and Sherwood numbers have quite similar behaviors for increasing values of mixed convection parameter  $\lambda$ , concentration buoyancy parameter  $N$  and Deborah number  $\beta_1$ .
- Larger values of heat sink parameter  $\beta^* < 0$  give rise to the local Nusselt number  $(-\theta'(0))$ . However Sherwood number  $(-\phi'(0))$  enhances with an increase in heat source  $\beta^* > 0$ .



## Chapter 7

# Soret and Dufour effects in three-dimensional flow of Maxwell fluid with chemical reaction and convective condition

This chapter addresses the heat and mass transfer effects in three-dimensional flow of Maxwell fluid over a stretching surface with convective boundary conditions. Mass transfer is considered in the presence of first order chemical reaction. Soret and Dufour effects in the conservation law of energy and concentration are considered. Convergent series solutions to the resulting nonlinear problems are developed. Plots of physical quantities of interest are analyzed.

### 7.1 Problems formulation

We consider the steady three-dimensional flow of an incompressible Maxwell fluid induced by a stretching surface at  $z = 0$ . The flow takes place in the domain  $z > 0$ . The ambient fluid temperature is taken as  $T_\infty$  while the surface temperature is maintained by convective heat transfer. Soret and Dufour effects in presence of mixed convection flow are taken into account. In addition the effect of first order chemical reaction in mass transfer is taken under

consideration. Flow diagram is as follows:

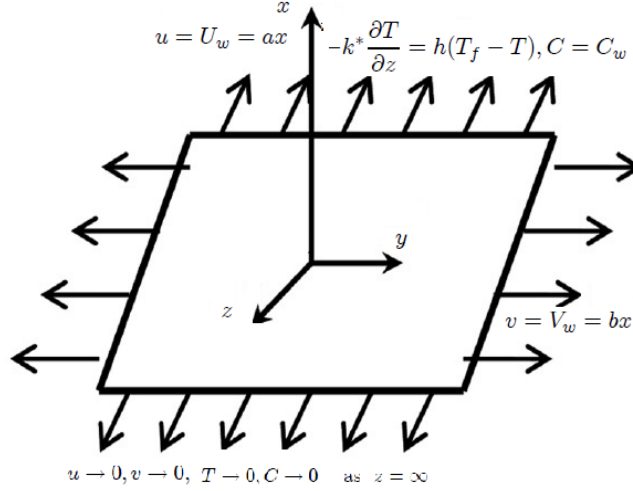


Fig. 7.1: Geometry of the problem

The governing boundary layer equations for three-dimensional flow of Maxwell fluid can be written as

$$\frac{\partial u}{\partial x} + \frac{\partial v}{\partial y} + \frac{\partial w}{\partial z} = 0, \quad (7.1)$$

$$\begin{aligned} u \frac{\partial u}{\partial x} + v \frac{\partial u}{\partial y} + w \frac{\partial u}{\partial z} = & \nu \frac{\partial^2 u}{\partial z^2} - \lambda_1 \left( u^2 \frac{\partial^2 u}{\partial x^2} + v^2 \frac{\partial^2 u}{\partial y^2} + w^2 \frac{\partial^2 u}{\partial z^2} + 2uv \frac{\partial^2 u}{\partial x \partial y} \right. \\ & \left. + 2vw \frac{\partial^2 u}{\partial y \partial z} + 2uw \frac{\partial^2 u}{\partial x \partial z} \right) \\ & + g\beta_T(T - T_\infty) + g\beta_C(C - C_\infty), \end{aligned} \quad (7.2)$$

$$u \frac{\partial v}{\partial x} + v \frac{\partial v}{\partial y} + w \frac{\partial v}{\partial z} = \nu \frac{\partial^2 v}{\partial z^2} - \lambda_1 \left( u^2 \frac{\partial^2 v}{\partial x^2} + v^2 \frac{\partial^2 v}{\partial y^2} + w^2 \frac{\partial^2 v}{\partial z^2} + 2uv \frac{\partial^2 v}{\partial x \partial y} + \right. \\ \left. 2vw \frac{\partial^2 v}{\partial y \partial z} + 2uw \frac{\partial^2 v}{\partial x \partial z} \right), \quad (7.3)$$

$$u \frac{\partial T}{\partial x} + v \frac{\partial T}{\partial y} + w \frac{\partial T}{\partial z} = \sigma \frac{\partial^2 T}{\partial z^2} + \frac{D_e k_T}{C_s C_p} \frac{\partial^2 C}{\partial z^2} + \frac{\mu}{\rho c_p} \left( \left( \frac{\partial u}{\partial z} \right)^2 + \left( \frac{\partial v}{\partial z} \right)^2 \right), \quad (7.4)$$

$$u \frac{\partial C}{\partial x} + v \frac{\partial C}{\partial y} + w \frac{\partial C}{\partial z} = D_e \frac{\partial^2 C}{\partial z^2} + \frac{D_e k_T}{T_m} \frac{\partial^2 T}{\partial z^2} - k_1(C - C_\infty). \quad (7.5)$$

In Eqs. (7.1) – (7.5) the respective velocity components in the  $x$ -,  $y$ - and  $z$ -directions are denoted by  $u$ ,  $v$  and  $w$ ,  $\lambda_1$  shows the relaxation time,  $T$  the fluid temperature,  $\sigma$  the thermal diffusivity of fluid,  $\nu = (\mu/\rho)$  the kinematic viscosity,  $\mu$  the dynamic viscosity of fluid,  $C$  the

concentration field,  $D_e$  the mass diffusivity,  $k_T$  the thermal diffusion ratio,  $C_p$  the specific heat,  $C_s$  the concentration susceptibility and  $\rho$  the density of fluid.

The boundary conditions appropriate to flow under consideration are given by

$$u = u_e = ax, \quad v = by, \quad w = 0, \quad -k \frac{\partial T}{\partial z} = h(T_f - T), \quad C = C_w \text{ at } z = 0, \quad (7.6)$$

$$u \rightarrow 0, \quad v \rightarrow 0, \quad T \rightarrow T_\infty, \quad C \rightarrow C_\infty \text{ as } z \rightarrow \infty, \quad (7.7)$$

where  $k^*$  indicates the thermal conductivity of fluid,  $T_f$  is the hot fluid temperature,  $C_\infty$  the ambient concentration and  $a$  and  $b$  have dimension inverse of time.

We now define

$$\begin{aligned} u &= axf'(\eta), \quad v = ayg'(\eta), \quad w = -\sqrt{a\nu}(f(\eta) + g(\eta)), \\ \theta(\eta) &= \frac{T - T_\infty}{T_f - T_\infty}, \quad \eta = z\sqrt{\frac{a}{\nu}}, \quad \phi(\eta) = \frac{C - C_\infty}{C_w - C_\infty}. \end{aligned} \quad (7.8)$$

Now the use of above variables satisfy Eq. (7.1) automatically while Eqs. (7.2)-(7.7) are reduced as follows:

$$f''' + (f + g)f'' - f'^2 + \beta_1[2(f + g)f'f'' - (f + g)^2f'''] + \lambda(\theta + N\phi) = 0, \quad (7.9)$$

$$g''' + (f + g)g'' - g'^2 + \beta_1[2(f + g)g'g'' - (f + g)^2g'''] = 0, \quad (7.10)$$

$$\theta'' + Pr(f + g)\theta' + Pr D_f \phi'' + Pr(E_1 f''^2 + E_2 g''^2) = 0, \quad (7.11)$$

$$\phi'' + Sc(f + g)\phi' - Sck^*\phi + ScSr\theta'' = 0, \quad (7.12)$$

$$f = 0, \quad g = 0, \quad f' = 1, \quad g' = \beta, \quad \theta' = -\gamma_1(1 - \theta(0)), \quad \phi = 1 \text{ at } \eta = 0, \quad (7.13)$$

$$f' \rightarrow 0, \quad g' \rightarrow 0, \quad \theta \rightarrow 0, \quad \phi \rightarrow 0 \text{ as } \eta \rightarrow \infty, \quad (7.14)$$

$$\begin{aligned}
\beta_1 &= \lambda_1 a, \lambda = \frac{Gr_x}{Re_x^2}, Gr_x = \frac{g\beta_T(T_f - T_\infty)x^3}{\nu^2}, N = \frac{\beta_C(C_w - C_\infty)}{\beta_T(T_f - T_\infty)}, Pr = \frac{\nu}{\sigma}, \\
D_f &= \frac{D_e k_T}{C_s C_p} \frac{(C_w - C_\infty)}{(T_f - T_\infty)\nu}, Sr = \frac{D_e k_T}{T_m \nu} \frac{(T_f - T_\infty)}{(C_w - C_\infty)}, E_1 = \frac{a^2 x^2}{C_p(T_f - T_\infty)}, E_2 = \frac{a^2 y^2}{C_p(T_f - T_\infty)}, \\
Sc &= \frac{\nu}{D_e}, k^* = \frac{k_1}{a}, \beta = \frac{b}{a}, \gamma_1 = \frac{h}{k^*} \sqrt{\frac{\nu}{a}}.
\end{aligned} \tag{7.15}$$

Here  $\beta_1$  is the Deborah number,  $\lambda$  the mixed convection parameter,  $Gr_x$  the local Grashof number,  $N$  the concentration buoyancy parameter,  $Pr$  the Prandtl number,  $D_f$  the Dufour number,  $Sr$  the Soret number,  $E_1$  and  $E_2$  the Eckert numbers along the  $x$  and  $y$  directions respectively,  $Sc$  the Schmidt number,  $k^*$  the chemical reaction parameter,  $\beta$  the ratio of rates parameters and  $\gamma_1$  the Biot number. All parameters are defined in a sequence in which they are written and prime shows the differentiation with respect to  $\eta$ .

Local Nusselt (dimensionless temperature gradient at the surface) and local Sherwood (dimensionless concentration gradient at the surface) numbers in dimensionless forms are given by

$$Nu/Re_x^{1/2} = -\theta'(0), \tag{7.16}$$

$$Sh/Re_x^{1/2} = -\phi'(0), \tag{7.17}$$

in which  $Re_x = u_e x / \nu$  is the local Reynolds number.

## 7.2 Homotopy analysis solutions

The initial approximations and auxiliary linear operators required for homotopy analysis solutions are presented below i.e.

$$f_0(\eta) = (1 - e^{-\eta}), \quad g_0(\eta) = \beta (1 - e^{-\eta}), \quad \theta_0(\eta) = \frac{\gamma_1 \exp(-\eta)}{1 + \gamma_1}, \quad \phi_0(\eta) = \exp(-\eta) \tag{7.18}$$

$$\mathcal{L}_f = f''' - f', \quad \mathcal{L}_g = g''' - g', \quad \mathcal{L}_\theta = \theta'' - \theta, \quad \mathcal{L}_\phi = \phi'' - \phi, \tag{7.19}$$

with the following properties of the defined operators in Eq. (7.18) i.e.

$$\begin{aligned}\mathcal{L}_f(C_1 + C_2 e^\eta + C_3 e^{-\eta}) &= 0, \quad \mathcal{L}_g(C_4 + C_5 e^\eta + C_6 e^{-\eta}) = 0, \\ \mathcal{L}_\theta(C_7 e^\eta + C_8 e^{-\eta}) &= 0, \quad \mathcal{L}_\phi(C_9 e^\eta + C_{10} e^{-\eta}) = 0\end{aligned}\tag{7.20}$$

where  $C_i$  ( $i = 1 - 10$ ) indicate the arbitrary constants.

The corresponding problems at the zeroth order are given in the following forms:

$$(1 - p) \mathcal{L}_f [\hat{f}(\eta; p) - f_0(\eta)] = p \hbar_f \mathcal{N}_f [\hat{f}(\eta; p), \hat{g}(\eta; p)], \tag{7.21}$$

$$(1 - p) \mathcal{L}_g [\hat{g}(\eta; p) - g_0(\eta)] = p \hbar_g \mathcal{N}_g [\hat{f}(\eta; p), \hat{g}(\eta; p)], \tag{7.22}$$

$$(1 - p) \mathcal{L}_\theta [\hat{\theta}(\eta; p) - \theta_0(\eta)] = p \hbar_\theta \mathcal{N}_\theta [\hat{f}(\eta; p), \hat{g}(\eta; p), \hat{\theta}(\eta; p), \hat{\phi}(\eta; p)], \tag{7.23}$$

$$(1 - p) \mathcal{L}_\phi [\hat{\phi}(\eta; p) - \phi_0(\eta)] = p \hbar_\phi \mathcal{N}_\phi [\hat{f}(\eta; p), \hat{g}(\eta; p), \hat{\theta}(\eta; p), \hat{\phi}(\eta; p)], \tag{7.24}$$

$$\begin{aligned}\hat{f}(0; p) &= 0, \quad \hat{f}'(0; p) = 1, \quad \hat{f}'(\infty; p) = 0, \quad \hat{g}(0; p) = 0, \quad \hat{g}'(0; p) = \beta, \quad \hat{g}'(\infty; p) = 0, \\ \hat{\theta}'(0; p) &= -\gamma_1[1 - \theta(0, p)], \quad \hat{\theta}(\infty, p) = 0, \quad \hat{\phi}(0, p) = 1, \quad \hat{\phi}(\infty, p) = 0\end{aligned}\tag{7.25}$$

$$\begin{aligned}\mathcal{N}_f[\hat{f}(\eta, p), \hat{g}(\eta, p)] &= \frac{\partial^3 \hat{f}(\eta, p)}{\partial \eta^3} - \left( \frac{\partial \hat{f}(\eta, p)}{\partial \eta} \right)^2 + (\hat{f}(\eta, p) + \hat{g}(\eta, p)) \frac{\partial^2 \hat{f}(\eta, p)}{\partial \eta^2} \\ &+ \beta_1 \left[ 2(\hat{f}(\eta, p) + \hat{g}(\eta, p)) \frac{\partial \hat{f}(\eta, p)}{\partial \eta} \frac{\partial^2 \hat{f}(\eta, p)}{\partial \eta^2} \right. \\ &\quad \left. - (\hat{f}(\eta, p) + \hat{g}(\eta, p))^2 \frac{\partial^3 \hat{f}(\eta, p)}{\partial \eta^3} \right] \\ &+ \lambda (\hat{\theta}(\eta, p) + N \hat{\phi}(\eta, p)),\end{aligned}\tag{7.26}$$

$$\begin{aligned}\mathcal{N}_g[\hat{g}(\eta, p), \hat{f}(\eta, p)] &= \frac{\partial^3 \hat{g}(\eta, p)}{\partial \eta^3} - \left( \frac{\partial \hat{g}(\eta, p)}{\partial \eta} \right)^2 + (\hat{f}(\eta, p) + \hat{g}(\eta, p)) \frac{\partial^2 \hat{g}(\eta, p)}{\partial \eta^2} \\ &+ \beta_1 \left[ 2(\hat{f}(\eta, p) + \hat{g}(\eta, p)) \frac{\partial \hat{g}(\eta, p)}{\partial \eta} \frac{\partial^2 \hat{g}(\eta, p)}{\partial \eta^2} \right. \\ &\quad \left. - (\hat{f}(\eta, p) + \hat{g}(\eta, p))^2 \frac{\partial^3 \hat{g}(\eta, p)}{\partial \eta^3} \right],\end{aligned}\tag{7.27}$$

$$\begin{aligned}
\mathcal{N}_\theta[\hat{\theta}(\eta, p), \hat{\phi}(\eta, p), \hat{f}(\eta, p), \hat{g}(\eta, p)] &= \frac{\partial^2 \hat{\theta}(\eta, p)}{\partial \eta^2} + \text{Pr}(\hat{f}(\eta, p) + \hat{g}(\eta, p)) \frac{\partial \hat{\theta}(\eta, p)}{\partial \eta} \\
&+ \text{Pr} D_f \frac{\partial^2 \hat{\phi}(\eta, p)}{\partial \eta^2} \\
&+ \text{Pr} \left( \begin{array}{c} E_1 \left( \frac{\partial^2 \hat{f}(\eta, p)}{\partial \eta^2} \right)^2 \\ + E_2 \left( \frac{\partial^2 \hat{g}(\eta, p)}{\partial \eta^2} \right)^2 \end{array} \right). \tag{7.28}
\end{aligned}$$

$$\begin{aligned}
\mathcal{N}_\phi[\hat{\phi}(\eta, p), \hat{\theta}(\eta, p), \hat{f}(\eta, p), \hat{g}(\eta, p)] &= \frac{\partial^2 \hat{\phi}(\eta, p)}{\partial \eta^2} + Sc(\hat{f}(\eta, p) + \hat{g}(\eta, p)) \frac{\partial \hat{\phi}(\eta, p)}{\partial \eta} \\
&- Sck^* \hat{\phi}(\eta, p) + ScSr \frac{\partial^2 \hat{\theta}(\eta, p)}{\partial \eta^2}. \tag{7.29}
\end{aligned}$$

Here  $p$  is an embedding parameter,  $\hbar_f$ ,  $\hbar_g$ ,  $\hbar_\theta$  and  $\hbar_\phi$  are the non-zero auxiliary parameters and  $\mathcal{N}_f$ ,  $\mathcal{N}_g$ ,  $\mathcal{N}_\theta$  and  $\mathcal{N}_\phi$  indicate the nonlinear operators. When  $p = 0$  and  $p = 1$  one has

$$\begin{aligned}
\hat{f}(\eta; 0) &= f_0(\eta), \quad \hat{\theta}(\eta, 0) = \theta_0(\eta), \quad \hat{\phi}(\eta, 0) = \phi_0(\eta) \\
\hat{f}(\eta; 1) &= f(\eta), \quad \hat{\theta}(\eta, 1) = \theta(\eta), \quad \hat{\phi}(\eta, 1) = \phi(\eta). \tag{7.30}
\end{aligned}$$

Clearly when  $p$  is increased from 0 to 1 then  $f(\eta, p)$ ,  $g(\eta, p)$ ,  $\theta(\eta, p)$  and  $\phi(\eta, p)$  vary from  $f_0(\eta)$ ,  $g_0(\eta)$ ,  $\theta_0(\eta)$  and  $\phi_0(\eta)$  to  $f(\eta)$ ,  $g(\eta)$ ,  $\theta(\eta)$  and  $\phi(\eta)$ . By Taylor's expansion we have

$$f(\eta, p) = f_0(\eta) + \sum_{m=1}^{\infty} f_m(\eta) p^m, \quad f_m(\eta) = \frac{1}{m!} \left. \frac{\partial^m f(\eta; p)}{\partial p^m} \right|_{p=0}, \tag{7.31}$$

$$g(\eta, p) = g_0(\eta) + \sum_{m=1}^{\infty} g_m(\eta) p^m, \quad g_m(\eta) = \frac{1}{m!} \left. \frac{\partial^m g(\eta; p)}{\partial p^m} \right|_{p=0}, \tag{7.32}$$

$$\theta(\eta, p) = \theta_0(\eta) + \sum_{m=1}^{\infty} \theta_m(\eta) p^m, \quad \theta_m(\eta) = \frac{1}{m!} \left. \frac{\partial^m \theta(\eta; p)}{\partial p^m} \right|_{p=0}, \tag{7.33}$$

$$\phi(\eta, p) = \phi_0(\eta) + \sum_{m=1}^{\infty} \phi_m(\eta) p^m, \quad \phi_m(\eta) = \frac{1}{m!} \left. \frac{\partial^m \phi(\eta; p)}{\partial p^m} \right|_{p=0}, \tag{7.34}$$

where the convergence of above series strongly depends upon  $\hbar_f$ ,  $\hbar_g$ ,  $\hbar_\theta$  and  $\hbar_\phi$ . Considering that  $\hbar_f$ ,  $\hbar_g$ ,  $\hbar_\theta$  and  $\hbar_\phi$  are selected properly so that Eqs. (7.31) – (7.34) converge at  $p = 1$  then

we can write

$$f(\eta) = f_0(\eta) + \sum_{m=1}^{\infty} f_m(\eta), \quad (7.35)$$

$$g(\eta) = g_0(\eta) + \sum_{m=1}^{\infty} g_m(\eta), \quad (7.36)$$

$$\theta(\eta) = \theta_0(\eta) + \sum_{m=1}^{\infty} \theta_m(\eta), \quad (7.37)$$

$$\phi(\eta) = \phi_0(\eta) + \sum_{m=1}^{\infty} \phi_m(\eta). \quad (7.38)$$

The resulting problems at  $m$ th order deformation can be constructed as follows:

$$\mathcal{L}_f[f_m(\eta) - \chi_m f_{m-1}(\eta)] = \hbar_f \mathcal{R}_f^m(\eta), \quad (7.39)$$

$$\mathcal{L}_g[g_m(\eta) - \chi_m g_{m-1}(\eta)] = \hbar_g \mathcal{R}_g^m(\eta), \quad (7.40)$$

$$\mathcal{L}_\theta[\theta_m(\eta) - \chi_m \theta_{m-1}(\eta)] = \hbar_\theta \mathcal{R}_\theta^m(\eta), \quad (7.41)$$

$$\mathcal{L}_\phi[\phi_m(\eta) - \chi_m \phi_{m-1}(\eta)] = \hbar_\phi \mathcal{R}_\phi^m(\eta). \quad (7.42)$$

$$\begin{aligned} f_m(0) &= f'_m(0) = f'_m(\infty) = 0, \quad g_m(0) = g'_m(0) = g'_m(\infty) = 0, \quad \theta'_m(0) - \gamma_1 \theta_m(0) = \theta_m(\infty) = 0, \\ \phi_m(0) &= \phi_m(\infty) = 0. \end{aligned} \quad (7.43)$$

$$\begin{aligned} \mathcal{R}_f^m(\eta) &= f'''_{m-1}(\eta) - \sum_{k=0}^{m-1} f'_{m-1-k} f'_k + \sum_{k=0}^{m-1} (f_{m-1-k} f''_k + g_{m-1-k} f''_k) \\ &+ \beta_1 \sum_{k=0}^{m-1} \sum_{l=0}^k (2(f_{m-1-k} + g_{m-1-k}) f'_{k-l} f''_l - (f_{m-1-k} f_{k-l} + g_{m-1-k} g_{k-l} + 2f_{m-1-k} g_{k-l}) f'''_l) \\ &+ \lambda (\theta_{m-1} + N \phi_{m-1}), \end{aligned} \quad (7.44)$$

$$\begin{aligned} \mathcal{R}_g^m(\eta) &= g'''_{m-1}(\eta) - \sum_{k=0}^{m-1} g'_{m-1-k} g'_k + \sum_{k=0}^{m-1} (f_{m-1-k} g''_k + g_{m-1-k} g''_k) \\ &+ \beta_1 \sum_{k=0}^{m-1} \sum_{l=0}^k [2(f_{m-1-k} + g_{m-1-k}) g'_{k-l} g''_l \\ &- (f_{m-1-k} f_{k-l} + g_{m-1-k} g_{k-l} + 2f_{m-1-k} g_{k-l}) g'''_l], \end{aligned} \quad (7.45)$$

$$\begin{aligned}\mathcal{R}_\theta^m(\eta) &= \theta''_{m-1} + Pr \sum_{k=0}^{m-1} (\theta'_{m-1-k} f_k + \theta'_{m-1-k} g_k) + Pr D_f \phi''_{m-1} \\ &\quad + Pr \left( E_1 \sum_{k=0}^{m-1} f''_{m-1-k} f''_k + E_2 \sum_{k=0}^{m-1} g''_{m-1-k} g''_k \right),\end{aligned}\quad (7.46)$$

$$\mathcal{R}_\phi^m(\eta) = \phi''_{m-1} + Sc \sum_{k=0}^{m-1} (\phi'_{m-1-k} f_k + \phi'_{m-1-k} g_k) - Sck^* \phi + ScSr \theta''_{m-1}, \quad (7.47)$$

$$\chi_m = \begin{cases} 0, & m \leq 1, \\ 1, & m > 1. \end{cases} \quad (7.48)$$

Solving the above  $m$ th order deformation problems we have

$$f_m(\eta) = f_m^*(\eta) + C_1 + C_2 e^\eta + C_3 e^{-\eta}, \quad (7.49)$$

$$g_m(\eta) = g_m^*(\eta) + C_4 + C_5 e^\eta + C_6 e^{-\eta}, \quad (7.50)$$

$$\theta_m(\eta) = \theta_m^*(\eta) + C_7 e^\eta + C_8 e^{-\eta}, \quad (7.51)$$

$$\phi_m(\eta) = \phi_m^*(\eta) + C_9 e^\eta + C_{10} e^{-\eta}, \quad (7.52)$$

in which the  $f_m^*$ ,  $g_m^*$ ,  $\theta_m^*$  and  $\phi_m^*$  indicate the special solutions.

### 7.3 Analysis and discussion

Obviously the homotopic solutions (7.35) – (7.38) involve the auxiliary parameters  $\hbar_f$ ,  $\hbar_g$ ,  $\hbar_\theta$  and  $\hbar_\phi$ . These parameters have pivotal role in adjusting and controlling the convergence of homotopic solutions. Hence the  $\hbar$ -curves are displayed at 18<sup>th</sup> order of approximations in order to determine the suitable ranges of  $\hbar_f$ ,  $\hbar_g$ ,  $\hbar_\theta$  and  $\hbar_\phi$ . Fig. 7.2 witness that the admissible values of  $\hbar_f$ ,  $\hbar_g$ ,  $\hbar_\theta$  and  $\hbar_\phi$  here are  $-1.25 \leq \hbar_f \leq -0.50$ ,  $-1.25 \leq \hbar_g \leq -0.50$ ,  $-1.40 \leq \hbar_\theta \leq -0.25$  and  $-1.20 \leq \hbar_\phi \leq -0.75$ . Table 7.1 ensures that the developed series solutions converge in the whole region of  $\eta$  when  $\hbar_f = \hbar_g = \hbar_\theta = \hbar_\phi = -1$ .

**Table 7.1:** Convergence of series solutions for different order of approximations when  $\beta_1 = 0.2$ ,  $\beta = 0.3$ ,  $Pr = 1.0$ ,  $Sr = 0.4$ ,  $D_f = 0.5$ ,  $Sc = 0.5$ ,  $k^* = 0.3$ ,  $\gamma_1 = 0.6$  and  $\hbar_f = \hbar_g =$



$$\hbar_\theta = \hbar_\phi = -1.0.$$

order of approximations	1	5	10	15	20	25	30	35
$-f''(0)$	1.1215	1.1323	1.1323	1.1323	1.1323	1.1323	1.1323	1.1323
$-g''(0)$	0.25735	0.25958	0.25951	0.25951	0.25951	0.25951	0.25951	0.25951
$-\theta'(0)$	0.24141	0.22468	0.22127	0.22061	0.22045	0.22041	0.22040	0.22040
$-\phi'(0)$	0.64583	0.56841	0.55948	0.55838	0.55820	0.55817	0.55816	0.55816

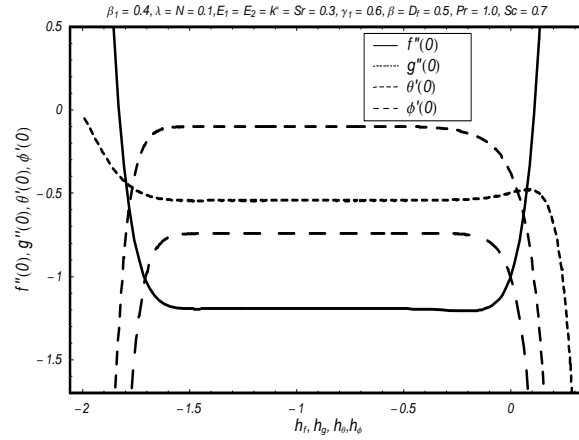


Fig.7.2:  $\hbar$ -curves for the function  $f, g, \theta$  and  $\phi$ .

Figs. 7.3 and 7.4 depict the behaviors of mixed convection parameter  $\lambda$  and concentration buoyancy parameter  $N$  on the velocity profile  $f'(\eta)$ . Fig. 7.3 is drawn to see the effect of mixed convection parameter  $\lambda$  on velocity profile  $f'(\eta)$ . It is noticed that momentum boundary layer thickness and velocity profile  $f'(\eta)$  increase with an increase in mixed convection parameter in case of assisting flow ( $\lambda > 0$ ) while reverse effect is noted in case of opposing flow ( $\lambda < 0$ ). This is due to the fact that buoyancy forces are more dominant to viscous forces in case of assisting flow ( $\lambda > 0$ ) while buoyancy forces reduce for opposing flow ( $\lambda < 0$ ). Effect of concentration buoyancy parameter  $N$  on the velocity profile  $f'(\eta)$  is analyzed in Fig. 7.4. It is seen that both the momentum boundary layer thickness and velocity profile  $f'(\eta)$  are increasing functions of

concentration buoyancy parameter  $N$ .

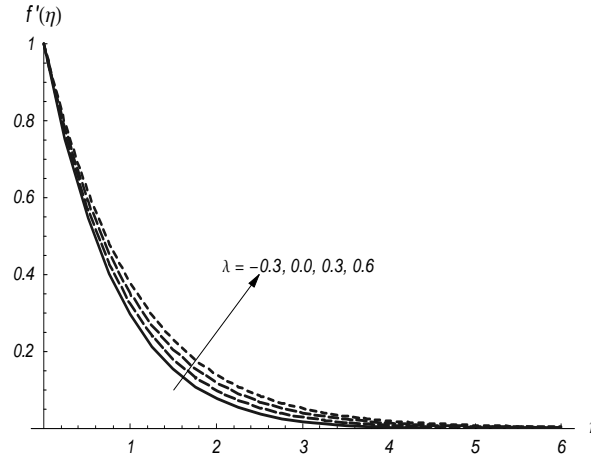


Fig. 7.3: Influence of  $\lambda$  on  $f'(\eta)$  when  $N = E_1 = E_2 = 0.3$  and  $\beta_1 = 0.5$ .

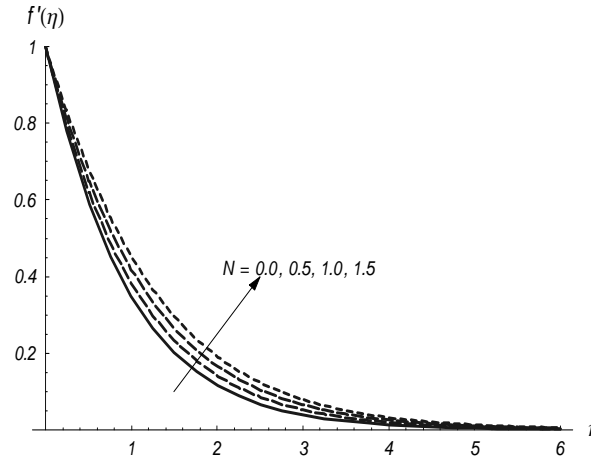


Fig. 7.4: Influence of  $N$  on  $f'(\eta)$  when  $\beta = \lambda = E_1 = E_2 = 0.3$  and  $\beta_1 = 0.5$ .

Figs. 7.5–7.9 examine the variation of Dufour number  $D_f$ , Eckert numbers  $E_1$  and  $E_2$ , mixed convection parameter  $\lambda$  and concentration buoyancy parameter  $N$  on the temperature  $\theta(\eta)$ . Effect of Dufour number  $D_f$  on temperature profile  $\theta(\eta)$  is presented in Fig. 7.5. As Dufour effect pointed out the generation of energy flux by composition gradient, then the thermal boundary layer thickness and temperature  $\theta(\eta)$  increase with an increase in  $D_f$ . Figs. 7.6 and 7.7 illustrate the effect of Eckert numbers  $E_1$  and  $E_2$  on the temperature  $\theta(\eta)$  along the  $x$  and  $y$  directions respectively. As the Eckert number expresses the relationship between the

kinetic energy in the flow and the enthalpy. It embodies the conversion of kinetic energy into internal energy by work done against the viscous fluid stresses. Greater viscous dissipative heat causes a rise in the temperature and thermal boundary layer thickness. Fig. 7.8 is drawn to see the influence of mixed convection parameter  $\lambda$  on the temperature  $\theta(\eta)$ . Thermal boundary layer thickness and temperature  $\theta(\eta)$  decrease in case of assisting flow ( $\lambda > 0$ ) while increase in case of opposing flow ( $\lambda < 0$ ). This is due to the fact that in case of assisting flow ( $\lambda > 0$ ) the buoyancy forces are more dominant to viscous forces which causes a reduction in the temperature  $\theta(\eta)$  while in case of opposing flow ( $\lambda < 0$ ) the viscous forces are more dominant than buoyancy forces which in results enhances the temperature  $\theta(\eta)$ . Influence of concentration buoyancy parameter  $N$  on the temperature  $\theta(\eta)$  is seen in Fig. 7.9. It is found that the associated boundary layer and temperature  $\theta(\eta)$  is decreasing function of  $N$ .

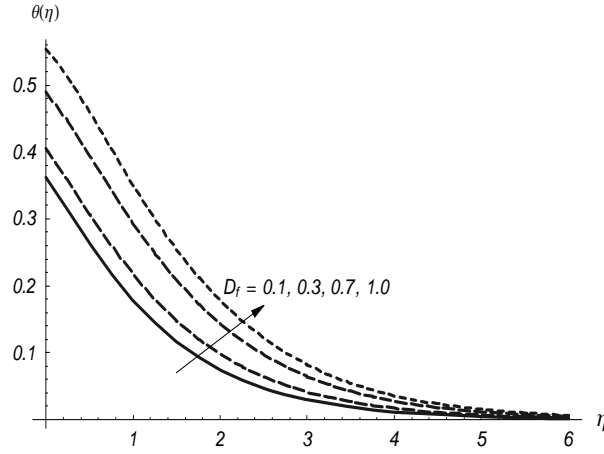


Fig. 7.5: Influence of  $D_f$  on  $\theta(\eta)$  when  $\beta_1 = k^* = 0.5, Pr = Sr = 0.5$

$$\lambda = E_1 = E_2 = N = \beta = Sc = 0.3 \text{ and } \gamma_1 = 0.4.$$

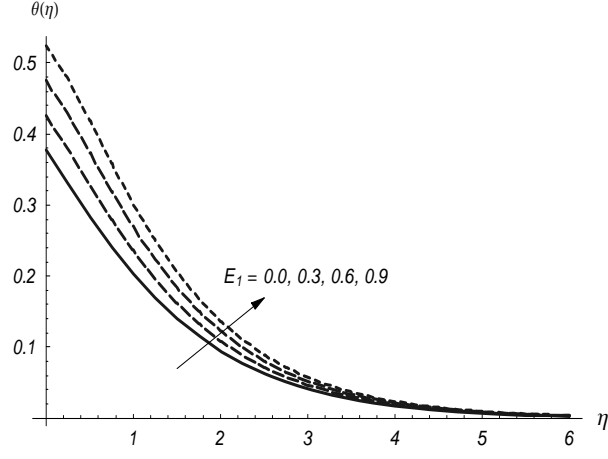


Fig. 7.6: Influence of  $E_1$  on  $\theta(\eta)$  when  $\beta_1 = k^* = 0.5, Pr = Sr = 0.5$ ,

$$\lambda = D_f = E_2 = N = \beta = Sc = 0.3 \text{ and } \gamma_1 = 0.4.$$

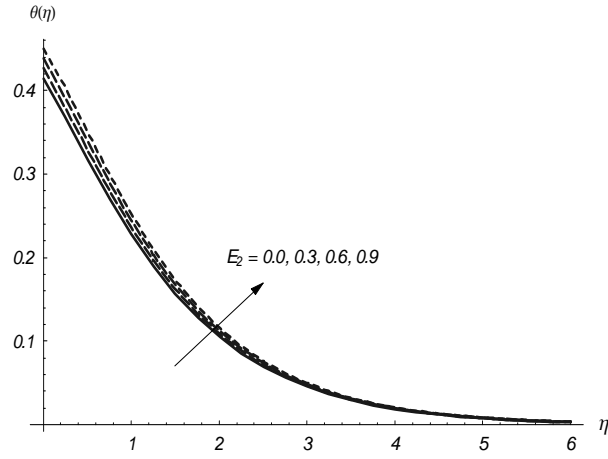


Fig. 7.7: Influence of  $E_2$  on  $\theta(\eta)$  when  $\beta_1 = k^* = 0.5, Pr = Sr = 0.5$

$$\lambda = D_f = E_1 = N = \beta = Sc = 0.3 \text{ and } \gamma_1 = 0.4.$$

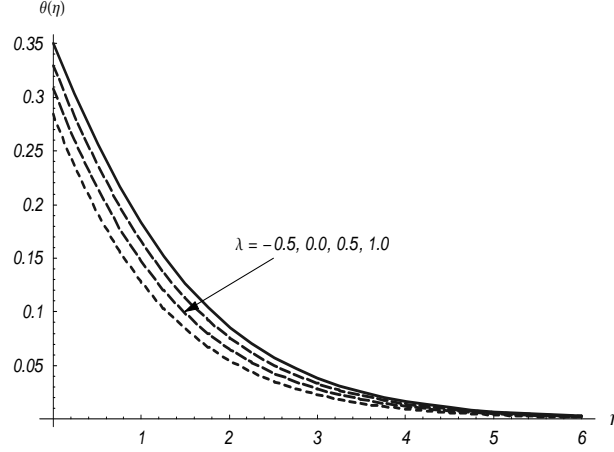


Fig. 7.8: Influence of  $\lambda$  on  $\theta(\eta)$  when  $\beta_1 = k^* = 0.5$ ,  $Pr = Sr = 0.5$

$$D_f = E_1 = E_2 = N = \beta = Sc = 0.3 \text{ and } \gamma_1 = 0.4.$$

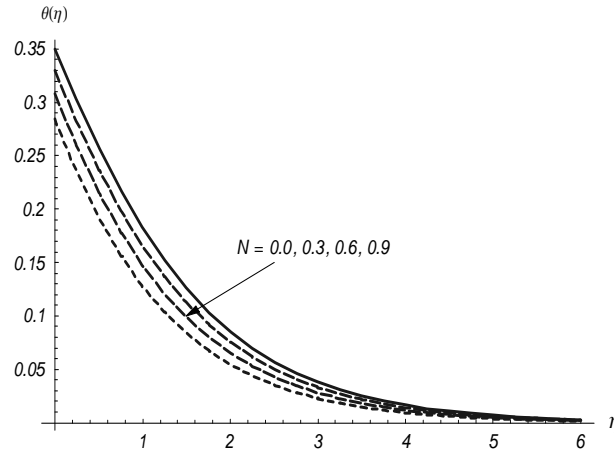


Fig.7.9: Influence of  $N$  on  $\theta(\eta)$  when  $\beta_1 = k^* = 0.5$ ,  $Pr = Sr = 0.5$

$$D_f = E_1 = E_2 = \lambda = \beta = Sc = 0.3 \text{ and } \gamma_1 = 0.4.$$

Figs. 7.10-7.13 are sketched to see the effects of Soret number  $Sr$ , generative/destructive chemical reaction  $k^*$ , mixed convection parameter  $\lambda$  and concentration buoyancy parameter  $N$  on concentration profile  $\phi(\eta)$ . Fig. 7.10 depicts the influence of Soret number  $Sr$  on concentration profile  $\phi(\eta)$ . As in Soret effect the temperature gradient causes the mass flux which in turn enhances the concentration profile  $\phi(\eta)$  and associated boundary layer thickness. Effect of destructive/generative chemical reaction  $k^*$  on the concentration profile  $\phi(\eta)$  is analyzed in

Fig. 11. It is found that in case of generative chemical reaction ( $k^* < 0$ ) the reduction in  $\phi(\eta)$  is noted while reverse is in case of destructive chemical reaction ( $k^* > 0$ ). Figs. 7.12 and 7.13 are presented to see the effects of mixed convection parameter  $\lambda$  and concentration buoyancy parameter  $N$  on the concentration profile  $\phi(\eta)$ . These Figs. show that  $\phi(\eta)$  reduces with the increase in  $\lambda$  and  $N$ . Also the associated boundary layer thickness are decreasing functions of  $\lambda$  and  $N$ .

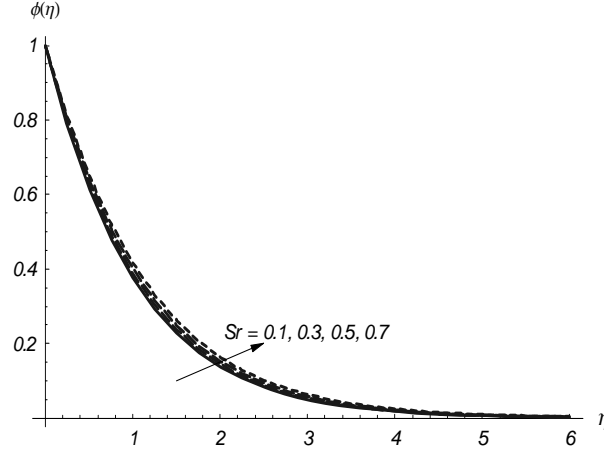


Fig. 7.10: Influence of  $Sr$  on  $\phi(\eta)$  when  $\beta_1 = k^* = 0.5, Pr = 0.5, \gamma_1 = 0.4$ ,

$$D_f = E_1 = E_2 = \lambda = N = \beta = Sc = 0.3,$$

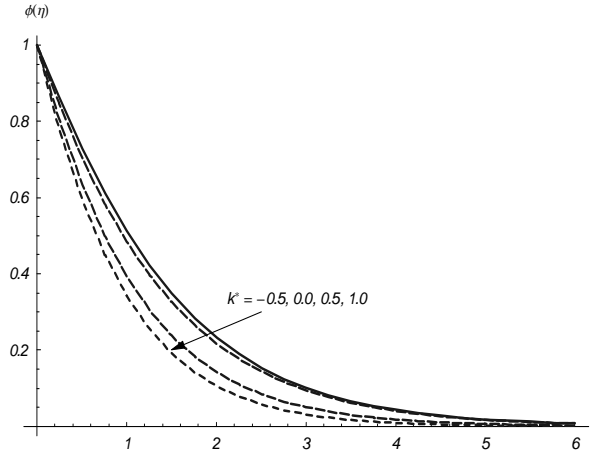


Fig. 7.11: Influence of  $k^*$  on  $\phi(\eta)$  when  $\beta_1 = 0.5, Pr = Sr = 0.5$ ,

$$D_f = E_1 = E_2 = \lambda = N = \beta = Sc = 0.3 \text{ and } \gamma_1 = 0.4.$$

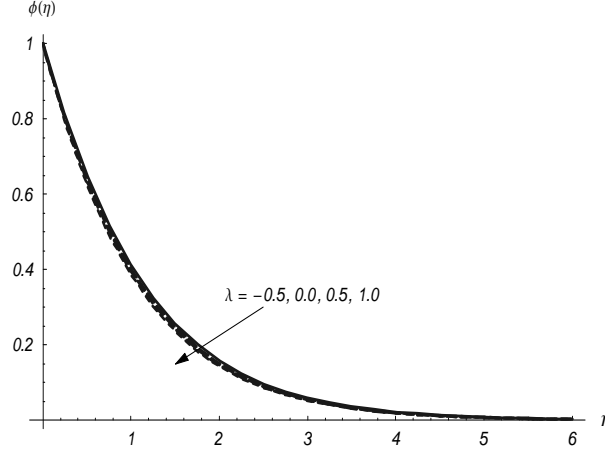


Fig. 7.12: Influence of  $\lambda$  on  $\phi(\eta)$  when  $\beta_1 = k^* = 0.5$ ,  $Pr = Sr = 0.5$ ,

$$D_f = E_1 = E_2 = N = \beta = Sc = 0.3 \text{ and } \gamma_1 = 0.4.$$

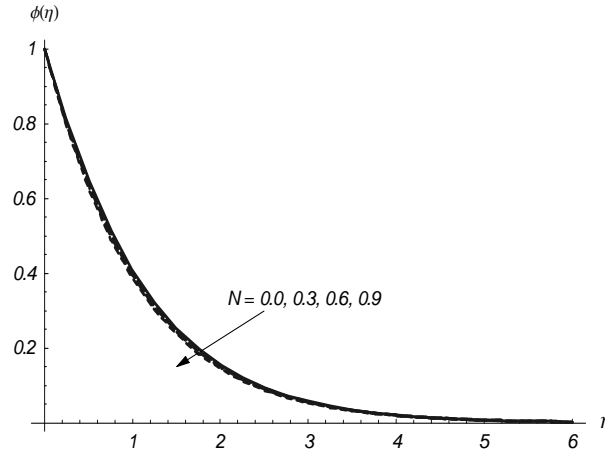


Fig. 7.13: Influence of  $N$  on  $\phi(\eta)$  when  $\beta_1 = k^* = 0.5$ ,  $Pr = Sr = 0.5$ ,

$$D_f = E_1 = E_2 = \lambda = \beta = Sc = 0.3 \text{ and } \gamma_1 = 0.4.$$

Table 7.1 presents the convergence of homotpic solutions. It is noted that computations are sufficient for  $15^{th}$  order iterations of velocity and  $35^{th}$  order iterations of the temperature and concentration profiles for convergent series solutions. Tables 7.2 and 7.3 are prepared to analyze numerical values of local Nusselt and Sherwood numbers. The values of  $-\theta'(0)$  and  $-\phi'(0)$  decrease by increasing Deborah number, mixed convection parameter and concentration buoyancy parameter. Here  $-\theta'(0)$  increases by increasing Prandtl number and Biot number

while reverse is the case of  $-\phi'(0)$ . It is also found that  $-\theta'(0)$  decreases by increasing Eckert numbers while opposite behavior of  $-\phi'(0)$ . Table 7.4 presents the comparison of  $-f''(0)$  and  $-g''(0)$  for various values of  $\beta$  in the limiting sense with ref. [13]. Table 7.5 ensures the values of local Nusselt number  $-\theta'(0)$  are in good agreement with ref. [39] in a limiting sense.

**Table 7.2:** Values of local Nusselt  $-\theta'(0)$  and Sherwood numbers  $-\phi'(0)$  for the different



values of the parameters  $\beta_1, \beta, Sc, Sr, D_f, k^*, Pr$  and  $\gamma_1$  when  $\lambda = N = E_1 = E_2 = 0.3$ .

$\beta_1$	$\beta$	$Pr$	$\gamma_1$	$Sc$	$Sr$	$D_f$	$k^*$	$-\theta'(0)$	$-\phi'(0)$
0.0	0.2	0.7	0.4	0.5	0.4	0.5	0.3	0.16023	0.56411
0.2								0.15399	0.55548
0.4								0.14858	0.54795
0.2	0.0							0.14266	0.53103
	0.2							0.15399	0.55548
	0.4							0.16269	0.57666
0.2	0.2	0.4						0.13249	0.55814
		0.8						0.16009	0.55462
		1.2						0.17597	0.55212
0.2	0.2	0.7	0.2					0.098922	0.56163
			0.4					0.15319	0.55548
			0.6					0.18962	0.55150
0.2	0.2	0.7	0.4	0.0				0.20797	0.11228
				0.5				0.15399	0.55548
				1.0				0.11405	0.85681
0.2	0.2	0.7	0.4	0.5	0.0			0.15406	0.56553
					0.5			0.15457	0.55288
					1.0			0.15565	0.53984
0.2	0.2	0.7	0.4	0.5	0.5	0.2		0.19480	0.54212
						0.5		0.15469	0.55287
						1.0		0.084902	0.57214
0.2	0.2	0.7	0.4	0.5	0.5	0.5	0.0	0.18113	0.35157
							0.3	0.15469	0.55212
							0.5	0.14153	0.65090

**Table 7.3:** Values of local Nusselt  $-\theta'(0)$  and Sherwood numbers  $-\phi'(0)$  for the different values of the parameters  $\lambda, N, E_1$  and  $E_2$  when  $\beta_1 = \beta = 0.2, Sc = D_f = 0.5, Sr = \gamma_1 = 0.4,$

$Pr = 0.7$  and  $k^* = 0.3$ .

$\lambda$	$N$	$E_1$	$E_2$	$-\theta'(0)$	$-\phi'(0)$
-0.3	0.3	0.3	0.3	0.0091701	0.71369
0.0				0.091253	0.73788
0.3				0.12419	0.75068
0.3	0.0			0.11837	0.74820
	0.3			0.12444	0.75042
	0.6			0.12978	0.75260
0.3	0.3	0.0		0.18952	0.73121
		0.1		0.16745	0.73772
		0.2		0.14557	0.74431
0.3	0.3	0.3	0.0	0.14414	0.74474
			0.1	0.13777	0.74657
			0.2	0.13110	0.74854

**Table 7.4:** Values of  $-f''(0)$  and  $-g''(0)$  with  $\beta$  when  $\beta_1 = \lambda = N = 0$  with HPM (Ariel [13])

and exact solution (Ariel [13]).

$\beta$	$-f''(0)$			$-g''(0)$		
	HAM	HPM[13]	Exact[13]	HAM	HPM[13]	Exact[13]
0.0	1	1	1	0	0	0
0.1	1.020260	1.017027	1.020260	0.066847	0.073099	0.066847
0.2	1.039495	1.034587	1.039495	0.148737	0.158231	0.148737
0.3	1.057955	1.052470	1.057955	0.243360	0.254347	0.243360
0.4	1.075788	1.070529	1.075788	0.349208	0.360599	0.349209
0.5	1.093095	1.088662	1.093095	0.465205	0.476290	0.465205
0.6	1.109946	1.106797	1.109947	0.590528	0.600833	0.590529
0.7	1.126397	1.124882	1.126398	0.724532	0.733730	0.724532
0.8	1.142488	1.142879	1.142489	0.866682	0.874551	0.866683
0.9	1.158254	1.160762	1.158254	1.016539	1.022922	1.016539
1.0	1.173720	1.178511	1.173721	1.173720	1.178511	1.173721

**Table 7.5:** Values of local Nusselt number  $-\theta'(0)$  for different values of  $\beta^*, \beta$  and Pr in a

limiting sense when  $\lambda = N = E_1 = E_2 = D_f = Sr = k^* = 0.0$  and  $\gamma_1 = 0.6$ .

$\beta_1$	$\beta$	Pr	Present Results	Hayat et al [39]
			$-\theta'(0)$	$-\theta'(0)$
0.0	0.5	1.0	0.330404	0.33040
0.3			0.321661	0.32160
0.8			0.308651	0.30799
1.2			0.299526	0.29873
0.4	0.0		0.287813	0.28908
	0.4		0.316638	0.31664
	0.7		0.330168	0.33017
	1.0		0.340702	0.34070
0.4	0.5	0.7	0.282787	0.28279
		1.2	0.340424	0.34042
		1.6	0.368405	0.36840
		2.0	0.388869	0.38887

## 7.4 Conclusions

Three dimensional mixed convection flow of Maxwell fluid over a stretching surface with convective condition is investigated. Effects of chemical reaction and Soret and Dufour are analyzed. The main observations are listed below.

- Momentum boundary layer thickness and velocity profile  $f'(\eta)$  increase with the increase in  $\lambda$  and  $N$ .
- Concentration profile  $\phi(\eta)$  is decreasing function of generative chemical reaction parameter ( $k^* > 0$ ) while increasing function of destructive chemical reaction ( $k^* < 0$ ) and Soret number  $Sr$ .
- Influences of  $\lambda$  and  $N$  on  $\theta(\eta)$  and  $\phi(\eta)$  are qualitatively similar.
- Thermal boundary layer thickness and temperature field increase when  $D_f$  increases.

- There are opposite effects of local Nusselt number and local Sherwood number when  $D_f$ ,  $Sr$ ,  $E_1$  and  $E_2$  increase.
- Local Nusselt and Sherwood numbers increase when  $k^*$ ,  $D_f$  and  $Sc$  are enhanced.
- Effects of local Nusselt number and local Sherwood number for  $Pr$ ,  $Sr$ ,  $\lambda$  and  $N$  are similar.

## Chapter 8

# Radiative mixed convection flow of an Oldroyd-B fluid by an inclined stretching surface

Mixed convection flow of an Oldroyd-B fluid in the presence of thermal radiation is investigated in this chapter. Flow is induced by an inclined stretching surface. The boundary layer equations of an Oldroyd-B fluid in the presence of heat transfer are used. Appropriate transformations reduce the partial differential equations into the ordinary differential equations. Computational analysis is performed for the convergent series solutions. The values of local Nusselt number are numerically analyzed. Effects of various parameters involved in the velocity and temperature are discussed.

### 8.1 Mathematical analysis

Consider the steady two-dimensional mixed convection flow of an incompressible Oldroyd-B fluid by an inclined stretching surface. The heat transfer is considered in the presence of thermal radiation using Rosseland approximation. Here  $x$ -axis is taken along the stretching surface and  $y$ -axis normal to the  $x$ -axis. Conservation laws of mass, linear momentum and energy in absence of viscous dissipation give

$$\frac{\partial u}{\partial x} + \frac{\partial v}{\partial y} = 0, \quad (8.1)$$

$$\begin{aligned} u \frac{\partial u}{\partial x} + v \frac{\partial u}{\partial y} = & \nu \frac{\partial^2 u}{\partial y^2} - \lambda_1 \left[ u^2 \frac{\partial^2 u}{\partial x^2} + v^2 \frac{\partial^2 u}{\partial y^2} + 2uv \frac{\partial^2 u}{\partial x \partial y} \right] \\ & + \nu \lambda_2 \left[ u \frac{\partial^3 u}{\partial x \partial y^2} + v \frac{\partial^3 u}{\partial y^3} - \frac{\partial u}{\partial x} \frac{\partial^2 u}{\partial y^2} - \frac{\partial u}{\partial y} \frac{\partial^2 v}{\partial y^2} \right] + g\beta_T(T - T_\infty) \cos \alpha, \end{aligned} \quad (8.2)$$

$$\rho c_p \left( u \frac{\partial T}{\partial x} + v \frac{\partial T}{\partial y} \right) = \frac{\partial}{\partial y} \left( \left( \frac{16\sigma_s T_\infty^3}{3k_e} + k \right) \frac{\partial T}{\partial y} \right), \quad (8.3)$$

where  $u$  and  $v$  are the velocity components in the  $x$ - and  $y$ -directions,  $\lambda_1$  and  $\lambda_2$  are the relaxation and retardation times, respectively,  $\nu = (\mu/\rho)$  is the kinematic viscosity,  $\sigma_s$  is the Stefan-Boltzmann constant,  $T$  is the fluid temperature,  $\rho$  is the fluid density,  $g$  is the gravitational acceleration,  $\beta_T$  is thermal expansion coefficient of temperature,  $c_p$  is the specific heat,  $k_e$  is the mean absorption coefficient and  $k$  is the thermal conductivity.

The appropriate boundary conditions are taken as follows:

$$u = cx, \quad v = 0, \quad T = T_w \text{ at } y = 0, \quad (8.4)$$

$$u \rightarrow 0, \quad T \rightarrow T_\infty \text{ as } y \rightarrow \infty \quad (8.5)$$

with the surface temperature  $T_w$  by

$$T_w(x, t) = T_\infty + bx, \quad (8.6)$$

where  $b$  and  $c$  are the positive constants. If  $\psi$  is the stream function then defining

$$\eta = \sqrt{\frac{c}{\nu}} y, \quad \psi = \sqrt{c\nu} x f(\eta), \quad \theta(\eta) = \frac{T - T_\infty}{T_w - T_\infty}, \quad (8.7)$$

$$u = \frac{\partial \psi}{\partial y}, \quad v = -\frac{\partial \psi}{\partial x}, \quad (8.8)$$

the incompressibility condition is clearly satisfied and the resulting problems for  $f$  and  $\theta$  satisfy the following equations

$$f''' + f f'' - f'^2 + \beta_1(2f f' f'' - f^2 f''') - \beta_2(f''^2 - f f'''' ) + \lambda \theta \cos \alpha = 0, \quad (8.9)$$

$$\left(1 + \frac{4}{3}R\right) \theta'' + \text{Pr} (f \theta' - f' \theta) = 0, \quad (8.10)$$

$$f(0) = 0, \quad f'(0) = 1, \quad f'(\infty) \rightarrow 0, \quad \theta(0) = 1, \quad \theta(\infty) \rightarrow 0. \quad (8.11)$$

In the above expressions  $\beta_1$  and  $\beta_2$  are the Deborah numbers,  $\lambda$  is mixed convection parameter,  $Gr_x$  is the local Grashof number,  $Re_x$  is the Reynold number,  $\text{Pr}$  is the Prandtl number,  $R$  is the radiation parameter and primes indicate the differentiation with respect to  $\eta$  i.e.

$$\begin{aligned} \beta_1 &= \lambda_1 c, \quad \beta_2 = \lambda_2 c, \quad \lambda = \frac{Gr_x}{Re_x^2}, \quad Gr_x = \frac{g \beta (T_w - T_\infty) x^3}{\nu^2}, \quad Re_x = \frac{u_w^2 x^2}{\nu^2}, \\ \text{Pr} &= \frac{\mu c_p}{k}, \quad R = \left( \frac{4 \sigma_s T_\infty^3}{k_e k} \right). \end{aligned} \quad (8.12)$$

Local Nusselt number  $Nu_x$  in terms of heat transfer  $q_w$  is

$$Nu_x = \frac{x q_w}{k(T_w - T_\infty)}, \quad q_w = -k \left( \frac{\partial T}{\partial y} \right)_{y=0}. \quad (8.13)$$

Above equation in dimensionless variables becomes

$$Nu/Re_x^{1/2} = -(1 + \frac{4}{3}R) \theta'(0). \quad (8.14)$$

Considering the set of base functions

$$\left\{ \eta^k \exp(-n\eta) | k \geq 0, n \geq 0 \right\} \quad (8.15)$$

one can express that

$$f_m(\eta) = \sum_{n=0}^{\infty} \sum_{k=0}^{\infty} a_{m,n}^k \eta^k \exp(-n\eta), \quad (8.16)$$

$$\theta_m(\eta) = \sum_{n=0}^{\infty} \sum_{k=0}^{\infty} b_{m,n}^k \eta^k \exp(-n\eta), \quad (8.17)$$

where  $a_{m,n}$  and  $b_{m,n}$  are the coefficients.



Initial guesses  $f_0$  and  $\theta_0$  and auxiliary linear operators  $\hbar_f$  and  $\hbar_\theta$  are chosen as follows:

$$f_0(\eta) = 1 - \exp(-\eta), \quad \theta_0(\eta) = \exp(-\eta), \quad (8.18)$$

$$\mathcal{L}_f = \frac{d^3 f}{d\eta^3} - \frac{df}{d\eta}, \quad \mathcal{L}_\theta = \frac{d^2 \theta}{d\eta^2} - \theta, \quad (8.19)$$

where

$$\mathcal{L}_f [C_1 + C_2 \exp(\eta) + C_3 \exp(-\eta)] = 0, \quad \mathcal{L}_\theta [C_4 \exp(\eta) + C_5 \exp(-\eta)] = 0 \quad (8.20)$$

in which  $C_i$  ( $i = 1 - 5$ ) are the arbitrary constants. Introducing  $p \in [0, 1]$  as the embedding parameter and  $\hbar_f$  and  $\hbar_\theta$  the non-zero auxiliary parameters, the deformation problems at the zeroth order are

$$(1 - p)\mathcal{L}_f[\hat{f}(\eta, p) - f_0(\eta)] = p\hbar_f \mathcal{N}_f [\hat{f}(\eta, p), \hat{\theta}(\eta, p)], \quad (8.21)$$

$$(1 - p)\mathcal{L}_\theta[\hat{\theta}(\eta, p) - \theta_0(\eta)] = p\hbar_\theta \mathcal{N}_\theta [\hat{f}(\eta, p), \hat{\theta}(\eta, p)], \quad (8.22)$$

$$\hat{f}(\eta; p)\Big|_{\eta=0} = 0, \quad \frac{\partial \hat{f}(\eta; p)}{\partial \eta}\Big|_{\eta=0} = 1, \quad \frac{\partial \hat{f}(\eta; p)}{\partial \eta}\Big|_{\eta=\infty} = 0, \quad (8.23)$$

$$\hat{\theta}(\eta; p)\Big|_{\eta=0} = 1, \quad \hat{\theta}(\eta; p)\Big|_{\eta=\infty} = 0, \quad (8.24)$$

$$\begin{aligned} \mathcal{N}_f[\hat{f}(\eta, p), \hat{\theta}(\eta, p)] &= \frac{\partial^3 \hat{f}(\eta, p)}{\partial \eta^3} - \hat{f}(\eta, p) \frac{\partial^2 \hat{f}(\eta, p)}{\partial \eta^2} - \left( \frac{\partial \hat{f}(\eta, p)}{\partial \eta} \right)^2 \\ &+ \beta_1 \left[ 2\hat{f}(\eta, p) \frac{\partial \hat{f}(\eta, p)}{\partial \eta} \frac{\partial^2 \hat{f}(\eta, p)}{\partial \eta^2} - (\hat{f}(\eta, p))^2 \frac{\partial^3 \hat{f}(\eta, p)}{\partial \eta^3} \right] \\ &+ \beta_2 \left[ \left( \frac{\partial^2 \hat{f}(\eta, p)}{\partial \eta^2} \right)^2 - \hat{f}(\eta, p) \frac{\partial^4 \hat{f}(\eta, p)}{\partial \eta^4} \right] \\ &+ \lambda \hat{\theta}(\eta, p) \cos \alpha, \end{aligned} \quad (8.25)$$

$$\mathcal{N}_\theta [\hat{f}(\eta; p), \hat{\theta}(\eta; p)] = \left( 1 + \frac{4}{3}R \right) \frac{\partial^2 \hat{\theta}(\eta, p)}{\partial \eta^2} + \text{Pr} \left( \hat{f}(\eta; p) \frac{\partial \hat{\theta}(\eta; p)}{\partial \eta} - \hat{\theta}(\eta; p) \frac{\partial \hat{f}(\eta; p)}{\partial \eta} \right). \quad (8.26)$$

For  $p = 0$  and  $p = 1$ , we have

$$\widehat{f}(\eta; 0) = f_0(\eta), \quad \widehat{f}(\eta; 1) = f(\eta), \quad (8.27)$$

$$\widehat{\theta}(\eta; 0) = \theta_0(\eta), \quad \widehat{\theta}(\eta; 1) = \theta(\eta) \quad (8.28)$$

and when  $p$  increases from 0 to 1 then  $\widehat{f}(\eta; p)$  and  $\widehat{\theta}(\eta; p)$  deform from  $f_0(\eta)$  and  $\theta_0(\eta)$  to  $f(\eta)$  and  $\theta(\eta)$  respectively. Further Taylor series expansion yields

$$\widehat{f}(\eta; p) = f_0(\eta) + \sum_{m=1}^{\infty} f_m(\eta) p^m, \quad (8.29)$$

$$\widehat{\theta}(\eta; p) = \theta_0(\eta) + \sum_{m=1}^{\infty} \theta_m(\eta) p^m, \quad (8.30)$$

$$f_m(\eta) = \frac{1}{m!} \left. \frac{\partial^m \widehat{f}(\eta; p)}{\partial p^m} \right|_{p=0}, \quad \theta_m(\eta) = \frac{1}{m!} \left. \frac{\partial^m \widehat{\theta}(\eta; p)}{\partial p^m} \right|_{p=0}. \quad (8.31)$$

The auxiliary parameters  $\hbar_f$  and  $\hbar_\theta$  are selected such that the series (8.29) and (8.30) converge at  $p = 1$ . Hence

$$f(\eta) = f_0(\eta) + \sum_{m=1}^{\infty} f_m(\eta), \quad \theta(\eta) = \theta_0(\eta) + \sum_{m=1}^{\infty} \theta_m(\eta). \quad (8.32)$$

The corresponding problems at  $m$ th order are given by

$$\mathcal{L}_f [f_m(\eta) - \chi_m f_{m-1}(\eta)] = \hbar_f \mathcal{R}_m^f(\eta), \quad \mathcal{L}_\theta [\theta_m(\eta) - \chi_m \theta_{m-1}(\eta)] = \hbar_\theta \mathcal{R}_m^\theta(\eta), \quad (8.33)$$

$$\begin{aligned} f_m(0) &= 0, \quad f'_m(0) = 0, \quad f'_m(\infty) = 0, \\ \theta_m(0) &= 0, \quad \theta_m(\infty) = 0, \quad \phi_m(0) = 0, \quad \phi_m(\infty) = 0, \end{aligned} \quad (8.34)$$

$$\begin{aligned}
\mathcal{R}_f^m(\eta) &= f_{m-1}'''(\eta) + \sum_{k=0}^{m-1} \left[ f_{m-1-k} f_k'' - f_{m-1-k}' f_k'' \right] \\
&+ \beta_1 \sum_{k=0}^{m-1} f_{m-1-k} \sum_{l=0}^k \{ 2f_{k-l}' f_l'' - f_{k-l} f_l''' - \lambda f_{m-1}'(\eta) \} \\
&+ \beta_2 \{ f_{m-1-k}' \sum_{k=0}^{m-1} f_k' - f_{m-1-k} \sum_{k=0}^{m-1} f_k^{iv} \} + \lambda \theta \cos \alpha,
\end{aligned} \tag{8.35}$$

$$\mathcal{R}_m^\theta(\eta) = \left( 1 + \frac{4}{3}R \right) \theta_{m-1}'' + \text{Pr} \sum_{k=0}^{m-1} (f_{m-1-k} \theta_k' - f_{m-1-k}' \theta_k) \tag{8.36}$$

$$\chi_m = \begin{cases} 0, & m \leq 1 \\ 1, & m > 1 \end{cases}. \tag{8.37}$$

The general solutions of Eq. (8.32) can be written as follows:

$$f_m(\eta) = f_m^*(\eta) + C_1 + C_2 \exp(\eta) + C_3 \exp(-\eta), \tag{8.38}$$

$$\theta_m(\eta) = \theta_m^*(\eta) + C_4 \exp(\eta) + C_5 \exp(-\eta), \tag{8.39}$$

where the special solutions are  $f_m^*(\eta)$  and  $\theta_m^*(\eta)$  and

$$\begin{aligned}
C_2 &= C_4 = 0, \\
C_1 &= -C_3 - f_m^*(0), \quad C_3 = \left. \frac{\partial f_m^*(\eta)}{\partial \eta} \right|_{\eta=0}, \\
C_5 &= -\theta_m^*(0).
\end{aligned} \tag{8.40}$$

## 8.2 Convergence of the series solutions

Clearly the series solutions contain the non-zero auxiliary parameters  $\hbar_f$  and  $\hbar_\theta$ . Hence the  $\hbar_f$  and  $\hbar_\theta$  curves are plotted for 20th-order of approximation in order to find the admissible values of  $\hbar_f$  and  $\hbar_\theta$ . It is found that the admissible values of  $\hbar_f$  and  $\hbar_\theta$  are  $-1.4 \leq \hbar_f$ ,  $\hbar_\theta \leq -0.25$  (Fig. 8.1). The series given by Eq. (8.36) converges in the whole region of  $\eta$  when  $\hbar_f = \hbar_\theta = -0.6$ .

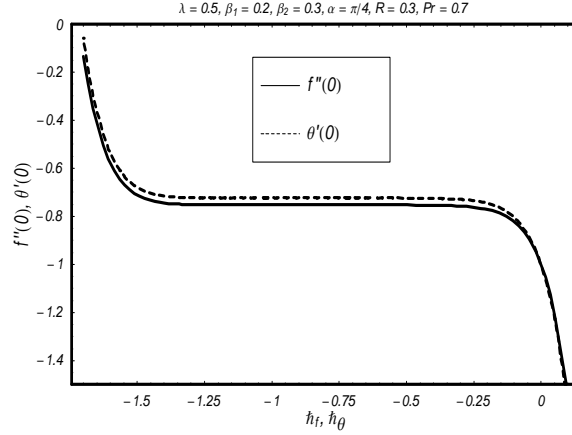


Fig.8.1:  $h$ -curves for the function  $f$  and  $\theta$ .

### 8.3 Discussion

This section examines the influence of physical parameters on the velocity  $f'(\eta)$  and temperature  $\theta(\eta)$ . Figs. 8.2 – 8.9 depict the graphical effects of inclination  $\alpha$ , Deborah numbers  $\beta_1$  and  $\beta_2$  and mixed convection parameter  $\lambda$ . Figs. 8.2 and 8.3 depict that fluid velocity decreases while the fluid temperature increases with the increase of inclination parameter  $\alpha$ . It is also observed that momentum boundary layer thickness is a decreasing function of  $\alpha$  while thermal boundary layer thickness is an increasing function of  $\alpha$ . Figs. 8.4 and 8.5 are sketched to analyze the effect of relaxation time parameter  $\beta_1$  on the velocity and temperature. As the relaxation time parameter increases the velocity profile decreases while the temperature profile is quite opposite to that of the velocity profile. Figs. 8.6 and 8.7 examine the influence of mixed convection parameter  $\lambda$  on the velocity and temperature. The fluid velocity and associated momentum boundary layer thickness increase by increasing  $\lambda$ . It is clear that the temperature has opposite effect when compared with velocity. We also noticed that the fluid velocity increases rapidly in comparison to the temperature with the increasing values of  $\lambda$ . Figs. 8.8 and 8.9 depict the effect of retardation time  $\beta_2$  on the temperature and velocity fields. Here we observed that  $\beta_2$  has quite opposite effect on the velocity and temperature. The fluid velocity increases with an

increase in  $\beta_2$ .

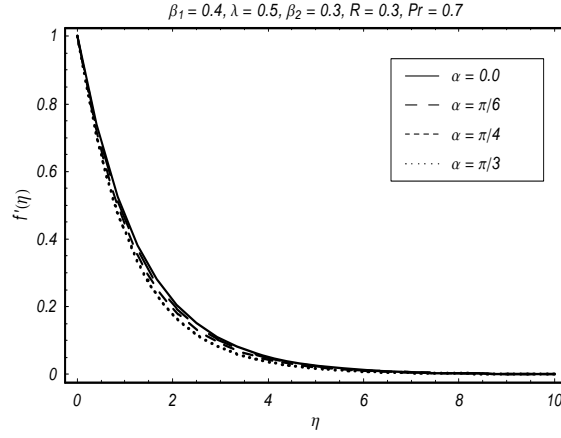


Fig. 8.2: Influence of sheet inclination  $\alpha$  on  $f'(\eta)$ .

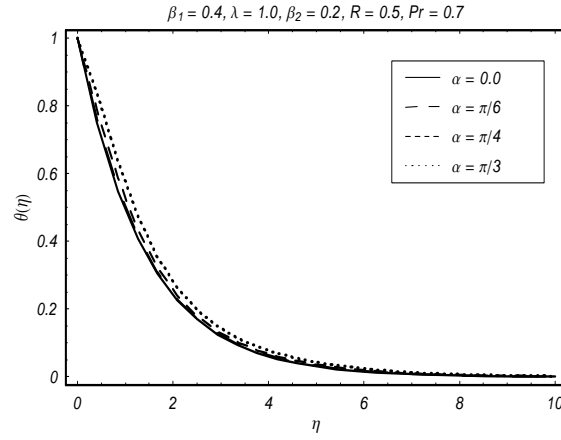


Fig. 8.3: Influence of sheet inclination  $\alpha$  on  $\theta(\eta)$ .

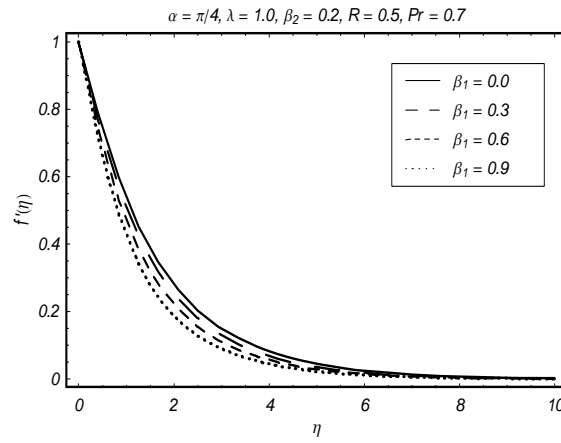


Fig.8.4: Influence of Deborah number  $\beta_1$  on  $f'(\eta)$ .

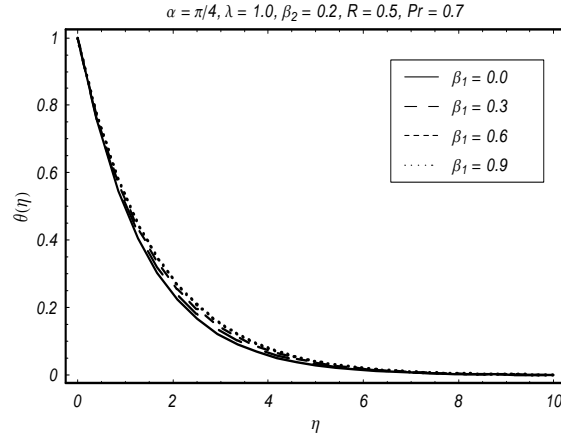


Fig. 8.5: Influence of Deborah number  $\beta_1$  on  $\theta(\eta)$ .

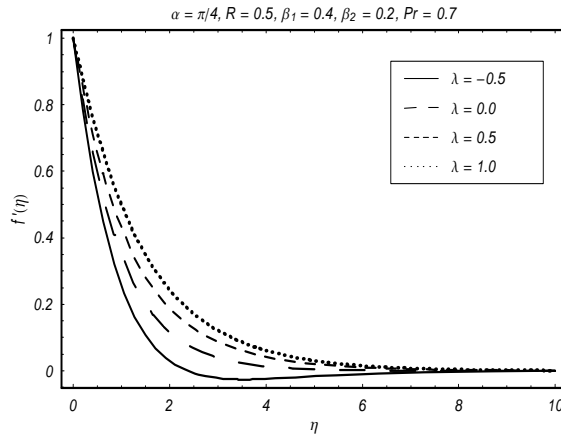


Fig. 8.6: Influence of mixed convection  $\lambda$  on  $f'(\eta)$ .

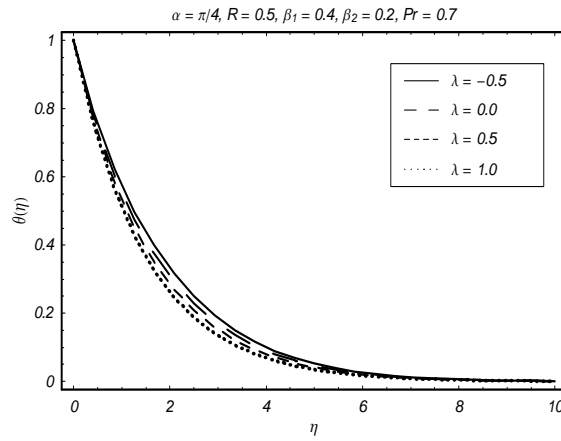


Fig. 8.7: Influence of mixed convection  $\lambda$  on  $\theta(\eta)$ .

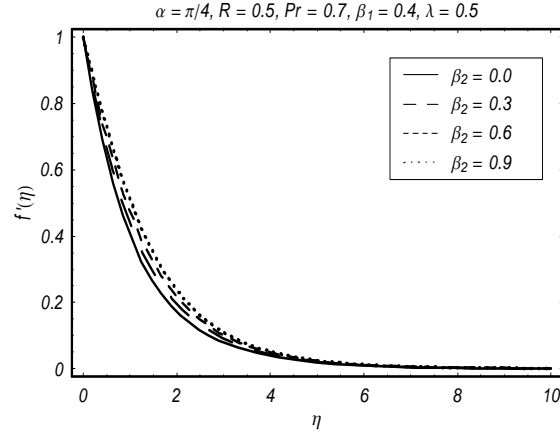


Fig. 8.8: Influence of Deborah number  $\beta_2$  on  $f'(\eta)$ .

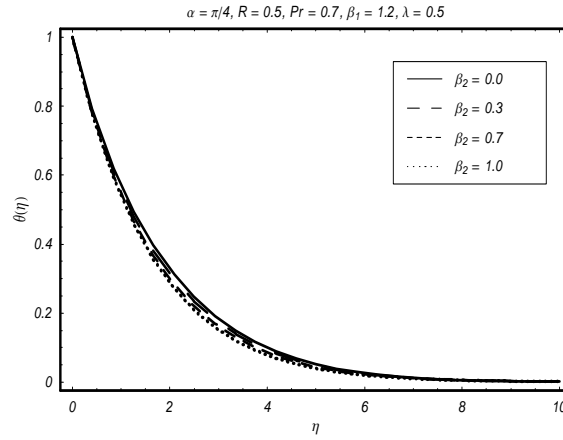


Fig. 8.9: Influence of Deborah number  $\beta_2$  on  $\theta(\eta)$ .

Table 8.1 also shows that the series solutions converge for 20th-order of deformations for both the velocity and temperature. Table 8.2 analyzes the numerical values of local Nusselt number for different values of  $\beta_1$ ,  $\beta_2$ ,  $\lambda$ ,  $Pr$  and  $R$ . We note that the numerical values of local Nusselt number increase with the increase of  $\beta_1$ ,  $\beta_2$ ,  $Pr$  and such values decrease for  $\lambda$  and  $R$ .

**Table 8.1:** Convergence of homotopy solutions for different order of approximations when

$\alpha = \pi/4$ ,  $\beta_1 = 0.2$ ,  $\lambda = 0.5$ ,  $\beta_2 = 0.3$ ,  $Pr = 0.7$  and  $R = 0.3$ .

Order of approximation	$-f''(0)$	$-\theta'(0)$
1	0.69555	0.73000
05	0.75163	0.72503
10	0.75241	0.72457
15	0.75240	0.72457
20	0.75239	0.72456
25	0.75239	0.72456
30	0.75239	0.72456

**Table 8.2:** Local Nusselt number and skin friction coefficient  $Re_x^{-1/2} Nu_x$  for some values of  $\beta_1$ ,  $\lambda$ ,  $Pr$ ,  $\beta_2$  and  $R$  when  $\alpha = \pi/4$ .

$\beta_1$	$\beta_2$	$\lambda$	$Pr$	$R$	$-(1 + \frac{4}{3}R) \theta'(0)$
0.1	0.2	0.5	0.7	0.3	0.73887
0.2					0.71284
0.3					0.70528
0.5	0.0				0.70729
	0.2				0.71925
	0.4				0.72951
	0.2	0.0			0.66787
		0.3			0.70324
		0.5			0.71924
		0.5	0.3		0.43757
			0.5		0.58961
			0.7	0.0	0.84020
				0.2	0.75419
				0.5	0.66085



## 8.4 Concluding remarks

This chapter examines the effect of thermal radiation on the mixed convection flow of an Oldroyd-B fluid over an inclined stretching sheet. The main observations of this study are as follows.

- Effect of mixed convection parameter  $\lambda$  on the velocity and temperature are quite opposite.
- Momentum and thermal boundary layers for  $\lambda$  have opposite effects.
- Decrease in temperature is more significant in comparison to velocity when Prandtl number  $Pr$  increases.
- Thermal boundary layer thickness is decreasing function of Prandtl number.
- Deborah numbers  $\beta_1$  and  $\beta_2$  have quite opposite effects for the velocity and temperature.

## Chapter 9

# Mixed convection flow of an Oldroyd-B fluid with power law heat flux and heat source

This chapter looks at the mixed convection flow of an Oldroyd-B fluid bounded by a porous stretching surface. Mathematical formulation is developed in the presence of heat source and power law heat flux. Velocity and temperature are computed. Plots for different parameters are analyzed. Numerical values of local Nusselt number are examined.

### 9.1 Development of problems

We consider the two-dimensional flow of an incompressible Oldroyd-B fluid over a porous surface. A Cartesian coordinate system is chosen in such a way that  $x$ -axis is taken along the flow direction and the  $y$ -axis perpendicular to the  $x$ -axis. The fluid fills the half space  $y > 0$ .

Heat source is present and power law heat flux is imposed. Flow geometry is shown in Fig. 9.1.

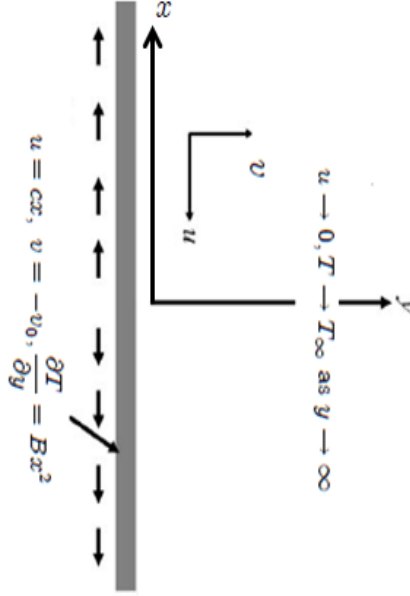


Fig. 9.1: Physical model of the problem

The present boundary layer flow is governed by the following expressions

$$\frac{\partial u}{\partial x} + \frac{\partial v}{\partial y} = 0, \quad (9.1)$$

$$\begin{aligned} u \frac{\partial u}{\partial x} + v \frac{\partial u}{\partial y} = & \nu \frac{\partial^2 u}{\partial y^2} - \lambda_1 \left[ u^2 \frac{\partial^2 u}{\partial x^2} + v^2 \frac{\partial^2 u}{\partial y^2} + 2uv \frac{\partial^2 u}{\partial x \partial y} \right] \\ & + \nu \lambda_2 \left[ u \frac{\partial^3 u}{\partial x \partial y^2} + v \frac{\partial^3 u}{\partial y^3} - \frac{\partial u}{\partial x} \frac{\partial^2 u}{\partial y^2} - \frac{\partial u}{\partial y} \frac{\partial^2 v}{\partial y^2} \right] + g\beta_T(T - T_\infty), \end{aligned} \quad (9.2)$$

$$u \frac{\partial T}{\partial x} + v \frac{\partial T}{\partial y} = \frac{k}{\rho c_p} \frac{\partial^2 T}{\partial y^2} + \frac{Q}{\rho c_p} (T - T_\infty). \quad (9.3)$$

In above equations  $u$  and  $v$  are the velocity components in the  $x$ - and  $y$ -directions,  $\lambda_1$  and  $\lambda_2$  are the relaxation and retardation times respectively,  $g$  the gravitational acceleration,  $\beta_T$  the thermal expansion coefficient,  $\nu = (\mu/\rho)$  the kinematic viscosity,  $T$  the fluid temperature,  $\rho$  the density of fluid,  $k$  the thermal conductivity of fluid,  $c_p$  the specific heat at constant pressure and  $Q$  the heat source coefficient.

The subjected boundary conditions are

$$u = cx, \quad v = -v_0, \quad \frac{\partial T}{\partial y} = Ax^2 \quad \text{at } y = 0, \quad (9.4)$$

$$u = 0, \quad T = T_\infty \quad \text{as } y \rightarrow \infty, \quad (9.5)$$

where  $A$  is the temperature coefficient and  $T_\infty$  is the ambient temperature.

The similarity transformations are given by

$$u = cx f'(\eta), \quad v = -\sqrt{c\nu} f(\eta), \quad T = T_\infty + A \sqrt{\frac{\nu}{c}} x^2 \theta(\eta), \quad \eta = \sqrt{\frac{c}{\nu}} y \quad (9.6)$$

in which  $c$  is a constant and prime denotes differentiation with respect to  $\eta$ . Eq. (9.1) is automatically satisfied and the Eqs. (9.2-9.5) are reduced as follows

$$f''' + f f'' - f'^2 + \beta_1(2f f' f'' - f^2 f''') - \beta_2(f''^2 - f f'''' ) + \lambda \theta = 0, \quad (9.7)$$

$$\theta'' + Pr f \theta' - 2Pr f' \theta + \beta^* \theta = 0, \quad (9.8)$$

$$f = S, \quad f' = 1, \quad \theta' = 1 \quad \text{at } \eta = 0, \quad (9.9)$$

$$f' = 0, \quad \theta = 0 \quad \text{as } \eta \rightarrow \infty, \quad (9.10)$$

in which  $\beta_1 = \lambda_1 c$  and  $\beta_2 = \lambda_2 c$  are the Deborah numbers,  $\lambda = \frac{Gr_x}{Re_x^2}$  the mixed convection parameter with  $Gr_x = \frac{g \beta_T (T - T_\infty) x^3}{\nu^2}$  the local Grashof number and  $Re_x = \frac{U x}{\nu}$  the local Reynolds number,  $S = \frac{v_0}{\sqrt{\nu c}}$  the suction/injection parameter,  $Pr = \frac{\mu c_p}{k}$  the Prandtl number and  $\beta^* = \frac{\nu Q}{k c}$  a heat generation/absorption parameter.

Expression of local Nusselt number  $Nu_x$  is

$$Nu_x = \frac{x q_w}{k(T - T_\infty)}, \quad q_w = -k \left( \frac{\partial T}{\partial y} \right)_{y=0}. \quad (9.11)$$

Dimensionless form of Eq. (9.11) is

$$Nu/Re_x^{1/2} = -\frac{1}{\theta(0)}. \quad (9.12)$$

## 9.2 Homotopy analysis solutions

Choosing the following set of base functions

$$\{\eta^k \exp(-n\eta) | k \geq 0, n \geq 0\} \quad (9.13)$$

we express  $f$  and  $\theta$  as follows

$$f(\eta) = a_{0,0}^0 + \sum_{n=0}^{\infty} \sum_{k=0}^{\infty} a_{m,n}^k \eta^k \exp(-n\eta), \quad (9.14)$$

$$\theta(\eta) = \sum_{n=0}^{\infty} \sum_{k=0}^{\infty} b_{m,n}^k \eta^k \exp(-n\eta), \quad (9.15)$$

where  $a_{m,n}^k$  and  $b_{m,n}^k$  are the coefficients. Initial approximations and auxiliary linear operators are taken in the following forms

$$f_0(\eta) = S + 1 - \exp(-\eta), \quad \theta_0(\eta) = -\exp(-\eta), \quad (9.16)$$

$$\mathcal{L}_f = f''' - f', \quad \mathcal{L}_\theta = \theta'' + \theta', \quad (9.17)$$

$$\mathcal{L}_f(C_1 + C_2 e^\eta + C_3 e^{-\eta}) = 0, \quad \mathcal{L}_\theta(C_4 + C_5 e^{-\eta}) = 0, \quad (9.18)$$

where  $C_i$  ( $i = 1 - 5$ ) are the arbitrary constants.

The corresponding zeroth order deformation problems are developed in the following fash-  
ions.

$$(1-p) \mathcal{L}_f [\hat{f}(\eta; p) - f_0(\eta)] = p h_f \mathcal{N}_f [\hat{f}(\eta; p), \hat{\theta}(\eta, p)], \quad (9.19)$$

$$(1-p) \mathcal{L}_\theta [\hat{\theta}(\eta; p) - \theta_0(\eta)] = p h_\theta \mathcal{N}_\theta [\hat{f}(\eta; p), \hat{\theta}(\eta, p)], \quad (9.20)$$

$$\hat{f}(0; p) = S, \quad \hat{f}'(0; p) = 1, \quad \hat{f}'(\infty; p) = 0, \quad \hat{\theta}'(0, p) = 1, \quad \hat{\theta}(\infty, p) = 0, \quad (9.21)$$

$$\begin{aligned}\mathcal{N}_f[\hat{f}(\eta, p)] &= \frac{\partial^3 \hat{f}(\eta, p)}{\partial \eta^3} - \hat{f}(\eta, p) \frac{\partial^2 \hat{f}(\eta, p)}{\partial \eta^2} - \left( \frac{\partial \hat{f}(\eta, p)}{\partial \eta} \right)^2 \\ &+ \beta_1 \left[ 2\hat{f}(\eta, p) \frac{\partial \hat{f}(\eta, p)}{\partial \eta} \frac{\partial^2 \hat{f}(\eta, p)}{\partial \eta^2} - (\hat{f}(\eta, p))^2 \frac{\partial^3 \hat{f}(\eta, p)}{\partial \eta^3} \right] +\end{aligned}\quad (9.22)$$

$$\beta_2 \left[ \left( \frac{\partial^2 \hat{f}(\eta, p)}{\partial \eta^2} \right)^2 - \hat{f}(\eta, p) \frac{\partial^4 \hat{f}(\eta, p)}{\partial \eta^4} \right] + \lambda \frac{\partial \hat{\theta}(\eta, p)}{\partial \eta}, \quad (9.23)$$

$$\mathcal{N}_\theta[\hat{\theta}(\eta, p), \hat{f}(\eta, p)] = \frac{\partial^2 \hat{\theta}(\eta, p)}{\partial \eta^2} + Pr \hat{f}(\eta, p) \frac{\partial \hat{\theta}(\eta, p)}{\partial \eta} - 2Pr \frac{\partial \hat{f}(\eta, p)}{\partial \eta} \hat{\theta}(\eta, p) + \beta^* \hat{\theta}(\eta, p), \quad (9.24)$$

in which  $p$  is an embedding parameter,  $h_f$  and  $h_\theta$  the non-zero auxiliary parameters and  $\mathcal{N}_f$  and  $\mathcal{N}_\theta$  the nonlinear operators. For  $p = 0$  and  $p = 1$  we have

$$\hat{f}(\eta; 0) = f_0(\eta), \quad \hat{\theta}(\eta, 0) = \theta_0(\eta) \text{ and } \hat{f}(\eta; 1) = f(\eta), \quad \hat{\theta}(\eta, 1) = \theta(\eta), \quad (9.25)$$

and when  $p$  increases from 0 to 1 then  $f(\eta, p)$  and  $\theta(\eta, p)$  vary from  $f_0(\eta), \theta_0(\eta)$  to  $f(\eta)$  and  $\theta(\eta)$ . Taylor's series yields

$$f(\eta, p) = f_0(\eta) + \sum_{m=1}^{\infty} f_m(\eta) p^m, \quad (9.26)$$

$$\theta(\eta, p) = \theta_0(\eta) + \sum_{m=1}^{\infty} \theta_m(\eta) p^m, \quad (9.27)$$

$$f_m(\eta) = \frac{1}{m!} \left. \frac{\partial^m f(\eta; p)}{\partial p^m} \right|_{p=0}, \quad \theta_m(\eta) = \frac{1}{m!} \left. \frac{\partial^m \theta(\eta; p)}{\partial p^m} \right|_{p=0}, \quad (9.28)$$

where the convergence of above series strongly depends upon  $h_f$  and  $h_\theta$ . The auxiliary parameters  $h_f$  and  $h_\theta$  are selected in such a way that (9.26) and (9.27) converge at  $p = 1$  and hence

$$f(\eta) = f_0(\eta) + \sum_{m=1}^{\infty} f_m(\eta), \quad (9.29)$$

$$\theta(\eta) = \theta_0(\eta) + \sum_{m=1}^{\infty} \theta_m(\eta). \quad (9.30)$$

The  $m$ th-order deformation problems are constructed by the following expressions

$$\mathcal{L}_f[f_m(\eta) - \chi_m f_{m-1}(\eta)] = h_f \mathcal{R}_f^m(\eta), \quad (9.31)$$

$$\mathcal{L}_\theta[\theta_m(\eta) - \chi_m \theta_{m-1}(\eta)] = h_\theta \mathcal{R}_\theta^m(\eta), \quad (9.32)$$

$$f_m(0) = f'_m(0) = f'_m(\infty) = 0, \quad \theta'_m(0) - \gamma \theta_m(0) = \theta_m(\infty) = 0, \quad (9.33)$$

$$\begin{aligned} \mathcal{R}_f^m(\eta) &= f_{m-1}'''(\eta) + \sum_{k=0}^{m-1} \left[ f_{m-1-k} f_k'' - f'_{m-1-k} f_k'' \right] \\ &+ \beta_1 \sum_{k=0}^{m-1} f_{m-1-k} \sum_{l=0}^k \{ 2f'_{k-l} f_l'' - f_{k-l} f_l''' - \lambda f'_{m-1}(\eta) \} \\ &+ \beta_2 \{ f'_{m-1-k} \sum_{k=0}^{m-1} f'_k - f_{m-1-k} \sum_{k=0}^{m-1} f_k^{iv} \} + \lambda \theta_{m-1}, \end{aligned} \quad (9.34)$$

$$\mathcal{R}_\theta^m(\eta) = \theta_{m-1}''(\eta) + Pr \sum_{k=0}^{m-1} \theta'_{m-1-k} f_k - 2Pr \sum_{k=0}^{m-1} \theta_{m-1-k} f'_k + \beta^* \theta_{m-1}(\eta), \quad (9.35)$$

$$\chi_m = \begin{cases} 0, & m \leq 1, \\ 1, & m > 1. \end{cases} \quad (9.36)$$

If  $f_m^*$  and  $\theta_m^*$  are the special solutions then the general solutions are

$$f_m(\eta) = f_m^*(\eta) + C_1 + C_2 e^\eta + C_3 e^{-\eta}, \quad (9.37)$$

$$\theta_m(\eta) = \theta_m^*(\eta) + C_4 + C_5 e^{-\eta}. \quad (9.38)$$

### 9.3 Convergence of the homotopy solutions

The auxiliary parameters  $\hbar_f$  and  $\hbar_\theta$  have significant role in the convergence of developed series solutions. Here the  $\hbar$ -curves are portrayed for 18<sup>th</sup> order of approximations in order to find the values of  $\hbar_f$  and  $\hbar_\theta$  ensuring convergence. Figs. 9.2 depict that the range of admissible values of  $\hbar_f$  and  $\hbar_\theta$  are  $-0.8 \leq \hbar_f \leq -0.2$  and  $-0.75 \leq \hbar_\theta \leq -0.2$ . The series solution converge in the whole region of  $\eta$  when  $\hbar_f = -0.4$  and  $\hbar_\theta = -0.4$ . Table 9.1 depicts that 25<sup>th</sup> order

deformations are sufficient for both the velocity and temperature expressions.

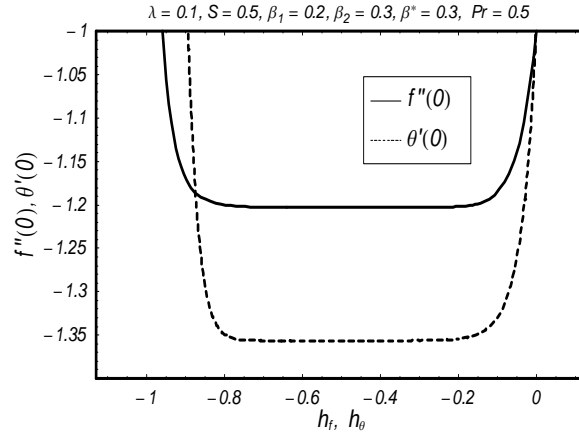


Fig.9.2:  $\hbar$ -curves for the function  $f$  and  $\theta$ .

**Table 9.1.** Convergence of homotopy solutions for different order of approximations when  $\beta_1 = 0.2$ ,  $\beta_2 = \beta^* = 0.3$ ,  $Pr = S = 0.5$ ,  $\lambda = 0.1$ ,  $\hbar_f = -0.4$  and  $\hbar_\theta = -0.4$ .

Order of approximation	$-f''(0)$	$-\theta''(0)$
1	1.10000	1.22000
5	1.19801	1.34636
10	1.20255	1.35611
15	1.20268	1.35640
20	1.20271	1.35642
25	1.20272	1.35643
30	1.20272	1.35643

## 9.4 Graphical results and discussion

The purpose of this section is to highlight the variations of interesting parameters through Figs. 9.3–9.7 for velocity and temperature. Figs. 9.3 and 9.4 show the behaviors of suction/injection parameter  $S$ , Deborah number  $\beta_1$  and mixed convection parameter  $\lambda$  on the velocity  $f'(\eta)$ . Fig. 9.3 shows the effects of suction/injection parameter  $S$  on the velocity profile  $f'(\eta)$ . Here  $S > 0$  corresponds to suction and  $S < 0$  for injection case. We observed that the velocity  $f'(\eta)$  is



lower for suction case in comparison to injection phenomenon. From physical point of view suction is an agent that resists the fluid flow. Such resistance in fluid flow creates a reduction in the velocity field and associated boundary layer thickness. Fig. 9.4 illustrates that both the fluid velocity and boundary layer thickness decrease when mixed convection parameter is increased. Note that the mixed convection parameter involves the buoyancy force. Buoyancy force is stronger for the larger mixed convection parameter and weaker for the smaller mixed convection parameter. This stronger buoyancy acts as an agent to creates a reduction in the velocity profile and momentum boundary layer thickness.

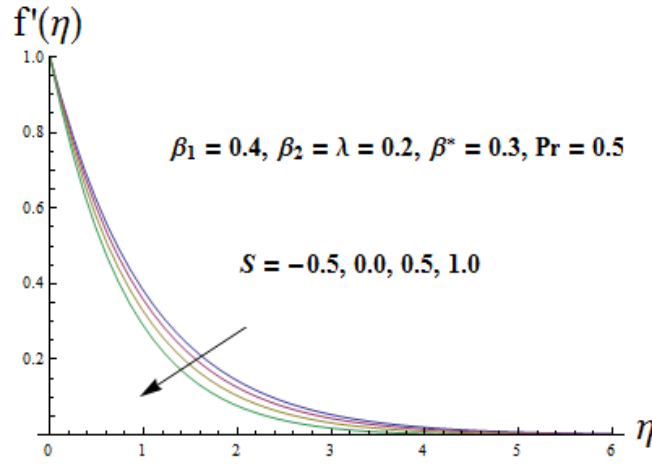


Fig. 9.3: Variation of  $S$  on  $f'(\eta)$ .

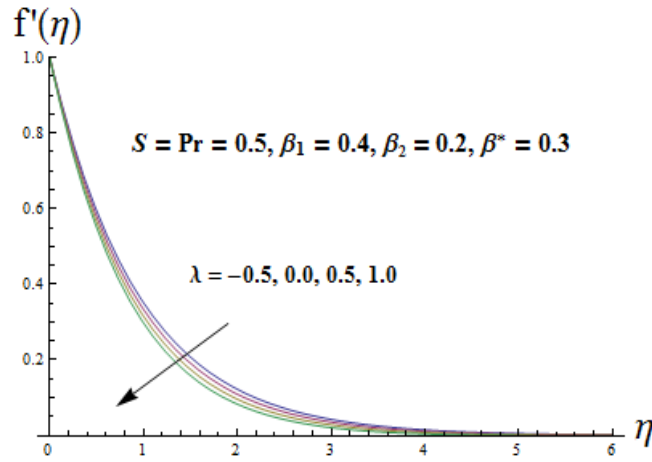


Fig. 9.4: Variation of  $\lambda$  on  $f'(\eta)$ .

Figs. 9.5 – 9.7 are displayed to examine the influence of arising parameters on dimensionless

temperature profile  $\theta(\eta)$ . Fig. 9.5 presents the variations in temperature  $\theta(\eta)$  for different values of suction/injection parameter  $S$ . From this Fig. it is analyzed that the temperature is higher for injection case when we compared it with suction case. The effects of suction parameter  $S$  on  $\theta(\eta)$  is qualitatively similar to that of the velocity. Both the temperature  $\theta(\eta)$  and thermal boundary layer thickness increase when mixed convection parameter  $\lambda$  increases (see Fig 9.6). Here buoyancy force is an agent that creates an enhancement in the temperature and thermal boundary layer thickness. Influence of heat source  $\beta^*$  on  $\theta(\eta)$  is presented in Fig. 9.7. Physically  $\beta^* > 0$  means that  $T_w > T_\infty$  and in this case heat is supplied to the flow region from the wall. The temperature boosts with heat source parameter  $\beta^* > 0$  while reduction in thermal boundary layer thickness and temperature is seen with heat sink parameter  $\beta^* < 0$ .

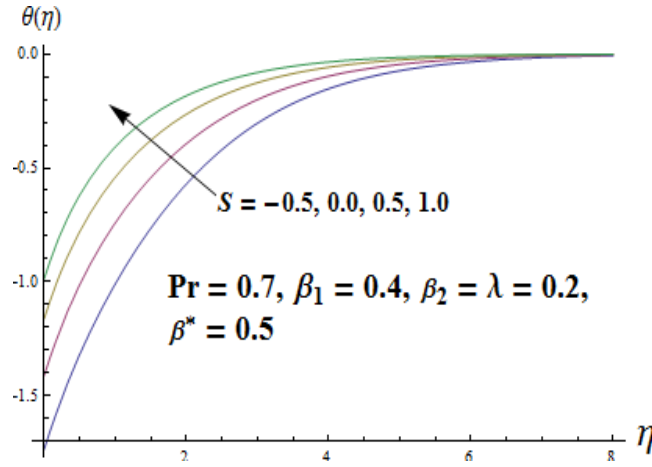


Fig. 9.5: Variation of  $S$  on  $\theta(\eta)$ .

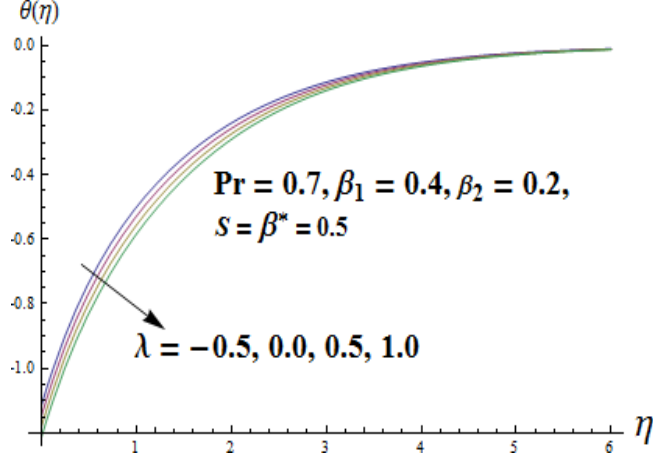


Fig. 9.6: Variation of  $\lambda$  on  $\theta(\eta)$ .

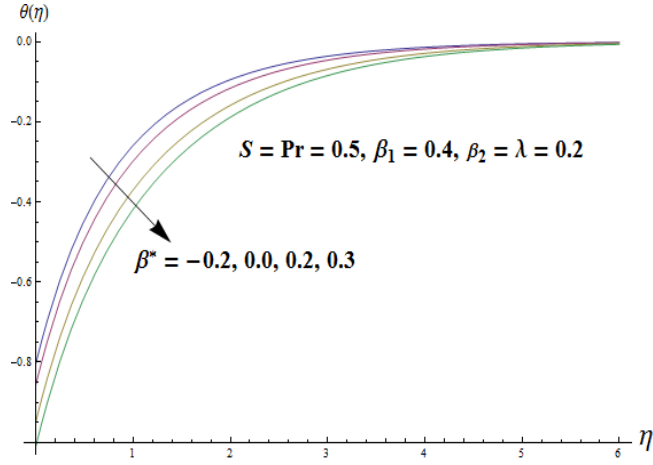


Fig. 9.7: Variation of  $\beta^*$  on  $\theta(\eta)$ .

Table 9.2 shows that the local Nusselt number has quite opposite behavior for  $\beta_1$  and  $\beta_2$ . The values of Nusselt number increases by increasing  $\beta^*$ ,  $Pr$  and  $S$ . However it decreases by increasing  $\lambda$ . Table. 9.3 ensures the validity of present results for  $f''(0)$  in a limiting sense.

**Table 9.2:** Values of local Nusselt number  $Nu/Re_x^{1/2}$  for the parameters  $\beta_1$ ,  $\beta_2$ ,  $\beta^*$ ,  $Pr$ ,  $S$

when  $\lambda = 0.1$ .

$\beta_1$	$\beta_2$	$\beta^*$	Pr	$S$	$\lambda$	$-Nu/Re_x^{1/2}$
0.0	0.3	0.3	0.5	0.5	0.1	1.20133
0.2						1.17496
0.4						1.14936
	0.4					1.18647
	0.5					1.19622
	0.6					1.20463
		-0.1				1.02500
		-0.2				1.09798
		-0.3				1.16099
			0.6			1.27668
			0.9			1.60523
			1.2			1.91014
				0.8		1.23081
				1.0		1.30323
				1.5		1.45103
					0.2	1.15381
					0.4	1.13613
					0.6	1.11294

**Table 9.3:** Comparison of  $f''(0)$  for different values of Maxwell parameter  $\beta_1$  when  $\beta_2 = S =$

$\lambda = 0$ .

	Abel et al. [38]	Present results
$\beta_1$	$-f''(0)$	$-f''(0)$
0.0	1.00000	1.00000
0.2	1.051948	1.051889
0.4	1.101850	1.101903
0.6	1.150163	1.150137
0.8	1.196692	1.196711
1.2	1.285257	1.285363
1.6	1.368641	1.368758
2.0	1.447617	1.447651

## 9.5 Final remarks

This chapter deals with the mixed convection flow of Oldroyd-B fluid over a stretching sheet with suction/injection, heat source/sink and power law heat flux. Effects of different involved parameters such as mixed convection parameter  $\lambda$  and heat source/sink  $\beta^*$  on the flow field and temperature are analyzed. The main observations are summarized as follows:

- Velocity profile and momentum boundary layer thickness reduce in case of suction  $S > 0$  while these enhance in case of injection  $S < 0$ .
- Thermal boundary layer thickness is increasing function of heat source parameter  $\beta^* > 0$  while it reduces with heat absorption parameter  $\beta^* < 0$ .
- Increase in mixed convection parameter  $\lambda$  yields an enhancement in the temperature and thermal boundary layer thickness while reduction in heat transfer rate at wall is noted.
- Behaviors of Deborah numbers  $\beta_1$  and  $\beta_2$  on the heat transfer rate at the wall are opposite. Heat transfer rate at wall increases with the heat absorption  $\beta^* < 0$  and suction parameters  $S > 0$ .

## Chapter 10

# Soret and Dufour effects in mixed convection flow of an Oldroyd-B fluid with convective boundary conditions

This chapter investigates the effects of heat and mass transfer in the mixed convection flow of an Oldroyd-B fluid over a stretching surface with convective boundary conditions. Emphasis is given to the analysis of Soret and Dufour effects. Relevant problems are first formulated and then computed by the homotopy analysis method (HAM). Velocity, temperature and concentration fields are computed and analyzed through plots. In addition, the local Nusselt and Sherwood numbers are examined through the numerical values.

### 10.1 Mathematical model

We choose  $x$ -axis along the stretching surface in the flow direction and  $y$ -axis is taken perpendicular to the surface. An incompressible Oldroyd-B fluid is considered. The surface satisfies the convective boundary conditions. Further, the Soret and Dufour effects are taken into account.

The resulting boundary layer equations for flow of an Oldroyd-B fluid are

$$\frac{\partial u}{\partial x} + \frac{\partial v}{\partial y} = 0, \quad (10.1)$$

$$\begin{aligned} u \frac{\partial u}{\partial x} + v \frac{\partial u}{\partial y} = & \nu \frac{\partial^2 u}{\partial y^2} - \lambda_1 \left[ u^2 \frac{\partial^2 u}{\partial x^2} + v^2 \frac{\partial^2 u}{\partial y^2} + 2uv \frac{\partial^2 u}{\partial x \partial y} \right] \\ & + \nu \lambda_2 \left[ u \frac{\partial^3 u}{\partial x \partial y^2} + v \frac{\partial^3 u}{\partial y^3} - \frac{\partial u}{\partial x} \frac{\partial^2 u}{\partial y^2} - \frac{\partial u}{\partial y} \frac{\partial^2 v}{\partial y^2} \right] \\ & + g[\beta_T(T - T_\infty) + \beta_C(C - C_\infty)], \end{aligned} \quad (10.2)$$

$$u \frac{\partial T}{\partial x} + v \frac{\partial T}{\partial y} = \alpha_m \frac{\partial^2 T}{\partial y^2} + \frac{D_e k_T}{C_s C_p} \frac{\partial^2 C}{\partial y^2}, \quad (10.3)$$

$$u \frac{\partial C}{\partial x} + v \frac{\partial C}{\partial y} = D_e \frac{\partial^2 C}{\partial y^2} + \frac{D_e k_T}{T_m} \frac{\partial^2 T}{\partial y^2}, \quad (10.4)$$

where  $u$  and  $v$  denote the velocity components in the  $x$ - and  $y$ -directions respectively,  $\lambda_1$  and  $\lambda_2$  the relaxation and retardation times respectively,  $T$  the fluid temperature,  $C$  the concentration field,  $\nu$  the kinematic viscosity,  $\rho$  the fluid density,  $D_e$  the mass diffusivity,  $\alpha_m$  the thermal conductivity,  $k_T$  the thermal-diffusion ratio,  $C_p$  the specific heat,  $C_s$  the concentration susceptibility,  $T_m$  the fluid mean temperature and  $\sigma$  the fluid electrical conductivity.

The boundary conditions are expressed in the following forms

$$u = u_w(x) = cx, \quad v = 0, \quad -k \frac{\partial T}{\partial y} = h(T_f - T), \quad C = C_w \text{ at } y = 0, \quad (10.5)$$

$$u \rightarrow 0, \quad T \rightarrow T_\infty, \quad C \rightarrow C_\infty \text{ as } y \rightarrow \infty \quad (10.6)$$

in which  $T_f$  denotes the convective fluid temperature,  $T_\infty$  the ambient temperature and  $k$  the thermal conductivity.

Setting the following transformations

$$\eta = y \sqrt{\frac{c}{\nu}}, \quad u = cx f'(\eta), \quad v = -\sqrt{c\nu} f(\eta), \quad \theta(\eta) = \frac{T - T_\infty}{T_f - T_\infty}, \quad \phi(\eta) = \frac{C - C_\infty}{C_w - C_\infty}, \quad (10.7)$$

incompressibility condition (10.1) is automatically satisfied and the other equations give

$$f''' + f f'' - f'^2 + \beta_1(2f f' f'' - f^2 f''') - \beta_2(f'^2 - f f''') + \lambda \theta + \lambda N \phi = 0, \quad (10.8)$$

$$\frac{1}{Pr} \theta'' + f \theta' + D_f \phi'' = 0, \quad (10.9)$$

$$\phi'' + Sc f \phi' + Sc \theta'' = 0, \quad (10.10)$$

$$f(0) = 0, \quad f'(0) = 1, \quad f'(\infty) = 0, \quad (10.11)$$

$$\theta'(0) = -\gamma_1(1 - \theta(0)), \quad \theta(\infty) = 0, \quad (10.12)$$

$$\phi(0) = 1, \quad \phi(\infty) = 0. \quad (10.13)$$

In above expressions the prime indicates the differentiation with respect to  $\eta$ ,  $\beta_1 = \lambda_1 c$  and  $\beta_2 = \lambda_2 c$  are the Deborah numbers,  $\lambda = \frac{Gr_x}{Re_x^2}$  the mixed convection parameter with  $Gr_x = \frac{g \beta_T (T - T_\infty) x^3}{\nu^2}$  as the Grashof number,  $Re_x = \frac{U x}{\nu}$  the local Reynold number,  $Pr = \nu / \alpha_m$  the Prandtl number,  $\gamma_1 = (h/k) \sqrt{\nu/c}$  the Biot number,  $Sc = \nu / De$  the Schmidt number,  $D_f$  the Dufour number and  $Sr$  the Soret number. The definition of  $D_f$  and  $Sr$  are

$$D_f = \frac{D_e k_T}{C_s C_p} \frac{(C_w - C_\infty)}{(T_f - T_\infty) \nu}, \quad Sr = \frac{D_e k_T}{T_m \nu} \frac{(T_w - T_\infty)}{(C_w - C_\infty)}. \quad (10.14)$$

Local Nusselt and local Sherwood numbers in dimensionless coordinates are expressed as follows:

$$Nu(Re_x)^{-1/2} = -\theta'(0), \quad (10.15)$$

$$Sh(Re_x)^{-1/2} = -\phi'(0). \quad (10.16)$$

In the next section we will develop the homotopy solutions for the resulting problems.

## 10.2 Series solutions

The initial guesses and auxiliary linear operators are taken as

$$f_0(\eta) = (1 - \exp(-\eta)), \quad \theta_0(\eta) = \frac{\gamma_1 \exp(-\eta)}{1 + \gamma_1}, \quad \phi_0(\eta) = \exp(-\eta) + \frac{\eta}{2} \exp(-\eta), \quad (10.17)$$



$$\mathcal{L}_f = \frac{d^3 f}{d\eta^3} - \frac{df}{d\eta}, \quad \mathcal{L}_\theta = \frac{d^2 \theta}{d\eta^2} - \theta, \quad \mathcal{L}_\phi = \frac{d^2 \phi}{d\eta^2} - \phi, \quad (10.18)$$

$$\mathcal{L}_f [C_1 + C_2 \exp(\eta) + C_3 \exp(-\eta)] = 0, \quad (10.19)$$

$$\mathcal{L}_\theta [C_4 \exp(\eta) + C_5 \exp(-\eta)] = 0, \quad \mathcal{L}_\phi [C_6 \exp(\eta) + C_7 \exp(-\eta)] = 0, \quad (10.20)$$

in which  $C_i$  ( $i = 1 - 7$ ) denote the arbitrary constants.

### 10.2.1 Zeroth and mth order deformation problems

Having the non-linear operators  $\mathcal{N}_f$ ,  $\mathcal{N}_\theta$  and  $\mathcal{N}_\phi$  in the forms

$$\begin{aligned} \mathcal{N}_f[\hat{f}(\eta, p), \hat{\theta}(\eta, p)] &= \frac{\partial^3 \hat{f}(\eta, p)}{\partial \eta^3} - \hat{f}(\eta, p) \frac{\partial^2 \hat{f}(\eta, p)}{\partial \eta^2} - \left( \frac{\partial \hat{f}(\eta, p)}{\partial \eta} \right)^2 \\ &+ \beta_1 \left[ 2\hat{f}(\eta, p) \frac{\partial \hat{f}(\eta, p)}{\partial \eta} \frac{\partial^2 \hat{f}(\eta, p)}{\partial \eta^2} - (\hat{f}(\eta, p))^2 \frac{\partial^3 \hat{f}(\eta, p)}{\partial \eta^3} \right] \\ &+ \beta_2 \left[ \left( \frac{\partial^2 \hat{f}(\eta, p)}{\partial \eta^2} \right)^2 - \hat{f}(\eta, p) \frac{\partial^4 \hat{f}(\eta, p)}{\partial \eta^4} \right] \\ &+ \lambda \hat{\theta}(\eta, p) + \lambda N \hat{\phi}(\eta, p), \end{aligned} \quad (10.21)$$

$$\mathcal{N}_\theta[\hat{f}(\eta, p), \hat{\theta}(\eta, p), \hat{\phi}(\eta, p)] = \frac{1}{Pr} \frac{\partial^2 \hat{\theta}(\eta, p)}{\partial \eta^2} + \hat{f}(\eta, p) \frac{\partial \hat{\theta}(\eta, p)}{\partial \eta} + D_f \frac{\partial^2 \hat{\phi}(\eta, p)}{\partial \eta^2}, \quad (10.22)$$

$$\mathcal{N}_\phi[\hat{f}(\eta, p), \hat{\theta}(\eta, p), \hat{\phi}(\eta, p)] = \frac{\partial^2 \hat{\phi}(\eta, p)}{\partial \eta^2} + Sc \hat{f}(\eta, p) \frac{\partial \hat{\phi}(\eta, p)}{\partial \eta} + Sr Sc \frac{\partial^2 \hat{\theta}(\eta, p)}{\partial \eta^2}, \quad (10.23)$$

the corresponding problems at the zeroth and  $m$ th orders can be expressed as follows:

$$(1 - p) \mathcal{L}_f[\hat{f}(\eta, p) - f_0(\eta)] = p \hbar_f \mathcal{N}_f[\hat{f}(\eta, p), \hat{\theta}(\eta, p), \hat{\phi}(\eta, p)], \quad (10.24)$$

$$(1 - p) \mathcal{L}_\theta[\hat{\theta}(\eta, p) - \theta_0(\eta)] = p \hbar_\theta \mathcal{N}_\theta[\hat{f}(\eta, p), \hat{\theta}(\eta, p), \hat{\phi}(\eta, p)], \quad (10.25)$$

$$(1 - p) \mathcal{L}_\phi[\hat{\phi}(\eta, p) - \phi_0(\eta)] = p \hbar_\phi \mathcal{N}_\phi[\hat{f}(\eta, p), \hat{\theta}(\eta, p), \hat{\phi}(\eta, p)], \quad (10.26)$$

$$\hat{f}(\eta; p) \Big|_{\eta=0} = 0, \quad \frac{\partial \hat{f}(\eta; p)}{\partial \eta} \Big|_{\eta=0} = 1, \quad \frac{\partial \hat{f}(\eta; p)}{\partial \eta} \Big|_{\eta=\infty} = 0, \quad (10.27)$$

$$\hat{\theta}'(\eta; p) \Big|_{\eta=0} = -\gamma[1 - \hat{\theta}(\eta; p) \Big|_{\eta=0}], \quad \hat{\theta}(\eta; p) \Big|_{\eta=\infty} = 0, \quad (10.28)$$

$$\hat{\phi}(\eta; p) \Big|_{\eta=0} = 1, \quad \hat{\phi}(\eta; p) \Big|_{\eta=\infty} = 0, \quad (10.29)$$

$$\mathcal{L}_f[f_m(\eta) - \chi_m f_{m-1}(\eta)] = \hbar_f \mathcal{R}_m^f(\eta), \quad (10.30)$$

$$\mathcal{L}_\theta[\theta_m(\eta) - \chi_m \theta_{m-1}(\eta)] = \hbar_\theta \mathcal{R}_m^\theta(\eta), \quad (10.31)$$

$$\mathcal{L}_\phi[\phi_m(\eta) - \chi_m \phi_{m-1}(\eta)] = \hbar_\phi \mathcal{R}_m^\phi(\eta), \quad (10.32)$$

$$\begin{aligned} f_m(0) &= 0, \quad f'_m(0) = 0, \quad f'_m(\infty) = 0, \quad \theta'_m(0) - \gamma \theta_m(0) = 0, \\ \theta_m(\infty) &= 0, \quad \phi_m(0) = 0, \quad \phi_m(\infty) = 0, \end{aligned} \quad (10.33)$$

$$\begin{aligned} \mathcal{R}_f^m(\eta) &= f_{m-1}'''(\eta) + \sum_{k=0}^{m-1} \left[ f_{m-1-k} f_k'' - f'_{m-1-k} f_k'' \right] \\ &+ \beta_1 \sum_{k=0}^{m-1} f_{m-1-k} \sum_{l=0}^k \{ 2f'_{k-l} f_l'' - f_{k-l} f_l''' - \lambda f'_{m-1}(\eta) \} \\ &+ \beta_2 \{ f'_{m-1-k} \sum_{k=0}^{m-1} f_k' - f_{m-1-k} \sum_{k=0}^{m-1} f_k^{iv} \} + \lambda \theta'_{m-1}(\eta) + \lambda N 1 \phi'_{m-1}(\eta), \end{aligned} \quad (10.34)$$

$$\mathcal{R}_m^\theta(\eta) = \frac{1}{P_r} \theta_{m-1}''(\eta) + \sum_{k=0}^{m-1} f_{m-1-k} \theta_k' + D_f \phi_{m-1}''(\eta), \quad (10.35)$$

$$\mathcal{R}_m^\phi(\eta) = \phi_{m-1}''(\eta) + S c \sum_{k=0}^{m-1} f_{m-1-k} \phi_k' + S c \theta_{m-1}''(\eta), \quad (10.36)$$

$$\chi_m = \begin{cases} 0, & m \leq 1 \\ 1, & m > 1, \end{cases} \quad (10.37)$$

where  $p \in [0, 1]$  is an embedding parameter and  $\hbar_f$ ,  $\hbar_\theta$  and  $\hbar_\phi$  are the nonzero auxiliary parameters. Taylor's series gives

$$\hat{f}(\eta; p) = f_0(\eta) + \sum_{m=1}^{\infty} f_m(\eta) p^m, \quad f_m(\eta) = \frac{1}{m!} \frac{\partial^m \hat{f}(\eta; p)}{\partial p^m} \Big|_{p=0}, \quad (10.38)$$

$$\hat{\theta}(\eta; p) = \theta_0(\eta) + \sum_{m=1}^{\infty} \theta_m(\eta) p^m, \quad \theta_m(\eta) = \frac{1}{m!} \frac{\partial^m \hat{\theta}(\eta; p)}{\partial p^m} \Big|_{p=0}, \quad (10.39)$$

$$\hat{\phi}(\eta; p) = \phi_0(\eta) + \sum_{m=1}^{\infty} \phi_m(\eta) p^m, \quad \phi_m(\eta) = \frac{1}{m!} \left. \frac{\partial^m \hat{\phi}(\eta; p)}{\partial p^m} \right|_{p=0}. \quad (10.40)$$

and when  $p = 0$  and  $p = 1$  then

$$\hat{f}(\eta; 0) = f_0(\eta), \quad \hat{f}(\eta; 1) = f(\eta), \quad (10.41)$$

$$\hat{\theta}(\eta; 0) = \theta_0(\eta), \quad \hat{\theta}(\eta; 1) = \theta(\eta), \quad (10.42)$$

$$\hat{\phi}(\eta; 0) = \phi_0(\eta), \quad \hat{\phi}(\eta; 1) = \phi(\eta). \quad (10.43)$$

We choose the auxiliary parameters in such a way that the series solutions converge for  $p = 1$  and so

$$f(\eta) = f_0(\eta) + \sum_{m=1}^{\infty} f_m(\eta), \quad (10.44)$$

$$\theta(\eta) = \theta_0(\eta) + \sum_{m=1}^{\infty} \theta_m(\eta), \quad (10.45)$$

$$\phi(\eta) = \phi_0(\eta) + \sum_{m=1}^{\infty} \phi_m(\eta). \quad (10.46)$$

The general solutions  $(f_m, \theta_m, \phi_m)$  in terms of special solutions  $(f_m^*, \theta_m^*, \phi_m^*)$  can be written as follows

$$f_m(\eta) = f_m^*(\eta) + C_1 + C_2 \exp(\eta) + C_3 \exp(-\eta), \quad (10.47)$$

$$\theta_m(\eta) = \theta_m^*(\eta) + C_4 \exp(\eta) + C_5 \exp(-\eta), \quad (10.48)$$

$$\phi_m(\eta) = \phi_m^*(\eta) + C_6 \exp(\eta) + C_7 \exp(-\eta). \quad (10.49)$$

### 10.3 Convergence of the homotopy solutions

The convergence analysis of the series solutions depends upon the auxiliary parameters  $\hbar_f$ ,  $\hbar_\theta$  and  $\hbar_\phi$ . Hence the  $\hbar$ -curves for the 17<sup>th</sup> order of approximations are plotted. It is found that the admissible ranges of  $\hbar_f$ ,  $\hbar_\theta$  and  $\hbar_\phi$  are  $-1.7 \leq \hbar_f \leq -0.20$ ,  $-1.5 \leq \hbar_\theta \leq -0.25$  and  $-1.5 \leq \hbar_\phi \leq -0.40$ . The series (10.44 – 10.46) converge in the whole region of  $\eta$  when  $\hbar_f = \hbar_\theta = \hbar_\phi = -1.0$  (see Fig. 10.1). Table 10.1 indicates that how much terms for each

physical quantity are required for the convergent solution. It is noticed that less number of terms are required in the convergent expression of velocity.

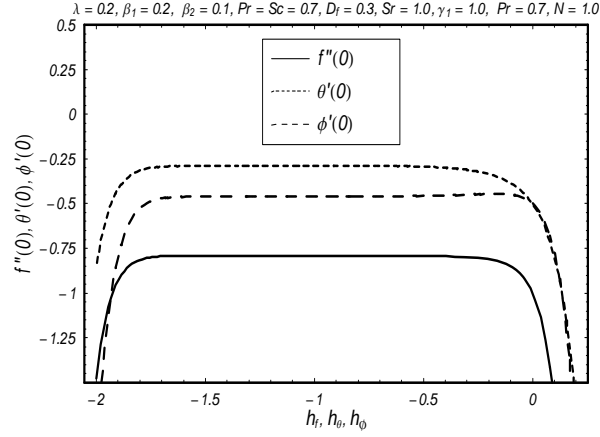


Fig.10.1 :  $\hbar$ -curves for the function  $f$ ,  $\theta$  and  $\phi$ .

**Table 10.1:** Convergence of homotopy solutions for different order of approximations when  $\beta_1 = 0.2$ ,  $\beta_2 = 0.1$ ,  $Pr = Sc = 0.7$ ,  $\gamma_1 = 1.0$ ,  $D_f = 0.3$ ,  $Sr = 0.2$ ,  $N = 1.0$ ,  $\hbar_f = \hbar_\theta = \hbar_\phi = -1.0$ .

Order of approximations	$-f''(0)$	$-\theta'(0)$	$-\phi'(0)$
1	0.82500	0.39104	0.43194
5	0.79502	0.30304	0.45255
10	0.79137	0.29030	0.46033
15	0.79129	0.28971	0.46071
20	0.79132	0.28991	0.46044
25	0.79133	0.28993	0.46042
30	0.79133	0.28993	0.46043

## 10.4 Discussion

Interest in this section is to analyze the variations of different emerging parameters on the physical quantities like temperature, concentration field, local Nusselt and Sherwood numbers. Figs. 10.2 – 10.9 are displayed to see the variations of mixed convection parameter  $\lambda$ , concentration buoyancy parameter  $N$ , Dufour number  $D_f$  and Soret number  $Sr$  on the temperature of fluid

$\theta(\eta)$ . Fig. 10.2 shows that the mixed convection parameter  $\lambda$  decreases the temperature  $\theta(\eta)$ . Also thermal boundary layer thickness reduces with an increase in mixed convection parameter  $\lambda$ . Fig. 10.3 illustrated that temperature and associated thermal boundary layer thickness are decreasing functions of  $N$ . Fig. 10.4 shows that temperature  $\theta(\eta)$  and thermal boundary layer thickness increase with an increase in Dufour number  $D_f$ . With an increase in Soret number  $Sr$ , temperature  $\theta(\eta)$  and thermal boundary layer thickness decrease as seen in Fig. 10.5.

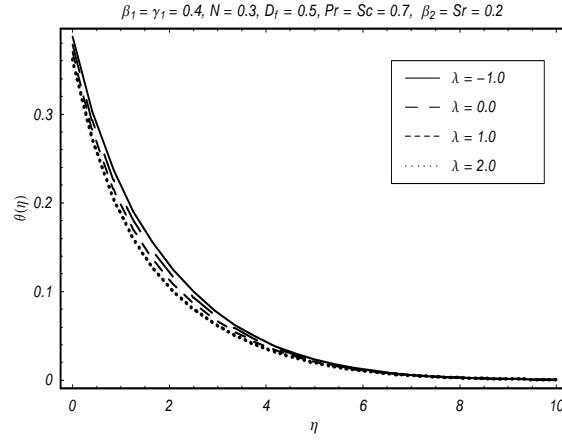


Fig. 10.2: Influence of  $\lambda$  on  $\theta(\eta)$ .

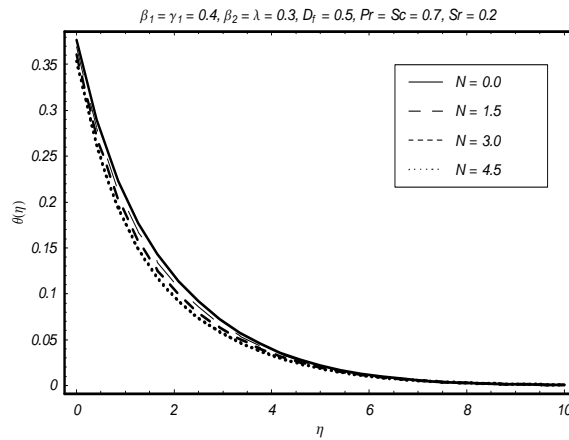


Fig. 10.3: Influence of  $N$  on  $\theta(\eta)$ .

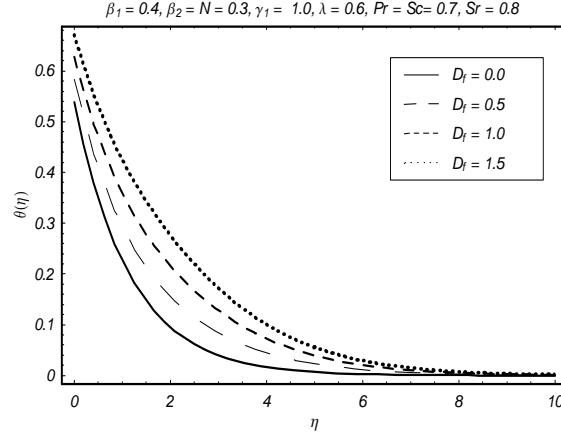


Fig. 10.4: Influence of  $D_f$  on  $\theta(\eta)$ .

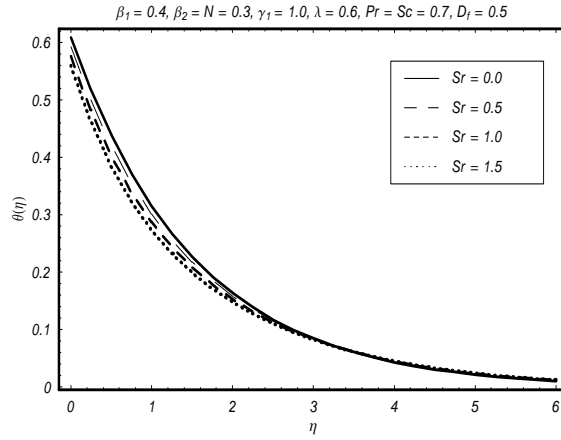


Fig. 10.5: Influence of  $Sr$  on  $\theta(\eta)$ .

Figs. 10.6 – 10.9 plot the effects of  $\lambda$ ,  $N$ ,  $D_f$  and  $Sr$  on the concentration field  $\phi(\eta)$ . From Fig. 10.6 it is found that the concentration field and associated boundary layer thickness show a decrease when mixed convection parameter  $\lambda$  increases. Effects of concentration buoyancy parameter  $N$  on the concentration are qualitatively similar to that of temperature (see Figs. 10.3 and 10.7). Figs. 10.4 and 10.8 show that the behaviors of the temperature and concentration profiles are quite opposite in case of Dufour number. This shows that the Dufour number corresponds to weaker concentration and stronger temperature. Fig. 10.9 pointed out

that the larger Soret number has a strong concentration.

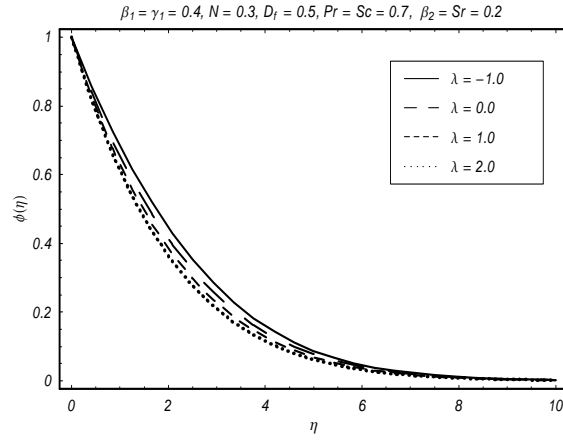


Fig. 10.6: Influence of  $\lambda$  on  $\phi(\eta)$ .

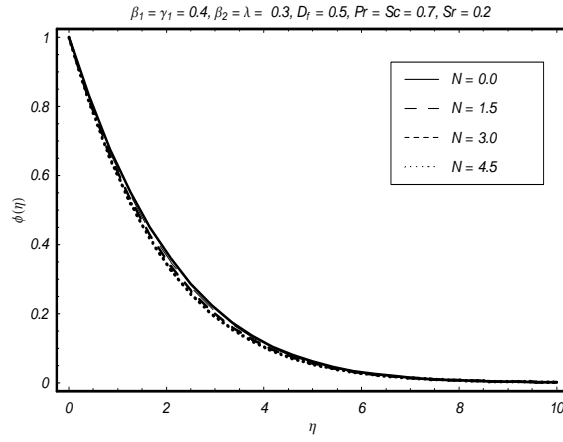


Fig. 10.7: Influence of  $N$  on  $\phi(\eta)$ .

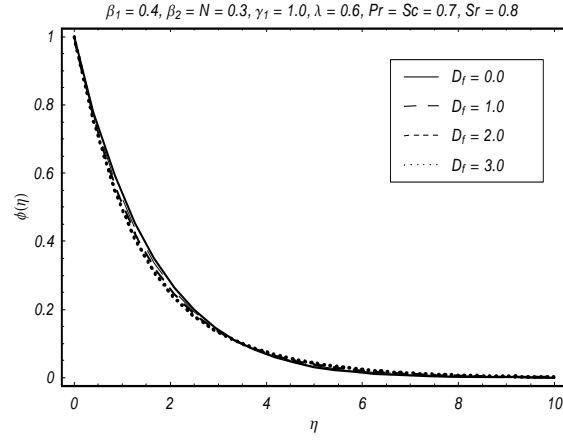


Fig. 10.8: Influence of  $D_f$  on  $\phi(\eta)$ .

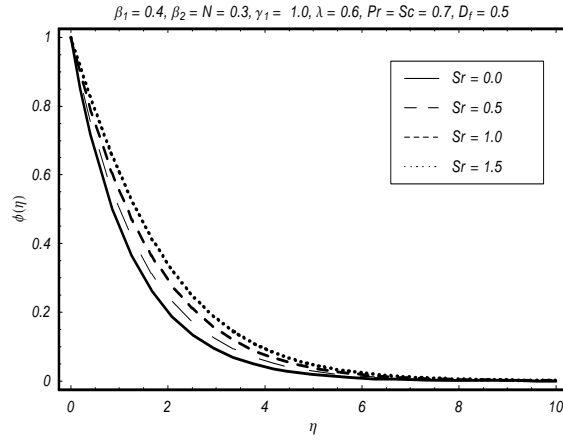


Fig. 10.9: Influence of  $Sr$  on  $\phi(\eta)$ .

**Table 10.2:** Values of local Nusselt number and Sherwood number for the parameters  $\beta_1$ ,



$\beta_2, Pr, Sr, D_f, \gamma_1$  and  $N$  when  $\lambda = 0.1$ .

$\beta_1$	$\beta_2$	$\lambda$	$Pr$	$Sr$	$D_f$	$Sc$	$\gamma_1$	$N$	$-\theta'(0)$	$-\phi'(0)$
0.0	0.2	0.1	0.7	0.5	0.8	1	1	1	0.29514	0.47225
0.2									0.28993	0.46033
0.4									0.28525	0.44998
0.2	0.0								0.28797	0.45592
	0.2								0.29176	0.46462
	0.4								0.29508	0.47226
0.2	0.2	0.0							0.27062	0.41866
		0.2							0.29176	0.46463
		0.4							0.30305	0.49095
0.2	0.2	0.2	0.8						0.30136	0.50625
			0.9						0.30891	0.54602
			1.0						0.31480	0.58434
			0.7	0.0					0.28679	0.49981
			0.2						0.29176	0.46462
			0.4						0.29679	0.42800
			0.2	0.0					0.33235	0.45353
				0.2					0.30546	0.46096
				0.4					0.27788	0.46830
				0.2	1.0				0.30546	0.46094
					1.2				0.30001	0.51681
					1.4				0.29513	0.56908
					1.0	1.0			0.30546	0.46094
						1.2			0.32396	0.45920
						1.4			0.33863	0.45781
						1.0	1.0		0.30546	0.46094
							1.2		0.30700	0.46444
							1.4		0.30846	0.46779

## 10.5 Conclusions

Mixed convection flow of an Oldroyd-B fluid is investigated in the presence of convective boundary condition and Soret and Dufour effects. The main observations are pointed out below.

- Effects of  $\lambda$  and  $N$  on temperature and concentration fields are similar.
- Effects of Soret number  $Sr$  on  $\theta(\eta)$  and  $\phi(\eta)$  are reverse.
- Thermal boundary layer thickness and temperature field increase when  $D_f$  increases.
- There are opposite effects of local Nusselt number and Sherwood number when  $D_f$ ,  $Sr$  and  $\gamma_1$  increase.
- local Nusselt and Sherwood numbers decrease when  $\beta_1$  increases.
- With an increase in  $\lambda$  and  $N$  both local Nusselt and Sherwood numbers are enhanced.

## Chapter 11

# Mixed convection Falkner-Skan wedge flow of an Oldroyd-B fluid in presence of thermal radiation

The present chapter examines the Falkner-Skan flow of rate type non-Newtonian fluid. Expressions of an Oldroyd-B fluid in the presence of mixed convection and thermal radiation are used in the development of relevant equations. The resulting partial differential equations are reduced into the ordinary differential equations employing appropriate transformations. Expressions of flow and heat transfer are constructed. Convergence of derived nonsimilar series solutions is guaranteed. Impact of various parameters involved in the flow and heat transfer is plotted and examined.

### 11.1 Problems development

Let us consider the two-dimensional Falkner-Skan flow of an Oldroyd-B fluid. We further consider the heat transfer. Cartesian coordinates  $(x, y)$  are used in such a way that  $x$ -axis is parallel to the wall and  $y$ -axis normal to it. An incompressible fluid occupies the region  $y \geq 0$ . The equations governing the present flow situation are based on the conservation laws of mass,

linear momentum and energy. Flow diagram of the problem is as follows:

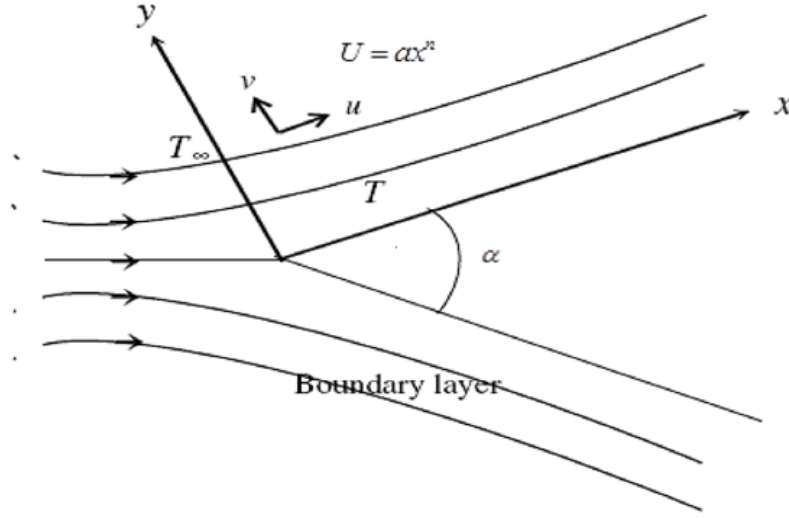


Fig. 11.1: Physical Model

Taking into account the aforementioned assumptions, the resulting boundary layer equations can be written as follows:

$$\frac{\partial u}{\partial x} + \frac{\partial v}{\partial y} = 0, \quad (11.1)$$

$$\begin{aligned} u \frac{\partial u}{\partial x} + v \frac{\partial u}{\partial y} = & \nu \frac{\partial^2 u}{\partial y^2} - \lambda_1 \left[ u^2 \frac{\partial^2 u}{\partial x^2} + v^2 \frac{\partial^2 u}{\partial y^2} + 2uv \frac{\partial^2 u}{\partial x \partial y} \right] \\ & + \nu \lambda_2 \left[ u \frac{\partial^3 u}{\partial x \partial y^2} + v \frac{\partial^3 u}{\partial y^3} - \frac{\partial u}{\partial x} \frac{\partial^2 u}{\partial y^2} - \frac{\partial u}{\partial y} \frac{\partial^2 v}{\partial y^2} \right] \\ & + g\beta_T (T - T_\infty) \sin \frac{\alpha}{2}, \end{aligned} \quad (11.2)$$

$$\rho c_p \left( u \frac{\partial T}{\partial x} + v \frac{\partial T}{\partial y} \right) = \frac{\partial}{\partial y} \left( \left( \frac{16\sigma_s T_\infty^3}{3k_e} + k \right) \frac{\partial T}{\partial y} \right). \quad (11.3)$$

The appropriate boundary conditions are

$$\begin{aligned} u &= U, \quad v = 0, \quad T = T_w = T_\infty + Ax^d \quad \text{at } y = 0, \\ u &\rightarrow 0, \quad T \rightarrow T_\infty \quad \text{as } y \rightarrow \infty \end{aligned} \quad (11.4)$$

where  $U (= ax^n)$  is the free stream velocity,  $\mu$  is the dynamic viscosity,  $\lambda_1$  is the relaxation

time,  $\lambda_2$  is the retardation time,  $\alpha$  is the wedge angle,  $k$  is the thermal conductivity,  $d$  is the surface temperature exponent,  $T$  and  $T_\infty$  are the temperatures of the fluid and ambient respectively and  $T_w$  is the wall temperature. We utilize

$$\begin{aligned} u &= U(x) f', \quad \eta = \sqrt{\frac{n+1}{2}} \sqrt{\frac{U}{\nu x}} y, \quad \psi = \sqrt{\frac{2}{n+1}} \sqrt{\nu x U} f(\eta), \\ v &= -\sqrt{\frac{n+1}{2}} \sqrt{\frac{\nu U}{x}} \left[ f(\eta) + \frac{n-1}{n+1} \eta f'(\eta) \right], \quad \theta(\eta) = \frac{T - T_\infty}{T_w - T_\infty}, \end{aligned} \quad (11.5)$$

where  $\eta$  is the similarity variable,  $\psi$  is the stream function,  $f$  is the dimensionless stream function and  $\theta$  is the dimensionless temperature. Now the continuity equation (11.1) is identically satisfied and Eqs. (11.2) – (11.4) lead to the following expressions

$$\begin{aligned} f''' + f f'' + \beta_1 \left( -2n \left( \frac{n-1}{n+1} \right) f'^3 + (3n-1) f f' f'' - \left( \frac{n+1}{2} \right) f^2 f''' + \left( \frac{n-1}{2} \right) \eta f'^2 f'' \right) \\ + \beta_2 \left( \left( \frac{3n-1}{2} \right) (f'')^2 - \left( \frac{n+1}{2} \right) f f'''' + (n-1) f' f''' \right) - \frac{2n}{n+1} f'^2 + \frac{2}{n+1} \lambda \theta \sin \frac{\alpha}{2} = 0, \end{aligned} \quad (11.6)$$

$$\left( 1 + \frac{4}{3} R \right) \theta'' + \text{Pr} (f \theta' - \frac{2d}{n+1} f' \theta) = 0, \quad (11.7)$$

$$f(0) = 0, \quad f'(0) = 1, \quad \theta(0) = 1, \quad f'(\infty) = 0, \quad \theta(\infty) = 0. \quad (11.8)$$

Here prime denotes the differentiation with respect to  $\eta$ ,  $\beta_1$  and  $\beta_2$  are the dimensionless material parameters,  $\lambda$  is mixed convection parameter,  $Gr_x$  is the local Grashof number,  $\text{Pr}$  is the Prandtl number and  $R$  is the radiation parameter. The definitions of these parameters are

$$\begin{aligned} \beta_1 &= \frac{\lambda_1 U}{x}, \quad \beta_2 = \frac{\lambda_2 U}{x}, \quad \lambda = \frac{Gr_x}{\text{Re}_x^2}, \quad \text{Pr} = \frac{\mu c_p}{k}, \\ R &= \left( \frac{4\sigma_s T_\infty^3}{k_e k} \right), \quad Gr_x = \frac{g \beta (T_w - T_\infty) x^3}{\nu^2}. \end{aligned} \quad (11.9)$$

Local Nusselt number ( $Nu_x$ ) along with heat transfer rate ( $q_w$ ) are

$$Nu_x = \frac{x q_w}{k (T_w - T_\infty)}, \quad q_w = -k \left( \frac{\partial T}{\partial y} \right)_{y=0} \quad (11.10)$$

which in dimensionless form gives

$$(\text{Re}_x)^{-1/2} Nu_x = -\theta'(0). \quad (11.11)$$

## 11.2 Series solutions

The initial guesses  $(f_0, \theta_0)$  and auxiliary linear operators  $(\mathcal{L}_f, \mathcal{L}_\theta)$  are taken as follows

$$f_0(\eta) = 1 - e^{-\eta}, \quad \theta_0(\eta) = e^{-\eta}, \quad (11.12)$$

$$\mathcal{L}_f(f) = \frac{d^3 f}{d\eta^3} - \frac{df}{d\eta}, \quad \mathcal{L}_\theta(\theta) = \frac{d^2 \theta}{d\eta^2} - \theta, \quad (11.13)$$

with

$$\mathcal{L}_f[C_1 + C_2 \exp(\eta) + C_3 \exp(-\eta)] = 0, \quad (11.14)$$

$$\mathcal{L}_\theta[C_4 \exp(\eta) + C_5 \exp(-\eta)] = 0, \quad (11.15)$$

where  $C_i$  ( $i = 1 - 5$ ) are the arbitrary constants. If  $p \in [0, 1]$  is the embedding parameter and  $\hbar_f$  and  $\hbar_\theta$  are the non-zero auxiliary parameters then the zeroth-order and  $m$ th order deformation problems are stated as follows.

### 11.2.1 Zeroth order problem

$$(1-p) \mathcal{L}_f [\hat{f}(\eta; p) - f_0(\eta)] = p \hbar_f \mathcal{N}_f [\hat{f}(\eta; p), \hat{\theta}(\eta; p)], \quad (11.16)$$

$$(1-p) \mathcal{L}_\theta [\hat{\theta}(\eta; p) - \theta_0(\eta)] = p \hbar_\theta \mathcal{N}_\theta [\hat{\theta}(\eta; p), \hat{f}(\eta; p)], \quad (11.17)$$

$$\hat{f}(0; p) = 0, \hat{f}'(0; p) = 0, \hat{f}'(\infty; p) = 1, \hat{\theta}(0; q) = 1, \hat{\theta}(\infty; q) = 0, \quad (11.18)$$

$$\begin{aligned}
\mathcal{N}_f [\hat{f}(\eta, p), \hat{\theta}(\eta; p)] &= \frac{\partial^3 f(\eta; p)}{\partial \eta^3} + f(\eta; p) \frac{\partial^2 f(\eta; p)}{\partial \eta^2} - \frac{2n}{n+1} \left( \frac{\partial f(\eta; p)}{\partial \eta} \right)^2 \\
&+ \beta_1 \left( -2n \frac{n-1}{n+1} \left( \frac{\partial f(\eta; p)}{\partial \eta} \right)^3 + (3n-1) f(\eta; p) \frac{\partial f(\eta; p)}{\partial \eta} \frac{\partial^2 f(\eta; p)}{\partial \eta^2} \right) \\
&- \beta_1 \left( \frac{n+1}{2} (f(\eta; p))^2 \frac{\partial^3 f(\eta; p)}{\partial \eta^3} + \frac{n-1}{2} \eta \left( \frac{\partial f(\eta; p)}{\partial \eta} \right)^2 \frac{\partial^2 f(\eta; p)}{\partial \eta^2} \right) \\
&+ \beta_2 \left( \left( \frac{3n-1}{2} \right) \left( \frac{\partial^2 f(\eta; p)}{\partial \eta^2} \right)^2 - \left( \frac{n+1}{2} \right) f(\eta; p) \frac{\partial^4 f(\eta; p)}{\partial \eta^4} \right) \\
&+ \beta_2 \left( (n-1) \frac{\partial f(\eta; p)}{\partial \eta} \frac{\partial^3 f(\eta; p)}{\partial \eta^3} \right) + \frac{2}{n+1} \lambda \hat{\theta}(\eta, p) \sin \frac{\alpha}{2}, \quad (11.19)
\end{aligned}$$

$$\begin{aligned}
\mathcal{N}_\theta [\hat{\theta}(\eta; p), \hat{f}(\eta; p)] &= \left( 1 + \frac{4}{3} R \right) \frac{\partial^2 \hat{\theta}(\eta, p)}{\partial \eta^2} + \text{Pr} \hat{f}(\eta; p) \frac{\partial \hat{\theta}(\eta; p)}{\partial \eta} \\
&- \text{Pr} \frac{2d}{n+1} \hat{\theta}(\eta; p) \frac{\partial \hat{f}(\eta; p)}{\partial \eta}. \quad (11.20)
\end{aligned}$$

### 11.2.2 $m$ th-order deformation problems

$$\mathcal{L}_f [f_m(\eta) - \chi_m f_{m-1}(\eta)] = \hbar_f \mathcal{R}_m^f(\eta), \quad (11.21)$$

$$\mathcal{L}_\theta [\theta_m(\eta) - \chi_m \theta_{m-1}(\eta)] = \hbar_\theta \mathcal{R}_m^\theta(\eta), \quad (11.22)$$

$$\begin{aligned}
f_m(0) &= f'_m(0) = f'_m(\infty) = f''_m(\infty) = 0, \\
\theta_m(0) &= \theta_m(\infty) = 0, \quad (11.23)
\end{aligned}$$

$$\begin{aligned}
\mathcal{R}_m^f(\eta) &= f'''_{m-1}(\eta) + \sum_{k=0}^{m-1} \left[ +\beta_1 \left( \begin{aligned} &f_{m-1-k} f''_k - \frac{2n}{n+1} f'_{m-1-k} f'_k \\ &-2n \frac{n-1}{n+1} f'_{m-1-k} \sum_{l=0}^k f'_{k-l} f'_l + (3n-1) f_{m-1-k} \sum_{l=0}^k f'_{k-l} f''_l \\ &-\frac{n+1}{2} f_{m-1-k} \sum_{l=0}^k f_{k-l} f'''_l + \frac{n-1}{2} \eta f'_{m-1-k} \sum_{l=0}^k f'_{k-l} f''_l \end{aligned} \right) \right. \\
&\quad \left. +\beta_2 \left( \begin{aligned} &\frac{3n-1}{2} f''_{m-1-k} f''_k \\ &-\frac{n+1}{2} f_{m-1-k} f'''_k \\ &+ (n-1) f'_{m-1-k} f'''_k \end{aligned} \right) \right] \\
&+ \frac{2}{n+1} \lambda \theta_{m-1} \sin \frac{\alpha}{2}, \quad (11.24)
\end{aligned}$$

$$\mathcal{R}_m^\theta(\eta) = \theta''_{m-1} + \Pr \sum_{k=0}^{m-1} \left( \theta'_{m-1-k} f_k - \frac{2d}{n+1} f'_{m-1-k} \theta_k \right), \quad (11.25)$$

$$\chi_m = \begin{cases} 0, & m \leq 1 \\ 1, & m > 1 \end{cases}. \quad (11.26)$$

For  $p = 0$  and  $p = 1$ , we have

$$\widehat{f}(\eta; 0) = f_0(\eta), \quad \widehat{f}(\eta; 1) = f(\eta), \quad (11.27)$$

$$\widehat{\theta}(\eta; 0) = \theta_0(\eta), \quad \widehat{\theta}(\eta; 1) = \theta(\eta), \quad (11.28)$$

and when  $p$  increases from 0 to 1 then  $\widehat{f}(\eta; p)$  and  $\widehat{\theta}(\eta; p)$  vary from the initial solutions  $f_0(\eta)$  and  $\theta_0(\eta)$  to final solutions  $f(\eta)$  and  $\theta(\eta)$  respectively. By Taylor's expansion one has

$$\widehat{f}(\eta; p) = f_0(\eta) + \sum_{m=1}^{\infty} f_m(\eta) p^m, \quad f_m(\eta) = \frac{1}{m!} \frac{\partial^m \widehat{f}(\eta; p)}{\partial p^m} \Big|_{p=0}, \quad (11.29)$$

$$\widehat{\theta}(\eta; p) = \theta_0(\eta) + \sum_{m=1}^{\infty} \theta_m(\eta) p^m, \quad \theta_m(\eta) = \frac{1}{m!} \frac{\partial^m \widehat{\theta}(\eta; p)}{\partial p^m} \Big|_{p=0}, \quad (11.30)$$

where the auxiliary parameters are so properly chosen that the series (11.29) and (11.31) converge at  $p = 1$  i.e.

$$f(\eta) = f_0(\eta) + \sum_{m=1}^{\infty} f_m(\eta), \quad (11.31)$$

$$\theta(\eta) = \theta_0(\eta) + \sum_{m=1}^{\infty} \theta_m(\eta). \quad (11.32)$$

The general solutions of Eqs. (11.32) and (11.33) are

$$f_m(\eta) = f_m^*(\eta) + C_1 + C_2 e^\eta + C_3 e^{-\eta}, \quad (11.33)$$

$$\theta_m(\eta) = \theta_m^*(\eta) + C_4 e^\eta + C_5 e^{-\eta}, \quad (11.34)$$

in which  $f_m^*$  and  $\theta_m^*$  are the special solutions.



### 11.3 Convergence

Note that the series solutions in Eqs. (11.32) and (11.33) contain two auxiliary parameters  $\hbar_f$  and  $\hbar_\theta$ . The convergence of series solutions depend upon these auxiliary parameters. For range of values of these parameters, the  $\hbar$ -curves at 15th-order of approximations have been plotted in Fig. 11.2. It is found that the admissible values of  $\hbar_f$  and  $\hbar_\theta$  are  $-1.3 \leq \hbar_f \leq -0.25$  and  $-1.2 \leq \hbar_\theta \leq -0.5$ . Table 11.1 further guarantees that the series solutions are convergent up to five decimal places when  $\hbar_f = \hbar_\theta = -0.5$ .

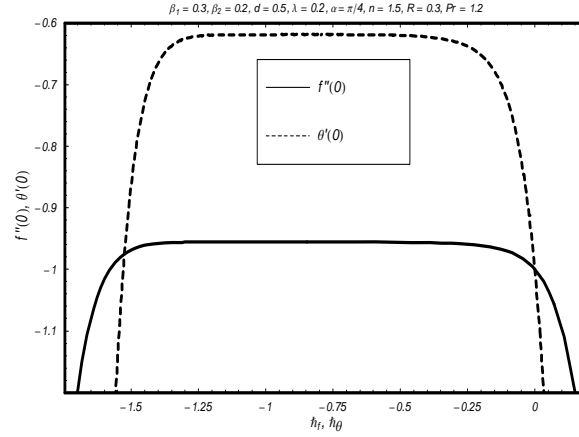


Fig.11.2 :  $\hbar$ -curves for the function  $f$  and  $\theta$ .

### 11.4 Discussion

The aim of this subsection is to present the effects of pertinent parameters on the velocity, temperature and surface heat transfer. Variation of parameter  $n$  on the velocity and temperature are sketched in the Figs. 11.3 and 11.4. Clearly the effects of  $n$  on the velocity and temperature profiles are quite reverse. Influence of mixed convection parameter  $\lambda$  on both the velocity and temperature profiles are given in the Figs. 11.5 and 11.6. It is observed that the velocity and momentum boundary layer thickness increase with the increase of mixed convection parameter  $\lambda$  while the temperature and thermal boundary layer thickness decrease. Figs. 11.7 and 11.8 are drawn to see the variation of  $\alpha$  on the velocity and temperature profiles. It is noticed that the velocity and momentum boundary layer thickness increase when  $\alpha$  increases. It is found that the temperature and thermal boundary layer thickness are decreasing functions of  $\alpha$ . Figs.

11.9 and 11.10 are sketched to see the variation of surface temperature parameter  $d$  on the velocity  $f'(\eta)$  and the temperature  $\theta(\eta)$ . Both  $f'(\eta)$  and  $\theta(\eta)$  decrease with the increase in  $d$ . It is also observed that both the momentum and thermal boundary layer thicknesses decrease when  $d$  increases.

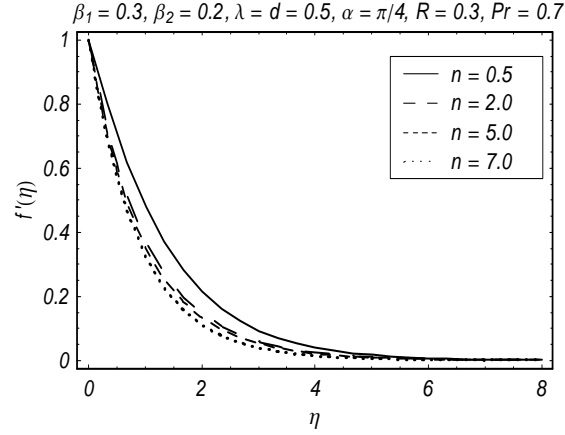


Fig. 11.3: Impact of  $n$  on  $f'(\eta)$ .

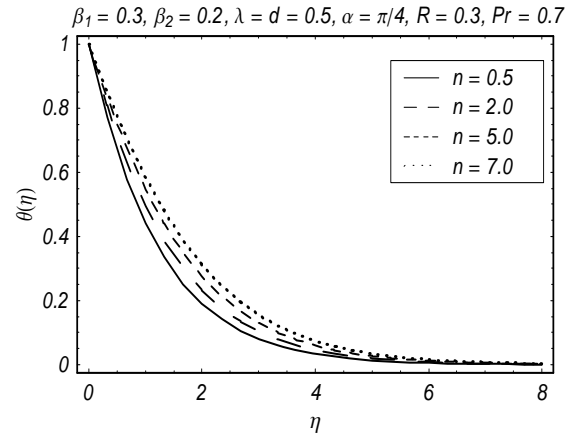


Fig. 11.4: Impact of  $n$  on  $\theta(\eta)$ .

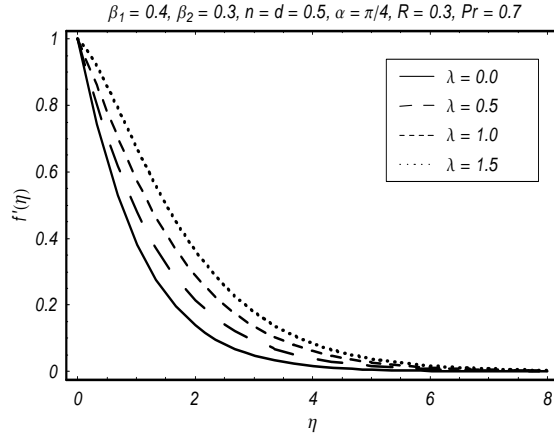


Fig. 11.5: Impact of  $\lambda$  on  $f'(\eta)$ .

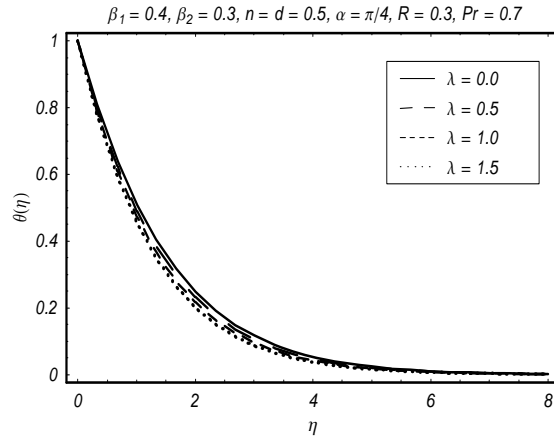


Fig. 11.6: Impact of  $\lambda$  on  $\theta(\eta)$ .

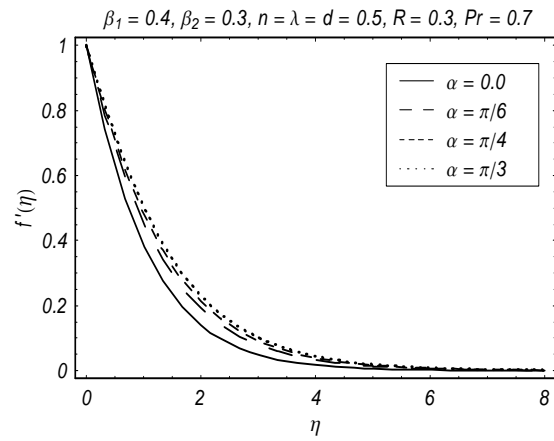


Fig. 11.7: Impact of  $\alpha$  on  $f'(\eta)$ .

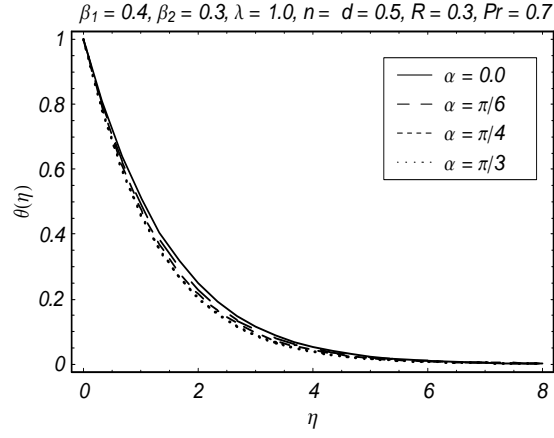


Fig. 11.8: Impact of  $\alpha$  on  $\theta(\eta)$ .

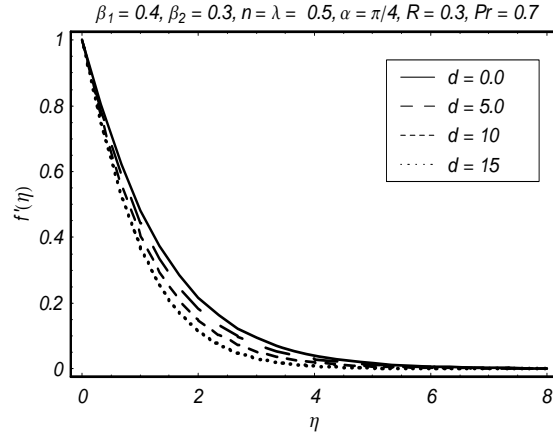


Fig. 11.9: Impact of  $d$  on  $f'(\eta)$ .

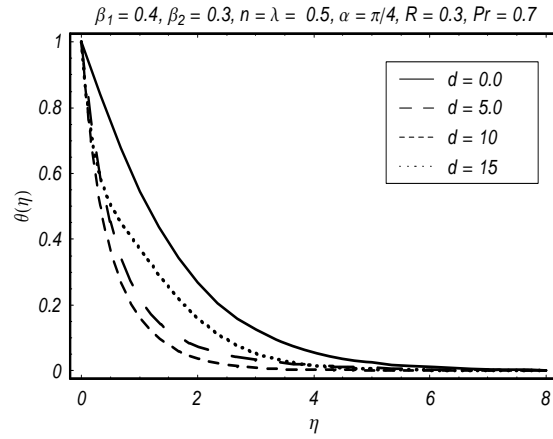


Fig. 11.10: Impact of  $d$  on  $\theta(\eta)$ .

Figs. 11.11 and 11.12 are drawn to see the influence of mixed convection parameter  $\lambda$ , wedge angle  $\alpha$ , surface temperature parameter  $d$  and velocity index  $n$  on the local Nusselt number  $-\theta'(0)$ . Fig. 11.11 depicts the effects of  $\lambda$  and  $\alpha$  on  $-\theta'(0)$ . It is noticed that  $-\theta'(0)$  increases through increase of mixed convection parameter  $\lambda$  and wedge angle  $\alpha$ . Fig. 11.12 depicts that variations of  $n$  and  $d$  have opposite effects on  $-\theta'(0)$ . A close look at Table 11.1 indicates that 25<sup>th</sup>-order approximation gives convergent series solutions.

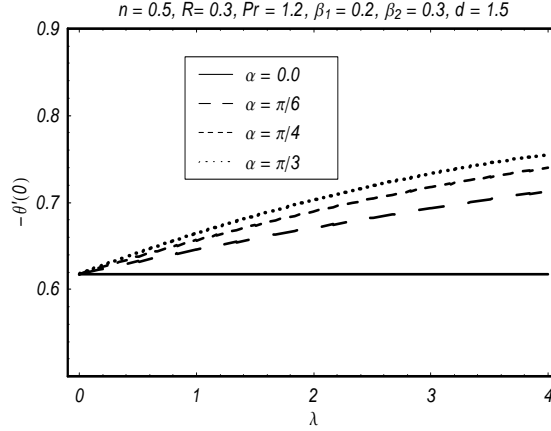


Fig. 11.11: Impacts of  $\lambda$  and  $\alpha$  on  $-\theta'(0)$ .

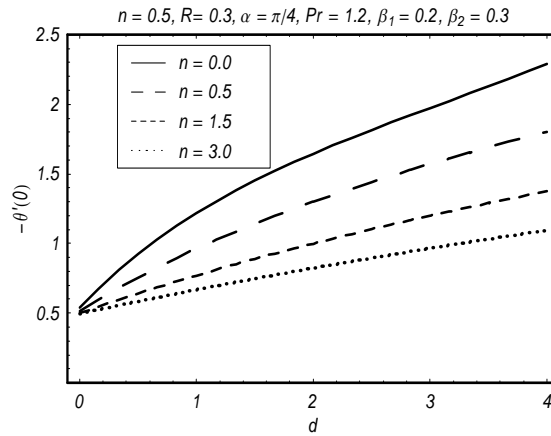


Fig. 11.12: Impacts of  $d$  and  $n$  on  $-\theta'(0)$ .

Table 11.1 : Convergence of the homotopy solutions for different order of approximation when  $Pr = 1.0$ ,  $\lambda = 0.3$ ,  $n = 1.5$ ,  $d = 0.5$ ,  $R = 0.3$ ,  $\alpha = \pi/4$ ,  $\beta_1 = 0.2$ ,  $\beta_2 = 0.3$  and

$$\hbar_f = \hbar_\theta = -0.5.$$

Order of approximation	$-f'''(0)$	$-\theta'(0)$
1	0.90330	0.78889
5	0.86304	0.64042
10	0.86077	0.62757
15	0.86047	0.62627
20	0.86045	0.62616
25	0.86044	0.62616
30	0.86044	0.62616

## 11.5 Conclusions

Mixed convection and thermal radiation effects in the Falkner-Skan wedge flow of an Oldroyd-B fluid are investigated. The following points are worth mentioning:

- Table 11.1 shows that convergence of the functions  $f$  and  $\theta$  are obtained at 25<sup>th</sup>-order approximations up to five decimal places when  $\hbar_f = \hbar_\theta = -0.5$ .
- Influence of mixed convection parameter  $\lambda$  increases the velocity and momentum boundary layer thickness while it decreases the temperature and thermal boundary layer thickness.
- Influence of wedge angle  $\alpha$  and radiation parameter  $R$  on both the temperature and velocity profiles are quite similar.
- Thermal boundary layer and momentum boundary layer thicknesses are decreasing functions of surface temperature exponent  $d$ .
- Surface heat transfer  $-\theta'(0)$  increases with an increase of wedge angle  $\alpha$ , mixed convection parameter  $\lambda$  and surface temperature exponent  $d$ .

# Bibliography

- [1] H. Schlichting, Boundary layer theory, 6th ed. Mc-Graw Hill, New York (1964).
- [2] B.C. Sakiadis, Boundary layer behavior on continuous solid surfaces: II Boundary on a continuous flat surface, *AIChE J.* 7 (1961) 221-225.
- [3] L.J. Crane, Flow past a stretching plate, *Z. Angew. Math. Phys.* 21 (1970) 645-647.
- [4] A. Chakrabarti and A. S. Gupta, Hydromagnetic flow and heat transfer over a stretching sheet, *Quarterly Appl. Math.* 37 (1979) 73-78.
- [5] C. K. Chen and M. I. Char, Heat transfer of a continuous stretching surface with suction or blowing, *J. Math. Anal. Appl.* 135 (1988) 568–580.
- [6] K. Vajravelu and A. Hadjinicolaou, Heat transfer in a viscous fluid over a stretching sheet with viscous dissipation and internal heat generation, *Int. Commun. Heat Mass Transf.* 20 (1993) 417-430.
- [7] H.I. Andersson, O.R. Hansen and B. Holmedal, Diffusion of a chemically reactive species from a stretching sheet, *Int. J. Heat Mass Transf.* 37 (1994) 659–664.
- [8] W. H. H. Banks, Similarity solutions of the boundary-layer equations for a stretching wall, *J. Méch. Théor. Appl.* 2 (1983) 375–392.
- [9] T. G. Fang, J. Zhang and S. Yao, Slip magnetohydrodynamic viscous flow over a permeable shrinking sheet, *Chin. Phys. Lett.* 27 (2010) 124702.

- [10] S. Mukhopadhyay, G. C. Layek and S. A. Samad, Study of MHD boundary layer flow over a heated stretching sheet with variable viscosity, *Int. J. Heat Mass Transf.* 48 (2005) 4460–4466.
- [11] C.Y. Wang, The three-dimensional flow due to a stretching flat surface, *Phys. Fluid* 27 (1984) 1915–1917.
- [12] C. D. S. Devi, H. S. Takhar and G. Nath, Unsteady three-dimensional, boundary-layer flow due to a stretching surface, *Int. J. Heat Mass Transf.* 29 (1986) 1996–1999.
- [13] P. D. Ariel, The three-dimensional flow past a stretching sheet and the homotopy perturbation method, *Computers Mathematics Appl.* 54 (2007) 920–925.
- [14] P. D. Ariel, On computation of the three dimensional flow past a stretching sheet, *Appl. Math. Comput.* 188 (2007) 1244–1250.
- [15] T. Hayat and T. Javed, On analytic solution for generalized three-dimensional MHD flow over a porous stretching sheet, *Phys. Lett. A* 370 (2007) 243–250.
- [16] M. Kumari and G. Nath, Analytic solution of unsteady three-dimensional MHD boundary layer flow and heat transfer due to impulsively stretched plane surface, *Commun. Nonlinear Sci. Numer. Simulat.* 14 (2009) 3339–3350.
- [17] K. Vajravelu, Viscous flow over a nonlinear stretching sheet, *Appl. Math. Comput.* 124 (2001) 281–288.
- [18] R. Cortell, Effects of viscous dissipation and radiation on the thermal boundary layer over a nonlinearly stretching sheet, *Phys. Lett. A* 372 (2008) 631–636.
- [19] T. Hayat, T. Javed and Z. Abbas, MHD flow of a micropolar fluid near a stagnation-point towards a non-linear stretching surface, *Nonlinear Analysis: Real World Appl.* 10 (2009) 1514–1526.
- [20] N. Afzal, Momentum and thermal boundary layers over a two-dimensional or axisymmetric non-linear stretching surface in a stationary fluid, *Int. J. Heat Mass Transf.* 53 (2010) 540–547.



- [21] P. S. Gupta and A. S. Gupta, Heat and mass transfer on a stretching sheet with suction or blowing, *Can. J. Chem. Eng.* 55 (1977) 744-746.
- [22] E. Magyari and B. Keller, Heat and mass transfer in the boundary layers on an exponentially stretching continuous surface, *J. Phys. D: Appl. Phys.* 32 (1999) 577—585.
- [23] E. M. A. Elbashbeshy, Heat transfer over an exponentially stretching continuous surface with suction, *Arch. Mech.* 53 (2001) 643-651.
- [24] M. Q. Al-Odat, R. A. Damesh and T. A. Al-Azab, Thermal boundary layer on an exponentially stretching continuous surface in the presence of magnetic field, *Int. J. Appl. Mech. Eng.* 11 (2006) 289-299.
- [25] I. C. Liu, H. H. Wang and Y. F. Peng, Flow and heat transfer for three dimensional flow over an exponentially stretching surface, *Chem. Eng. Commun.* 200 (2013) 253-268.
- [26] B. S. Dandapat and A. S. Gupta, Flow and heat transfer in a viscoelastic fluid over a stretching sheet, *Int. J. Non-Linear Mech.* 24 (1989) 215-219.
- [27] C. K. Chen, M. I. Char and J. W. Cleaver, Temperature field in non-Newtonian flow over a stretching plate, *J. Math. Anal. Appl.* 151 (1990) 301-307.
- [28] K. Vajravelu and D. Rollins, Heat transfer in a viscoelastic fluid over a stretching sheet, *J. Math. Anal. Appl.* 158 (1991) 241–255.
- [29] T. Hayat, M. Sajid and I. Pop, Three-dimensional flow over a stretching surface in a viscoelastic fluid, *Nonlinear Analysis: Real World Appl.* 9 (2008) 1811 – 1822.
- [30] I. C. Liu, Flow and heat transfer of an electrically conducting fluid of second grade over a stretching sheet subject to a transverse magnetic field, *Int. J. Heat Mass Transf.* 47 (2004) 4427–4437.
- [31] M. M. Nandeppanavar, M. S. Abel and K. Vajravelu, Flow and heat transfer characteristics of a viscoelastic fluid in a porous medium over an impermeable stretching sheet with viscous dissipation, *Int. J. Heat Mass Transf.* 53 (2010) 4707–4713.

- [32] J. J. Choi, Z. Rusak and J. A. Tichy, Maxwell fluid suction flow in a channel, *J. Non-Newtonian Fluid Mech.* 85 (1999) 165.
- [33] K. Sadeghy, A. H. Najafi and M. Saffaripour, Sakiadis flow of an upper-convected Maxwell fluid, *Int. J. Non-Linear Mech.* 40 (2005) 1220 – 1228.
- [34] A. A. Pahlavan, V. Aliakbar, F. V. Farahani and K. Sadeghy, MHD flows of UCM fluids above porous stretching sheets using two-auxiliary-parameter homotopy analysis method, *Commun. Nonlinear Sci. Numer. Simulat.* 14 (2009) 473–488.
- [35] V. Aliakbar, A. A. Pahlavan and K. Sadeghy, The influence of thermal radiation on MHD flow of Maxwellian fluids above stretching sheets, *Commun. Nonlinear Sci. Numer. Simulat.* 14 (2009) 779–794.
- [36] C. Fetecau, M. Athar and C. Fetecau, Unsteady flow of a generalized Maxwell fluid with fractional derivative due to a constantly accelerating plate, *Comput. Math. Appl.* 57 (2009) 596-603.
- [37] M. Kumari and G. Nath, Steady mixed convection stagnation-point flow of upper convected Maxwell fluids with magnetic field, *Int. J. Non-Linear Mech.* 44 (2009) 1048–1055.
- [38] M. S. Abel, J. V. Tawade and M. M. Nandeppanavar, MHD flow and heat transfer for the upper-convected Maxwell fluid over a stretching sheet, *Meccanica* 47 (2012) 385—393.
- [39] T. Hayat, S. A. Shehzad and A. Alsaedi, Study on three-dimensional flow of Maxwell fluid over a stretching surface with convective boundary conditions, *Int. J. Phys. Sci.* 7 (2012) 761 - 768.
- [40] R. K. Bhatnagar, G. Gupta and K. R. Rajagopal, Flow of an Oldroyd-B fluid due to stretching sheet in the presence of a free stream velocity, *Int. J. Non-Linear Mech.* 30 (1995) 391-405.
- [41] K.R. Rajagopal, On an exact solution for the flow of an Oldroyd-B fluid, *Bull. Tech. Univ. Istanbul* 49 (1996) 617-623.
- [42] T. Hayat, K. Hutter, S. Asghar and A. M. Siddiqui, MHD Flows of an Oldroyd-B Fluid, *Math. Comput. Modell.* 36 (2002) 987-995.

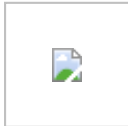
- [43] M. D. Smith, Y. L. Joo, R. C. Armstrong and R. A. Brown, Linear stability analysis of flow of an Oldroyd-B fluid through a linear array of cylinders, *J. Non-Newtonian Fluid Mech.* 109 (2003) 13–50.
- [44] S. Asghar, S. Parveen, S. Hanif, A. M. Siddiqui and T. Hayat, Hall effects on the unsteady hydromagnetic flows of an Oldroyd-B fluid, *Int. J. Eng. Sci.* 41 (2003) 609–619.
- [45] C. Fetecau and C. Fetecau, Unsteady flows of Oldroyd-B fluids in a channel of rectangular cross-section, *Int. J. Non-Linear Mech.* 40 (2005) 1214 – 1219.
- [46] J. Niu, C. Fu and W. Tan, Stability of thermal convection of an Oldroyd-B fluid in a porous medium with Newtonian heating, *Phys. Lett. A* 374 (2010) 4607-4613.
- [47] J. Mewis, Thixotropy – a general review. *J. Non-Newtonian Fluid Mech.* 6 (1979) 1–20.
- [48] H. A. Barnes, Thixotropy – a review, *J. Non-Newtonian Fluid Mech.* 70 (1997) 1-33.
- [49] J. Harris, A continuum theory of time-dependent inelastic flow, *Rheol. Acta* 6 (1967) 6.
- [50] J. Harris, *Rheology and non-Newtonian flow*, London: Longman (1977).
- [51] S. Sadeqi, N. Khabazi and K. Sadeghy, Blasius flow of thixotropic fluids: A numerical study, *Commun. Nonlinear Sci. Numer. Simulat.* 16 (2011) 711–721.
- [52] J. J. M. Sillekens, C. C. M. Rindt and A. A. V. Steenhoven, Development of laminar mixed convection in a horizontal square channel with heated side walls, *Int. J. Heat and Fluid Flow* 19 (1998) 270-281.
- [53] G.P. Celata, A. Chiaradia, M. Cumo and F. D. Annibale, Heat transfer enhancement by air injection in upward heated mixed-convection flow of water, *Int. J. Multiphase Flow* 25 (1999) 1033-1052.
- [54] A. Barletta, Analysis of flow reversal for laminar mixed convection in a rectangular duct with one or more isothermal walls, *Int. J. Heat Mass Transf.* 44 (2001) 3481-3497.
- [55] E. Magyari, I. Pop and B. Keller, Mixed convection boundary layer flow past a horizontal permeable flat plate, *Fluid Dynamics Research* 31 (2002) 215-225.

- [56] R. Nazar, N. Amin and I. Pop, Unsteady mixed convection boundary layer flow near the stagnation point on a vertical surface in a porous medium, *Int. J. Heat Mass Transf.* 47 (2004) 2681–2688.
- [57] M. A. Hossain, S. Bhowmick and R. S. R. Gorla, Unsteady mixed-convection boundary layer flow along a symmetric wedge with variable surface temperature, *Int. J. Eng. Sci.* 44 (2006) 607–620.
- [58] H. A. Mohammed and Y. K. Salman, Experimental investigation of mixed convection heat transfer for thermally developing flow in a horizontal circular cylinder, *Appl. Therm. Eng.* 27 (2007) 1522–1533.
- [59] H. A. Mohammed, Laminar mixed convection heat transfer in a vertical circular tube under buoyancy-assisted and opposed flows, *Energy Conv. Manag.* 49 (2008) 2006–2015.
- [60] M. Kotouc, G. Bouchet and J. Dusek, Loss of axisymmetry in the mixed convection, assisting flow past a heated sphere, *Int. J. Heat Mass Transf.* 51 (2008) 2686–2700.
- [61] M. Mahmood, S. Asghar and M. A. Hossain, Transient mixed convection flow arising due to thermal diffusion over a porous sensor surface inside a squeezing horizontal channel, *Int. J. Therm. Sci.* 48 (2009) 1619–1626.
- [62] T. Hayat, M. Mustafa and I. Pop, Heat and mass transfer for Soret and Dufour’s effect on mixed convection boundary layer flow over a stretching vertical surface in a porous medium filled with a viscoelastic fluid, *Commun. Nonlinear Sci. Numer. Simulat.* 15 (2010) 1183–1196.
- [63] A. J. Chamkha, Thermal radiation and buoyancy effects on hydromagnetic flow over an accelerating permeable surface with heat source or sink, *Int. J. Eng. Sci.* 38 (2000) 1699–1712.
- [64] S. Abel, K. V. Prasad and A. Mahaboob, Buoyancy force and thermal radiation effects in MHD boundary layer visco-elastic fluid flow over continuously moving stretching surface, *Int. J. Therm. Sci.* 44 (2005) 465–476.

- [65] S. Mukhopadhyay and G.C. Layek, Effects of thermal radiation and variable fluid viscosity on free convective flow and heat transfer past a porous stretching surface, *Int. J. Heat Mass Transf.* 51 (2008) 2167–2178.
- [66] S. Mukhopadhyay, Effect of thermal radiation on unsteady mixed convection flow and heat transfer over a porous stretching surface in porous medium, *Int. J. Heat Mass Transf.* 52 (2009) 3261–3265.
- [67] C. H. Chen, Magnetohydrodynamic mixed convection of a power-law fluid past a stretching surface in the presence of thermal radiation and internal heat generation/absorption, *Int. J. Non-Linear Mech.* 44 (2009) 596–603.
- [68] K. Vajravelu and D. Rollins, Heat transfer in an electrically conducting fluid over a stretching surface, *Int. J. Non-Linear Mech.* 27 (1992) 265–277.
- [69] M. S. Abel and M. M. Nandeppanavar, Heat transfer in MHD viscoelastic boundary layer flow over a stretching sheet with non-uniform heat source/sink, *Commun. Nonlinear Sci. Numer. Simulat.* 14 (2009) 2120–2131.
- [70] O. A. Beg, J. Zueco, R. Bhargava and H. S. Takhar, Magnetohydrodynamic convection flow from a sphere to a non-Darcian porous medium with heat generation or absorption effects: network simulation, *Int. J. Therm. Sci.* 48 (2009) 913–921.
- [71] R. Kandasamy, K. Periasamy and K. K. S. Prabhu, Chemical reaction, heat and mass transfer on MHD flow over a vertical stretching surface with heat source and thermal stratification effects, *Int. J. Heat Mass Transf.* 48 (2005) 4557–4561.
- [72] M. A. Mansour, N. F. E. Anssary and A. M. Aly, Effects of chemical reaction and thermal stratification on MHD free convective heat and mass transfer over a vertical stretching surface embedded in a porous media considering Soret and Dufour numbers, *Chem. Eng. J.* 145 (2008) 340–345.
- [73] D. Pal and B. Talukdar, Buoyancy and chemical reaction effects on MHD mixed convection heat and mass transfer in a porous medium with thermal radiation and Ohmic heating, *Commun. Nonlinear Sci. Numer. Simulat.* 15 (2010) 2878–2893.

- [74] G. Singh, P. R. Shrma and A. J. Chamkha, Mass transfer with chemical reaction in MHD mixed convective flow along a vertical stretching sheet, *Int. J. Energy Tech.* 4 (2012) 1-12.
- [75] S. J. Liao, Homotopy Analysis Method: A new analytic technique for nonlinear problems, *Commun. Nonlinear Sci. Numer. Simulat.* 2 (1997) 95-100.
- [76] S. J. Liao, Beyond perturbation: introduction to Homotopy Analysis Method, Chapman & Hall, Boca Raton (2003).
- [77] S. Abbasbandy, Approximate solution for the nonlinear model of diffusion and reaction in porous catalysts by means of the homotopy analysis method, *Chem. Eng. J.* 136 (2008) 144-150.
- [78] M. Sajid and T. Hayat, The application of homotopy analysis method to thin film flows of a third order fluid, *Chaos Solitons Fractals* 38 (2008) 506-515.
- [79] S. J. Liao, A short review on the homotopy analysis method in fluid mechanics, *J. Hydrodyn.* 22 (2010) 882-884.
- [80] M. Turkyilmazoglu, A note on the homotopy analysis method, *Appl. Math. Lett.* 23 (2010) 1226-1230.
- [81] S. J. Liao, Homotopy analysis method in nonlinear differential equations, Higher Edu. Press, Beijing and Springer-Verlag Berlin Heidelberg (2012).
- [82] S. Abbasbandy, E. Shivanian and K. Vajravelu, Mathematical properties of image-curve in the frame work of the homotopy analysis method, *Commun. Nonlinear Sci. Numer. Simulat.* 16 (2011) 4268-4275.
- [83] M. M. Rashidi, S. A. M. Pour, T. Hayat and S. Obaidat, Analytic approximate solutions for steady flow over a rotating disk in porous medium with heat transfer by homotopy analysis method, *Comput. Fluids* 54 (2012) 1-9.
- [84] I. Ahmad, M. Ahmed, Z. Abbas and M. Sajid, Hydromagnetic flow and heat transfer over a bidirectional stretching surface in a porous medium, *Thermal Sci.* 15 (2011) S205-S220.

- [85] M. Turkyilmazoglu, Series solution of nonlinear two-point singularly perturbed boundary layer problems, *Comput. Math. Appl.* 60 (2010) 2109-2114.



## Turnitin Originality Report

PHD Final Thesis by Bilal Ashraf

From Bilal (8899)

Processed on 03-Jul-2014 16:44 PKT

ID: 437813038

Word Count: 37678

Similarity Index

14%

### Similarity by Source

Internet Sources:	3%
Publications:	13%
Student Papers:	0%

### sources:

1

2% match (publications)

[International Journal of Numerical Methods for Heat & Fluid Flow, Volume 24, Issue 2 \(2014-03-28\)](#)

2

2% match (publications)

[Hayat, T., S. A. Shehzad, and A. Alsaedi. "MHD Three-Dimensional Flow by an Exponentially Stretching Surface with Convective Boundary Condition", Journal of Aerospace Engineering, 2014.](#)

3

2% match (publications)

[International Journal of Numerical Methods for Heat & Fluid Flow, Volume 23, Issue 7 \(2013-09-07\)](#)

4

1% match (publications)

[International Journal of Numerical Methods for Heat & Fluid Flow, Volume 24, Issue 2 \(2014-03-28\)](#)

5

1% match (publications)

[Sadeqi, S.. "Blasius flow of thixotropic fluids: A numerical study". Communications in Nonlinear Science and Numerical Simulation, 201102](#)

6

1% match (publications)

[Shateyi, Stanford Motsa, Sandile Sydney . "The effects of thermal radiation, hall currents, Soret, and Dufour on MHD flow by mixed convection o", Mathematical Problems in Engineering, Annual 2010 Issue](#)

7

1% match (publications)

[International Journal of Numerical Methods for Heat & Fluid Flow, Volume 24, Issue 2 \(2014-03-28\)](#)

8

< 1% match (publications)

[Poornima, T. and Reddy, N. Bhaskar. "EFFECTS OF THERMAL RADIATION AND CHEMICAL REACTION ON MHD FREE CONVECTIVE FLOW PAST A SEMI-INFINITE VERTICAL POROUS MOVING PLATE", International Journal of Applied Mathematics & Mechanics, 2013.](#)



- 9 < 1% match (Internet from 15-May-2009)  
<http://hal.physast.uga.edu/~jss/1120L/data/RCJ/orionstars.fit>
- 
- 10 < 1% match (Internet from 29-Aug-2008)  
<http://hal.physast.uga.edu/~jss/1120L/data/CCJD/Lab%20%232/Jupiter25sempy.fit>
- 
- 11 < 1% match (publications)  
[Liu, I.C.. "Flow and heat transfer of an electrically conducting fluid of second grade over a stretching sheet subject to a transverse magnetic field", International Journal of Heat and Mass Transfer, 200409](#)
- 
- 12 < 1% match (Internet from 07-Feb-2012)  
[http://www.rckazan.ru/upload/blank/zayav\\_o\\_vidach\\_pasp.rtf](http://www.rckazan.ru/upload/blank/zayav_o_vidach_pasp.rtf)
- 
- 13 < 1% match (Internet from 23-Jan-2013)  
<http://thermalscience.vinca.rs/pdfs/papers-2012/ThSci-46PQYKBUBK.pdf>
- 
- 14 < 1% match (Internet from 07-Aug-2013)  
[http://journal-enertech.eu/papers-archive/doc\\_download/31-paper-26-2010-17.html](http://journal-enertech.eu/papers-archive/doc_download/31-paper-26-2010-17.html)
- 
- 15 < 1% match (publications)  
[Mahmoud, Mostafa A.A.. "A note on variable viscosity and chemical reaction effects on mixed convection heat and mass transfe", Mathematical Problems in Engineering, Annual 2007 Issue](#)
- 
- 16 < 1% match (publications)  
[Shateyi, Stanford Motsa, Sandile Sydney. "Thermal radiation effects on heat and mass transfer over an unsteady stretching surface.\(Research Ar", Mathematical Problems in Engineering, Annual 2009 Issue](#)
- 
- 17 < 1% match (Internet from 01-Nov-2013)  
[http://permraion.ru/\\_res/fs/file11785.wmf](http://permraion.ru/_res/fs/file11785.wmf)
- 
- 18 < 1% match (Internet from 09-May-2013)  
<http://www.cobrahealth.com/COBRAalternativenotice.rtf>
- 
- 19 < 1% match (publications)  
[Odat, Mohammed Q. Al- Azab, Tariq A. Al-. "Transient MHD double-diffusive natural convection over a vertical surface embedded in a non-darcy po", Mathematical Problems in Engineering, Annual 2009 Issue](#)
- 
- 20 < 1% match (publications)  
[Wong, Sin Wei, M. A. Omar Awang, Anuar Ishak, and Ioan Pop. "Boundary Layer Flow and Heat Transfer over an Exponentially Stretching/Shrinking Permeable Sheet with Viscous](#)

Dissipation". Journal of Aerospace Engineering. 2014.

21 < 1% match (publications)  
[Mahmoud, Mostafa Waheed, Shima. "Effects of slip and heat generation/absorption on MHD mixed convection flow of a micropolar fluid ov". Mathematical Problems in Engineering. Annual 2010 Issue](#)

22 < 1% match (publications)  
[Mahmoud, Mostafa A. A. and Waheed, Shima E.. "Heat and Mass Transfer for a Maxwell Fluid Flow Near a Stagnation Point with Variable Wall Heat and Mass Flux in the Presence of Heat Generation or Absorption". International Review of Physics. 2013.](#)

23 < 1% match (publications)  
[Hsiao, Kai-Long Chen, Guan-Bang. "Conjugate heat transfer of mixed convection for viscoelastic fluid past a stretching sheet.\(Research". Mathematical Problems in Engineering. Annual 2007 Issue](#)

24 < 1% match (Internet from 21-May-2012)  
<http://q3.atdan.net/pub/maps/defrag/lick-sux.pk3>

25 < 1% match (Internet from 10-Nov-2005)  
[http://unseen.free.fr/photoshop/brush/vered\\_useful\\_brush.abr](http://unseen.free.fr/photoshop/brush/vered_useful_brush.abr)

26 < 1% match (publications)  
[International Journal of Numerical Methods for Heat & Fluid Flow, Volume 23, Issue 7 \(2013-09-07\)](#)

27 < 1% match (publications)  
[Aziz, Mohamed Abd El-. "The effects of variable fluid properties and viscous dissipation on forced convection of viscoelasti". Canadian Journal of Physics. August 2010 Issue](#)

28 < 1% match (publications)  
[Ratkiewicz, Bogusław\(Cieśliński, Jan Leszek\). "Dyskretyzacja niektórych modeli fizycznych: od podejścia standardowego do dyskretyzacji geometrycznej". Repozytorium Uniwersytetu im Adama Mickiewicza AMUR, 2011.](#)

29 < 1% match (publications)  
[Mdzinarishvili, Tengiz and Sherman, Simon. "Basic Equations and Computing Procedures for Frailty Modeling of Carcinogenesis: Application to Pancreatic Cancer Data", Cancer Informatics. 2013.](#)

30 < 1% match (Internet from 20-Oct-2010)  
[http://data.astronomycamp.org/2001/SpringAdult/raw/camp\\_0401\\_0027.fits](http://data.astronomycamp.org/2001/SpringAdult/raw/camp_0401_0027.fits)

31 < 1% match (publications)  
[Farhani, Sahbi and Rejeb, Jaleddine Ben. "Link between Economic Growth and Energy](#)

Consumption in Over 90 Countries". Interdisciplinary Journal of Contemporary Research in Business, 2012.

32

&lt; 1% match (Internet from 20-Jun-2011)

[http://data.astronomycamp.org/2005/AdvancedTeen/PrimeFocus/01\\_05JUL01\\_S03251\\_0004.arch](http://data.astronomycamp.org/2005/AdvancedTeen/PrimeFocus/01_05JUL01_S03251_0004.arch)

33

&lt; 1% match (Internet from 26-Nov-2005)

<http://pc-isa2.dacya.ucm.es/controldigitalF/RespuesTemporal.pdf>

34

&lt; 1% match (publications)

[Kimiaiefar, A.; Bagheri, G. H.; Barari, A.; Arabsolghar, A. R. and Rahimpour, M.. "On the Analytical Solution of Non-Orthogonal Stagnation Point Flow towards a Stretching Sheet", International Journal of Applied Mathematics, 2011.](#)

35

&lt; 1% match (publications)

[Trocha, Piotr\(Barnaś, Józef\). "Wpływ efektów interferencyjnych i korelacji kulombowskich na transport elektronowy przez układy kropek kwantowych", Repozytorium Uniwersytetu im Adama Mickiewicza AMUR, 2011.](#)

36

&lt; 1% match (publications)

[Kapcia, Konrad, Jerzy\(Robaszkiewicz, Stanisław\). "Uporządkowania elektronowe i ich separacje w rozszerzonych modelach Hubbarda", Repozytorium Uniwersytetu im Adama Mickiewicza AMUR, 2014.](#)

37

&lt; 1% match (publications)

[Sveinsson, Oli G. B., Jose D. Salas, and Duane C. Boes. "Regional Frequency Analysis of Extreme Precipitation in Northeastern Colorado and Fort Collins Flood of 1997", Journal of Hydrologic Engineering, 2002.](#)

## paper text:

### Preface

14**The boundary layer flows over a moving surface have**

vital importance due to their ever increasing usage in the industries. In such industrial processes, the kinematics of stretching and heat transfer through rate of cooling have substantial impact in the improvement of final product of better quality. No doubt, the thermal buoyancy force arising due to cooling or heating of a moving surface may alter significantly the flow and thermal fields and thereby the heat transfer behavior in the manufacturing process. In several practical applications, the order of magnitudes of buoyancy and viscous forces are comparable for moderate flow velocities and large surface temperature differences and convective heat transfer process is thus called as mixed convection. The buoyancy forces due to temperature and concentration differences are significant in mixed convection thermal and concentration diffusions. In fact the buoyancy forces causing a pressure gradient in the boundary layer modify

8the velocity, temperature and concentration distributions and consequently the rate of

heat and mass transfer between the surface and fluid. Specifically the mixed convection flows are encountered in industrial processes like solar central receivers exposed to the wind currents, nuclear reactors called during emergency shutdown, electronic devices cooled by fans and heat exchangers etc. The mixed convection flows with heat and mass transfer are relevant to energy related engineering problems that include both metal and polymer sheets. Mostly, the fluids in industrial processes are non-Newtonian. Certain oils, paints, blood at low shear rate, shampoos, cosmetic products body fluids, pasta, ice cream, ice, mud etc are few examples of non-Newtonian fluids. Keeping all the aforementioned facts in mind, the present thesis is structured as follows. Chapter one covers literature survey and laws of conservation of mass, linear momentum and energy. Boundary layer equations of second grade, Maxwell, Oldroyd-B and thixotropic fluids are presented. Basic idea of homotopy analysis method is also given. Chapter two deliberates the mixed convection

4boundary layer flow of thixotropic fluid with thermophoresis over a stretched sheet. Fluid is electrically conducting in the

presence of constant applied

6magnetic field. Heat and mass transfer

effects are considered

8in the presence of Joule heating and thermal radiation.

Series solutions are obtained to analyze the velocity, temperature and concentration fields.

1Numerical values of local Nusselt and Sherwood numbers for different values of emerging parameters

are computed and analyzed. A comparative study

7with the previous solutions in a limiting sense is made. The leading results of

this problem are published in "Journal of Thermophysics and Heat Transfer 27 (2013) 733-740". Three-dimensional

2mixed convection flow of second grade fluid over an exponentially stretching

## surface

are studied in chapter three. Convective boundary conditions are utilized for the heat transfer analysis. Analysis is carried out in the presence of thermal radiation. The series solutions are established through a newly developed method recognized as the homotopy analysis method. The convergent analysis of velocity components and temperature are derived. Graphs are plotted and analyzed for interesting physical parameters. A systematic study is performed to analyze the impacts of the significant

13 **parameters on the velocity and temperature**, the **skin friction** coefficients and the **local Nusselt number**.

The contents of this chapter are published in "Plos One 9 (2014) e90038". Chapter four reports the

6 **heat and mass transfer** effects in three-dimensional **mixed convection flow**

of viscoelastic fluid with internal heat source/sink and chemical reaction. An exponential stretching surface is employed for flow generation. Magnetic field normal to the direction of flow is taken under consideration. Convective conditions at boundary surface are also encountered. An analytical approach

7 **homotopy analysis method** is used to develop **the solution** expressions of the **problem**.

Impacts of different controlling parameters such as stretching ratio parameter, Hartman number, internal heat source/sink, chemical reaction, mixed convection, concentration buoyancy parameter and Biot numbers

19 **on the velocity, temperature and concentration profiles** are analyzed graphically. **The local Nusselt number and Sherwood numbers**

are sketched and examined. The results of present chapter are submitted for possible publication in "Applied Mathematics and Computation". Chapter 5 provides the three-dimensional mixed convection

3 **flow of viscoelastic fluid over a stretching surface in presence of**

thermophoresis.

7 **Soret and Dufour effects are also**

taken into account. Series solutions are constructed.

15 **Dimensionless velocity, temperature and concentration** distributions **are shown graphically**

for different values of involved parameters.

26 **Numerical values of local Nusselt and Sherwood numbers** are **computed** and analyzed. **The**

contents of this chapter are submitted for possible publication in “Engineering Applications of Computational Fluid Mechanics”.

2 **Three-dimensional flow of Maxwell fluid over a stretching surface is**

addressed in chapter six. Analysis is prepared in presence of concentration and thermal buoyancy effects. Convective boundary conditions for heat and mass transfer are explored. Series solutions of ii the resulting problem are established. Results are displayed to examine the influence of physical

1 **parameters on the velocity, temperature and concentration** fields. Main observations **of**

this chapter are accepted for publication in “Journal of Central South University”. Chapter seven is prepared to examine the

11 **heat and mass transfer** effects **in** three-dimensional **flow of Maxwell fluid over a stretching**

2 **surface with convective boundary conditions.** Mass transfer **is considered in the**

presence of first order chemical reaction. Conservation laws of energy and concentration are based upon the Soret and Dufour effects. Convergent series solutions to the resulting nonlinear problems are developed. The relevant results are accepted for publication in “International Journal of Numerical Method for Heat and Fluid Flow”. Mixed convection

2 **flow by an inclined stretching surface with**

thermal radiation is investigated in chapter eight. The

**2boundary layer equations of an Oldroyd-B fluid**

**1in the presence of heat transfer are**

used. Suitable transformations reduce the

**2partial differential equations into the ordinary differential equations.**

Computational analysis is implemented for the convergent series solutions.

**4The values of local Nusselt number are**

numerically analyzed. Effects of various parameters involved in the velocity and temperature are discussed. The contents of this chapter are accepted for publication in “Journal of Applied Mechanics and Technical Physics”. Chapter nine provides

**23the mixed convection flow of an Oldroyd-B fluid bounded by a stretching**

surface with suction/injection. Mathematical formulation is developed

**3in the presence of heat source and power law heat flux. Velocity and**

temperature are computed. Numerical

**4values of local Nusselt number are**

examined. Results are computed in a limiting sense with existing literature. The contents of this chapter are published in “Journal of the Brazilian Society of Mechanical Sciences and Engineering DOI 10.1007/s40430-014- 0165-8”. Chapter ten investigates the effects of

**6heat and mass transfer in the mixed convection**

**1flow of an Oldroyd-B fluid over a stretching surface with convective boundary conditions.**

Stress is given to the analysis of Soret and Dufour effects. Related problems are first modeled and then computed by homotopy analysis method (HAM).

**1 Velocity, temperature and concentration fields are given. In addition, the**

**1 local Nusselt and Sherwood numbers are**

examined through numerical values. These observations are submitted for publication in "Thermophysics and Aeromechanics". iii Falkner-Skan flow of rate type non-Newtonian fluid is analyzed in chapter eleven. Expressions of an Oldroyd-B fluid are used in the development of relevant equations. Analysis has been carried out in presence of mixed convection and thermal radiation. Expressions of flow and heat transfer are assembled.

**7 Convergence of derived nonsimilar series solutions is**

provided. This research is submitted for publication in "Journal of Aerospace Engineering". . iv Contents 1 Literature survey and methodology 5 1.1 Introduction . . . . . 5 1.2 Background . . . . . 5 1.3 Fundamental laws . . . . . 12 1.3.1 Law of conservation of mass . . . . . 12 1.3.2 Law of conservation of linear momentum . . . . . 12 1.3.3 Equation of heat transfer . . . . . 13 1.3.4 Diffusion equation . . . . . 13 1.4 Boundary layer equations of nonlinear fluids . . . . . 14 1.4.1 Second grade fluid . . . . . 14 1.4.2 Maxwell fluid . . . . . 15 1.4.3 Oldroyd-B fluid . . . . . 16 1.4.4 Thixotropic fluid . . . . . 17 1.5 Homotopy analysis method (HAM) . . . . . 18 2 MHD mixed convection flow of thixotropic fluid with thermophoresis, Joule heating and thermal radiation 21 2.1 Mathematical formulation . . . . . 21 2.2 Series solutions . . . . . 25 2.3 Convergence analysis and discussion . . . . . 28 2.4 Closing remarks . . . . . 40 3 Three-dimensional

**3 mixed convection flow of viscoelastic fluid with thermal radiation and**

convective conditions 41 3.1 Mathematical analysis . . . . . 42 3.2 Solutions development . . . . . 45 3.3 Convergence analysis . . . . . 49 3.4 Discussion of results . . . . . 50 3.5 Conclusions . . . . . 58 4 Convective

**6 heat and mass transfer in three-dimensional mixed convection flow of viscoelastic fluid with**



chemical reaction and heat source/sink	60
4.1 Mathematical modeling	61
4.2 Series solutions	63
4.3 Convergence analysis and discussion	67
4.4 Closing remarks	75
5 Thermophoresis and MHD mixed convection flow with Soret and Dufour effects	76
5.1 Mathematical analysis	76
5.2 Construction of solutions	79
5.3 Analysis	83
5.4 Conclusions	90

#### 4 Three-dimensional flow of Maxwell fluid over a stretching surface with heat source and

convective conditions	92
6.1 Governing problems	92
6.2 Series solutions	95
6.3 Convergence analysis and discussion	98
6.3.1 Conclusions	105
7 Soret and Dufour effects in three-dimensional	

#### 2 flow of Maxwell fluid with chemical reaction and convective condition

7.1 Problems formulation	107
7.2 Homotopy analysis solutions	110
7.3 Analysis and discussion	114
7.4 Conclusions	126
8 Radiative mixed convection flow of an Oldroyd-B fluid by an inclined stretching surface	128
8.1 Mathematical analysis	128
8.2 Convergence of the series solutions	133
8.3 Discussion	134
8.4 Concluding remarks	139
9 Mixed convection flow of an Oldroyd-B	

#### 3 fluid with power law heat flux and heat source

9.1 Development of problems	141
9.2 Homotopy analysis solutions	144
9.3 Convergence of the homotopy solutions	146
9.4 Graphical results and discussion	147
9.5 Final remarks	152
10	152

#### 1 Soret and Dufour effects in mixed convection flow of an Oldroyd-B fluid

with convective boundary conditions	153
10.1 Mathematical model	153
10.2 Series solutions	155
10.2.1 Zeroth and mth order deformation problems	156
10.3 Convergence of the homotopy solutions	158
10.4 Discussion	159
10.5 Conclusions	165
11	165

## 2Mixed convection Falkner-Skan wedge flow of an Oldroyd-B fluid

in presence of thermal radiation 166 11.1 Problems development . . . . . 169 11.2 Series solutions . . . . . 169 11.2.1 Zeroth order problem . . . . . 169 11.2.2 ?th-order deformation problems . . . . . 170 11.3 Convergence . . . . . 172 11.4 Discussion . . . . . 172 11.5 Conclusions . . . . . 177 Chapter 1 Literature survey and methodology 1.1 Introduction This chapter contains the literature review related to the considered flow problems. Boundary layer equations of thixotropic, second grade, Maxwell and Oldroyd-B fluids are presented. Brief idea of homotopy analysis method (HAM) are also provided. 1.2 Background External flows around streamlined bodies have viscous (shear and no-slip) effects confined close to the body surfaces and its wake but are nearly inviscid far from the body are termed as bound- ary layer flows [1] which occur in aerodynamics (airplanes, rockets, projectiles), hydrodynamics (ships, submarines, torpedoes), transportation (automobiles, trucks, cycles), wind engineering (buildings, bridges, water towers) and ocean engineering (buoys, breakwaters, cables). The boundary layer flow problem over stretching sheet have many industrial applications such as polymer sheet or filament extrusion from a dye or long thread between feed roll or wind-up roll, glass fiber and paper production, drawing of plastic films and liquid films in condensation process. Due to the high applicability of this problem in such industrial phenomena, Sakiadis [2] initiated the work for flow by moving surface. After the pioneering work of Sakiadis, researchers have studied the flow over stretching surfaces under various aspects for viscous and nonlinear fluids. A similarity solution of viscous fluid

## 14over a stretching surface which is stretched with the velocity

proportional to the distance from origin was presented by Crane [3]. Chakrabarti and Gupta [4] analyzed the hydromagnetic

## 23flow over a stretching surface. Heat

## 13transfer over a continuous stretching surface with suction and injection

was analyzed by Chen and Char [5]. Vajravelu and Hadjinicolaou [6] reported the heat transfer features

## 8in the laminar boundary layer flow of viscous fluid over a linearly stretching surface with

variable wall temperature. Ef- fects of suction and injection are present. They attained the solutions of the problem in Kumar functions. Andersson et al. [7] found the solutions

13over a stretching surface in presence of first order chemical

reactions. Similarity solutions of the boundary layer equations over stretching wall was obtained by Banks [8]. Closed form solution of magnetohydrodynamic (MHD) flow under slip condition

7over a permeable stretching surface was obtained by Fang et al. [9].  
Mukhopadhyay et al. [10] obtained the solution of

MHD

16boundary layer flow over a heated stretching sheet with

variable viscosity. Wang [11] extended the boundary layer flow of Crane [3] for three-dimensional stretching surface. Devi et al. [12] extended the flow of ref. [11] for

16unsteady stretching surface in presence of heat and mass transfer

effects. An approximate analytical solutions of the steady, laminar three

20-dimensional flow for an incompressible viscous fluid past a stretching sheet

were proposed by Ariel [13,14]. Hayat and Javed [15] analyzed the three

3-dimensional flow of an incompressible viscous fluid over a porous stretching surface in presence of

magnetic field by employing homotopy analysis method. Kumari and Nath [16] discussed the unsteady magnetohydrodynamic viscous fluid with heat transfer induced by a bilateral stretching surface. An analysis for

14heat transfer over a non-linearly stretching surface for a viscous fluid

was provided by Vajravelu [17]. Cortell [18] extended the work of ref. [17] in presence of thermal radiation and viscous dissipation over a non-linearly stretching surface. Two-dimensional magnetohydrodynamic

3stagnation point flow of an incompressible micropolar fluid over a non-linearly stretching surface was explored by

Hayat et al. [19]. The laminar boundary layer flow over an axisymmetric plane was provided by Afzal [20]. It has been noted by Gupta and Gupta [21] that stretching mechanism in all realistic situation is not linear. For instance the stretching is not linear in plastic and paper production industries. Besides these the

20flow and heat transfer by an exponentially stretching

surface has been studied by Magyari and Keller [22].

20In this attempt the two-dimensional flow of an incompressible viscous fluid

is considered. The solutions of laminar boundary layer equations describing heat and flow in a quiescent fluid driven by an exponentially permeable stretching surface were numerically analyzed by Elbashbasy [23]. Al-Odat et al. [24] numerically discussed the thermal boundary layer flow with an exponential temperature distribution. Here magnetohydrodynamic flow was addressed. Liu et al. [25] studied the three-dimensional

13boundary layer flow of a viscous fluid over an exponentially stretching surface by using the

Ackroyd and Runge-Kutta methods. Analysis of non-linear fluids

1is an active area of research

for the last few years. In many fields such as food industry, drilling operations and bioengineering, the fluids, either synthetic or natural, are mixtures of different stuffs such as water, particle, oils, red cells and other long chain molecules. Such combination imparts strong rheological properties to the resulting liquids. The dynamic viscosity in non-linear materials varies non-linearly with the shear rate. These fluids in terms of their different rheological features cannot be described by a single constitutive relationship. Hence several relationships for the non-linear fluids are proposed. In fact the additional parameters in such non-linear fluids are the main culprit which makes the resulting systems more nonlinear, higher order and complex than the Navier-Stokes equations. The rheological fluids in general have been classified into three categories known as the differential, integral and rate types. Second grade fluid is a subclass of differential type fluids which exhibits the normal stress effects. To predict these effects many researchers studied second grade fluid under various aspects. Dandapat and Gupta [26] discussed the flow

23of an incompressible second-order fluid due to stretching

surface under boundary layer assumptions. Chen et al. [27] delivered the temperature distribution in

11 viscoelastic fluid of Walters' B Model over a horizontal stretching plate. The

velocity of the plate is proportional to the distance from the slit. Vajravelu and Rollins [28] carried out the heat transfer effects in viscoelastic

8 fluid over a stretching surface with frictional heating and internal heat generation

or absorption.

2 Hayat et al. [29] studied the three-dimensional flow

over stretching surface in a viscoelastic fluid by applying homotopy analysis method. Liu [30] presented

11 analytical solutions for the flow and heat transfer in steady laminar boundary flow of an electrically conducting fluid of second grade subject to transverse uniform magnetic field past a semi-infinite stretching sheet with power-law surface temperature or power-law surface heat flux. The effects of viscous dissipation, internal heat generation or absorption, work done due to deformation and Joule heating were also considered in the energy equation.

1 Flow and heat transfer characteristics of viscoelastic fluid with porous medium over a stretching surface with

viscous dissipation was governed by Nandeppanavar et al. [31]. Differential type models do not predict the relaxation and retardation time effects while these effects can be anticipated by rate type fluids. Maxwell fluid is a

7 simplest subclass of rate type fluids.

Channel

1 flow of an upper convected Maxwell fluid (UCM)

induced by suction was presented by Choi et al. [32]. Sadeghy [33] discussed the

**22flow of an upper-convected Maxwell (UCM) fluid above a rigid plate moving steadily.**

Pahlavan et al. [34] studied the

**7MHD flows of UCM fluids above porous stretching sheets**

using two-auxiliary-parameter homotopy analysis method. Maxwellian MHD flow induced by a linearly stretched with thermal radiations was investigated by Aliakbar et al. [35].

**3Unsteady flow of generalized Maxwell fluid with fractional derivative induced by**

an accelerating plate was provided by Fetecau et al. [36]. Kumari and Nath [37] analyzed the

**22Maxwell fluid over stretching sheet in presence of mixed convection. Abel et al. [38] proposed the**

MHD

**22flow and heat transfer for the upper-convected Maxwell fluid over a stretching sheet. Hayat et al. [39] presented the three -dimensional**

Maxwell fluid over stretching

**2surface with convective boundary conditions. Bhatanagar et al.**

[40] initiated to analyze the boundary layer flow of rate type fluids. They obtained the solutions of two-dimensional flow over

**8a stretching surface with variable free stream velocity. Exact solutions of**

unidirectional

**2flow of an Oldroyd-B fluid**

between two parallel plates was presented by Rajagopal [41]. Exact solutions for flows

**8 of an electrically conducting Oldroyd-B fluid over an infinite oscillatory plate in**

the presence of a transverse magnetic field when the entire system rotates about an axis normal to the plate was obtained by Hayat et al. [42]. The linear stability of the

**2 flow of an Oldroyd-B fluid through a**

linear array of cylinders confined in a channel was analyzed by Smith et al. [43]. They computed solutions for both the steady state and linear stability of these states by employing finite element analysis. Exact solutions for the influence of Hall current and rotation in the oscillatory flows by an infinite plate were obtained by Asghar et al. [44]. Fetecau and Fetecau [45] analyzed the unsteady flows of Oldroyd-B fluids in a channel of rectangular cross-section. A linear stability analysis determining the onset of oscillatory convection of an Oldroyd-B fluid in a two-dimensional rectangular porous medium generated by Newtonian heating was presented by Niu et al. [46]. In nonlinear fluids sometimes

**5 nonlinearity introduced by their shear-dependent viscosity and/or elasticity often gives rise to a formidable mathematical task which cannot be solved.**

**5 Obviously, the situation becomes much more complicated when the viscosity of the fluid is time- dependent. Time-dependent fluid systems are quite frequent in industrial applications with the common effect being a drop in viscosity by the progress of time. Complex fluid systems such as drilling muds, foodstuff, paints, cosmetics, pharmaceuticals, suspensions, grease, and the like belong to this class of fluids-the so-called thixotropic fluids. Physiological fluids such as blood, synovial fluid, and mucus may also exhibit thixotropic behavior depending on the time scale of the observation.**

**5 A common effect among thixotropic fluids is that their viscosity is decreased even when the shear rate is constant**

[47,48]. Harris [49,50]

**5 tried to address boundary layer flows of thixotropic fluids.**

Harris presented

**5a simple thixotropic fluid model (the so called Harris model) to investigate the effects of a fluid's thixotropic behavior on the characteristics of the momentum boundary layer formed above a fixed plate**

[50].

**5Two-dimensional flow of an incompressible thixotropic fluid obeying Harris rheological model over a fixed semi-infinite plate**

was investigated by Sadeqi et al. [51]. Mixed convection flows or combined free and forced convection flows occur in many technological and industrial applications and in nature for example, in solar receivers exposed to wind currents, electronic devices cooled by fans, nuclear reactors cooled during emergency shutdown, heat exchanges placed in a low-velocity environment, flows in the ocean and in the atmosphere, and many more. Finite element method was utilized for detailed analysis of mixed-convection flow in a horizontal channel heated from the side walls were computed by Sillekens [52]. Heat transfer enhancement by air injection in upward heated mixed-convection flow of water was studied by Celata et al. [53]. Barletta [54] provided the analysis of the laminar and fully developed mixed convection flow in a vertical rectangular duct with one or more isothermal walls. Magyari et al. [55] analyzed the

**6boundary layer mixed convection flow over a**

permeable horizontal plate. The unsteady

**20mixed convection boundary layer flow near the region of a stagnation point on a vertical surface embedded in a Darcian fluid-saturated porous medium**

was investigated by Nazar et al. [56]. They employed Keller—Box method to obtain the solutions. Laminar two-dimensional unsteady mixed convection

**20boundary-layer flow of viscous incompressible fluid past a sharp wedge**

was developed by Hussain et al. [57]. Perturbation solutions were obtained for small and large dimensionless time. Experimental investigation was presented on mixed (free and forced) convection to study the local and average heat transfer for hydrodynamically and thermally developed laminar air flow in a horizontal circular cylinder was analyzed by Mohammed and Salman [58]. Laminar mixed convection heat transfer for assisted and opposed air flows in the entrance region of a vertical circular tube with wall heat flux boundary condition had been experimentally investigated by Mohammed [59]. Kotouc et al. [60] also provided the loss of axisymmetry in the mixed convection assisting flow past a heated sphere. A transient laminar mixed convection flow of viscous incompressible fluid generated by thermal buoyancy force over a horizontal porous sensor surface placed inside a squeezing channel was discussed by Mahmood et al.



[61]. The implicit finite difference approximation together with Keller box method was employed for the solution of small and large time regimes.

**6Heat and mass transfer characteristics in mixed convection boundary layer flow past a linearly stretching vertical surface in a porous medium filled with a viscoelastic fluid**

with Dufour and Soret effects was governed by Hayat et al. [62]. Radiative mixed convection has gained much importance amongst the recent researchers due to number of applications in geophysical and energy storage problems such as in furnaces, ovens and boilers and the interest in our environment and in no conventional energy sources, such as the use of salt gradient solar ponds for energy collection and storage. Similarity equations governing steady hydromagnetic boundary-layer flow over an accelerating permeable surface

**6in the presence of thermal radiation, thermal buoyancy and**

heat generation or absorption effects were obtained by Chamka [63]. Buoyancy force and thermal radiation effects in MHD boundary layer viscoelastic fluid flow over continuously moving

**4stretching surface was** investigated by Abel et al.

[64]. Mukhopadhyay and Layek [65] presented the free convective boundary layer

**21flow and heat transfer of a fluid** with variable viscosity **over a porous stretching vertical surface in presence of**

thermal radiation. Results were obtained by Lie group transformations. Also Mukhopadhyay [66] analyzed the

**6effects of thermal radiation on unsteady boundary layer mixed convection heat transfer problem from a vertical porous stretching surface embedded in porous medium.**

Magnetohydrodynamic mixed convective flow and heat

**6transfer of an electrically conducting power-law fluid past a stretching surface in the presence of heat generation/absorption and thermal**

radiation was studied by Chen [67]. Numerical solutions were generated by an implicit finite-difference technique for the non-similar coupled flow. A

8study of utilizing heat source or sink in moving fluids

has been a subject of interest of many researchers. This is because of its possible application to geophysical sciences, astrophysical sciences, and in cosmic studies. Such flows arise either due to unsteady motion of the boundary or the boundary temperature. The study of fluctuating flow is important in the paper industry and many other technological fields. Many investigators stressed

6on the magnetohydrodynamic flow of an electrically conducting fluid

because of numerous applications in metallurgical industry such as in drawing, annealing,

2in the purification of molten metals from non-metallic inclusions,

electromagnetic pumps, MHD generators etc. Several studies have been presented by the authors in

22presence of transverse magnetic field and heat

source/sink over a stretching surface.

8Heat transfer characteristics in an electrically conducting fluid over a stretching sheet with

variable wall temperature and heat source/sink was investigated by Vajravelu and Rollins [68]. Abel et al. [69] presented

4the study of momentum and heat transfer characteristics in hydromagnetic flow

of viscoelastic liquid

16over a stretching sheet with non-uniform heat source,

where the flow was generated due to a linear stretching of the sheet and influenced by uniform magnetic field applied vertically. Beg et al. [70] examined the magnetohydrodynamic free

6convection from a sphere embedded in an electrically-conducting fluid-

## saturated porous

regime with heat generation. The present trend in the field of chemical reaction analysis is to give a mathematical model for the system to predict the reactor performance. A large amount of research work has been reported in this field. In particular, the

## 6study of heat and mass transfer

with chemical reaction is of considerable importance in chemical and hydrometallurgical industries. MHD flow with

## 6heat and mass transfer characteristics of an incompressible viscous electrically conducting and Boussinesq fluid due to a vertical stretching

surface with chemical reaction and thermal stratification effects was presented by Kandasamy et al. [71].

## 6Mansour et al. [72] studied the effects of chemical reaction, thermal stratification, Soret and Dufour numbers on MHD free convective heat and mass transfer of a viscous incompressible and electrically conducting fluid over a vertical stretching surface embedded in a saturated porous medium.

The

## 6combined effect of mixed convection with thermal radiation and chemical reaction on MHD flow of viscous and electrically conducting fluid past a vertical permeable surface in presence of porous medium was analyzed

by Pal and Talukdar [73]. Mass transfer with

## 8chemical reaction in MHD mixed convective flow along a vertical

stretching sheet was investigated by Singh et al. [74]. 1.3 Fundamental laws 1.3.1 Law of conservation of mass The equation of continuity (law of conservation of mass) can be represented by  $\nabla \cdot (\rho V) = 0$  (1.1) where ?

## 3is the density of fluid and V is the fluid

velocity. For an incompressible fluid Eq. (1.1) can be expressed as follows:  $\nabla \cdot V = 0$  (1.2) 1.3.2 Law of

conservation of linear momentum Generalized equation of motion can be expressed as  $\rho \frac{Dv}{Dt} = \nabla \cdot \tau + \rho b$  (1.3) For an incompressible flow  $\tau = -pI + S$  (1.4) in which

$\tau$  is the Cauchy stress tensor,  $p$  is the pressure,  $I$  is the identity tensor,  $S$  is the

extra stress tensor,  $b$  is the body force and  $\frac{D}{Dt}$  is the material time derivative. The Cauchy stress tensor and the velocity field for three-dimensional flow can be described in the forms  $T = \begin{bmatrix} T_{11} & T_{12} & T_{13} \\ T_{21} & T_{22} & T_{23} \\ T_{31} & T_{32} & T_{33} \end{bmatrix}$   $V = [v_1, v_2, v_3]^T$  (1.5) (1.6) where  $T_{11}, T_{22}, T_{33}$  and  $T_{12}, T_{13}, T_{23}$  represent the normal stresses,  $T_{12}, T_{13}, T_{23}$  and  $T_{21}, T_{31}, T_{32}$  show the shear stresses and  $v_1, v_2, v_3$

are the velocity components along the  $x, y$  and  $z$ -directions respectively.

Equation (1.3) in component form can be written as follows:  $\rho \frac{Dv_i}{Dt} = \frac{\partial \tau_{ij}}{\partial x_j} + \rho b_i$  (1.7)  $\tau_{ij} = -p\delta_{ij} + S_{ij}$  (1.8)  $\mu \left( \frac{\partial v_i}{\partial x_j} + \frac{\partial v_j}{\partial x_i} \right) = S_{ij}$  (1.9)  $\mu \left( \frac{\partial v_i}{\partial x_j} + \frac{\partial v_j}{\partial x_i} \right) = S_{ij}$  where  $b_1, b_2$  and  $b_3$  show the components of body force along the  $x, y$  and  $z$ -axes, respectively. The above equations for two-dimensional flow become  $\rho \frac{Dv_x}{Dt} = \frac{\partial \tau_{xx}}{\partial x} + \frac{\partial \tau_{xy}}{\partial y} + \rho b_x$   $\rho \frac{Dv_y}{Dt} = \frac{\partial \tau_{xy}}{\partial x} + \frac{\partial \tau_{yy}}{\partial y} + \rho b_y$  (1.10)  $\tau_{xx} = -p + 2\mu \frac{\partial v_x}{\partial x}$   $\tau_{yy} = -p + 2\mu \frac{\partial v_y}{\partial y}$   $\tau_{xy} = \mu \left( \frac{\partial v_x}{\partial y} + \frac{\partial v_y}{\partial x} \right)$  (1.11) According to first law of thermodynamics the heat transfer equation can be written as  $\rho \frac{Dh}{Dt} = \nabla \cdot q + \rho \dot{q}$  (1.12) where  $h$  is the internal energy,  $\dot{q}$  the specific heat,  $T$  the temperature,  $L = \nabla V$  the velocity gradient,  $q = -k \nabla T$  the heat flux,  $k$  the thermal conductivity and  $\dot{q}$  the radiative heating. The above equation in absence of radiative heating is given below  $\rho \frac{Dh}{Dt} = \nabla \cdot q$  (1.13) 1.3.4 Diffusion equation Mass transfer occurs whenever fluid flows that is some mass is transferred from one place to another. According to Fick's law  $J = -D \nabla C$  (1.14) where

$C$  is the concentration,  $D$  is the coefficient of mass diffusivity and  $J$  is the

reaction rate diffusing species. 1.4 Boundary layer equations of nonlinear fluids 1.4.1 Second grade fluid Extra stress tensor  $S$  for a second grade fluid can be expressed as  $S = \alpha_1 A_1 + \alpha_2 A_2$  where  $A_1$  is the first Rivlin-Erickson tensor can be defined by  $A_1 = \text{grad } V + (\text{grad } V)^T$  For three-dimensional flow one obtains  $A_1 = \begin{bmatrix} 2\frac{\partial v_1}{\partial x_1} & \frac{\partial v_1}{\partial x_2} + \frac{\partial v_2}{\partial x_1} & \frac{\partial v_1}{\partial x_3} + \frac{\partial v_3}{\partial x_1} \\ \frac{\partial v_2}{\partial x_1} + \frac{\partial v_1}{\partial x_2} & 2\frac{\partial v_2}{\partial x_2} & \frac{\partial v_2}{\partial x_3} + \frac{\partial v_3}{\partial x_2} \\ \frac{\partial v_3}{\partial x_1} + \frac{\partial v_1}{\partial x_3} & \frac{\partial v_3}{\partial x_2} + \frac{\partial v_2}{\partial x_3} & 2\frac{\partial v_3}{\partial x_3} \end{bmatrix}$  and the second Rivlin-Erickson tensor  $A_2$  can be computed through  $A_2 = A_1 A_1 - I A_1 + L A_1 + L^T A_1$  (1.15) (1.16) (1.17) (1.18) For thermodynamic stability the second grade model should obey the inequality given below:  $\alpha_1 \geq 0, \alpha_2 \geq 0, \alpha_1 + \alpha_2 = 0$  (1.19) From the boundary layer theory [1], the order of  $\alpha_1$  and  $\alpha_2$  are 1 while the order of  $\mu$  and  $\rho$  are  $\frac{1}{2}$  Three-dimensional boundary layer equations for second grade fluid can be written as  $\rho \frac{Dv_i}{Dt} = \frac{\partial \tau_{ij}}{\partial x_j} + \rho b_i$   $\tau_{ij} = -p\delta_{ij} + S_{ij}$   $S_{ij} = \alpha_1 \left( \frac{\partial v_i}{\partial x_j} + \frac{\partial v_j}{\partial x_i} \right) + \alpha_2 \left( \frac{\partial v_i}{\partial x_k} \frac{\partial v_k}{\partial x_j} + \frac{\partial v_j}{\partial x_k} \frac{\partial v_k}{\partial x_i} \right) + \alpha_3 \left( \frac{\partial v_i}{\partial x_j} \frac{\partial v_j}{\partial x_k} + \frac{\partial v_j}{\partial x_i} \frac{\partial v_i}{\partial x_k} \right) + \alpha_4 \left( \frac{\partial v_i}{\partial x_k} \frac{\partial v_k}{\partial x_j} + \frac{\partial v_j}{\partial x_k} \frac{\partial v_k}{\partial x_i} \right) + \alpha_5 \left( \frac{\partial v_i}{\partial x_j} \frac{\partial v_j}{\partial x_k} + \frac{\partial v_j}{\partial x_i} \frac{\partial v_i}{\partial x_k} \right)$  (1.20)  $\alpha_1 = \mu$   $\alpha_2 = \mu$   $\alpha_3 = \mu$   $\alpha_4 = \mu$   $\alpha_5 = \mu$  (1.21) 1.4.2 Maxwell fluid The extra stress tensor  $S$  for Maxwell fluid can be expressed by the following relation  $\tau = \mu \left( \frac{Dv}{Dt} + \frac{1}{\lambda} \tau \right)$  (1.22)  $\mu$  is the viscosity,  $\lambda$  is the relaxation time,  $\frac{D}{Dt}$  the covariant differentiation,  $\tau$  denotes the

kinematic viscosity and  $A_1$  the first Rivlin-Ericksen tensor. For a tensor  $S$  of rank two, a vector  $b_1$  and a scalar  $\mu$  we get  $\mu S + (V \cdot \nabla)S - S(\text{grad } V) = -(\text{grad } V)S$  (1.23)  $\mu b_1 + (V \cdot \nabla)b_1 - (\text{grad } V)b_1 =$  (1.24)  $\mu + (V \cdot \nabla)\mu =$  (1.25) Implementation of 1 +  $\mu$  on Eq. (1.3), we have the following relations in the absence of body force  $\rho \frac{D}{Dt} \mu = -\mu \nabla \cdot V + \mu \nabla^2$  (1.26)  $\mu \nabla^2 \mu = \mu \nabla^2 \mu$  By adopting the procedure  $\mu = \mu(\nabla^2 A_1)$  (1.27)  $\mu \nabla^2 \mu = \mu \nabla^2 \mu$  Hence the above relations in absence of pressure gradient is  $\mu \nabla^2 \mu = \mu \nabla^2 \mu$  (1.28)  $\mu \nabla^2 \mu = \mu \nabla^2 \mu$  By using the boundary layer theory [1], the order of  $\mu$  and  $\mu$  is 1 and order of  $\mu$  and  $\mu$  is  $\mu$  The  $\mu$ -momentum equation vanishes identically because it has order  $\mu$  Hence the boundary layer equations for three-dimensional flow of Maxwell fluid are  $\mu \nabla^2 \mu + \mu \nabla^2 \mu + \mu \nabla^2 \mu = \mu \nabla^2 \mu$  (1.29)  $\mu \nabla^2 \mu = \mu \nabla^2 \mu$  (1.30) The boundary layer equation for

## 2two-dimensional flow of Maxwell fluid

are given below  $\mu \nabla^2 \mu + \mu \nabla^2 \mu + \mu \nabla^2 \mu = \mu \nabla^2 \mu$  (1.31)  $\mu \nabla^2 \mu = \mu \nabla^2 \mu$  1.4.3 Oldroyd-B fluid The extra stress tensor for an Oldroyd-B fluid model can be expressed as  $S = S + \mu \nabla^2 S$  (1.32)  $\mu \nabla^2 \mu = \mu \nabla^2 \mu$  where  $\mu$  denotes the retardation time and law of conservation of momentum in absence of pressure gradient and body force can be written as follows:  $\mu \nabla^2 \mu = \mu \nabla^2 \mu$  The scalar forms of boundary layer equations in this case are  $\mu \nabla^2 \mu + \mu \nabla^2 \mu + \mu \nabla^2 \mu = \mu \nabla^2 \mu$  (1.33) (1.34)  $\mu \nabla^2 \mu + \mu \nabla^2 \mu + \mu \nabla^2 \mu = \mu \nabla^2 \mu$  and the governing boundary layer equation for two-dimensional flow is  $\mu \nabla^2 \mu + \mu \nabla^2 \mu + \mu \nabla^2 \mu = \mu \nabla^2 \mu$  (1.35)  $\mu \nabla^2 \mu = \mu \nabla^2 \mu$  1.4.4 Thixotropic fluid Stress tensor  $\tau$  for thixotropic fluid model  $\tau = 2\mu(\dot{\gamma})\dot{\gamma}$  where the

5viscosity is allowed to be time-dependent through allowing the second invariant of the deformation-rate tensor to be time-dependent,  $\mu$  is

5the second invariant of the deformation- rate tensor

and  $\mu = (\mu_0 + \mu_1 \dot{\gamma})$  (1.37) In the simple Harris

5model, a quadratic form is used for the  $\mu$  so that we have,

$\mu = (\mu_0 + \mu_1 \dot{\gamma} + \mu_2 \dot{\gamma}^2)$  (1.38)  $\mu \nabla^2 \mu = \mu \nabla^2 \mu$  ! For the

### 5 viscosity function, in the SH model we have

[49,50]  $\mu = \mu_0 - \mu_1 \frac{\partial u}{\partial y} + \mu_2 \frac{\partial^2 u}{\partial y^2}$  (1.39) where  $\frac{\partial}{\partial y}$  is the material derivative defined as  $\frac{\partial}{\partial y} = \frac{\partial}{\partial y} + (u \frac{\partial}{\partial x} + v \frac{\partial}{\partial y})$  (1.40)  $\mu_1$  and  $\mu_2$  are the material constants. For boundary layer analysis the viscosity function becomes  $\mu = \mu_0 - \mu_1 \frac{\partial u}{\partial y} + \mu_2 \frac{\partial^2 u}{\partial y^2} + 4\mu_2 \frac{\partial^3 u}{\partial y^3} + \mu_3 \frac{\partial^4 u}{\partial y^4}$  (1.41)  $\mu_3$  By using boundary layer analysis the  $y$ -momentum equation is completely dropped for two-dimensional flow.

### 5 On the other hand, the $x$ -momentum equation is reduced to

$\rho \frac{\partial u}{\partial t} + \rho u \frac{\partial u}{\partial x} + \rho v \frac{\partial u}{\partial y} = \rho \frac{\partial^2 u}{\partial y^2} - \frac{\partial p}{\partial x} + \mu \frac{\partial^3 u}{\partial y^3} + \mu_1 \frac{\partial^4 u}{\partial y^4} + \mu_2 \frac{\partial^5 u}{\partial y^5}$  (1.42) 1.5 Homotopy analysis method (HAM) In the absence of analytical solutions before the advent of computers, the researchers mainly directed their efforts at obtaining some forms of approximate solutions. One of the key issues of approximate solutions has always been the accuracy of the solutions. The accuracy, generally speaking, is measured in terms of the norm of the error in Banach space. The error being the difference of the approximate solution from the exact solution. In the absence of an exact solution (analytical or numerical) a heuristic approach consisting of the convergence of successive approximations has been chosen to judge the merit of an approximate solution. With the advent of computers the approximate solutions in fluid dynamics have lost some of their importance as more and better numerical algorithms have been developed to solve the increasingly realistic, but more complicated problems numerically. Nevertheless, approximate analytical solutions still have their relevance for the following reasons: Firstly, they give the solutions for each point within the domain of interest unlike the numerical solutions which are available for a particular run only for a set of discrete points in the domain. Secondly, compared to a numerical solution a nicely produced approximate solution, requiring a minimal effort and having a reasonable amount of accuracy is always handy for an engineer, scientist or an applied mathematician, who can obtain a solution completely, thereby gaining a valuable insight into the essentials of the problem. Thirdly, even with most of the scientific packages, some initial guess is required for the solution, as the algorithms, in general are not globally convergent. In such situations, approximate solutions can provide an excellent starting guess, which can be rapidly refined to the exact numerical solution in a few iterations. Homotopy analysis method is proposed by Liao [75-76] and is very useful to obtain the series solutions of the nonlinear ordinary and partial differential equations [77-85]. According to Liao [75-76], this method distinguishes itself from other analytical methods in the following five aspects 1. HAM is not dependent on physical parameters. Therefore the technique can be used for both strong/weak nonlinear problems. 2. It is valid for strongly nonlinear problems even if a given nonlinear problem does not contain any small/large parameter. 3. It provides us with a convenient way to adjust

### 3 the convergence region and rate of approximation of the series

solution. 4. HAM provides freedom to choose base functions to approximate the solution of nonlinear problem. 5. This method can be coupled with many other mathematical methods such as integral transform methods, series expansion methods, numerical methods and so on. This technique is applicable in the development of results to numerous problems [78 - 88]. Idea behind the HAM is as follows. Nonlinear

differential equation can be written as follows:  $\mathcal{N}(\eta) + \mathcal{H}(\eta) = 0$  (1.43) where  $\mathcal{N}$  is a nonlinear operator,  $\mathcal{H}(\eta)$  is an unknown function to be determined and  $\mathcal{H}_0(\eta)$  is a known function. The homotopic equation is  $(1 - \gamma)\mathcal{L}[\mathcal{H}(\eta) - \mathcal{H}_0(\eta)] = \gamma\{\mathcal{N}(\eta) - \mathcal{H}_0(\eta)\}$  (1.44) where  $\mathcal{H}_0(\eta)$  is initial guess,  $\mathcal{L}$  is auxiliary linear operator,  $\gamma$  is auxiliary parameter or convergence control parameter,  $\gamma \in [0, 1]$  is an embedding parameter and  $\mathcal{H}(\eta)$  is an unknown function. By expanding Taylor's series about  $\gamma$  one obtains  $\mathcal{H}(\eta) = \mathcal{H}_0(\eta) + \gamma\mathcal{H}_1(\eta) + \gamma^2\mathcal{H}_2(\eta) + \gamma^3\mathcal{H}_3(\eta) + \dots$  (1.45)  $\gamma=1$   $\mathcal{H}(\eta) = \mathcal{H}_0(\eta) + \mathcal{H}_1(\eta) + \mathcal{H}_2(\eta) + \mathcal{H}_3(\eta) + \dots$  The convergence of above series firmly depends upon  $\gamma$ . The value of  $\gamma$  is chosen in such a way that series solution is convergent at  $\gamma = 1$ . Substituting  $\gamma = 1$  one obtains The  $n$ -th order deformation problems are  $\mathcal{L}[\mathcal{H}_n(\eta) - \mathcal{H}_{n-1}(\eta)] = \gamma\mathcal{R}_n(\eta)$  (1.46)  $\mathcal{L}[\mathcal{H}_n(\eta) - \mathcal{H}_{n-1}(\eta)] = \gamma\mathcal{R}_n(\eta)$  (1.47) where  $0 \leq \gamma \leq 1$   $\mathcal{R}_n(\eta) = \mathcal{N}(\eta) - \mathcal{H}_0(\eta) + \mathcal{H}_1(\eta) + \mathcal{H}_2(\eta) + \dots + \mathcal{H}_{n-1}(\eta) - \mathcal{H}_0(\eta)$  (1.48)  $\mathcal{R}_n(\eta) = \mathcal{N}(\eta) - \mathcal{H}_0(\eta) + \mathcal{H}_1(\eta) + \mathcal{H}_2(\eta) + \dots + \mathcal{H}_{n-1}(\eta) - \mathcal{H}_0(\eta)$  (1.49)  $\mathcal{H}_0(\eta) = \mathcal{H}_0(\eta)$  Chapter 2

## 21 MHD mixed convection flow of thixotropic fluid

with thermophoresis, Joule heating and thermal radiation This chapter deals with the magnetohydrodynamic (MHD) mixed convection

## 4 flow of thixotropic fluid over a moving surface. Heat transfer is considered in the

presence of thermophoresis, Joule heating and radiative effects. Dimensionless nonlinear problem is computed by homotopy analysis method (HAM). The convergent solutions are plotted and examined for various parameters of interest. Numerical values of wall shear stress and heat transfer rate are computed and discussed. 2.1 Mathematical formulation We consider

## 3 Cartesian coordinate system in such a way that $x$ -axis is along the stretching surface and $y$ -axis is perpendicular to it. The

magnetohydrodynamic

## 3 boundary layer flow of thixotropic fluid is

## 1 taken into account. Heat and mass transfer characteristics are

accounted

## 8 in the presence of thermal radiation and thermophoresis effects.

Uniform temperature of the surface  $T_w$  is

## 8 higher than the ambient fluid temperature $T_\infty$ Further the species



## 25/97



the Eckert number and  $Pr = \frac{\mu}{\rho \alpha}$  the Schmidt number. It is further seen that both  $Pr_1$  and  $Pr_2$  are functions of  $Pr$ . Hence the fluid flow in present situation lacks a self-similar solution. This is striking difference when compared present case with that of Blasius flow of viscous fluid i.e. in Blasius flow there is self-similar solution. Here  $Pr_2$  especially indicates the fluids' thixotropic behavior. The

**1 skin friction coefficient, local Nusselt number and local Sherwood number**

in non-dimensional form can be written as follows:  $\theta''(0) = \theta(0) - \theta(1)6[\theta(0)]^3$   $\phi''(0) - \phi(0) = -\theta(0)$  and  $\phi''(0) - \phi(0) = -\theta(0)$  (2.14) Here we noticed

**5 that the wall shear stress at given  $\eta$ -location is only affected by**

$\theta_1$  but only indirectly by  $\theta_2$  (i.e. through  $\theta(0)$ ) [51]. We have serious limitation in a simplified Harris model for representing true thixotropic fluid. 2.2 Series solutions The homotopic solutions for  $\theta$  and  $\phi$  in a set of base functions  $\{\theta \exp(-\eta^2) \mid \eta \geq 0, \theta \geq 0\}$  (2.15) are given by  $\sum_{n=0}^{\infty} \theta_n(\eta) = \theta(\eta) \exp(-\eta^2)$   $X \theta = 0$  (2.16)  $\sum_{n=0}^{\infty} \phi_n(\eta) = \phi(\eta) \exp(-\eta^2)$  (2.17)

**28  $X \theta = 0$   $X \phi = 0$**   $\sum_{n=0}^{\infty} \theta_n(\eta) = \theta(\eta) \exp(-\eta^2)$  (2.18)  **$X \theta = 0$   $X \phi = 0$**

where  $\theta_n$ ,  $\phi_n$  and  $\eta$  are  $\eta$

**4 are the coefficients.** The appropriate **initial approximations and auxiliary linear operators are**

$\theta_0(\eta) = 1 - \exp(-\eta^2)$   $\theta_0(\eta) = \exp(-\eta^2)$   $\theta_0(\eta) = \exp(-\eta^2)$   $L \theta = \theta'''' - \theta$   $L \theta = \theta'' - \theta$   $L \theta = \theta'' - \theta$  (2.19) (2.20) with  $L(\theta_1 + \theta_2 + \theta_3 - \theta) = 0$ ,  $L(\theta_4 + \theta_5 - \theta) = 0$   $L(\theta_6 + \theta_7 - \theta)$  (2.21) in which  $\theta_i$  ( $i = 1-7$ ) denote

**4 the arbitrary constants and the zeroth order deformation problems**

are  $(1 - \eta) L \theta^*(\eta; \eta) - \theta_0(\eta) = \eta^{-1} N$

**37  $\theta^*(\eta; \eta) \theta^*(\eta; \eta) \theta^*(\eta; \eta)$  (2.22)  $(1 - \eta) L \theta^*(\eta; \eta) - \theta_0(\eta)$**

$= \eta^{-1} N$

**10  $\theta^*(\eta; \eta) \theta^*(\eta; \eta) \theta^*(\eta; \eta)$  (2.23)  $(1 - \eta) L \theta^*(\eta; \eta) - \theta_0(\eta) = \eta^{-1} N$**   
 **$\theta^*(\eta; \eta) \theta^*(\eta; \eta) \theta^*(\eta; \eta)$**

$$12 \quad \begin{aligned} \mathcal{P}^0(0; ?) = 0 \quad \mathcal{P}^0(0; ?) = 1 \quad \mathcal{P}^0(\infty; ?) = 0 \quad \mathcal{P}^{00}(\infty; ?) = 0 \quad \mathcal{P}^0(0; ?) = 1, \quad \mathcal{P}^0(\infty; ?) = \\ 0 \quad \mathcal{P}^0(0; ?) = 1 \text{ and } \mathcal{P}^0(\infty; ?) = 0 \end{aligned}$$

3embedding parameter,  $\sim ? ? \sim ?$  and  $\sim ?$  the non-zero auxiliary parameters and the nonlinear operators  $N_1$ ,  $N_2$  and

$24^{(?? ?)} + ^{(?? ?)} 22^{(?? ?)} ??^{(?? ?)} \geq N? [^{(?? ?)} ? ^{(?; ?)} ? ^{(?; ?)}] = -$

$??3 ??2 \tilde{A} ?? ! 2_{+?1(?) } \tilde{A} ?2^{(??}$

$$17^{?^{(? ?)} ??2}! ? ?3 ?^{(???) } ?2^{?(???) } ?3 ?^{(???) } 2^{+?2(?)} \square ?2 ?^{??^{(??^3)} ??2} ? ?3 + ?2 ?^{?(??2??)} - ?^{(? ?)} 4 ?3 ?^{(???' )} \square ? ?2 ? ?3 2 - ?^{(? ?)}^3 ? ? ? ?$$

17^('??2??')^2 ?4 ??^?(? 4??) □ +?^(?? ?) + ??^(?; ?) - ?2 □^3 '??^(?? ?)^3 ' □ □  
 ?? ? (2. 26) N ?[?^(?? ?)? ?^(?; ?)? ?^(?;

9??2!-? ?^((? ?) ?^((? ?) + ? ?^((? ?) ?^((? ?) ?? ?? ?^((??) ?2 ?^((??) ?  
4 +?2? ??? □ □ -?^((? ?)??3 ?^3((?3??)?? 2?2 ?^((? ? 2??) 3□ ? (2.27) □ ^ 3'□  
□ N [?(? ?) ? ^(?; ?) ? ^(?; ?)] = ?2?(???) +?? ?^((??)??^((??) ?^((??) ?  
^((??) ??2Ä ?? - ?? ! -? ?? Ä ??^((? ?) ?^((? ?) - ?^((? ?

27/97

2.34) converge at  $\eta = 1$ . Hence  $\theta(\eta) = \theta_0(\eta) + \theta_1(\eta)\eta^\infty$  (2.35)  $\theta = 1$   $P(\eta) = \theta_0(\eta) + \theta_1(\eta)\eta^\infty$  (2.36)  $\theta = 1$   
 $P^\infty(\eta) = \theta_0(\eta) + \theta_1(\eta)\eta^\infty$  (2.37)  $\theta = 1$  If we denote the special solutions  $\theta_1^*(\eta)$ ,  $\theta_2^*(\eta)$  and  $\theta_3^*(\eta)$  then  
 the general solutions  $\theta(\eta)$ ,  $P(\eta)$  and  $\eta(\eta)$  are  $\theta(\eta) = \theta_1^*(\eta) + \theta_1 + \theta_2\eta + \theta_3\eta - \theta_1\eta(\eta) = \theta_1^*(\eta)$   
 $+ \theta_4\eta + \theta_5\eta - \theta_1\eta(\eta) = \theta_1^*(\eta) + \theta_6\eta + \theta_7\eta - \theta_1\eta$  (2.38) (2.39) (2.40) 2.3 Convergence analysis and  
 discussion We recall that the auxiliary parameters  $\sim\eta$ ,  $\sim\eta$  and  $\sim\eta$  are useful in controlling and adjusting the  
 convergence of the series solutions. We draw the  $\sim$ -curves at 14th order of approximation in obtaining the  
 ranges for  $\sim\eta$ ,  $\sim\eta$  and  $\sim\eta$ . It is noticed from Fig. 2.2 that the admissible values of  $\sim\eta$ ,  $\sim\eta$  and  $\sim\eta$  are  $-0.7 \leq \sim\eta \leq -0.25$ ,  $-0.95 \leq \sim\eta \leq -0.5$  and  $-0.95 \leq \sim\eta \leq -0.5$ . Further

3the series solutions converge in the whole region of  $\eta$  when  $\sim\eta = \sim\eta = \sim\eta = -0.7$   
 6? Table 2.1

is presented to see the convergent values

1for different order of approximations at  $\sim\eta = \sim\eta = \sim\eta = -0.7$

6? This Table indicates

4that the series solutions for velocity converge from 20th order of deformations  
 and

temperature and concentration converge from 25th order of deformations. Hence 25th order deformations  
 are computed to find a convergent series solutions.

$K_1=0.1, K_2=0.2, l=0.4, t=0.3, M=0.6, Sc=0.7, Ec=0.5, Pr=1.0, N=0.3, R=0.4 -0$

1.5 -1  $f''(\eta)$ ,  $q'(\eta)$ ,  $f'(\eta)$  -1 .5

-2  $f''(\eta)$  -2.5  $g'(\eta)$   $q'(\eta)$  -1.2 -1 -0.8 -0.6 -0.4 -0.2 0 0.2  $\tilde{N}_f$ ,  $\tilde{N}_q, \tilde{N}_f$  Fig. 2. 2:  $\sim$ -curves for the functions  $\theta$   
 $\eta$  and  $\eta$  Table 2.1:

1Convergence of series solutions for different order of approximations when

$\eta_1 = 0.71$   $\eta_2 = 0.72$   $\eta = 0.74$   $\eta = 0.73$   $\eta = 0.76$   $\eta = 0.77$   $\eta = 0.75$   $\eta = 1.70$   $\eta = 0.73$   $\eta = 0.74$  and  
 $\sim\eta = \sim\eta = \sim\eta = -0.76$  Order of approximations  $-\eta$   $\theta_0(0)$   $-\eta_0(0)$   $-\eta_0(0)$  1 0.86800 0.63500 0.85000 5  
 0.82753 0.60365 0.71921 10 0.82461 0.60732 0.69473 20 0.82425 0.60872 0.68636 25 0.82425 0.60886  
 0.68578 30 0.82425 0.60886 0.68578 35 0.82425 0.60886 0.68578 Figs. 2.3- 2.7 are sketched to analyze  
 the variations of thixotropic parameters  $\eta_1$  and  $\eta_2$  local buoyancy parameter  $\eta$  Hartman number  $\eta$  and  
 concentration buoyancy parameter  $\eta$  on the fluid velocity  $\theta_0(\eta)$  Figs. 2.3 and 2.4 depict

1that the fluid velocity and momentum boundary layer thickness are increasing

## functions of

thixotropic parameters. By increasing thixotropic parameters, the values of material parameters  $\eta_1$  and  $\eta_2$  increase. An increase in the material parameters give rise to the fluid velocity and momentum boundary layer thickness. Fig. 2.5 shows that an increase in local buoyancy parameter gives rise to the fluid velocity and its associated boundary layer thickness. Increase in buoyancy parameter corresponds to stronger buoyancy force. Buoyancy force is an agent that causes

13an increase in the fluid flow and its related boundary layer thickness.

2An increase in Hartman number reduces the fluid velocity.

Hartman number involves the Lorentz force and

2an increase in Lorentz force reduces the fluid velocity and boundary layer thickness

(see Fig. 2.6). The Lorentz force provides a resistance to flow. From Fig. 2.7 it is observed that concentration buoyancy parameter enhances the velocity. To see the impacts of different parameters on the temperature  $\theta(\eta)$  Figs. 2.8-2.15 are portrayed. From Figs. 2.8 and 2.9, we have seen that the thixotropic parameters  $\eta_1$  and  $\eta_2$  are decreasing functions of

2temperature and thermal boundary layer thicknesses. Larger values of

$\eta_1$  and  $\eta_2$  correspond to stronger  $\eta_1$  and  $\eta_2$  showing a reduction in the temperature. We also noted that the thixotropic parameters have quite opposite effects on the fluid velocity and temperature. Figs. 2.10 and 2.11 present the effects of local buoyancy parameter and concentration buoyancy parameter

4on the temperature. It is found that the temperature and thermal boundary layer thickness

become smaller for larger values of local buoyancy parameter and concentration buoyancy parameter. Physically, both  $\eta_1$  and  $\eta_2$  depend on the buoyancy force. Larger values of  $\eta_1$  and  $\eta_2$  lead to the stronger buoyancy force. Such stronger buoyancy force reduced

13the temperature and thermal boundary layer thickness. Fig. 2.12 is

plotted to analyze the influence of Eckert number

4on the temperature. Here it is revealed that the temperature and thermal boundary layer thickness

are increased for larger Eckert number. This is because of the reason that

27heat energy is always stored in the liquid due to the frictional heating.

Such increase in Eckert number enhances the temperature at any point in the thermal boundary layer region. From Fig. 2.13, one can see that temperature is an increasing function of Hartman number. Larger values of Hartman number posses stronger Lorentz force. This stronger Lorentz force

13enhances the temperature and thermal boundary layer thickness.

Impact

2of Prandtl number ?? on the temperature ??(?) is analyzed in Fig.

2.14.

2Thermal boundary layer thickness and temperature ??(?) are decreasing functions of

??? This is due to the fact that with an enhancement in Prandtl number ??, thermal diffusivity decreases

2which leads to a reduction in temperature ??(?) Fig.

2.15 shows that temperature ??(?) increases with an increase in radiation parameter ?. Also thermal boundary layer thickness enhances with ? which is due to the fact that as thermal radiation parameter increases, the mean absorption coefficient ?? decreases which in results give rise to the divergence of radiative heat flux. Hence

16the rate of radiative heat transferred to the fluid

shoot up so that the fluid temperature increases. Figs. 2.16-2.22 are plotted to see the variations of ?1? ? 2? ?? ?? ??, ? and ? on the concentration ??(?)? Figs. 2.16 and 2.17 show the influence of thixotropic parameters on the concentration. From these Figs. we observed that increase in thixotropic parameters reduced the concentration and its related boundary thickness. We also analyzed that the effects of thixotropic parameters

26 on the temperature and concentration are similar in a qualitative sense.

A comparison of Figs. 2.8, 2.9, 2.16 and 2.17 show that the variation in temperature are dominant in comparison to variation in concentration due to thixotropic parameters. Local buoyancy parameter and concentration buoyancy parameter are decreasing functions of concentration (see Figs. 2.18 and 2.19). Fig. 2.20 shows

4 that an increase in Eckert number leads to a decrease in the concentration and its related boundary layer thickness.

For higher Eckert number, concentration specie diffuses due to which the concentration field decreases. Fig. 2.21 illustrates the variations of Hartman number on the fluid concentration. It is revealed that concentration is a decreasing function of Hartman number. We conclude that the variations in temperature are more dominant when compared with the variations in the concentration.

27 From Fig. 2. 22 it is observed that the associated boundary layer thickness

and concentration profile decrease when thermophoretic parameter  $\gamma$  increases.  $K_2 = 0.2, l = 0.4, t = 0.3, M = 0.6, Sc = 0.7, Ec = 0.5, Pr = 1.0, N = 0.3, R = 0.4$  1 0.8  $K_1 = 0.0$   $K_1 = 1.0$  0.6  $K_1 = 2.0$   $K_1 = 3.0$   $f''h?$  0.4 0.2 0 0 1 2 3 4 5 h Fig. 2.3: Influence of  $\gamma_1$  on  $\theta_0(\gamma)$

$K_1 = 0.1, l = 0.4, t = 0.3, M = 0.6, Sc = 0.7, Ec = 0.5, Pr = 1.0, N = 0.3, R = 0.4$  1  $K_2 = 0.0$   $K_2 = 0.7$  0.8  $K_2 = 1.4$   $K_2 = 2.0$

4  $f''h?$  0.6 0.4 0.2 0 0 1 2 3 4 5 h

Fig. 2.4: Influence of  $\gamma_2$  on  $\theta_0(\gamma)$  1  $l = -0.5$  0.8

3  $l = 0.0$   $l = 0.5$  0.6  $l = 1.0$

$f''h?$  0.4 0.2 0 0 2 4 6 8 h Fig. 2.5: Influence of  $\gamma$  on  $\theta_0(\gamma)$

$K_1 = 0.1, K_2 = 0.2, l = 0.4, t = 0.3, Sc = 0.7, Ec = 0.5, Pr = 1.0, N = 0.3, R = 0.4$

4 1  $M = 0.0$  0.8  $M = 0.5$   $M = 1.0$  0.6  $M = 1.5$   $f''h?$  0.4 0.2 0

0 2 4 6 8 h Fig. 2.6: Influence of  $\gamma$  on  $\theta_0(\gamma)$   $K_1 = 0.1, K_2 = 0.2, l = 0.4, t = 0.3, M = 0.6, Sc = 0.7, Ec = 0.5, Pr = 1.0, R = 0.4$  1 0.8

14  $N = 0.0$   $N = 0.5$  0.6  $N = 1.0$   $N = 1.5$

f?h? 0.4 0.2 0 0 2 4 6 8 h Fig. 2.7: Influence of ? on ?(?) 1 0.8 K1 = 0.0 K1 = 1.0 0.6 K1 = 2.0 K1 = 3.0

1q?h? 0.4 0.2 0 0 2 4 6 8 h

Fig. 2.8: Influence of ?1 on ?(?) K1 = 0.1, l = 0.4, t = 0.3, M = 0.6, Sc = 0.7, Ec = 0.5, Pr = 1.0, N = 0.3, R = 0.4 1 0.8 K2 = 0.0 K2 = 0.7 0.6 K2 = 1.4 K2 = 2.0

1q?h? 0.4 0.2 0 0 2 4 6 8 h

Fig. 2.9: Influence of ?2 on ?(?) K1=0.1,K2=0.2,t=0.3,M=0.6,Sc=0.7,Ec=0.5,Pr=1.0,N=0.3,R=0.4 1 0.8 l = -0.5

3l = 0.0 0.6 l = 0.5 l = 1.0

1q?h? 0.4 0.2 0 0 2 4 6 8 h

Fig. 2.10: Influence of ? on ?(?) 1 0.8 N = 0.0 N = 1.5 0.6 N = 3.0 N = 4.5

1q?h? 0.4 0.2 0 0 2 4 6 8 h

Fig. 2.11: Influence of ? on ?(?) K1=0.1,K2=0.2,l=0.4,t=0.3,M=0.6,Sc=0.7,Pr=1.0,N=0.3,R=0.4 1 Ec=0.0 0.8

11Ec = 0.5 Ec = 1.0 0.6 Ec = 1.5

1q?h? 0.4 0.2 0 0 2 4 h 6 8

Fig. 2.12: Influence of ?? on ?(?) K1=0.1,K2=0.2,l=0.4,t=0.3,Sc=0.7,Ec=0.5,Pr=1.0,N=0.3,R=0.4 1 0.8

4M=0.0 M=0.5 0.6 M=1.0 M=1.5 q ?h? 0.4 0.2 0

0 2 4 6 8 h Fig. 2.13: Influence of ? on ?(?) 1 0.8 Pr = 0.5 Pr = 1.0 0.6 Pr = 1.5 Pr = 2.0

1q?h? 0.4 0.2 0 0 2 4 6 8 h

Fig. 2.14: Influence of Pr on ?(?) K1 = 0.1, K2 = 0.2, l = 0.4, t = 0.3, M = 0.6, Sc = 0.7, Ec = 0.5, Pr = 1.0, N = 0.3 1 0.8 R = 0.0 R = 0.4 0.6 R = 0.8 R = 1.2

1 **q?h? 0.4 0.2 0 0 2 4** 6 8 h

Fig. 2.15: Influence of ? on ?(?)  $K_2 = 0.2, I = 0.4, t = 0.3, M = 0.6, Sc = 0.7, Ec = 0.5, Pr = 1.0, N = 0.3, R = 0.4$  1 0.8  $K_1 = 0.0$   $K_1 = 1.0$  0.6  $K_1 = 2.0$   $K_1 = 3.0$  f?h? 0.4 0.2 0 0 1 2 3 4 5 6 7 h Fig. 2.16: Influence of ?1 on ?(?) 1 0.8  $K_2 = 0.0$   $K_2 = 0.7$  0.6  $K_2 = 1.4$   $K_2 = 2.0$  f?h? 0.4 0.2 0 0 1 2 3 4 5 6 7 h Fig. 2.17: Influence of ?2 on ?(?)  $K_1=0.1, K_2=0.2, t=0.3, M=0.6, Sc=0.7, Ec=0.5, Pr=1.0, N=0.3, R=0.4$  1 0.8 I = -0.5

3 **I = 0.0** 0.6 **I = 0.5** **I = 1.0**

f?h? 0.4 0.2 0 0 1 2 3 4 5 6 7 h Fig. 2.18: Influence of ? on ?(?)  $K_1=0.1, K_2=0.2, I=0.4, t=0.3, M=0.6, Sc=0.7, Ec=0.5, Pr=1.0, R=0.4$  1 0.8

14 **N = 0.0** **N = 0.5** 0.6 **N = 1.0** **N = 1.5**

f?h? 0.4 0.2 0 0 2 4 6 8 h Fig. 2.19: Influence of ? on ?(?) 1  $Ec = 0.0$  0.8

11 **Ec = 0.5** **Ec = 1.0** 0.6 **Ec = 1.5** f?h? **0.**

4 0.2 0 0 2 4 6 8 h Fig. 2.20: Influence of ?? on ?(?)  $K_1 = 0.1, K_2 = 0.2, I = 0.4, t = 0.3, Sc = 0.7, Ec = 0.5, Pr = 1.0, N = 0.3, R = 0.4$

41 **M = 0.0** 0.8 **M = 0.5** **M = 1.0** 0.6 **M = 1.5** f?h? **0.4** **0.2** **0**

0 2 4 6 8 h Fig. 2.21: Influence of ? on ?(?)  $K_1 = 0.1, K_2 = 0.2, I = 0.4, M = 0.6, Sc = 0.7, Ec = 0.5, Pr = 1.0, N = 0.3, R = 0.4$  1 t = 0.0 0.8 t = 0.7 t = 1.4 0.6 t = 2.0 f?h? 0.4 0.2 0 0 1 2 3 4 5 6 7 h Fig. 2.22: Influence of ? on ?(?) Table 2.2 is made to find

4 **the numerical values of skin-friction coefficient for various values of**

?1? ?2? ?? ? and ? when the other parameters are fixed. We noted that the values of skin-friction coefficient are decreased by increasing ?1? ?2 and ?? However reverse situation is noted for ? and ?? Table 2. 3 analyzes the

1 **numerical values of local Nusselt number and local Sherwood number for different values of emerging parameters**

in viscous and non-Newtonian cases. We observed that the



## 7 values of local Nusselt number and local Sherwood number is large in

the case of non-Newtonian fluid when compared with the case of viscous fluid. Table 2.4 is computed for the comparison of  $\theta_{00}(0)$  and  $\theta_0(0)$  through different values of Prandtl number and local buoyancy parameter when all other parameters are zero. From this Table, it is analyzed that our series solutions have a good agreement with the numerical solutions in a limiting case. Table 2.2:

## 4 Numerical values of skin-friction coefficient for different values of

$\eta_1$   $\eta_2$   $\eta_3$   $\eta_4$  and  $\eta$  when  $\eta = 0.3$ ,  $\eta = 0.4$ ,  $\eta = 1.0$ ,  $\eta = 0.5$  and  $\eta = 0.7$   $\eta_1$   $\eta_2$   $\eta_3$   $\eta_4$   $\eta$   $-\eta_1\eta_2\eta_3\eta_4\eta$  0.0 0.2 0.6 0.4 0.4 0.84799 0.3 0.79227 0.5 0.76088 0.2 0.0 0.6 0.4 0.4 0.84923 0.3 0.79373 0.5 0.76247 0.2 0.2 0.0 0.4 0.4 0.71906 0.5 0.80959 1.0 1.01672 0.2 0.2 0.5 0.0 0.4 0.95561 0.4 0.76145 0.8 0.56391 0.2 0.2 0.5 0.3 0.0 0.80923 1.0 0.81003 2.0 0.81106 Table 2.3:

## 1 Numerical values of local Nusselt number and local Sherwood number for different values of

$\eta_1$   $\eta_2$   $\eta_3$   $\eta_4$  and  $\eta$  when  $\eta = 0.3$  and  $\eta = 0.4$   $\eta_1$   $\eta_2$   $\eta_3$   $\eta_4$   $\eta$   $-\theta_0(0) -\theta_0(0) \eta_1 = \eta_2 = 0.2 -\theta_0(0) -\theta_0(0) \eta_1 = \eta_2 = 0.2$  0.0 0.5 1.0 0.5 0.7 0.5 1.0 1.5 0.5 0.5 1.0 1.0 0.3 0.3 0.4 0.4 0.67883 0.58160 0.29936 0.58763 0.57572 0.57065 0.87335 0.86284 0.83862 0.62245 1.10358 1.45081 0.69254 0.60339 0.36075 0.60862 0.59829 0.59387 0.88088 0.86671 0.84058 0.68707 1.10750 1.45463 0.5 0.7 0.3 0.6 0.8 1.0 0.3 0.4 0.66211 0.54179 0.46338 0.84754 0.87021 0.88469 0.67841 0.56632 0.49302 0.85318 0.87341 0.88618 0.5 0.7 0.5 0.5 0.8 1.3 0.3 0.4 0.41490 0.52313 0.65577 0.88107 0.86855 0.85452 0.42578 0.54006 0.68482 0.88426 0.87243 0.85721 0.5 0.7 0.5 1.0 0.0 0.5 1.0 0.4 0.55688 0.59650 0.62949 0.85559 0.86737 0.87800 0.58355 0.61561 0.64317 0.85988 0.87109 0.88142 0.5 0.7 0.5 1.0 0.3 0.0 0.5 1.0 0.70547 0.55912 0.47505 0.84788 0.86538 0.87469 0.73986 0.57908 0.48877 0.85133 0.86942 0.87958 Table 2.4: Comparison of  $\theta_{00}(0)$  and  $\theta_0(0)$  with Singh et al. [76] for different values of  $\eta_1$  and  $\eta_2$  Singh et al. [76] Present solutions  $\theta_{00}(0)$   $\theta_0(0)$   $\theta_{00}(0)$   $\theta_0(0)$   $\eta = 0.7$  -1.00 -0.79366 -1.00000 -0.79373  $\eta = 0.2$   $\eta = 0.7$  -0.50751 -0.89613 -0.50767 -0.89614  $\eta = 1.0$   $\eta = 0.7$  2.57771 -1.17244 2.57789 -1.17287  $\eta = 1.0$   $\eta = 1.0$  -1.00 -3.72067 -1.00000 -3.72033  $\eta = 0.2$   $\eta = 1.0$  -0.82568 -3.74856 -0.82529 -3.74718  $\eta = 1.0$   $\eta = 1.0$  0.61966 -3.95235 0.61940 -3.95266  $\eta = 1.0$  2.4 Closing remarks Effects of Joule heating, thermophoresis and thermal radiation in MHD flow of thixotropic fluid are analyzed. The main observations are listed below. • The non-Newtonian parameters  $\eta_1$  and  $\eta_2$  have similar effects on the velocity in a qualitative sense. • The effects of  $\eta$  and  $\eta$  on the velocity field are quite opposite. • The variations of  $\eta_1$  and  $\eta_2$  on temperature and concentration are opposite in comparison to velocity. •

## 13 An increase in Schmidt number corresponds to a smaller variation in

concentration field. Chapter 3 Three-dimensional

### 3 mixed convection flow of viscoelastic fluid with thermal radiation and

convective conditions The objective of this chapter is to examine the thermal radiation effect in three-dimensional

### 21 mixed convection flow of viscoelastic fluid. The

resulting

### 14 partial differential equations are reduced into a system of nonlinear ordinary differential equations

using appropriate transformations. The series solutions are developed through a modern technique known as the homotopy analysis method. The convergent expressions of the velocity components and temperature are derived. The solutions obtained are dependent on seven sundry parameters including the viscoelastic parameter, mixed convection parameter, ratio parameter, temperature exponent, Prandtl number, Biot number and radiation parameter. Discussion to these parameters is made via plots. 3.1 Mathematical analysis Let us consider three-dimensional

### 23 mixed convection flow of second grade fluid due to an exponentially stretching surface. The

surface coincides with the plane  $y = 0$  and the flow is confined in the region  $y \geq 0$ . The surface also possess the convective boundary condition. Influence of thermal radiation through Rosseland's approximation is taken into account. Flow configuration is given below. Fig. 3.1: Geometry of problem The governing boundary layer equations for steady three-dimensional flow of viscoelastic fluid can be put into the forms:  $u \frac{\partial u}{\partial x} + v \frac{\partial u}{\partial y} + w \frac{\partial u}{\partial z} = 0$  + + (3.1)  $u \frac{\partial v}{\partial x} + v \frac{\partial v}{\partial y} + w \frac{\partial v}{\partial z} = \frac{\mu}{\rho} \frac{\partial^2 v}{\partial y^2} + \frac{\mu}{\rho} \frac{\partial^2 v}{\partial z^2} + \frac{\mu}{\rho} \frac{\partial^2 v}{\partial x^2} + \frac{\mu}{\rho} \frac{\partial^2 v}{\partial y \partial z} + \frac{\mu}{\rho} \frac{\partial^2 v}{\partial y \partial x} + \frac{\mu}{\rho} \frac{\partial^2 v}{\partial z \partial x}$   $u \frac{\partial w}{\partial x} + v \frac{\partial w}{\partial y} + w \frac{\partial w}{\partial z} = \frac{\mu}{\rho} \frac{\partial^2 w}{\partial y^2} + \frac{\mu}{\rho} \frac{\partial^2 w}{\partial z^2} + \frac{\mu}{\rho} \frac{\partial^2 w}{\partial x^2} + \frac{\mu}{\rho} \frac{\partial^2 w}{\partial y \partial z} + \frac{\mu}{\rho} \frac{\partial^2 w}{\partial y \partial x} + \frac{\mu}{\rho} \frac{\partial^2 w}{\partial z \partial x}$   $\frac{\partial \theta}{\partial x} + v \frac{\partial \theta}{\partial y} + w \frac{\partial \theta}{\partial z} = \frac{k}{\rho c_p} \frac{\partial^2 \theta}{\partial y^2} + \frac{k}{\rho c_p} \frac{\partial^2 \theta}{\partial z^2} + \frac{k}{\rho c_p} \frac{\partial^2 \theta}{\partial x^2} + \frac{k}{\rho c_p} \frac{\partial^2 \theta}{\partial y \partial z} + \frac{k}{\rho c_p} \frac{\partial^2 \theta}{\partial y \partial x} + \frac{k}{\rho c_p} \frac{\partial^2 \theta}{\partial z \partial x}$  (3.2)  $\frac{\partial \theta}{\partial x} + v \frac{\partial \theta}{\partial y} + w \frac{\partial \theta}{\partial z} = \frac{k}{\rho c_p} \frac{\partial^2 \theta}{\partial y^2} + \frac{k}{\rho c_p} \frac{\partial^2 \theta}{\partial z^2} + \frac{k}{\rho c_p} \frac{\partial^2 \theta}{\partial x^2} + \frac{k}{\rho c_p} \frac{\partial^2 \theta}{\partial y \partial z} + \frac{k}{\rho c_p} \frac{\partial^2 \theta}{\partial y \partial x} + \frac{k}{\rho c_p} \frac{\partial^2 \theta}{\partial z \partial x}$  (3.3)  $\frac{\partial \theta}{\partial x} + v \frac{\partial \theta}{\partial y} + w \frac{\partial \theta}{\partial z} = \frac{k}{\rho c_p} \frac{\partial^2 \theta}{\partial y^2} + \frac{k}{\rho c_p} \frac{\partial^2 \theta}{\partial z^2} + \frac{k}{\rho c_p} \frac{\partial^2 \theta}{\partial x^2} + \frac{k}{\rho c_p} \frac{\partial^2 \theta}{\partial y \partial z} + \frac{k}{\rho c_p} \frac{\partial^2 \theta}{\partial y \partial x} + \frac{k}{\rho c_p} \frac{\partial^2 \theta}{\partial z \partial x}$  (3.4) where  $u, v$  and  $w$

1 are the velocity components in the  $x$ – $y$ – and  $z$ –directions respectively,  $\theta$  is the material fluid parameter,  $\nu = (\mu/\rho)$  is the kinematic viscosity,  $\mu$  is the dynamic viscosity,  $\rho$  is the

fluid density,  $\theta$

1 is the fluid temperature,  $g$  is the gravitational acceleration,  $T_\infty$  is thermal

expansion **coefficient of**

temperature, ??

**1 is the specific heat, ? is the thermal conductivity and ?? the**

radiative heat flux.

**8 By using the Rosseland approximation, the radiative heat flux ?? is given by**

$q_r = -\frac{4}{3} \sigma T^3 \frac{dT}{dy}$  (3.5)

**14 where ?? is the Stefan-Boltzmann constant and ?? the mean absorption coefficient.**

**8 By using the Rosseland approximation, the present analysis is limited to optically thick fluids. If the temperature differences are sufficiently small then Eq. (3.5) can be linearized by expanding ? into the Taylor series about  $T_\infty$ , which after neglecting higher order terms takes the form:**

$T = T_\infty + \theta$  By using Eqs. (3.5) and (3.6), Eq. (3.4) reduces to  $\frac{d}{dy} \left( \frac{1}{Pr} \frac{d\theta}{dy} \right) + \frac{d}{dy} \left( \frac{1}{Pr} \frac{d\theta}{dy} \right) = -\theta$  The boundary conditions can be expressed as follows:  $\theta = 0$  at  $y = 0$ ,  $\theta = 0$  at  $y = \infty$ ,  $\theta = 0$  at  $y = 0$ ,  $\theta = 0$  at  $y = \infty$  as  $y \rightarrow \infty$  (3.6) (3.7) (3.8) where subscript ? corresponds to the wall condition, ?

**3 is the thermal conductivity, ?? is the hot fluid temperature, ? is the heat**

transfer coefficient and  $T_\infty$  is the free stream temperature. The velocities and temperature are taken in the following forms:  $u = u_0 + u_1 y$ ,  $v = v_0 + v_1 y$ ,  $T = T_\infty + T_0 y$  (3.9) in which  $u_0, v_0$  are the constants, ? is the reference length and ? is the temperature exponent. The

**14 mathematical analysis of the problem is simplified by using the**

transformations [25]:  $\eta = y \sqrt{u_0}$ ,  $\theta = T - T_\infty$ ,  $\psi = \frac{1}{\sqrt{u_0}} \int u dy$ ,  $\theta = -\frac{1}{2} \frac{d\theta}{d\eta}$  (3.10)  $\mu \frac{d}{d\eta}$  Incompressibility condition is now clearly satisfied whereas Eqs. (3.2) – (3.8) give  $\frac{d}{d\eta} \left( \frac{1}{Pr} \frac{d\theta}{d\eta} \right) + \frac{d}{d\eta} \left( \frac{1}{Pr} \frac{d\theta}{d\eta} \right) = -\theta$  (3.11)  $\frac{d}{d\eta} \left( \frac{1}{Pr} \frac{d\theta}{d\eta} \right) + \frac{d}{d\eta} \left( \frac{1}{Pr} \frac{d\theta}{d\eta} \right) = -\theta$







## parameter

?? This is due to the fact that with the increase of ratio parameter ?? the  $\eta$ -component of velocity coefficient decreases which

**2leads to a decrease in both the momentum boundary layer and**

velocity component  $u_0(\eta)$ ? Fig. 3.4 illustrates the influence of viscoelastic parameter  $\eta$  on the velocity component  $u_0(\eta)$ ? It is clear that both the boundary layer and velocity component  $u_0(\eta)$  increase when the viscoelastic parameter increases. Influence of mixed convection parameter  $\eta$  on the velocity component  $u_0(\eta)$  is analyzed in Fig. 3.5. Increase in mixed convection parameter  $\eta$  shows an increase in velocity component  $u_0(\eta)$ . This is due to the fact that the buoyancy forces are much more effective rather than the viscous forces. Figs. 3.6 and 3.7 illustrate the variations of ratio parameter  $\eta$  and viscoelastic parameter  $\eta$  on the velocity component  $u_0(\eta)$ ? Variation of ratio parameter  $\eta$  is analyzed in Fig. 3.6. Through comparative study with Fig. 3.3 it is noted that  $u_0(\eta)$  decreases while  $\eta_0(\eta)$  increases when  $\eta$  increases. Physically, when  $\eta$  increases from zero, the lateral surface starts moving in  $\eta$ -direction and thus the velocity component  $u_0(\eta)$  increases and the velocity component  $\eta_0(\eta)$  decreases. Fig. 3.7 is plotted to see the variation of viscoelastic parameter  $\eta$  on the velocity component  $u_0(\eta)$ ?

**1It is found that both the velocity component  $u_0(\eta)$  and momentum boundary layer thicknesses are increasing functions of**

$\eta$ . It is revealed from Figs. 3.4 and 3.7 that the effect of  $\eta$  on both the velocities are qualitatively similar. Figs. 3.8-3.14 are sketched to see the effects of ratio parameter ?? viscoelastic parameter  $\eta$ , the temperature exponent ?? Biot number  $Bi$ ? mixed convection parameter ?? Radiation parameter  $Ra$  and Prandtl number  $Pr$  on the temperature  $\theta(\eta)$ ? Fig. 3.8 is drawn to see the impact of ratio parameter  $\eta$

**4on the temperature  $\theta(\eta)$ . It is noted that the temperature  $\theta(\eta)$  and also the thermal boundary layer thickness**

decrease with increasing  $\eta$ . Variation of the viscoelastic parameter  $\eta$  on the temperature  $\theta(\eta)$  is shown in Fig. 3?9. Here both

**2the temperature and thermal boundary layer thickness are decreasing functions of**

$\eta$ . Variation of mixed convection parameter  $\eta$  is analyzed in Fig. 3?10. It is seen that both the

**2temperature  $\theta(\eta)$  and thermal boundary layer thickness are decreasing functions of mixed convection parameter**

Fig. 3.11 presents the plots for the variation of Biot number. Note that  $B_i$  increases when  $A$  increases. The

**thermal boundary layer thickness** is also **increasing** function of

It is also noted that the fluid temperature is zero when the Biot number vanishes. Influence of temperature exponent  $n$  is displayed in Fig. 3.12.

**It is found that both the temperature  $T_f$  and thermal boundary layer thickness decrease when  $A$  is increased.**

Also both the

**temperature  $T_f$  and thermal boundary layer thickness are increasing functions of**

thermal radiation parameter  $\beta$  (see Fig. 3.13). It is observed that an increase in  $\beta$  has the ability to increase the thermal boundary layer. It is due to the fact that when the thermal radiation parameter increases, the mean absorption coefficient  $\mu_a$  will be decreased which in turn increases the

**divergence of the radiative heat flux.**

Hence

**the rate of radiative heat transfer to the fluid is increased and consequently the fluid temperature increases.** Fig. 3.14 is

plotted to see the effects of  $Pr$  on  $T_f$ .

**It is noticed that both the temperature profile and thermal boundary layer thickness**

are decreasing functions of  $Pr$ . In fact when  $Pr$  increases then thermal diffusivity decreases. This indicates reduction in energy transfer ability and ultimate it results in the decrease of thermal boundary layer. Fig. 3.3: Influence of  $\beta$  on the velocity  $u$ . Fig. 3.4: Influence of  $\beta$  on the velocity  $u$ . Fig. 3.5: Influence of





4.3173603 0.2 5.16586 3.97055 0.3 5.42622 3.96130 0.3 0.0 3.72170 1.65409 0.2 4.30247 2.34617 0.5  
5.42622 3.96130 Table 3.4:

### 3 Values of local Nusselt number $-?_0(0)$ for different values

of the parameters  $?$ ,  $??$   $??$   $??$   $??$   $Pr$  and  $?1$ .  $?$   $?$   $?$   $?1$   $?$   $Pr$   $?$   $-(1 + 43?)?_0(0)$  0.0 0.5 0.5 0.5 0.3 1.2 0.2  
0.297492 0.3 0.308234 0.5 0.311853 0.2 0.0 0.303062 0.3 0.304775 0.5 0.305738 0.2 0.5 0.0 0.282007  
0.3 0.297135 0.5 0.305738 0.1 0.0885730 0.3 0.216850 0.5 0.305738 0.2 0.5 0.5 0.5 0.0 0.329701 0.3  
0.305738 0.5 0.292750 0.2 0.5 0.5 0.5 0.3 1.0 0.292152 1.2 0.305738 1.5 0.321826 0.2 0.5 0.5 0.5 0.3  
1.2 0.0 0.288530 0.2 0.305738 0.5 0.325492 3.5 Conclusions Three-dimensional mixed convection

2 flow of viscoelastic fluid over an exponentially stretching surface is analyzed.  
The

analysis is carried out in the presence of thermal radiation and convective boundary conditions. The main observations can be summarized as follows. • Influence of ratio parameter  $?$  on the velocities  $?_0(?)$  and  $?_0(?)$  is quite opposite. However the effect of viscoelastic parameter  $?$  on the velocities  $?_0(?)$  and  $?_0(?)$  is qualitatively similar. •

2 Momentum boundary layer thickness increases for  $?_0(?)$  when ratio parameter  $?$  is

large. Effect of  $?$  on  $?_0(?)$  is opposite to that of  $?_0(?)$ . • Velocity component  $?_0(?)$  is increasing function of mixed convection parameter  $??$  However  $?_0(?)$

14 decreases with an increase of mixed convection parameter  $?$ . The impacts of

Biot number  $?1$  and radiation parameter  $?$  on  $?_0(?)$  and  $?_0(?)$  are qualitatively similar. • Momentum boundary layer is an increasing function of mixed convection parameter  $?$  while thermal boundary layer is decreasing function of mixed convection parameter  $??$ . • Increase

4 in Prandtl number decreases the temperature  $?_0(?)$ . • Thermal boundary layer thickness

decreases when ratio parameter  $??$  viscoelastic parameter  $?$ , mixed convection parameter  $??$  Prandtl number  $Pr$  and temperature exponent  $?$  are increased. • Influence of viscoelastic parameter  $?$  on the  $?$  and  $?$  directions of skin friction coefficients is opposite. • Both components of skin friction coefficient increase through an increase in ratio parameter  $??$ . • Local Nusselt number is an increasing function of Prandtl number  $Pr$ ? ratio parameter  $??$  viscoelastic parameter  $?$ , mixed convection parameter  $??$  Biot number  $?1$  and temperature exponent  $?$  while it decreases for radiation parameter  $?$ . Chapter 4 Convective

**6**heat and mass transfer in three-dimensional mixed **convection flow** of viscoelastic fluid **with**

chemical reaction and heat source/sink This chapter investigates the

**6**heat and mass transfer effects **in** three-dimensional **mixed**

con-vection flow of viscoelastic fluid with internal heat source/sink and chemical reaction. An exponential stretching surface induces the flow. Magnetic field normal to the direction of flow is applied. Convective conditions at boundary surface are also encountered. Appropriate similarity transformations are utilized to reduce the boundary layer

**2**partial differential equations into ordinary differential equations. Analytical solutions of the

resulting systems are obtained. Convergence of the obtained solutions is discussed explicitly. The

**1**local Nusselt and Sherwood numbers **are** sketched **and**

examined. 4.1 Mathematical modeling We consider the three-dimensional mixed convection

**1**boundary layer flow of viscoelastic fluid past **an exponentially stretching**

surface. Mathematical analysis has been carried out in

**1**presence of internal **heat source/sink and**

generative/destructive chemical reaction.

**6**Magnetic field is applied to the normal direction of flow. The

surface coincides

**23**with the plane at  $\eta = 0$  and the flow is confined in the region  $0 \leq \eta < \infty$

Convective boundary conditions for both

## 23 heat and mass transfer on the sheet

are taken into account. The governing equations for three-dimensional flow are expressed as follows: ??

$$\frac{\partial u}{\partial x} + \frac{\partial v}{\partial y} + \frac{\partial w}{\partial z} = 0 \quad (4.1)$$

$$\rho \left( u \frac{\partial u}{\partial x} + v \frac{\partial u}{\partial y} + w \frac{\partial u}{\partial z} \right) = \mu \nabla^2 u + \rho \beta (T - T_\infty) \quad (4.2)$$

$$\rho \left( u \frac{\partial v}{\partial x} + v \frac{\partial v}{\partial y} + w \frac{\partial v}{\partial z} \right) = \mu \nabla^2 v \quad (4.3)$$

$$\rho \left( u \frac{\partial w}{\partial x} + v \frac{\partial w}{\partial y} + w \frac{\partial w}{\partial z} \right) = \mu \nabla^2 w \quad (4.4)$$

$$\rho c_p \left( u \frac{\partial T}{\partial x} + v \frac{\partial T}{\partial y} + w \frac{\partial T}{\partial z} \right) = k \nabla^2 T + \dot{q}''' \quad (4.5)$$

In the above equations,  $u$  and  $v$

are the velocity components in the  $x$ - $y$ - and  $z$ -directions respectively,  $\rho$  the material fluid parameter,  $\beta$  the thermal expansion coefficient,  $k$  the

concentration expansion coefficient,  $\mu$  the electrical conductivity,  $B_0$  the magnitude of applied magnetic field,  $\rho$  the density of fluid,  $g$  the gravitational acceleration,  $\nu = (\mu/\rho)$  the kinematic viscosity,  $\mu$  the dynamic viscosity,  $\alpha$  the thermal diffusivity,  $T$  the fluid temperature,  $c_p$  the specific heat of the fluid,  $\dot{q}'''$  the uniform volumetric heat generation/absorption,  $C$  the concentration field,  $\rho$  the mass diffusivity and prime denotes the

15 differentiation with respect to  $\eta$ . The boundary conditions are given by

$u = v = w = 0$ ,  $T = T_\infty$ ,  $C = C_\infty$  at  $\eta = 0$ ;  $u \rightarrow U_\infty$ ,  $T \rightarrow T_\infty$ ,  $C \rightarrow C_\infty$  as  $\eta \rightarrow \infty$  (4.6) (4.7) where subscript  $w$  corresponds to the wall condition,  $h$  is the heat transfer coefficient,  $h_c$  is the concentration transfer coefficient,  $T_\infty$

16 is the ambient fluid temperature and  $C_\infty$  is the ambient fluid concentration. At wall the

velocities, temperature and concentration distributions are defined as:  $u = U_\infty f'(\eta)$ ,  $T = T_\infty + (T_w - T_\infty) \theta(\eta)$ ,  $C = C_\infty + (C_w - C_\infty) \phi(\eta)$  (4.8) where  $U_\infty$ ,  $T_\infty$ ,  $C_\infty$  are the constants,  $\eta$  is the reference length,  $\eta_\infty$

15 is the ambient temperature,  $C_\infty$  is the ambient concentration,  $\theta$  is the temperature exponent and  $\phi$  is the

concentration exponent. By using similarity transformations [25]:  $\eta = y \sqrt{U_\infty / \nu}$ ,  $\theta = (T - T_\infty) / (T_w - T_\infty)$ ,  $\phi = (C - C_\infty) / (C_w - C_\infty)$  (4.9)  $\mu$  equation (4.1) is identically satisfied and Eqs. (4.2) - (4.9) give:  $\theta'' + f\theta' - \theta = 0$  (4.10)  $\phi'' + f\phi' - \phi = 0$  (4.11)  $\theta'' + f\theta' - \theta = 0$  (4.12)  $\phi'' + f\phi' - \phi = 0$  (4.13)

46/97

$$\begin{aligned} 18 \quad & \mathbb{P}^0(0; ?) = 0? \quad \mathbb{P}^0(0; ?) = 1? \quad \mathbb{P}^0(\infty; ?) = 0? \quad \mathbb{P}^0(0; ?) = 0? \quad \mathbb{P}^0(0; ?) = ?? \quad \mathbb{P}^0(\infty; ?) = \\ & 0? \quad \mathbb{P}^0(0? ?) = -?1[1 - \mathbb{P}(0? ?)]? \quad \mathbb{P}^0(\infty ? ?) = 0? \quad \mathbb{P}^0(0? ?) = -?2[1 - \mathbb{P}(0? ?)]? \quad \mathbb{P}^0(\infty \\ & ?) = 0? \end{aligned}$$

10[?(?; ?)? ?^(?; ?)? ^?(?; ?)? ?^(?; ?)] = ?3 ??^(?? 3? ?) ??^(?? ?) ??^(?? ?) ??  
^((? ?) -2 Å ?? + ?? ! ?? + □ ?^((? ?) ?2 ?^((? ?) ) + 2? ^((? ? ?) + ?^((? ? ?) □ - ? ??  
^((? ?) ) ??2 □ +??^(?; ?) □ ?? □ □ □ ?2 ?^((???) 3 □ 6 ???^(?????)? 3 ??^(??3??) +  
??2 □ □ -3?2 ??^(??2??) +??3 ?^((? ? 3??) □ □ +? ?2 ??^(?? 2??) + □ □ □ +24  
???^?(? 2 ?????^(??? 2)??) □ ?3 ??^(??

10<sup>7</sup>(<sup>7</sup>□<sup>7</sup>?)<sup>7</sup>+<sup>7</sup>(<sup>7</sup>??<sup>7</sup>(<sup>7</sup>?)<sup>7</sup> ?) 74 <sup>7</sup>??<sup>7</sup>(<sup>7</sup> 4??) □ □ +? ?? □ □ □ □ □ □ N ?[<sup>7</sup>(<sup>7</sup>;  
?)<sup>7</sup> ?<sup>7</sup>(<sup>7</sup>; ?)<sup>7</sup> ?<sup>7</sup>(<sup>7</sup>; ?)<sup>7</sup> ?<sup>7</sup>(<sup>7</sup>; ?)] = 73<sup>7</sup>??(<sup>7</sup>??3 ?) <sup>7</sup>??<sup>7</sup>(<sup>7</sup>??)-2 ?? <sup>7</sup>??<sup>7</sup>(<sup>7</sup>?) +??  
<sup>7</sup>(<sup>7</sup>????) □ ?? + ?<sup>7</sup>(?? ?) ?2 ?<sup>7</sup>(?? ?) □ □ +<sup>7</sup>(?? ?) □ ??2 □6 <sup>7</sup>??<sup>7</sup>(<sup>7</sup>????) ?3 ??  
<sup>7</sup>(<sup>7</sup>?? 3□??) □ □ +? □ + 3 ?2 ?<sup>7</sup>(<sup>7</sup>??) ??2 - □ □ □ 3 ?2 <sup>7</sup>??<sup>7</sup>(<sup>7</sup>??2??)+?? 3 <sup>7</sup>??<sup>7</sup>(<sup>7</sup>?  
3??) □ □ □ □ ?2<sup>7</sup>(<sup>7</sup>??) <sup>7</sup>??<sup>7</sup>(<sup>7</sup>??)□ □ □ ??2 + 4 ?? ?3 ?<sup>7</sup>(<sup>7</sup>??)

9+2??2??^(?? 2??) □ ??3 □ +? ?^(?□??)+?^????) ?4 ?^????)□ - □ □ ??4 □ +? ??  
 ^?(????) -? □??^(?? ?□) □ □ □ ?? ? (4.30) N ?[?^(?; ?)? ?^(?; ?)? ?^(?; ?)? ?^(?  
 ?)] = ?2^?(?? ?) ???2 + Pr □ (?^??? ?) ?^?(?? ?) + Pr ?\*^?(?? ?) +?^?(? ?) □ ?? -  
 Pr ? Ã ????^?(??□?) ????^?(?? ?□) ?^?(?? ?)? + (4.31) ?? ?? ! N ?[?^(?; ?)? ?^(?; ?)? ?  
 ^(?; ?)? ?^(?; ?)] = ?2 ?^(?; ?) ?^?(?? ?) ???2 + ?? □ +?^?(? ?) □ ???^(?; ?) - ???\* ?  
 ^(?; ?) ?? -? ?? Ã ????^?(?? ?□) ????^?(?? ?) ?^(?;

3 is an embedding parameter, the non-zero auxiliary parameters are  $\sim \eta$   $\sim \eta$   $\sim \eta$  and  $\sim \eta$  and the nonlinear operators

are  $N''', N'', N'$  and  $N$ . Taking  $\eta = 0$  and  $\eta = 1$  we get

$$12\eta'(\eta;0) = \eta_0(\eta) \eta'(\eta;0) = \eta_0(\eta) \eta'(\eta;0) = \eta_0(\eta) \eta'(\eta;0) = \eta_0(\eta) \text{ and } \eta'(\eta;1) = \eta(\eta) \eta'(\eta;1) = \eta(\eta) \eta'(\eta;1) = \eta(\eta) \eta'(\eta;1)$$

$1) = \eta(\eta)$  (4.33) As  $\eta$  enhances from 0 to 1 then  $\eta(\eta;0)$ ,  $\eta(\eta;1)$  and  $\eta(\eta;1)$  differ from  $\eta_0(\eta)$ ,  $\eta_0(\eta)$ ,  $\eta_0(\eta)$  and  $\eta_0(\eta)$  to  $\eta(\eta)$ ,  $\eta(\eta)$  and  $\eta(\eta)$ . Applying Taylor's expansion we have  $\eta(\eta;1) = \eta_0(\eta) + \eta_1(\eta) \eta'(\eta;1) + \eta_2(\eta) \eta''(\eta;1) + \eta_3(\eta) \eta'''(\eta;1) + \dots$  (4.34)  $\eta(\eta;1) = \eta_0(\eta) + \eta_1(\eta) \eta'(\eta;1) + \eta_2(\eta) \eta''(\eta;1) + \eta_3(\eta) \eta'''(\eta;1) + \dots$  (4.35)  $\eta(\eta;1) = \eta_0(\eta) + \eta_1(\eta) \eta'(\eta;1) + \eta_2(\eta) \eta''(\eta;1) + \eta_3(\eta) \eta'''(\eta;1) + \dots$  (4.36)  $\eta(\eta;1) = \eta_0(\eta) + \eta_1(\eta) \eta'(\eta;1) + \eta_2(\eta) \eta''(\eta;1) + \eta_3(\eta) \eta'''(\eta;1) + \dots$  (4.37)  $\eta(\eta;1) = \eta_0(\eta) + \eta_1(\eta) \eta'(\eta;1) + \eta_2(\eta) \eta''(\eta;1) + \eta_3(\eta) \eta'''(\eta;1) + \dots$  The

**3convergence of above series strongly depends upon  $\eta$ ,  $\eta$ ,  $\eta$  and  $\eta$**   
**Considering that  $\eta$ ,  $\eta$ ,  $\eta$  and  $\eta$  are selected properly so that**

Eqs. (4.34) – (4.37) converge at  $\eta = 1$ . Therefore  $\eta(\eta) = \eta_0(\eta) + \eta_1(\eta) \eta'(\eta;1) + \eta_2(\eta) \eta''(\eta;1) + \eta_3(\eta) \eta'''(\eta;1) + \dots$

$$33\mathbf{P} \eta(\eta) = \eta_0(\eta) + \eta_1(\eta) \eta'(\eta;1) + \eta_2(\eta) \eta''(\eta;1) + \eta_3(\eta) \eta'''(\eta;1) + \dots$$

The general solution expressions can be written as  $\eta(\eta) = \eta_0(\eta) + \eta_1(\eta) \eta'(\eta;1) + \eta_2(\eta) \eta''(\eta;1) + \eta_3(\eta) \eta'''(\eta;1) + \dots$  (4.38) (4.39) (4.40) (4.41) (4.42) (4.43) (4.44) (4.45) 4.3 Convergence analysis and discussion Homotopic solutions (4.38) – (4.41) obviously depend on the auxiliary parameters  $\eta$ ,  $\eta$ ,  $\eta$  and  $\eta$ . In order to control the convergence of series solutions' these auxiliary parameters play a central role. To obtain the convergence region, the  $\eta$ -curves have been plotted at 14<sup>th</sup> order of approximations in Fig. 4.1. This Fig. clearly shows that the acceptable values of  $\eta$ ,  $\eta$ ,  $\eta$  and  $\eta$  are  $-1.0 \leq \eta \leq -0.4$ ,  $-1.0 \leq \eta \leq -0.2$ ,  $-1.2 \leq \eta \leq -0.1$  and  $-1.2 \leq \eta \leq -0.1$ . Table 4.1 ensures that the

**1series solutions converge in the whole region of  $\eta$  when  $\eta = \eta = \eta = \eta = -0.5$  f " $\eta$ ", g " $\eta$ ",**

$q'(0), f'(0), b^*=b=A=B=0.2, M=K=0.1, g_1=g_2=0.5, Pr=0.7, Sc=0.8, l=N=k^*=0.3, 0.0-0.5, g''(0)$

$$1\mathbf{f'(0)} \mathbf{q'(0)} -1.0 \mathbf{f''(0)} -1.5 -1.0$$

-0.5 0.0 hf, hg, hq, hf Fig. 4.1:  $\eta$ -curves for the functions  $\eta$ ,  $\eta$  and  $\eta$  Table 4

**2.1: Convergence of series solutions for different order of approximations**

when

$\eta = \eta = 0.1$ ?  $\eta = \eta = \eta^* = \eta = 0.2$ ?  $\eta = \eta = \eta^* = 0.3$ ?  $\eta_1 = \eta_2 = 0.5$ ?  $Pr = 0.7$ ?  $\eta = 0.8$  and  $\sim \eta = \sim \eta = \sim \eta = \sim \eta - 0.6$ ? order of approximations 1 5 10 15 20 25 30 35  $-\eta$  00 (0) 1.155 1.104 1.078 1.068 1.065 1.064 1.064 1.064  $-\eta$  00 (0) 0.2359 0.2395 0.2414 0.2420 0.2422 0.2422 0.2422 0.2422  $-\eta$  00 (0) 0.3084 0.2620 0.2437 0.2373 0.2349 0.2341 0.2340 0.2340  $-\eta$  00 (0) 0.3300 0.3318 0.3336 0.3340 0.3341 0.3341 0.3341 0.3341 Figs. 4.2 and 4.3 are plotted to see the effects of Hartman number  $\eta$  on the velocity profile  $\eta$  and  $\eta$ . The velocity profiles  $\eta$  and  $\eta$  are decreased when we increase the values of  $\eta$ . Also the

2momentum boundary layer thicknesses are decreasing functions of  $\eta$ . Fig.

4.4 is drawn to see the influence of internal heat source/ sink parameter  $\eta^*$  on the velocity profile  $\eta$ ? Clearly in case of heat sink parameter  $\eta^* \eta > 0$  both momentum boundary layer thickness and  $\eta$  decrease while in case of heat source parameter  $\eta^* \eta < 0$  kinetic energy of the fluid particles increases due to which the velocity profile  $\eta$  increases. Outcome of mixed convection parameter  $\eta$  on the velocity profile  $\eta$  in both assisting and opposing flows is seen in Fig. 4.5. In case of assisting flow  $\eta \eta > 0$  both  $\eta$  and momentum boundary layer thickness are enhanced while reverse effect is observed for opposing flow  $\eta \eta < 0$ ? Fig. 4.6 exhibits the variation of concentration buoyancy parameter  $\eta$  on the velocity profile  $\eta$ ? It is examined that an enhancement in  $\eta$  gives rise to the velocity profile  $\eta$ . Fig. 4.7 depicts the influence of internal heat source/sink parameter  $\eta^*$  on the temperature  $\eta$ ? With an increase in internal heat source  $\eta^* \eta > 0$  both the thermal boundary layer thickness and  $\eta$  increase while in case of heat sink parameter  $\eta^* \eta < 0$  both the thermal boundary layer thickness and  $\eta$  decrease. Figs. 4.8-4.10 are sketched to see the variations of chemical reaction parameter  $\eta^*$ , concentration exponent  $B$  and mass transfer Biot number  $\eta_2$  on the concentration profile  $\eta$ ? Fig. 4.8 is presented to analyze the variation of chemical reaction parameter  $\eta^*$  on the concentration profile  $\eta$ ? It is noted that the associated boundary layer thickness and concentration profile  $\eta$  decrease for generative chemical reaction  $\eta^* \eta > 0$  while reverse phenomena is noted for destructive chemical reaction  $\eta^* \eta < 0$ . With an enhancement in concentration exponent  $\eta$  both the concentration profile  $\eta$  and the boundary layer thickness decrease (see Fig. 4.9). Variation of mass transfer Biot number  $\eta_2$  on the concentration profile  $\eta$  is displayed in Fig. 4.10. Here we examined that the effect of  $\eta_2$  on the concentration profile  $\eta$  and associated boundary layer thickness are increasing? Figs. 4.11-4.13 are displayed to see the impacts of mixed convection parameter  $\eta$  concentration buoyancy parameter  $\eta$ , ratio parameter  $\eta$  Hartman number  $\eta$ , internal heat source/sink  $\eta^*$  and heat transfer

2Biot number  $\eta_1$  on the local Nusselt number

$-\eta$  00)? Fig. 4.11 shows that the

2heat transfer rate at the wall increases for

assisting flow  $\eta \eta > 0$  while it decreases for opposing flow  $\eta \eta < 0$ ? It is also examined



2that the heat transfer rate at wall is

increasing function of concentration buoyancy parameter  $\beta$ . Fig. 4.12 exhibited that the larger values of ratio parameter  $\beta$  corresponds to a higher heat transfer rate  $-q''(0)$ . Also it is to be noted that with an increase in Hartman number heat transfer rate decreases. Fig. 4.13 depicts that

20the heat transfer rate at the wall  $-q''(0)$  decreases

with internal heat source  $\beta \neq 0$  while increases with internal heat sink  $\beta \neq 0$ . Variations of mixed convection parameter  $\beta$ , concentration buoyancy parameter  $\beta$ , ratio parameter  $\beta$ , Hartman number  $M$ , chemical reaction  $\beta$  and mass transfer Biot number  $B$  on Sherwood number  $-q''(0)$  are plotted in the Figs. 4.14-4.16. Fig. 4.14 is drawn to see the influences of mixed convection parameter  $\beta$  and concentration buoyancy parameter  $\beta$  on the Sherwood number  $-q''(0)$ . It is seen that the Sherwood number  $-q''(0)$  is increasing function of  $\beta$  and  $\beta$  in case of assisting flow  $\beta \geq 0$  while decreasing function for opposing flow case. Fig. 4.15 depicts that the Sherwood number  $-q''(0)$  decreases with an enhancement in Hartman number  $M$  while it increases with an increase in ratio parameter  $\beta$ . Fig. 4.16 exhibits that the mass transfer at the wall  $-q''(0)$  enhances with generative chemical reaction  $\beta \neq 0$  while it reduces with destructive chemical reaction  $\beta \neq 0$ . It is also observed that the mass transfer at the wall  $-q''(0)$  is an increasing function of mass transfer Biot number  $B$ . Table 4.2 ensures the validity of present results with Liu et al. [25] in the limiting sense.  $f''(h)$  1.0 0.8  $b = b^* = k^* = A = B = 0.2$ ,  $g_1 = g_2 = 0.3$ ,  $0.6$   $Pr = Sc = 0.7$ ,  $K = I = N = 0.5$  0.4 0.2  $M = 0.0, 0.3, 0.6, 0.9$  0 1 2 3 4 5 6  $h$  Fig. 4.2: Influence of  $\beta$  on velocity  $q''(0)$ .  $g''(h)$  0.20  $b = k^* = A = B = 0.2$ ,  $g_1 = g_2 = 0.3$ ,  $Pr = Sc = 0.7$ ,  $b^* = K = I = N = 0.5$  0.15 0.10 0.05  $M = 0.0, 0.3, 0.6, 0.9$  1 2 3 4 5 6  $h$  Fig. 4.3: Influence of  $\beta$  on velocity  $q''(0)$ .  $f''(h)$  1.0  $b = k^* = A = B = 0.2$ ,  $M = g_1 = g_2 = 0.3$ ,  $Pr = Sc = 0.7$ ,  $K = I = N = 0.5$  0.8 0.6 0.4  $b^* = -3.0, 0.0, 0.3, 7.0$  0.2 0 1 2 3 4 5 6  $h$

2Fig. 4. 4: Influence of  $\beta$  on velocity  $q''(0)$ .  $f$

$q''(h)$  1.0  $k^* = A = B = 0.2$ ,  $g_1 = g_2 = M = b = 0.3$ ,  $Pr = Sc = 0.7$ ,  $b^* = K = N = 0.5$  0.8 0.6 0.4  $I = -0.5, 0.0, 0.5, 0.9$  0.2 0 1 2 3 4 5 6  $h$

2Fig. 4. 5: Influence of  $\beta$  on velocity  $q''(0)$ .  $f$

$q''(h)$  1.0 0.8  $k^* = A = B = 0.2$ ,  $g_1 = g_2 = M = b = 0.3$ ,  $Pr = Sc = 0.7$ ,  $b^* = K = I = 0.5$  0.6 0.4  $N = 0.0, 1.5, 3.0, 4.5$  0.2 0 1 2 3 4 5 6  $h$  Fig. 4.6: Influence of  $\beta$  on velocity  $q''(0)$ .  $q''(h)$  0.30 0.25  $b = k^* = A = B = 0.2$ ,  $g_1 = g_2 = M = 0.3$ ,  $Pr = Sc = 0.7$ ,  $K = I = N = 0.5$  0.20 0.15  $b^* = -0.3, 0.0, 0.3, 0.6$  0.10 0.05 1 2 3 4 5 6  $h$  Fig. 4.7: Influence of  $\beta$  on temperature  $q''(0)$ .  $f''(h)$  0.25 0.20  $b = A = B = 0.2$ ,  $g_1 = g_2 = M = 0.3$ ,  $Pr = Sc = 0.7$ ,  $K = I = N = b^* = 0.5$  0.15 0.10 0.05  $k^* = -0.2, 0.0, 0.2, 0.4$  1 2 3 4 5 6  $h$  Fig. 4.8: Influence of  $\beta$  on  $q''(0)$ .  $f''(h)$  0.25 0.20  $b = A = k^* = 0.2$ ,  $g_1 = g_2 = M = 0.3$ ,  $Pr = Sc = 0.7$ ,  $K = I = N = b^* = 0.5$  0.15 0.10 0.05  $B = 0.0, 0.2, 0.4, 0.6$  1 2 3 4 5 6  $h$  Fig. 4.9: Influence of  $\beta$  on concentration  $q''(0)$ .  $f''(h)$  0.4  $b = A = B = k^* = 0.2$ ,  $g_1 = M = 0.3$ ,  $Pr = Sc = 0.7$ ,  $K = I = N = b^* = 0.5$  0.3 0.2  $g_2 = 0.1, 0.3, 0.5, 0.7$  0.1 1 2 3 4 5 6  $h$  Fig. 4.10: Influence of  $B$  on  $q''(0)$ .  $-q''(0)$   $A = B = b = b^* = k^* = 0.2$ ,  $M = 0.1, 0.276$   $K = g_1 = g_2 = 0.5$ ,  $Pr = 0.7$ ,  $Sc = 0.8$   $I = -0.5, 0.0, 0.5, 1.0$  0.274 0.272 0.270 0.268 0.266 0.5 1.0 1.5 2.0  $N$  Fig. 4.11: Influence of  $\beta$  and  $B$

on  $-\eta(0)$ .  $-q''(0)$  0.32  $A = B = b^* = k^* = 0.2$ ,  $I = N = 0.3$ ,  $K = g_1 = g_2 = 0.5$ ,  $Pr = 0.7$ ,  $Sc = 0.8$  0.31 0.30  
 0.29 0.28  $M = 0.0, 0.5, 1.0, 1.5$  0.27 0.5 1.0 1.5 2.0  $b$  Fig. 4.11: Influence of  $\eta$  and  $\eta$  on  $-\eta(0)$ .  $-q''(0)$   $A =$   
 $B = k^* = b = 0.2$ ,  $I = N = 0.3$ , 0.4  $K = g_2 = 0.5$ ,  $Pr = 0.7$ ,  $M = 0.1$ ,  $Sc = 0.8$  0.3 0.2  $b^* = -0.3, 0.0, 0.3, 0.6$  0.1  
 0.2 0.4 0.6 0.8 1.0  $g_1$  Fig. 4.13: Influence of  $\eta^*$  and  $\eta_1$  on  $-\eta(0)$ .  $-f''(0)$  0.340  $A = B = b = b^* = k^* = 0.2$ ,  
 $M = 0.1$ ,  $K = g_1 = g_2 = 0.5$ ,  $Pr = 0.7$ ,  $Sc = 0.8$  0.335 0.330  $I = -0.5, 0.0, 0.5, 1.0$  0.5 1.0 1.5 2.0  $N$  Fig. 4.14:  
 Influence of  $\eta$  and  $\eta$  on  $-\eta(0)$ .  $-f''(0)$  0.336  $A = B = b^* = k^* = 0.2$ ,  $I = N = 0.3$ ,  $K = g_1 = g_2 = 0.5$ ,  $Pr = 0.7$ ,  
 $Sc = 0.8$  0.334 0.332 0.330 0.328  $M = 0.0, 0.5, 1.0, 1.5$  0.326 0.2 0.4 0.6 0.8 1.0  $b$  Fig. 4.15: Influence of  $\eta$   
 and  $\eta$  on  $-\eta(0)$ .  $-f''(0)$  0.5  $A = B = b = b^* = 0.2$ ,  $M = 0.1$ ,  $I = N = 0.3$   $K = g_1 = 0.5$ ,  $Pr = 0.7$ ,  $Sc = 0.8$  0.4 0.3  
 $k^* = -0.3, 0.0, 0.3, 0.5$  0.2 0.1 0.2 0.4 0.6 0.8 1.0  $g_2$  Fig. 4.16: Influence of  $\eta^*$  and  $\eta_1$  on  $-\eta(0)$ . Table  
 4.2: Comparative values of  $-\eta(0)$ ,  $-\eta(0)$  and  $\eta(\infty) + \eta(\infty)$  for different values of  $\eta$  when  $\eta = \eta = \eta = \eta_1$   
 $= \eta_2 = \eta^* = \eta^* = 0$  Liu et al. [25] Present results  $-\eta(0)$   $-\eta(0)$   $\eta(\infty) + \eta(\infty)$   $-\eta(0)$   $-\eta(0)$   $\eta(\infty) +$   
 $\eta(\infty)$  0.0 1.28180856 0 0.50 1.56988846 0.78494423 1.00 1.81275105 1.81275105 0.90564383  
 1.10918263 1.28077378 1.28181 0 0.90564 1.56989 0.78494 1.10918 1.81275 1.81275 1.28077 4.4  
 Closing remarks The present chapter deals with the three-dimensional

#### 4 mixed convection flow of MHD viscoelastic fluid over

an exponentially

#### 1 stretching surface in presence of heat source/sink and

generative/destructive chemical reaction. The main outcomes are as follows. • Velocity profiles  $\eta(\eta)$  and  $\eta(\eta)$  reduce with an increase in Hartman number  $\eta$ . • Momentum boundary layer thickness

#### 2 decreases with an increase in ratio parameter $\eta\eta$ • Both the

velocity profile  $\eta(\eta)$  and

#### 2 momentum boundary layer thicknesses are increasing functions of internal heat source parameter

$\eta^* \eta_0$  assisting flow case  $\eta \eta_0$  and concentration buoyancy parameter  $\eta$  while decreasing functions of internal heat sink parameter  $\eta^* \eta_0$  and opposing flow case  $\eta \eta_0$  • Thermal boundary layer thickness and temperature  $\eta(\eta)$  decrease with an increase in internal heat sink  $\eta^* \eta_0$  while thermal boundary layer thickness and temperature  $\eta(\eta)$  increase with an increase in internal heat source  $\eta^* \eta_0$ . • With an enhancement in generative chemical reaction  $\eta^* \eta_0$ , concentration exponent  $\eta$  and Schmidt number  $\eta\eta$  decreases the concentration profile  $\eta(\eta)$  The concentration boundary layer thickness increases for larger mass transfer Biot number  $\eta_2$  and destructive chemical reaction  $\eta^* \eta_0$  • Heat transfer rate  $-\eta(0)$  boosts up in case of assisting flow  $\eta \eta_0$  concentration buoyancy parameter  $\eta$ , ratio parameter  $\eta\eta$  heat transfer Biot number  $\eta_1$  and internal heat sink parameter  $\eta^* \eta_0$  while heat transfer rate  $-\eta(0)$  reduces with opposing flow  $\eta \eta_0$  Hartman number  $\eta$  and internal heat source  $\eta^* \eta_0$  • With an increase in assisting flow  $\eta \eta_0$  concentration buoyancy parameter  $\eta$ , ratio parameter  $\eta\eta$  mass transfer Biot number  $\eta_2$  and

generative chemical reaction parameter  $\gamma$  the Sherwood number  $Sh(0)$  enhances while reverse behavior is noted in case of opposing flow  $\gamma < 0$  Hartman number  $M$  and destructive chemical reaction parameter  $\gamma < 0$  Chapter 5 Thermophoresis and MHD mixed convection flow

**1with Soret and Dufour effects** This chapter investigates **the**

**4heat and mass transfer** effects in **three-dimensional**

mixed convec- tion flow of viscoelastic fluid over a

**4stretching surface with convective boundary conditions. The fluid is electrically conducting in the presence of constant applied magnetic field.**

Conservation laws of energy and concentration are based upon the Soret and Dufour effects. First order chemical reaction effects are also taken into account.

**15Dimensionless velocity, temperature and concentration** distributions **are shown graphically**

**7for different values of** involved **parameters. Numerical**

values of

**1local Nusselt and Sherwood** numbers **are** computed **and analyzed.** 5.1 **Mathematical** analysis **We consider the steady**

three-dimensional magnetohydrodynamic mixed convection

**7flow of an incompressible** viscoelastic **fluid over a stretching** surface **at**

$\gamma = 0$  The flow takes place in the domain  $0 \leq y \leq 1$  Heat and mass transfer characteristics are taken into account

**6in the presence of Soret and Dufour** and thermophoresis **effects. The**

ambient fluid temperature is taken as  $T_\infty$  while the surface temperature is maintained by convective heat



1 is the Prandtl number,  $\gamma$  is the Dufour number,  $\beta$  is the Schmidt number,  $\gamma$  is the Soret number,  $\beta^*$  is the chemical reaction parameter,  $\beta$  is the

thermophoretic parameter,  $\beta$  is ratio of rates parameters,  $\beta$

2 is the Biot number and prime shows the differentiation with respect to

?. These are given by  $\beta = \frac{\mu}{\rho \alpha} \frac{v}{L}$ ,  $\gamma = \frac{D}{\alpha} \frac{v}{L}$ ,  $\beta = \frac{D}{\alpha} \frac{v}{L}$ ,  $\gamma = \frac{D}{\alpha} \frac{v}{L}$ ,  $\beta^* = \frac{D}{\alpha} \frac{v}{L}$ ,  $\beta = \frac{D}{\alpha} \frac{v}{L}$ . Local Nusselt and Sherwood numbers in dimensionless forms are given by  $Nu = \frac{hL}{k}$  (5.15)  $Sh = \frac{hL}{D}$  (5.16) in which  $Re$  is the local Reynolds number. 5.2 Construction of solutions The initial approximations and auxiliary linear operators required for homotopy analysis solutions are presented below i.e.  $\phi_0(\eta) = 1 - \eta$ ,  $\psi_0(\eta) = \eta$ ,  $\theta_0(\eta) = \exp(-\eta)$  (5.17)  $\phi_1(\eta) = \phi_0(\eta) + L_1(\eta)$ ,  $\psi_1(\eta) = \psi_0(\eta) + L_2(\eta)$ ,  $\theta_1(\eta) = \theta_0(\eta) + L_3(\eta)$  with the following properties of the defined operators in Eq. (5.18) i.e.  $L_1(\eta) = -\phi_0(\eta)$ ,  $L_2(\eta) = -\psi_0(\eta)$ ,  $L_3(\eta) = -\theta_0(\eta)$  where  $\eta$  ( $\eta = 1 - 10$ ) indicate the arbitrary constants. (5.18) (5.19) The corresponding problems at the zeroth order are given in the following forms:  $(1 - \eta) L_1[\phi_1(\eta) - \phi_0(\eta)] = \eta N_1(\phi_0, \psi_0, \theta_0)$  (5.20)  $(1 - \eta) L_2[\psi_1(\eta) - \psi_0(\eta)] = \eta N_2(\phi_0, \psi_0, \theta_0)$  (5.21)  $(1 - \eta) L_3[\theta_1(\eta) - \theta_0(\eta)] = \eta N_3(\phi_0, \psi_0, \theta_0)$

29  $\phi_1(\eta) = \phi_0(\eta) + L_1(\eta)$ ,  $\psi_1(\eta) = \psi_0(\eta) + L_2(\eta)$ ,  $\theta_1(\eta) = \theta_0(\eta) + L_3(\eta)$

(5.22)  $(1 - \eta) L_1[\phi_1(\eta) - \phi_0(\eta)] = \eta N_1(\phi_0, \psi_0, \theta_0)$

25  $\phi_1(\eta) = \phi_0(\eta) + L_1(\eta)$ ,  $\psi_1(\eta) = \psi_0(\eta) + L_2(\eta)$ ,  $\theta_1(\eta) = \theta_0(\eta) + L_3(\eta)$

12  $\phi_1(\eta) = \phi_0(\eta) + L_1(\eta)$ ,  $\psi_1(\eta) = \psi_0(\eta) + L_2(\eta)$ ,  $\theta_1(\eta) = \theta_0(\eta) + L_3(\eta)$

(5.24) 2 N?

10  $\phi_1(\eta) = \phi_0(\eta) + L_1(\eta)$ ,  $\psi_1(\eta) = \psi_0(\eta) + L_2(\eta)$ ,  $\theta_1(\eta) = \theta_0(\eta) + L_3(\eta)$

$$\begin{aligned}
 & 3??) - \square^2 ??^{\square}(\square) \square \square \square (5.26) ?? N [??^{\square}(\square) ??^{\square}(\square) ??^{\square}(\square) ??^{\square}(\square)] \\
 & = ??^2 ??^{\square}(\square) + \Pr (??^{\square}(\square) + ??^{\square}(\square)) ??^{\square}(\square) + \Pr ?? ??^2 ??^{\square}(\square) ? \\
 & (5.27) N [??^{\square}(\square) ??^{\square}(\square) ??^{\square}(\square) ??^{\square}(\square)] = ??^2 ??^{\square}(\square) + ??^{\square}(\square) \\
 & + ??^{\square}(\square) ??^{\square}(\square) - ??? * ??^{\square}(\square) + ??? ??^2 ??^{\square}(\square) - ??? (?? ??^{\square}(\square) \\
 & ??^{\square}(\square) ?? - ??^{\square}(\square)
 \end{aligned}$$

?) ??^2 ??^{\square}(\square) )? (5.28) Here ?

4 is an embedding parameter,  $\sim ?? \sim ?$ ,  $\sim ?$  and  $\sim ?$  are the non-zero auxiliary parameters and  $N?? N?$ ,  $N?$  and  $N?$  indicate the nonlinear operators. When  $\square = 0$  and  $\square = 1$  one has

$$\begin{aligned}
 12 ??^{\square}(\square; 0) &= ??(\square) ??^{\square}(\square; 0) = ??(\square) ??^{\square}(\square; 0) = ??(\square) ??^{\square}(\square; 1) = ??(\square) ??^{\square}(\square; 1) = ? \\
 (\square) ??^{\square}(\square; 1) &= ??(\square)
 \end{aligned}$$

? (5.29) Clearly when  $\square$  is increased from 0 to 1 then  $??(\square)$ ,  $??(\square)$  and  $??(\square)$  vary from  $??(\square)$  to  $??(\square)$  and  $??(\square)$  to  $??(\square)$  and  $??(\square)$  and  $??(\square)$ . By Taylor's expansion we have  $??(\square) = ??(\square) + \square = 1 ??(\square) ??(\square) = ?1! ???(\square; ?) \square = 0 \infty ?$  (5.30)  $??(\square) = ??(\square) + \square = 1 ??(\square) ??(\square) = ?1! ???(\square; ?) \square = 0 \infty ?$  (5.31)  $P ??(\square) = ??(\square) = P1 ??(\square) ??(\square) = ?1! ???(\square; ?) \square = 0 \infty ?$  (5.32)  $P ??(\square) = ?0(\square) \infty ??(\square) ??(\square) = ?1! ???(\square; ?) \square = 0 \infty ?$  (5.33)  $\square = 1$

3 where the convergence of above series strongly depends upon  $\sim ?? \sim ?$ ,  $\sim ?$  and  $\sim ?$ . Considering that  $\sim ?? \sim ?$ ,  $\sim ?$  and  $\sim ?$  are selected properly so that

Eqs. (5.30)–(5.33) converge at  $\square = 1$  then we can write  $??(\square) = ??(\square) + ??(\square) \infty$  (5.34)  $\square = 1$   $P ??(\square) = ??(\square) + ??(\square) \infty \square = 1$   $??(\square) = ??(\square) + P \infty ??(\square) \square = 1$   $P \infty ??(\square) = ??(\square) + ??(\square) \square = 1$   $P$  The resulting problems at  $m$ th order deformation can be constructed as follows:  $L[??(\square) - ???-1(\square)] = \sim R??(\square)$   $L[??(\square) - ???-1(\square)] = \sim R??(\square)$   $L[??(\square) - ???-1(\square)] = \sim R??(\square)$  (5.35) (5.36) (5.37) (5.38) (5.39) (5.40) (5.41)  $??(0) = ??(0) = ??(\infty) = 0?$  (5.42)  $??(0) = ??(0) = ??(\infty) = 0?$  (5.43)  $??(0) - ?1 ??(0) = ??(\infty) = 0?$   $??(0) = ??(\infty) = 0?$  (5.44)  $R??(\square) = ??(0) - ??(1) - ??(2) + (??-1-??(0) + ??-1-??(0)) ?-1 ?-1 ?=0 ?=0 ?-P1 ??-1-??(0) + ??-1-??(0) ?P-1 \square ?=0 ?=0 + P ?-1 ??(0) - ??(0) - P ?-1 \square -? ?(0) - ??(0) ?=0 ?=0 -2 ?P-1 ??(0) - ??(0) - 2P ?-1 ??(0) - ??(0) 000 ?=0 ?=0 -? 2 \square ??(0) - P ?? + ?? ? \square P \square \square$  (5.45)  $R??(\square) = ??(0) - ??(1) - ??(2) + (??-1-??(0) + ??-1-??(0)) ?-1 ?-1 ?=0 ?=0 ?-P1 ??-1-??(0) + ??-1-??(0) ?P-1 \square ?=0 ?=0 P ?-1 ??(0) - ??(0) - P ?-1 ?(0) - ??(0) \square -? +$  (5.46)  $\square = 0 ?=0 - ??(0) - 2 ?P-1 ??(0) - ??(0) - 2P ?-1 ??(0) - ??(0) \square ?=0 ?=0 P P \square \square$   $R??(\square) = ??(0) - ??(1) - ??(2) + (??-1-??(0) + ??-1-??(0)) ?-1 ?-1 ?=0 ?=0 P R??(\square) = ??(0) - ??(1) - ??(2) + (??-1-??(0) + ??-1-??(0)) ?-1 ?-1 ?=0 ?=0 P ?? = 0 ? \leq 1 ? \square 1 ? ? 1 ?$  (5.49) Solving the above  $m$ th order deformation problems we have  $\square ??(\square) = ??(\square) + ?1 + ??(2) + ??(3) - ??$  (5.50)  $??(\square) = ??$

$\phi(\eta) + \eta^4 + \eta^5 \eta \eta + \eta^6 \eta - \eta \eta$  (5.51)  $\eta \eta(\eta) = \eta \eta \eta(\eta) + \eta \eta \eta \eta + \eta \eta \eta - \eta \eta$  (5.52)  $\eta \eta(\eta) = \eta \eta \eta(\eta) + \eta \eta \eta \eta + \eta \eta \eta \eta - \eta \eta$  (5.53) in which the  $\eta \eta \eta \eta$ ,  $\eta \eta \eta$  and  $\eta \eta \eta$  indicate the special solutions. 5.3 Analysis Obviously the series solutions (5.34)–(5.37) contain the auxiliary parameters  $\eta \eta \eta$ ,  $\eta \eta$  and  $\eta \eta$ . These parameters are very important in adjusting and controlling the convergence of homotopic solutions. Hence the

**1  $\eta \eta$ -curves are plotted at 10 $\eta \eta$  order of approximations in**

order to find the suitable ranges of  $\eta \eta \eta$ ,  $\eta \eta$  and  $\eta \eta$ . Fig. 5.1 indicate that the admissible values of  $\eta \eta \eta$ ,  $\eta \eta \eta$  and  $\eta \eta$  here are  $-1.75 \leq \eta \eta \leq -0.40$ ,  $-1.4 \leq \eta \eta \leq -0.30$ ,  $-1.40 \leq \eta \eta \leq -0.25$  and  $-1.40 \leq \eta \eta \leq -0.20$ . Table 5.1 presents the convergence of homotopic solutions. It is noted that computations are sufficient for 45 $\eta \eta$  order iterations of velocity and 35 $\eta \eta$  order iterations of the temperature and concentration profiles for the convergent series solutions.  $1 \text{ K} = t = 0.2$ ,  $l = N = k^* = 0.3$ ,  $b = Sc = Df = 0.5$ ,  $M = 0.7$ ,  $g_1 = 0.6$ ,  $Df = 0.3$ ,  $Sr = 0.4$ ,  $Pr = 1.0$   $f''(0) = 0.5$   $g''(0) =$

**7  $q''(0) = f''(0)$ ,  $g''(0)$ ,  $q''(0)$ ,  $f''(0)$  0  $f''(0)$**

- 0.5 -1 - 1.5 -1.5 -1 -0.5 0  $h_f, h_g, h_q, h_k$  Fig. 5.1:  $\eta \eta$ -curves for the functions  $\eta \eta \eta$ ,  $\eta \eta$  and  $\eta \eta$  Table 5.1:

**1 Convergence of series solutions for different order of approximations when**

$\eta \eta = \eta \eta = 0.2 \eta \eta \eta = \eta \eta \eta = 0.5 \eta \eta \eta = 1 \eta \eta \eta = 0.4 \eta \eta = 0.7 \eta \eta = \eta \eta = \eta \eta = 0.3 \eta \eta = 0.6$  and  $\eta \eta = \eta \eta = \eta \eta = -0.7 \eta \eta$  order of approximations  $\eta \eta$  00 (0)  $\eta \eta$  00 (0)  $\eta \eta$  (0)  $\eta \eta$  (0) 1 1.31063 0.632417 0.284766 0.763750 5 1.47588 0.746614 0.230340 0.599613 10 1.49331 0.762859 0.221636 0.578386 15 1.49592 0.764867 0.220665 0.575416 20 1.49650 0.765053 0.220797 0.574753 25 1.49664 0.765041 0.220916 0.574545 30 1.49667 0.765030 0.220950 0.574483 35 1.49667 0.765027 0.220953 0.574471 40 1.49667 0.765027 0.220953 0.574471 Figs. 5.2 – 5.5 depict the behaviors of mixed convection parameter  $\eta \eta$  and concentration buoyancy parameter  $\eta \eta$  on  $\eta \eta(\eta)$  and  $\eta \eta(\eta)$ . Figs. 5.2 and 5.3 are drawn to analyze the effects of mixed convection parameter  $\eta \eta$  on the velocity components  $\eta \eta(\eta)$  and  $\eta \eta(\eta)$ . It is shown that  $\eta \eta(\eta)$  and  $\eta \eta(\eta)$  increase with an increase in  $\eta \eta$ . Effect of concentration buoyancy parameter  $\eta \eta$  on the velocity components  $\eta \eta(\eta)$  and  $\eta \eta(\eta)$  are shown in the Figs. 5.4 and 5.5. It is examined that the concentration buoyancy parameter  $\eta \eta$  shows the similar effects on momentum boundary layer thicknesses and velocity components  $\eta \eta(\eta)$  and  $\eta \eta(\eta)$  as we observed for mixed convection parameter  $\eta \eta$ . Figs. 5.6 – 5.9 examine the variation

**7 of Dufour number  $\eta \eta$  and Soret number  $\eta \eta$  on the temperature  $\eta \eta(\eta)$  and concentration  $\eta \eta(\eta)$**

$\eta \eta(\eta)$  Variations of  $\eta \eta$  on temperature  $\eta \eta(\eta)$  and concentration  $\eta \eta(\eta)$  are analyzed in the Figs. 5.6 and 5.7. It is noted from these Figs. that  $\eta \eta$  has reverse effects on temperature  $\eta \eta(\eta)$  and concentration  $\eta \eta(\eta)$ . Figs. 5.8 and 5.9 are displayed to see the variation of  $\eta \eta$  on the temperature  $\eta \eta(\eta)$  and concentration profiles  $\eta \eta(\eta)$ . We noticed

2that the temperature  $\theta(\eta)$  and thermal boundary layer are reduced for an increase in  $\eta$ . The

concentration profile  $\theta(\eta)$  increases when  $\eta$  is increased. To analyze the effect of thermophoretic parameter  $\eta$  on the concentration  $\theta(\eta)$  profile we have sketched Fig. 5.10.

4It is found that an increase in thermophoretic parameter  $\eta$  leads to a decrease in both concentration profile  $\theta(\eta)$  and concentration boundary layer thickness.

1  $K = M = Sr = 0.5$ ,  $b = N = Sc = 0.3$ ,  $Df = k^* = 0.3$ ,  $t = 0.1$ ,  $g_1 = 0.4$ ,  $Pr = 0.7$

3  $\eta = 0.0$   $\eta = 0.8$   $\eta = 0.5$   $\eta = 1.0$   $\eta = 0.6$   $\eta$

$\eta = 1.5$   $\eta = 0.4$   $\eta = 0.2$   $\eta = 0$   $\eta = 1$   $\eta = 2$   $\eta = 3$   $\eta = 4$   $\eta = 5$   $\eta = 6$  h Fig. 5.2: Influence of  $\eta$  on  $\theta(\eta)$ ?  $K = M = Sr = 0.5$ ,  $b = N = Sc = 0.3$ ,  $Df = k^* = 0.3$ ,  $t = 0.1$ ,  $g_1 = 0.4$ ,  $Pr = 0.7$   $\eta = 0.3$   $\eta = 0.25$   $\eta = 0.2$

3  $\eta = 0.0$   $\eta = 0.5$   $\eta = 1.0$   $\eta$

$\eta = 1.5$  g

4  $\eta = 0.15$   $\eta = 0.1$   $\eta = 0.05$   $\eta = 0$   $\eta = 1$   $\eta = 2$   $\eta = 3$   $\eta = 4$   $\eta = 5$   $\eta = 6$  h Fig. 5.3: Influence of  $\eta$  on

$\theta(\eta)$ ?  $K = M = Sr = \eta = 0.5$ ,  $b = N = Sc = 0.3$ ,  $Df = k^* = 0.3$ ,  $t = 0.1$ ,  $g_1 = 0.4$ ,  $Pr = 0.7$   $N = 0.0$   $N = 0.8$   $N = 0.5$   $N = 1.0$   $N = 0.6$   $N = 1.5$   $\eta = 0.4$   $\eta = 0.2$   $\eta = 0$   $\eta = 1$   $\eta = 2$   $\eta = 3$   $\eta = 4$   $\eta = 5$   $\eta = 6$  h Fig. 5.4: Influence of  $\eta$  on  $\theta(\eta)$ ?  $K = M = Sr = 0.5$ ,  $b = N = Sc = 0.3$ ,  $Df = k^* = 0.3$ ,  $t = 0.1$ ,  $g_1 = 0.4$ ,  $Pr = 0.7$   $\eta = 0.3$   $\eta = 0.25$

14  $N = 0.0$   $N = 0.5$   $N = 0.2$   $N = 1.0$   $N = 1.5$

g

4  $\eta = 0.15$   $\eta = 0.1$   $\eta = 0.05$   $\eta = 0$   $\eta = 1$   $\eta = 2$   $\eta = 3$   $\eta = 4$   $\eta = 5$   $\eta = 6$  h Fig. 5.5: Influence of  $\eta$  on

$\theta(\eta)$ ?  $K = M = \eta = N = Sr = 0.5$ ,  $b = N = Sc = 0.3$ ,  $k^* = t = 0.2$ ,  $g_1 = 0.4$ ,  $Pr = 0.7$   $0.5$   $Df = 0.1$   $Df = 0.4$   $0.4$   $Df = 0.7$   $Df = 1.0$

4  $q(\eta) = 0.3$   $q(\eta) = 0.2$   $q(\eta) = 0.1$   $q(\eta) = 0$   $q(\eta) = 2$   $q(\eta) = 4$   $q(\eta) = 6$   $q(\eta) = 8$  h



Fig. 5.6: Influence of  $Pr$  on  $Nu_{local}$ ?  $K = M = I = N = Sr = 0.5$ ,  $b = N = Sc = 0.3$ ,  $k^* = t = 0.2$ ,  $g_1 = 0.4$ ,  $Pr = 0.7$  1 0.8 Df = 0.1 Df = 0.4 0.6 Df = 0.7 Df = 1.0 f?h? 0.4 0.2 0 0 2 4 6 8 h Fig. 5.7: Influence of  $Pr$  on  $Nu_{local}$ ?  $K = M = I = N = Df = 0.5$ ,  $b = N = Sc = 0.3$ ,  $k^* = t = 0.2$ ,  $g_1 = 0.4$ ,  $Pr = 0.7$  0.4 Sr = 0.1 Sr = 0.4 Sr = 0.7 0.3 Sr = 1.0

1q?h? 0.2 0.1 0 0 2 4 6 8 h

Fig. 5.8: Influence of  $Pr$  on  $Nu_{local}$ ?  $K = M = I = N = Df = 0.5$ ,  $b = N = Sc = 0.3$ ,  $k^* = t = 0.2$ ,  $g_1 = 0.4$ ,  $Pr = 0.7$  1 0.8 Sr = 0.1 Sr = 0.4 0.6 Sr = 0.7 Sr = 1.0 f?h? 0.4 0.2 0 0 2 4 6 8 h Fig. 5.9: Influence of  $Pr$  on  $Nu_{local}$ ?  $K = M = I = N = Df = 0.5$ ,  $b = N = Sc = 0.3$ ,  $k^* = Sr = 0.2$ ,  $g_1 = 0.4$ ,  $Pr = 0.7$  1 0.8 t = 0.1 t = 0.4 0.6 t = 0.7 t = 1.0 f?h? 0.4 0.2 0 0 2 4 6 8 h Fig. 5.10: Influence of  $Pr$  on  $Nu_{local}$ ? Table 5.2 is prepared to analyze

1numerical values of local Nusselt and Sherwood numbers. The values of

$Nu_{local}$  and  $Sh_{local}$  decrease by increasing Deborah number. Here  $Nu_{local}$  increases by increasing Prandtl and Biot numbers while reverse is the case of  $Sh_{local}$ . Table 5.3 shows that local Nusselt  $Nu_{local}$  and Sherwood numbers  $Sh_{local}$  decrease with the increase in Hartman and Soret numbers.

1Values of local Nusselt  $Nu_{local}$  and Sherwood numbers

$Nu_{local}$  are opposite for Schmidt, Dufour, thermophoretic and chemical reaction parameters. Table 5.2:

1Values of local Nusselt  $Nu_{local}$  and Sherwood numbers  $Sh_{local}$  for different values of the parameters

?? ?? ?? ?? ? ?? and ?1 when ?? = ?? = 0?5? ?? = 0?4? ? = 0?2? ?\* = 0?3 and ? = 0?5. ? ? ? ? ? ?1  
 $Nu_{local}$   $Sh_{local}$  0.0 0.2 0.4 0.2 0.5 0.0 0.2 0.4 0.5 0.3 1.0 0.6 0.24700 0.23486 0.18422 0.21393 0.22444  
 0.23200 0.61363 0.59297 0.51482 0.55535 0.57294 0.58714 0.2 0.2 0.0 0.3 0.5 0.19606 0.21647  
 0.22444 0.54490 0.56327 0.57295 0.2 0.2 0.5 0.0 0.3 0.5 0.21880 0.22446 0.22772 0.56592 0.57285  
 0.57750 0.2 0.2 0.5 0.3 1.0 0.22443 0.57291 1.5 0.24490 0.56585 2.0 0.25725 0.56080 0.2 0.2 0.5 0.3  
 1.0 0.2 0.10779 0.58240 0.5 0.20254 0.57481 0.7 0.24341 0.57118 Table 5.3:

1Values of local Nusselt  $Nu_{local}$  and Sherwood numbers  $Sh_{local}$  for different values of the parameters

??? ??? ?? ??? ?\* and ? when ? = ? = 0?2? ? = 0?5? ?1 = 0?3? ?? = 1 and ? = 0?6? ?? ?? ?? ?\* ? -?  
 $Nu_{local}$   $Sh_{local}$  0.2 0.4 0.5 0.2 0.3 0.5 0.26950 0.32824 0.5 0.22446 0.57285 0.7 0.19729 0.71482 0.5 0.2  
 0.22285 0.58265 0.5 0.22530 0.56786 0.7 0.22690 0.55779 0.5 0.4 0.2 0.27834 0.52746 0.5 0.22695  
 0.55765 0.7 0.18905 0.57984 0.5 0.4 0.5 0.4 0.22160 0.58610 0.7 0.21705 0.60820 1.0 0.21164 0.63434  
 0.5 0.4 0.5 0.2 0.5 0.20529 0.67118 0.7 0.18854 0.75605 1.0 0.16638 0.86737 0.5 0.4 0.5 0.2 0.3 0.6  
 0.22122 0.56859 0.8 0.21345 0.55880 1.0 0.20402 0.54895 5.4 Conclusions

**2MHD three-dimensional flow of viscoelastic fluid over a stretching surface is analyzed in the presence of thermophoresis and**

convective condition.

**6Effects of chemical reaction and Soret and Dufour**

are analyzed. The main observations are listed below. • Effects of mixed convection parameter  $\lambda$  and buoyancy concentration parameter  $N_b$  on

**1the velocity profiles and momentum boundary layer thickness are similar. • Effects of**

$\lambda$  and  $N_b$  on  $f''(0)$  and  $\theta'(0)$  are opposite. • Thermal boundary layer thickness and temperature field increase when  $N_b$  increases. • Concentration  $C(0)$  and associated

**2boundary layer thickness are decreasing functions of thermophoretic parameter**

$\lambda$  • There are opposite effects of

**1local Nusselt number and local Sherwood number** when  $\lambda$  increases,  $N_b$  increases,  $N_t$  increases and

$N_t$  increase. • Qualitative effects of

**1local Nusselt number and local Sherwood number are similar** when  $\lambda$ ,  $N_b$  and

$N_t$  increase. Chapter 6

**4Three-dimensional flow of Maxwell fluid over a stretching surface with heat source and**

convective conditions

**11Heat and mass transfer effects in three-dimensional flow of Maxwell fluid over a**

## 60/97



given in the following forms:  $(1 - \gamma) L \gamma \gamma(\gamma; \gamma) - \gamma_0(\gamma) = \gamma \sim \gamma N \gamma \gamma(\gamma; \gamma)?$

$$10 \gamma \gamma(\gamma; \gamma) \gamma \gamma(\gamma \gamma \gamma) \gamma \gamma(\gamma \gamma \gamma) \gamma \gamma (6.21) (1 - \gamma) L \gamma [\gamma \gamma(\gamma; \gamma) - \gamma_0(\gamma)] = \gamma \sim \gamma N \gamma \gamma(\gamma; \gamma) \gamma \gamma(\gamma; \gamma) \gamma \gamma(\gamma \gamma \gamma) \gamma \gamma(\gamma \gamma \gamma)$$

$\gamma) \gamma \gamma \gamma \gamma (6.22) (1 - \gamma) L \gamma \gamma(\gamma; \gamma) - \gamma_0(\gamma) = \gamma \sim \gamma N \gamma$

$$17 \gamma \gamma(\gamma; \gamma) \gamma \gamma(\gamma; \gamma) \gamma \gamma(\gamma \gamma \gamma) \gamma \gamma(\gamma \gamma \gamma) \gamma \gamma \gamma (1 - \gamma) L \gamma \gamma(\gamma; \gamma) - \gamma_0(\gamma) = \gamma \sim \gamma N \gamma \gamma(\gamma; \gamma) \gamma \gamma(\gamma; \gamma) \gamma \gamma(\gamma \gamma \gamma) \gamma \gamma(\gamma \gamma \gamma)$$

$\gamma) \gamma$

25 **h i h i h i h i**

(6.23) (6.24)

$$18 \gamma \gamma(0; \gamma) = 0 \gamma \gamma_0(0; \gamma) = 1 \gamma \gamma_0(\infty; \gamma) = 0 \gamma \gamma(0; \gamma) = 0 \gamma \gamma_0(0; \gamma) = \gamma \gamma \gamma_0(\infty; \gamma) = 0 \gamma \gamma_0(0 \gamma \gamma) = -\gamma_1[1 - \gamma(0 \gamma \gamma)] \gamma \gamma(\infty \gamma \gamma) = 0 \gamma \gamma_0(0 \gamma \gamma) = -\gamma_2[1 - \gamma(0 \gamma \gamma)] \gamma \gamma(\infty \gamma \gamma) = 0$$

(6.25)  $N \gamma$

$$9 [\gamma \gamma(\gamma \gamma \gamma) \gamma \gamma(\gamma \gamma \gamma) \gamma \gamma(\gamma \gamma \gamma) \gamma \gamma(\gamma \gamma \gamma)] = \gamma_3 \gamma \gamma(\gamma \gamma \gamma) \gamma \gamma(\gamma \gamma \gamma) 2 \gamma \gamma_3 - \tilde{A} \gamma \gamma ! + (\gamma \gamma(\gamma \gamma \gamma) + \gamma \gamma(\gamma \gamma \gamma)) \gamma_2 \gamma \gamma(\gamma \gamma \gamma) \gamma \gamma_2 2 (\gamma \gamma(\gamma \gamma \gamma) + \gamma \gamma(\gamma \gamma \gamma)) + \gamma_1 \square \gamma \gamma \gamma(\gamma \gamma \gamma) \gamma_2 \gamma \gamma(\gamma \gamma \gamma) \gamma \gamma \gamma_2 \square \square - (\gamma \gamma(\gamma \gamma \gamma) + \gamma \gamma(\gamma \gamma \gamma)) 2 \gamma_3 \gamma \gamma \gamma(\gamma \gamma \gamma \gamma \gamma) + [\gamma \gamma \square(\gamma \gamma \gamma) + \gamma_1 \gamma \gamma(\gamma \gamma \gamma)] \gamma \square \square \square (6.26) N \gamma [\gamma \gamma(\gamma \gamma \gamma) \gamma \gamma(\gamma \gamma \gamma) \gamma \gamma(\gamma \gamma \gamma) \gamma \gamma(\gamma \gamma \gamma)] = \gamma_3 \gamma \gamma(\gamma \gamma \gamma) \gamma \gamma_3 - \gamma \gamma \gamma(\gamma \gamma \gamma) 2 + (\gamma \gamma(\gamma \gamma \gamma) + \gamma \gamma(\gamma \gamma \gamma)) \gamma_2 \gamma \gamma(\gamma \gamma \gamma) \mu \gamma \gamma \gamma \gamma \gamma_2 2 (\gamma \gamma(\gamma \gamma \gamma) + \gamma \gamma(\gamma \gamma \gamma)) + \gamma_1 \square \gamma \gamma \gamma(\gamma \gamma \gamma) \gamma_2 \gamma \gamma(\gamma \gamma \gamma) \gamma \gamma \gamma_2 \square \gamma (6.27) \square - (\gamma \gamma(\gamma \gamma \gamma) + \gamma \gamma(\gamma \gamma \gamma)) 2 \gamma_3 \gamma \gamma \gamma(\gamma \gamma \gamma \gamma \gamma) \square \square \square N \gamma [\gamma \gamma(\gamma \gamma \gamma) \gamma \gamma(\gamma \gamma \gamma) \gamma \gamma(\gamma \gamma \gamma) \gamma \gamma(\gamma \gamma \gamma)] = \gamma_2 \gamma \gamma(\gamma \gamma \gamma \gamma \gamma) + \text{Pr} (\gamma \gamma(\gamma \gamma \gamma) + \gamma \gamma(\gamma \gamma \gamma)) \gamma \gamma(\gamma \gamma \gamma \gamma \gamma) + \gamma * \gamma \gamma(\gamma \gamma \gamma) \gamma (6.28) N \gamma [\gamma \gamma(\gamma \gamma \gamma) \gamma \gamma(\gamma \gamma \gamma) \gamma \gamma(\gamma \gamma \gamma) \gamma \gamma(\gamma \gamma \gamma)] = \gamma_2 \gamma \gamma(\gamma \gamma \gamma) + \gamma \gamma(\gamma \gamma \gamma \gamma \gamma) + \gamma \gamma(\gamma \gamma \gamma) \gamma \gamma \gamma(\gamma \gamma \gamma)$$

$\gamma) \gamma (6.29) \gamma \gamma \gamma \gamma$  Here  $\gamma$

**3 is an embedding parameter, the non-zero auxiliary parameters are  $\gamma \gamma \gamma \gamma$ ,  $\gamma \gamma$ ,  $\gamma \gamma$  and  $\gamma \gamma$  and the nonlinear operators**

are  $N??$ ,  $N?$ ,  $N?$  and  $N?$ . When  $? = 0$  and  $? = 1$  one has

$$12^{?^?}(?;0) = ?0(?)? ?^?(??0) = ?0(?)? ^?(??0) = ?0(?)? ^?(??0) = ?0(?)? ?^?(?; 1) = ?$$

$$(?)? ?^?(?? 1) = ?(?)? ^?(?? 1) = ?(?)? ?^?(?? 1) = ?0(?)?$$

(6.30) Clearly when  $?$  is increased from 0 to 1 then  $?(???)?$ ,  $?(???)$  and  $?(???)$  vary from  $?0(?)?$ ,  $0(?)?$ ,  $?0(?)$  and  $?0(?)$  to  $?(?)?$ ,  $?(?)?$ ,  $?(?)$  and  $?(?)$ . By Taylor's expansion we have  $?(???) = ?0(?) + ? = 1??$   
 $(?)?? ?^?(?) = ?1! ?^{??}(??;?)^{-?} = 0 \infty ?$  (6.31)  $?(???) = ?0(?) + ? = 1??(?)?? ?^?(?) = ?1! ?^{??}(??;?)^{-?} = 0$   
 $\infty ?$  (6.32)  $P^{-} ?(?? ?) = ?0(?) ? = P1??(?)?? ?^?(?) = ?1! ?^{??}(??;?)^{-?} = 0 \infty ?$  (6.33)  $P^{-} ?(?? ?) =$   
 $?0(?) \infty ?$  (6.34)  $? = 1 ?(?)?? ?^?(?) = ?1! ?^{??}(??; ?)^{-?} = 0$

**3 where the convergence of above series strongly depends upon  $\sim ? ? \sim ?$   
 $\sim ?$  and  $\sim ?$ . Considering that  $\sim ? ? \sim ?$  and  $\sim ?$  are selected properly so  
 that**

Eqs. (6.31)–(6.34) converge at  $? = 1$  then we have  $?(?) = ?0(?) + ??(?)? \infty ? = 1$   $P^{\infty} ?(?) = ?0(?) + ??(?)?$   
 $? = 1$   $P^{\infty} ?(?) = ?0(?) + ??(?)? ? = 1$   $P^{\infty} ?(?) = ?0(?) + ??(?)? ? = 1$  The general solutions can be expressed  
 below:  $P ?(??) = ??*(?) + ?1 + ?2?? + ?3? - ?? ?(??) = ??*(?) + ?4 + ?5?? + ?6? - ?? ?(??) = ?*?(?) + ?$   
 $7?? + ?8? - ?? ?(??) = ?*?(?) + ?9?? + ?10? - ??$  in which the  $??*?$ ,  $??*$  and  $??*$  indicate the  
 special solutions. (6.35) (6.36) (6.37) (6.38) (6.39) (6.40) (6.41) (6.42) 6.3 Convergence analysis and  
 discussion Clearly the homotopic series solutions (6.35) – (6.38) depend on the auxiliary parameters  $\sim ? ?$   
 $\sim ? ? \sim ?$  and  $\sim ? ?$ . These parameters have important role in the convergence of series solutions. For this  
 purpose, the  $\sim$ -curves are drawn at 15 $??$  order of approximations to determine the suitable ranges of  
 these auxiliary parameters. Fig. 6.1 shows that the acceptable values of  $\sim ? ? \sim ? ? \sim ?$  and  $\sim ?$  are  $-1?4 \leq$   
 $\sim ? \leq -0?20$   $-1?6 \leq \sim ? \leq -0?40$  and  $-1?50 \leq \sim ? ? \sim ? \leq -0?30$ . Table 6.1 ensures the convergence of  
 homotopic

**1 series solutions in the whole region of  $?$  when  $\sim ? = \sim ? = \sim ? = \sim ? = -0? 5? f''?$   
 $0?$ ,  $g''?0?$ ,**

$q'?0?$ ,  $f'?0?$  0.5  $b1 = b = b^* = g1 = g2 = 0.2$ ,  $l = N = 0.5$ ,  $Pr = Sc = 0.7$   $g''(0)$   $f'(0)$  0.0 -0.5.  $q'(0)$   $f''(0)$  -10. -15.  
 -10. -0.5 0.0  $hf, hg, hq, hf$  Fig. 6.1:  $\sim$ -curves for the functions  $?? ?$ ,  $?$  and  $??$  Table 6

**2.1: Convergence of series solutions for different order of approximations  
 when**

$? = ?1 = ?* = 0?2?$   $?2 = ? = ? = 0?3?$   $?1 = 0?5?$   $?? = 1?0?$   $?? = 1?2$  and  $\sim ? = \sim ? = \sim ? = \sim ? = -0?5?$   
 order of approximations  $-?00(0)$   $-?00(0)$   $-?0(0)$   $-?0(0)$  1 1.018 0.1497 0.3133 0.2228 5 1.029 0.06217  
 0.2782 0.2095 10 1.028 0.03940 0.2703 0.2067 15 1.029 0.03866 0.2702 0.2066 20 1.029 0.03982  
 0.2705 0.2066 25 1.029 0.03993 0.2705 0.2066 30 1.029 0.03993 0.2705 0.2066 Figs. 6.2-6.7 show the  
 effects of Deborah number  $?1?$  mixed convection parameter  $??$  con- centration buoyancy parameter  $?$  and

internal heat source/sink parameter  $\gamma^*$  on the velocity profiles  $u_0(\eta)$  and  $u_1(\eta)$ ? Figs. 6.2 and 6.3 are drawn to see the behavior of Deborah number  $\gamma_1$  on the velocity profiles  $u_0(\eta)$  and  $u_1(\eta)$ ? It is found that both the velocity profiles  $u_0(\eta)$  and  $u_1(\eta)$  decrease with an enhancement in  $\gamma_1$ ? It is also examined from these Figs. that associated boundary layer thicknesses are decreasing functions of  $\gamma_1$ ? This is due to the fact that  $\gamma_1$  depends on relaxation time. Larger relaxation time offers more resistance to the flow due to which the velocities are decreased. Figs. 6.4 and 6.5 are displayed to see the impact of mixed convection parameter  $\gamma$  on the velocity profiles  $u_0(\eta)$  and  $u_1(\eta)$ ? It is seen that both the velocity profiles  $u_0(\eta)$  and  $u_1(\eta)$  increase with an enhancement in  $\gamma$ ? Also momentum boundary layer thicknesses are increased with an increase in  $\gamma$ ? In fact an increase in  $\gamma$  enhances the buoyancy forces which are more dominant to viscous forces. Variations of concentration buoyancy parameter  $\gamma$  on the velocity profiles  $u_0(\eta)$  and  $u_1(\eta)$  are displayed in the Figs. 6.6 and 6.7. Similar behavior of  $\gamma$  is noted on the velocity profiles  $u_0(\eta)$  and  $u_1(\eta)$ ? Figs. 6.8 and 6.9 are plotted to see the variations of internal heat source/sink parameter  $\gamma^*$  and heat transfer

**2 Biot number  $\gamma_1$  on the temperature  $\theta(\eta)$ ? Fig.**

6.8 depicts that the

**13 thermal boundary layer thickness and temperature  $\theta(\eta)$  are increasing functions of**

internal heat source parameter  $\gamma^* \geq 0$  and decreasing functions of internal heat sink  $\gamma^* \leq 0$ ? With an increase in heat transfer Biot number  $\gamma_1$ ? both the thermal boundary layer thickness and temperature  $\theta(\eta)$  are enhanced (see Fig. 6.9). The reason is that as  $\gamma_1$  depends on heat transfer coefficient  $h$  which leads to an increase in temperature  $\theta(\eta)$ ? Figs. 6.10 is displayed to analyze the behavior of concentration  $\phi(\eta)$  for different values of mass transfer Biot number  $\gamma_2$ . It is observed that as  $\gamma_2$  increases the associated boundary layer thickness and concentration profile  $\phi(\eta)$  grow. As mass transfer Biot number  $\gamma_2$  depends on mass transfer coefficient  $h_m$  so with an enhancement in  $\gamma_2$  the mass transfer coefficient increases which leads to an increase in concentration profile  $\phi(\eta)$ ? Impacts of mixed convection parameter  $\gamma$  concentration buoyancy parameter  $\gamma$  Deborah number  $\gamma_1$  and internal heat source/sink parameter  $\gamma^*$  on the local Nusselt number  $(-u_0'(0))$  are displayed in the Figs. 6.11 and 6.12. It is found that local Nusselt number  $(-u_0'(0))$  enhances with an increase in  $\gamma$  and  $\gamma_1$  (see Fig. 6.11). Local Nusselt number  $(-u_0'(0))$  reduces with internal heat source parameter  $\gamma^* \geq 0$  while it increases with internal heat sink parameter  $\gamma^* \leq 0$  (see Fig. 6.12). It is also noticed from Fig. 6.12 that local Nusselt number  $(-u_0'(0))$  decreases with an increase in  $\gamma_1$ ? Figs. 6.13 and 6.14 are sketched to see the variations of mixed convection parameter  $\gamma$  concentration buoyancy parameter  $\gamma$  Deborah number  $\gamma_1$  and internal heat source/sink parameter  $\gamma^*$  on the Sherwood number  $(-\phi_0'(0))$ . Fig. 6.13 shows that the Sherwood number  $(-\phi_0'(0))$  increases with an increase in  $\gamma$  and  $\gamma_1$ . Fig. 6.14 indicates that the Sherwood number  $(-\phi_0'(0))$  increases by increasing internal heat source  $\gamma^* \geq 0$  while reverse effect is examined with an increase in Deborah number  $\gamma_1$ ?  $f''(h)$  1.0 0.8  $b = b^* = g_1 = g_2 = 0.2$ ,  $l = N = 0.5$ ,  $Pr = Sc = 0.7$  0.6 0.4  $b_1 = 0.0, 0.3, 0.6, 1.0$  0.2 0 1 2 3 4 5 6  $h$  Fig. 6.2: Variation of  $\gamma_1$  on  $u_0(\eta)$ ?  $g''(h)$  0.20  $b = b^* = g_1 = g_2 = 0.2$ ,  $l = N = 0.5$ ,  $Pr = Sc = 0.7$  0.15 0.10  $b_1 = 0.0, 0.3, 0.6, 1.0$  0.05 1 2 3 4 5 6  $h$  Fig. 6.3: Variation of  $\gamma_1$  on  $u_0(\eta)$ ?  $f''(h)$  1.0 0.8  $b_1 = b = b^* = g_1 = g_2 = 0.2$ ,  $N = 0.5$ ,  $Pr = Sc = 0.7$  0.6 0.4  $l = 0.0, 0.5, 1.0, 1.5$  0.2 0 1 2 3 4 5 6  $h$  Fig. 6.4: Variation of  $\gamma$  on  $u_0(\eta)$ ?  $g''(h)$  0.20  $b_1 = b = b^* = g_1 = g_2 = 0.2$ ,  $N = 0.5$ ,  $Pr = Sc = 0.7$  0.15 0.10  $l = 0.0, 0.5, 1.0, 1.5$  0.05 1 2

3 4 5 6 h Fig. 6.5: Variation of  $\eta$  on  $\eta(0)$ ?  $f''(0)$ ? 1.0 0.8  $b_1 = b = b^* = g_1 = g_2 = 0.2$ ,  $I = 0.5$ ,  $Pr = Sc = 0.7$  0.6 0.4  $N = 0.0, 1.5, 3.0, 4.5$  0.2 0 1 2 3 4 5 6 h Fig. 6.6: Variation of  $\eta$  on  $\eta(0)$ ?  $g''(0)$ ? 0.20  $b_1 = b = b^* = g_1 = g_2 = 0.2$ ,  $I = 0.5$ ,  $Pr = Sc = 0.7$  0.15  $N = 0.0, 1.5, 3.0, 4.5$  0.10 0.05 1 2 3 4 5 6 h Fig. 6.7: Variation of  $\eta$  on  $\eta(0)$ ?  $q''(0)$ ? 0.20  $b = b_1 = g_1 = g_2 = 0.2$ ,  $I = N = 0.5$ ,  $Pr = Sc = 0.7$  0.15 0.10  $b^* = -0.4, -0.2, 0.0, 0.2, 0.4$  0.05 1 2 3 4 5 6 h Fig. 6.8: Variation of  $\eta^*$  on  $\eta(0)$ ?  $q''(0)$ ? 0.35 0.30  $b = b_1 = b^* = g_2 = 0.2$ ,  $I = N = 0.5$ ,  $Pr = Sc = 0.7$  0.25 0.20 0.15  $g_1 = 0.1, 0.2, 0.3, 0.4$  0.10 0.05 1 2 3 4 5 6 h Fig. 6.9: Variation of  $\eta_1$  on  $\eta(0)$ ?  $f''(0)$ ? 0.35 0.30  $b = b_1 = b^* = g_1 = 0.2$ ,  $I = N = 0.5$ ,  $Pr = Sc = 0.7$  0.25 0.20 0.15  $g_2 = 0.1, 0.2, 0.3, 0.4$  0.10 0.05 1 2 3 4 5 6 h Fig. 6.10: Variation of  $\eta_2$  on  $\eta(0)$ ?  $-q''(0)$ ? 0.33 0.32  $b_1 = b^* = g_1 = 0.2$ ,  $g_2 = 0.3$ ,  $Pr = Sc = 0.7$  0.31  $N = 0.0, 0.5, 1.0, 1.5$  0.30 0.29 0.28 1 2 3 4 5 6 7 I Fig. 6.11: Variations of  $\eta$  and  $\eta$  on  $-\eta(0)$ ?  $-q''(0)$ ? 0.32  $b^* = 0.2, 0.1, 0.0, -0.1, -0.2$  0.31 0.30 0.29 0.28  $I = N = 0.5$ ,  $g_1 = 0.2$ ,  $g_2 = 0.3$ ,  $Pr = Sc = 0.7$  1 2 3 4  $b_1$  Fig. 6.12: Variations of  $\eta^*$  and  $\eta_1$  on  $-\eta(0)$ ?  $-f''(0)$ ? 0.295  $b_1 = b^* = g_1 = 0.2$ ,  $g_2 = 0.3$ ,  $Pr = Sc = 0.7$  0.290 0.285  $N = 0.0, 0.5, 1.0, 1.5$  0.280 0.275 1 2 3 4 5 6 7 I Fig. 6.13: Variations of  $\eta$  and  $\eta$  on  $-\eta(0)$ ?  $??''(0)$ ? 0.2748  $I = N = 0.5$ ,  $g_1 = 0.2$ ,  $g_2 = 0.3$ ,  $Pr = Sc = 0.7$  0.2746 0.2744 0.2742 0.2740 0.2738  $b_1 = 0.1, 0.2, 0.3, 0.4$  0.2736 \* 1 2 3 4  $b$  Fig. 6.14: Variations of  $\eta_1$  and  $\eta^*$  on  $-\eta(0)$ ? 6.3.1 Conclusions

Three-dimensional mixed

1 **convection flow of Maxwell fluid over a stretching sheet**

2 **with internal heat generation/** absorption is analyzed. **Convective boundary**

conditions for both heat and mass transfer are considered. The main observations are mentioned below. • Variations of mixed convection parameter  $\eta$  and concentration buoyancy parameter  $\eta$  enhance the velocity profiles and associated boundary layer thicknesses. • Velocity profiles and temperature increase in case of internal heat source  $\eta^* \geq 0$  while these reduce for heat sink  $\eta^* \leq 0$ . • Heat transfer Biot number  $\eta_1$

16 **increases the thermal boundary layer thickness and**

tem- perature. Also concentration and its associated boundary layer are enhanced with an increase in mass transfer Biot number  $\eta_2$ . • The

7 **local Nusselt and Sherwood numbers have** quite similar behaviors **for** increasing values of

mixed convection parameter  $\eta$ ? concentration buoyancy parameter  $\eta$  and Deborah number  $\eta_1$ . • Larger values of heat sink parameter  $\eta^* \leq 0$  give rise to the local Nusselt number ( $-\eta(0)$ ). However Sherwood number ( $-\eta(0)$ ) enhances with an increase in heat source  $\eta^* \geq 0$ . Chapter 7 Soret and Dufour effects in three-dimensional

2 **flow of Maxwell fluid with** chemical reaction and **convective condition**



# 11 heat and mass transfer effects in three-dimensional flow of Maxwell fluid over a stretching

2 **surface with convective boundary conditions.** Mass transfer **is considered** in the

## 1 Soret and Dufour effects in the conservation law of

energy and concentration are considered. Convergent series solutions to the resulting nonlinear problems are developed. Plots of physical quantities of interest are analyzed.

### 7.1 Problems formulation

3 We consider the steady three-dimensional flow of an incompressible Maxwell fluid induced by a stretching surface

[illegible]

$0 \leq \eta \leq 1$  as  $\eta \rightarrow \infty$  (7.9) (7.10) (7.11) (7.12) (7.13) (7.14)  $\eta_1 = \eta_1 \eta_2 \eta_3 \eta_4 \eta_5 \eta_6 \eta_7 \eta_8 \eta_9 \eta_{10} \eta_{11} \eta_{12} \eta_{13} \eta_{14} \eta_{15} \eta_{16} \eta_{17} \eta_{18} \eta_{19} \eta_{20} \eta_{21} \eta_{22} \eta_{23} \eta_{24} \eta_{25} \eta_{26} \eta_{27} \eta_{28} \eta_{29} \eta_{30} \eta_{31} \eta_{32} \eta_{33} \eta_{34} \eta_{35} \eta_{36} \eta_{37} \eta_{38} \eta_{39} \eta_{40} \eta_{41} \eta_{42} \eta_{43} \eta_{44} \eta_{45} \eta_{46} \eta_{47} \eta_{48} \eta_{49} \eta_{50} \eta_{51} \eta_{52} \eta_{53} \eta_{54} \eta_{55} \eta_{56} \eta_{57} \eta_{58} \eta_{59} \eta_{60} \eta_{61} \eta_{62} \eta_{63} \eta_{64} \eta_{65} \eta_{66} \eta_{67} \eta_{68} \eta_{69} \eta_{70} \eta_{71} \eta_{72} \eta_{73} \eta_{74} \eta_{75} \eta_{76} \eta_{77} \eta_{78} \eta_{79} \eta_{80} \eta_{81} \eta_{82} \eta_{83} \eta_{84} \eta_{85} \eta_{86} \eta_{87} \eta_{88} \eta_{89} \eta_{90} \eta_{91} \eta_{92} \eta_{93} \eta_{94} \eta_{95} \eta_{96} \eta_{97} \eta_{98} \eta_{99}$   
 $-2\eta_{100}) \eta_{101} \eta_{102} \eta_{103} \eta_{104} \eta_{105} \eta_{106} \eta_{107} \eta_{108} \eta_{109} \eta_{110} \eta_{111} \eta_{112} \eta_{113} \eta_{114} \eta_{115} \eta_{116} \eta_{117} \eta_{118} \eta_{119} \eta_{120} \eta_{121} \eta_{122} \eta_{123} \eta_{124} \eta_{125} \eta_{126} \eta_{127} \eta_{128} \eta_{129} \eta_{130} \eta_{131} \eta_{132} \eta_{133} \eta_{134} \eta_{135} \eta_{136} \eta_{137} \eta_{138} \eta_{139} \eta_{140} \eta_{141} \eta_{142} \eta_{143} \eta_{144} \eta_{145} \eta_{146} \eta_{147} \eta_{148} \eta_{149} \eta_{150} \eta_{151} \eta_{152} \eta_{153} \eta_{154} \eta_{155} \eta_{156} \eta_{157} \eta_{158} \eta_{159} \eta_{160} \eta_{161} \eta_{162} \eta_{163} \eta_{164} \eta_{165} \eta_{166} \eta_{167} \eta_{168} \eta_{169} \eta_{170} \eta_{171} \eta_{172} \eta_{173} \eta_{174} \eta_{175} \eta_{176} \eta_{177} \eta_{178} \eta_{179} \eta_{180} \eta_{181} \eta_{182} \eta_{183} \eta_{184} \eta_{185} \eta_{186} \eta_{187} \eta_{188} \eta_{189} \eta_{190} \eta_{191} \eta_{192} \eta_{193} \eta_{194} \eta_{195} \eta_{196} \eta_{197} \eta_{198} \eta_{199} \eta_{200}$   
 Here  $\eta_1$  is the Deborah number,  $\eta$  the mixed convection parameter,  $\eta_{10}$  the local Grashof number,  $\eta_{20}$  the concentration buoyancy parameter,  $\eta_{30}$  the Prandtl number,  $\eta_{40}$  the Dufour number,  $\eta_{50}$  the Soret number,  $\eta_1$  and  $\eta_2$  the Eckert numbers along the  $x$  and  $y$  directions respectively,  $\eta_{10}$  the Schmidt number,  $\eta_{20}$  the chemical reaction parameter,  $\eta_{30}$  the ratio of rates parameters and  $\eta_1$  the Biot number. All parameters are defined in a sequence in which they are written and prime shows the differentiation with respect to  $\eta$ . Local Nusselt (dimensionless temperature gradient at the surface) and local Sherwood (dimensionless concentration gradient at the surface) numbers in dimensionless forms are given by  $\eta_{100} = -\eta_{101}(0)$  (7.16)  $\eta_{102} = -\eta_{103}(0)$  (7.17) in which  $\eta_{104} = \eta_{105}$  is the local Reynolds number.

7.2 Homotopy analysis solutions The initial approximations and auxiliary linear operators required for homotopy analysis solutions are presented below i.e.  $\eta_{106}(\eta) = 1 - \eta_{107} \eta_{108} \eta_{109}(\eta) = \eta_{110} 1 - \eta_{111} \eta_{112} \eta_{113}(\eta) = \eta_{114} \exp(\eta_{115} \eta_{116} \eta_{117}) \eta_{118}(\eta) = \exp(-\eta_{119})$  (7.18)  $\eta_{120} \eta_{121} \eta_{122} \eta_{123} \eta_{124} \eta_{125} \eta_{126} \eta_{127} \eta_{128} \eta_{129} \eta_{130} \eta_{131} \eta_{132} \eta_{133} \eta_{134} \eta_{135} \eta_{136} \eta_{137} \eta_{138} \eta_{139} \eta_{140} \eta_{141} \eta_{142} \eta_{143} \eta_{144} \eta_{145} \eta_{146} \eta_{147} \eta_{148} \eta_{149} \eta_{150} \eta_{151} \eta_{152} \eta_{153} \eta_{154} \eta_{155} \eta_{156} \eta_{157} \eta_{158} \eta_{159} \eta_{160} \eta_{161} \eta_{162} \eta_{163} \eta_{164} \eta_{165} \eta_{166} \eta_{167} \eta_{168} \eta_{169} \eta_{170} \eta_{171} \eta_{172} \eta_{173} \eta_{174} \eta_{175} \eta_{176} \eta_{177} \eta_{178} \eta_{179} \eta_{180} \eta_{181} \eta_{182} \eta_{183} \eta_{184} \eta_{185} \eta_{186} \eta_{187} \eta_{188} \eta_{189} \eta_{190} \eta_{191} \eta_{192} \eta_{193} \eta_{194} \eta_{195} \eta_{196} \eta_{197} \eta_{198} \eta_{199} \eta_{200}$  with the following properties of the defined operators in Eq. (7.18) i.e.  $\eta_{201}(\eta_{202} + \eta_{203} \eta_{204} + \eta_{205} \eta_{206}) = 0$   $\eta_{207}(\eta_{208} + \eta_{209} \eta_{210} + \eta_{211} \eta_{212}) = 0$   $\eta_{213}(\eta_{214} + \eta_{215} \eta_{216} + \eta_{217} \eta_{218}) = 0$  (7.20) where  $\eta_{219}$  ( $\eta_{220} = 1 - 10$ ) indicate the

2 arbitrary constants. The corresponding problems at the zeroth order are

given in the following forms:  $(1 - \eta_{221}) \eta_{222} \eta_{223}(\eta_{224}; \eta_{225}) - \eta_{226}(\eta_{227}) = \eta_{228} \eta_{229} \eta_{230} \eta_{231} \eta_{232} \eta_{233} \eta_{234} \eta_{235} \eta_{236} \eta_{237} \eta_{238} \eta_{239} \eta_{240} \eta_{241} \eta_{242} \eta_{243} \eta_{244} \eta_{245} \eta_{246} \eta_{247} \eta_{248} \eta_{249} \eta_{250} \eta_{251} \eta_{252} \eta_{253} \eta_{254} \eta_{255} \eta_{256} \eta_{257} \eta_{258} \eta_{259} \eta_{260} \eta_{261} \eta_{262} \eta_{263} \eta_{264} \eta_{265} \eta_{266} \eta_{267} \eta_{268} \eta_{269} \eta_{270} \eta_{271} \eta_{272} \eta_{273} \eta_{274} \eta_{275} \eta_{276} \eta_{277} \eta_{278} \eta_{279} \eta_{280} \eta_{281} \eta_{282} \eta_{283} \eta_{284} \eta_{285} \eta_{286} \eta_{287} \eta_{288} \eta_{289} \eta_{290} \eta_{291} \eta_{292} \eta_{293} \eta_{294} \eta_{295} \eta_{296} \eta_{297} \eta_{298} \eta_{299} \eta_{300}$   
 $[\eta_{301}(\eta_{302}; \eta_{303}) - \eta_{304}(\eta_{305})] = \eta_{306} \eta_{307} \eta_{308} \eta_{309} \eta_{310} \eta_{311} \eta_{312} \eta_{313} \eta_{314} \eta_{315} \eta_{316} \eta_{317} \eta_{318} \eta_{319} \eta_{320} \eta_{321} \eta_{322} \eta_{323} \eta_{324} \eta_{325} \eta_{326} \eta_{327} \eta_{328} \eta_{329} \eta_{330} \eta_{331} \eta_{332} \eta_{333} \eta_{334} \eta_{335} \eta_{336} \eta_{337} \eta_{338} \eta_{339} \eta_{340} \eta_{341} \eta_{342} \eta_{343} \eta_{344} \eta_{345} \eta_{346} \eta_{347} \eta_{348} \eta_{349} \eta_{350} \eta_{351} \eta_{352} \eta_{353} \eta_{354} \eta_{355} \eta_{356} \eta_{357} \eta_{358} \eta_{359} \eta_{360} \eta_{361} \eta_{362} \eta_{363} \eta_{364} \eta_{365} \eta_{366} \eta_{367} \eta_{368} \eta_{369} \eta_{370} \eta_{371} \eta_{372} \eta_{373} \eta_{374} \eta_{375} \eta_{376} \eta_{377} \eta_{378} \eta_{379} \eta_{380} \eta_{381} \eta_{382} \eta_{383} \eta_{384} \eta_{385} \eta_{386} \eta_{387} \eta_{388} \eta_{389} \eta_{390} \eta_{391} \eta_{392} \eta_{393} \eta_{394} \eta_{395} \eta_{396} \eta_{397} \eta_{398} \eta_{399} \eta_{400}$

29  $\eta_{401}(\eta_{402}; \eta_{403}) \eta_{404}(\eta_{405}; \eta_{406}) \eta_{407}(\eta_{408} \eta_{409}) \eta_{410}(\eta_{411} \eta_{412}) \eta_{413} \eta_{414}$

(7.23)  $(1 - \eta_{415}) \eta_{416} \eta_{417}(\eta_{418}; \eta_{419}) - \eta_{420}(\eta_{421}) = \eta_{422} \eta_{423} \eta_{424} \eta_{425} \eta_{426} \eta_{427} \eta_{428} \eta_{429} \eta_{430} \eta_{431} \eta_{432} \eta_{433} \eta_{434} \eta_{435} \eta_{436} \eta_{437} \eta_{438} \eta_{439} \eta_{440} \eta_{441} \eta_{442} \eta_{443} \eta_{444} \eta_{445} \eta_{446} \eta_{447} \eta_{448} \eta_{449} \eta_{450} \eta_{451} \eta_{452} \eta_{453} \eta_{454} \eta_{455} \eta_{456} \eta_{457} \eta_{458} \eta_{459} \eta_{460} \eta_{461} \eta_{462} \eta_{463} \eta_{464} \eta_{465} \eta_{466} \eta_{467} \eta_{468} \eta_{469} \eta_{470} \eta_{471} \eta_{472} \eta_{473} \eta_{474} \eta_{475} \eta_{476} \eta_{477} \eta_{478} \eta_{479} \eta_{480} \eta_{481} \eta_{482} \eta_{483} \eta_{484} \eta_{485} \eta_{486} \eta_{487} \eta_{488} \eta_{489} \eta_{490} \eta_{491} \eta_{492} \eta_{493} \eta_{494} \eta_{495} \eta_{496} \eta_{497} \eta_{498} \eta_{499} \eta_{500}$

25  $\eta_{501} \eta_{502} \eta_{503} \eta_{504} \eta_{505} \eta_{506} \eta_{507} \eta_{508} \eta_{509} \eta_{510} \eta_{511} \eta_{512} \eta_{513} \eta_{514} \eta_{515} \eta_{516} \eta_{517} \eta_{518} \eta_{519} \eta_{520} \eta_{521} \eta_{522} \eta_{523} \eta_{524} \eta_{525} \eta_{526} \eta_{527} \eta_{528} \eta_{529} \eta_{530} \eta_{531} \eta_{532} \eta_{533} \eta_{534} \eta_{535} \eta_{536} \eta_{537} \eta_{538} \eta_{539} \eta_{540} \eta_{541} \eta_{542} \eta_{543} \eta_{544} \eta_{545} \eta_{546} \eta_{547} \eta_{548} \eta_{549} \eta_{550} \eta_{551} \eta_{552} \eta_{553} \eta_{554} \eta_{555} \eta_{556} \eta_{557} \eta_{558} \eta_{559} \eta_{560} \eta_{561} \eta_{562} \eta_{563} \eta_{564} \eta_{565} \eta_{566} \eta_{567} \eta_{568} \eta_{569} \eta_{570} \eta_{571} \eta_{572} \eta_{573} \eta_{574} \eta_{575} \eta_{576} \eta_{577} \eta_{578} \eta_{579} \eta_{580} \eta_{581} \eta_{582} \eta_{583} \eta_{584} \eta_{585} \eta_{586} \eta_{587} \eta_{588} \eta_{589} \eta_{590} \eta_{591} \eta_{592} \eta_{593} \eta_{594} \eta_{595} \eta_{596} \eta_{597} \eta_{598} \eta_{599} \eta_{600}$

18  $\eta_{601}(0; \eta_{602}) = 0$   $\eta_{603}(0; \eta_{604}) = 1$   $\eta_{605}(\infty; \eta_{606}) = 0$   $\eta_{607}(0; \eta_{608}) = 0$   $\eta_{609}(0; \eta_{610}) = \eta_{611} \eta_{612} \eta_{613}(\infty; \eta_{614}) = 0$   $\eta_{615}(0; \eta_{616}) = -\eta_{617} [1 - \eta_{618}(0; \eta_{619})] \eta_{620}(\infty; \eta_{621}) = 0$   $\eta_{622}(0; \eta_{623}) = 1$   $\eta_{624}(\infty; \eta_{625}) = 0$  (7.25)  $\eta_{626} \eta_{627} \eta_{628} \eta_{629} \eta_{630} \eta_{631} \eta_{632} \eta_{633} \eta_{634} \eta_{635} \eta_{636} \eta_{637} \eta_{638} \eta_{639} \eta_{640} \eta_{641} \eta_{642} \eta_{643} \eta_{644} \eta_{645} \eta_{646} \eta_{647} \eta_{648} \eta_{649} \eta_{650} \eta_{651} \eta_{652} \eta_{653} \eta_{654} \eta_{655} \eta_{656} \eta_{657} \eta_{658} \eta_{659} \eta_{660} \eta_{661} \eta_{662} \eta_{663} \eta_{664} \eta_{665} \eta_{666} \eta_{667} \eta_{668} \eta_{669} \eta_{670} \eta_{671} \eta_{672} \eta_{673} \eta_{674} \eta_{675} \eta_{676} \eta_{677} \eta_{678} \eta_{679} \eta_{680} \eta_{681} \eta_{682} \eta_{683} \eta_{684} \eta_{685} \eta_{686} \eta_{687} \eta_{688} \eta_{689} \eta_{690} \eta_{691} \eta_{692} \eta_{693} \eta_{694} \eta_{695} \eta_{696} \eta_{697} \eta_{698} \eta_{699} \eta_{700}$

$\eta_{701}] = \eta_{702}$

9  $\eta_{703}[\eta_{704}(\eta_{705} \eta_{706}) \eta_{707}(\eta_{708} \eta_{709})] = \eta_{710} \eta_{711} \eta_{712} \eta_{713} \eta_{714} \eta_{715} \eta_{716} \eta_{717} \eta_{718} \eta_{719} \eta_{720} \eta_{721} \eta_{722} \eta_{723} \eta_{724} \eta_{725} \eta_{726} \eta_{727} \eta_{728} \eta_{729} \eta_{730} \eta_{731} \eta_{732} \eta_{733} \eta_{734} \eta_{735} \eta_{736} \eta_{737} \eta_{738} \eta_{739} \eta_{740} \eta_{741} \eta_{742} \eta_{743} \eta_{744} \eta_{745} \eta_{746} \eta_{747} \eta_{748} \eta_{749} \eta_{750} \eta_{751} \eta_{752} \eta_{753} \eta_{754} \eta_{755} \eta_{756} \eta_{757} \eta_{758} \eta_{759} \eta_{760} \eta_{761} \eta_{762} \eta_{763} \eta_{764} \eta_{765} \eta_{766} \eta_{767} \eta_{768} \eta_{769} \eta_{770} \eta_{771} \eta_{772} \eta_{773} \eta_{774} \eta_{775} \eta_{776} \eta_{777} \eta_{778} \eta_{779} \eta_{780} \eta_{781} \eta_{782} \eta_{783} \eta_{784} \eta_{785} \eta_{786} \eta_{787} \eta_{788} \eta_{789} \eta_{790} \eta_{791} \eta_{792} \eta_{793} \eta_{794} \eta_{795} \eta_{796} \eta_{797} \eta_{798} \eta_{799} \eta_{800}$   
 $\eta_{801} \eta_{802} \eta_{803} \eta_{804} \eta_{805} \eta_{806} \eta_{807} \eta_{808} \eta_{809} \eta_{810} \eta_{811} \eta_{812} \eta_{813} \eta_{814} \eta_{815} \eta_{816} \eta_{817} \eta_{818} \eta_{819} \eta_{820} \eta_{821} \eta_{822} \eta_{823} \eta_{824} \eta_{825} \eta_{826} \eta_{827} \eta_{828} \eta_{829} \eta_{830} \eta_{831} \eta_{832} \eta_{833} \eta_{834} \eta_{835} \eta_{836} \eta_{837} \eta_{838} \eta_{839} \eta_{840} \eta_{841} \eta_{842} \eta_{843} \eta_{844} \eta_{845} \eta_{846} \eta_{847} \eta_{848} \eta_{849} \eta_{850} \eta_{851} \eta_{852} \eta_{853} \eta_{854} \eta_{855} \eta_{856} \eta_{857} \eta_{858} \eta_{859} \eta_{860} \eta_{861} \eta_{862} \eta_{863} \eta_{864} \eta_{865} \eta_{866} \eta_{867} \eta_{868} \eta_{869} \eta_{870} \eta_{871} \eta_{872} \eta_{873} \eta_{874} \eta_{875} \eta_{876} \eta_{877} \eta_{878} \eta_{879} \eta_{880} \eta_{881} \eta_{882} \eta_{883} \eta_{884} \eta_{885} \eta_{886} \eta_{887} \eta_{888} \eta_{889} \eta_{890} \eta_{891} \eta_{892} \eta_{893} \eta_{894} \eta_{895} \eta_{896} \eta_{897} \eta_{898} \eta_{899} \eta_{900}$





by composition gradient, then the thermal boundary layer thickness and temperature  $\theta(\eta)$  increase with an increase in  $\eta$ . Figs. 7.6 and 7.7 illustrate the effect of Eckert numbers  $Ec_1$  and  $Ec_2$  on the temperature  $\theta(\eta)$  along the  $x$  and  $y$  directions respectively. As the Eckert number expresses the relationship between the kinetic energy in the flow and the enthalpy. It embodies the conversion of kinetic energy into internal energy by work done against the viscous fluid stresses. Greater viscous dissipative heat causes a rise

13in the temperature and thermal boundary layer thickness. Fig. 7.8 is

drawn to see the influence of mixed convection parameter  $\lambda$  on

2the temperature  $\theta(\eta)$ ? Thermal boundary layer thickness

and temperature  $\theta(\eta)$  decrease in case of assisting flow ( $\lambda > 0$ ) while increase in case of opposing flow ( $\lambda < 0$ ). This is due to the fact that in case of assisting flow ( $\lambda > 0$ ) the buoyancy forces are more dominant to viscous forces which causes a reduction in the temperature  $\theta(\eta)$  while in case of opposing flow ( $\lambda < 0$ ) the viscous forces are more dominant than buoyancy forces which in results enhances the temperature  $\theta(\eta)$ . Influence of concentration buoyancy parameter  $N$  on the temperature  $\theta(\eta)$  is seen in Fig. 7.9. It is found that the associated boundary layer and temperature  $\theta(\eta)$  is decreasing function of  $N$ .  $q^*h$  0.5 0.4 0.3 0.2 0.1 0.0 0.1 1 2 3 4 5 6 h Fig. 7.5: Influence of  $\lambda$  on  $\theta(\eta)$  when  $\lambda_1 = \lambda_2 = 0.5$   $\eta = 0.5$   $\eta = 1$   $\eta = 2$   $\eta = 3$  and  $\lambda_1 = 0.4$   $q^*h$  0.5 0.4 0.3 0.2 0.1 0.0 0.1 1 2 3 4 5 6 h Fig. 7.6: Influence of  $\lambda_1$  on  $\theta(\eta)$  when  $\lambda_1 = \lambda_2 = 0.5$   $\eta = 0.5$   $\eta = 1$   $\eta = 2$   $\eta = 3$  and  $\lambda_1 = 0.4$   $q^*h$  0.4 0.3 0.2 0.1 0.0 0.1 1 2 3 4 5 6 h Fig. 7.7: Influence of  $\lambda_2$  on  $\theta(\eta)$  when  $\lambda_1 = \lambda_2 = 0.5$   $\eta = 0.5$   $\eta = 1$   $\eta = 2$   $\eta = 3$  and  $\lambda_1 = 0.4$   $q^*h$  0.35 0.3 0.25 0.2 0.15 0.1 0.05 0.1 1 2 3 4 5 6 h Fig. 7.8: Influence of  $\lambda$  on  $\theta(\eta)$  when  $\lambda_1 = \lambda_2 = 0.5$   $\eta = 0.5$   $\eta = 1$   $\eta = 2$   $\eta = 3$  and  $\lambda_1 = 0.4$   $q^*h$  0.35 0.3 0.25 0.2 0.15 0.1 0.05 0.1 1 2 3 4 5 6 h Fig. 7.9: Influence of  $N$  on  $\theta(\eta)$  when  $\lambda_1 = \lambda_2 = 0.5$   $\eta = 0.5$   $\eta = 1$   $\eta = 2$   $\eta = 3$  and  $\lambda_1 = 0.4$  Figs. 7.10-7.13 are sketched to see the effects of Soret number  $Sr$  generative/destructive chemical reaction  $k^*$  mixed convection parameter  $\lambda$  and concentration buoyancy parameter  $N$  on concentration profile  $\phi(\eta)$ . Fig. 7.10 depicts the influence of Soret number  $Sr$  on concentration profile  $\phi(\eta)$ . As in Soret effect the temperature gradient causes the mass flux which in turn enhances the concentration profile  $\phi(\eta)$  and associated boundary layer thickness. Effect of destructive/generative chemical reaction  $k^*$  on the concentration profile  $\phi(\eta)$  is analyzed in Fig. 11. It is found that in case of generative chemical reaction ( $k^* > 0$ ) the reduction in  $\phi(\eta)$  is noted while reverse is in case of destructive chemical reaction ( $k^* < 0$ ). Figs. 7.12 and 7.13 are presented to see the effects of mixed convection parameter  $\lambda$  and concentration buoyancy parameter  $N$  on the concentration profile  $\phi(\eta)$ . These Figs. show that  $\phi(\eta)$  reduces with the increase in  $\lambda$  and  $N$ . Also the associated boundary layer thickness are decreasing functions of  $\lambda$  and  $N$ .  $f^*h$  1 0.8 0.6 0.4 0.2 0.1 0.0 0.1 1 2 3 4 5 6 h Fig. 7.10: Influence of  $Sr$  on  $\phi(\eta)$  when  $\lambda_1 = \lambda_2 = 0.5$   $Pr = 0.5$   $\lambda_1 = 0.4$   $\eta = 1$   $\eta = 2$   $\eta = 3$   $\eta = 4$   $\eta = 5$   $\eta = 6$   $f^*h$  1 0.8 0.6 0.4 0.2 0.1 0.0 0.1 1 2 3 4 5 6 h Fig. 7.11: Influence of  $k^*$  on  $\phi(\eta)$  when  $\lambda_1 = 0.5$   $\eta = 0.5$   $\eta = 1$   $\eta = 2$   $\eta = 3$  and  $\lambda_1 = 0.4$   $f^*h$  1 0.8 0.6 0.4 0.2 0.1 0.0 0.1 1 2 3 4 5 6 h Fig. 7.12: Influence of  $\lambda$  on  $\phi(\eta)$  when  $\lambda_1 = \lambda_2 = 0.5$   $\eta = 0.5$   $\eta = 1$   $\eta = 2$   $\eta = 3$  and  $\lambda_1 = 0.4$   $f^*h$  1 0.8 0.6 0.4 0.2 0.1 0.0 0.1 1 2 3 4 5 6 h Fig. 7.13: Influence of  $N$  on  $\phi(\eta)$  when  $\lambda_1 = \lambda_2 = 0.5$   $\eta = 0.5$   $\eta = 1$   $\eta = 2$   $\eta = 3$  and  $\lambda_1 = 0.4$  Table 7.1 presents the convergence of homotopic solutions. It is noted that computations are sufficient for 15<sup>th</sup> order iterations of velocity and 35<sup>th</sup> order iterations of the temperature and

concentration profiles for convergent series solutions. Tables 7.2 and 7.3 are prepared to analyze

**1 numerical values of local Nusselt and Sherwood numbers.** The values of

$- \theta(0)$  and  $- \phi(0)$  decrease by increasing Deborah number, mixed convection parameter and concentration buoyancy parameter. Here  $- \theta(0)$  increases by increasing Prandtl number and Biot number while reverse is the case of  $- \phi(0)$ . It is also found that  $- \theta(0)$  decreases by increasing Eckert numbers while opposite behavior of  $- \phi(0)$ . Table 7.4 presents the comparison of  $- \theta(0)$  and  $- \phi(0)$  for various values of  $\gamma$  in the limiting sense with ref. [13]. Table 7.5 ensures

**4 the values of local Nusselt number  $- \theta(0)$  are in good agreement with**

ref. [39] in a limiting sense. Table 7.2:

**1 Values of local Nusselt  $- \theta(0)$  and Sherwood numbers  $- \phi(0)$  for the different values of the parameters**

$\gamma$  1 2 3 4 5 6 7 8 9 10 11 12 13 14 15 16 17 18 19 20 21 22 23 24 25 26 27 28 29 30 31 32 33 34 35 36 37 38 39 40 41 42 43 44 45 46 47 48 49 50 51 52 53 54 55 56 57 58 59 60 61 62 63 64 65 66 67 68 69 70 71 72 73 74 75 76 77 78 79 80 81 82 83 84 85 86 87 88 89 90 91 92 93 94 95 96 97 98 99 100 101 102 103 104 105 106 107 108 109 110 111 112 113 114 115 116 117 118 119 120 121 122 123 124 125 126 127 128 129 130 131 132 133 134 135 136 137 138 139 140 141 142 143 144 145 146 147 148 149 150 151 152 153 154 155 156 157 158 159 160 161 162 163 164 165 166 167 168 169 170 171 172 173 174 175 176 177 178 179 180 181 182 183 184 185 186 187 188 189 190 191 192 193 194 195 196 197 198 199 200 201 202 203 204 205 206 207 208 209 210 211 212 213 214 215 216 217 218 219 220 221 222 223 224 225 226 227 228 229 230 231 232 233 234 235 236 237 238 239 240 241 242 243 244 245 246 247 248 249 250 251 252 253 254 255 256 257 258 259 260 261 262 263 264 265 266 267 268 269 270 271 272 273 274 275 276 277 278 279 280 281 282 283 284 285 286 287 288 289 290 291 292 293 294 295 296 297 298 299 300 301 302 303 304 305 306 307 308 309 310 311 312 313 314 315 316 317 318 319 320 321 322 323 324 325 326 327 328 329 330 331 332 333 334 335 336 337 338 339 340 341 342 343 344 345 346 347 348 349 350 351 352 353 354 355 356 357 358 359 360 361 362 363 364 365 366 367 368 369 370 371 372 373 374 375 376 377 378 379 380 381 382 383 384 385 386 387 388 389 390 391 392 393 394 395 396 397 398 399 400 401 402 403 404 405 406 407 408 409 410 411 412 413 414 415 416 417 418 419 420 421 422 423 424 425 426 427 428 429 430 431 432 433 434 435 436 437 438 439 440 441 442 443 444 445 446 447 448 449 450 451 452 453 454 455 456 457 458 459 460 461 462 463 464 465 466 467 468 469 470 471 472 473 474 475 476 477 478 479 480 481 482 483 484 485 486 487 488 489 490 491 492 493 494 495 496 497 498 499 500 501 502 503 504 505 506 507 508 509 510 511 512 513 514 515 516 517 518 519 520 521 522 523 524 525 526 527 528 529 530 531 532 533 534 535 536 537 538 539 540 541 542 543 544 545 546 547 548 549 550 551 552 553 554 555 556 557 558 559 560 561 562 563 564 565 566 567 568 569 570 571 572 573 574 575 576 577 578 579 580 581 582 583 584 585 586 587 588 589 590 591 592 593 594 595 596 597 598 599 600 601 602 603 604 605 606 607 608 609 610 611 612 613 614 615 616 617 618 619 620 621 622 623 624 625 626 627 628 629 630 631 632 633 634 635 636 637 638 639 640 641 642 643 644 645 646 647 648 649 650 651 652 653 654 655 656 657 658 659 660 661 662 663 664 665 666 667 668 669 670 671 672 673 674 675 676 677 678 679 680 681 682 683 684 685 686 687 688 689 690 691 692 693 694 695 696 697 698 699 700 701 702 703 704 705 706 707 708 709 710 711 712 713 714 715 716 717 718 719 720 721 722 723 724 725 726 727 728 729 730 731 732 733 734 735 736 737 738 739 740 741 742 743 744 745 746 747 748 749 750 751 752 753 754 755 756 757 758 759 760 761 762 763 764 765 766 767 768 769 770 771 772 773 774 775 776 777 778 779 780 781 782 783 784 785 786 787 788 789 790 791 792 793 794 795 796 797 798 799 800 801 802 803 804 805 806 807 808 809 810 811 812 813 814 815 816 817 818 819 820 821 822 823 824 825 826 827 828 829 830 831 832 833 834 835 836 837 838 839 840 841 842 843 844 845 846 847 848 849 850 851 852 853 854 855 856 857 858 859 860 861 862 863 864 865 866 867 868 869 870 871 872 873 874 875 876 877 878 879 880 881 882 883 884 885 886 887 888 889 890 891 892 893 894 895 896 897 898 899 900 901 902 903 904 905 906 907 908 909 910 911 912 913 914 915 916 917 918 919 920 921 922 923 924 925 926 927 928 929 930 931 932 933 934 935 936 937 938 939 940 941 942 943 944 945 946 947 948 949 950 951 952 953 954 955 956 957 958 959 960 961 962 963 964 965 966 967 968 969 970 971 972 973 974 975 976 977 978 979 980 981 982 983 984 985 986 987 988 989 990 991 992 993 994 995 996 997 998 999 1000 1001 1002 1003 1004 1005 1006 1007 1008 1009 1010 1011 1012 1013 1014 1015 1016 1017 1018 1019 1020 1021 1022 1023 1024 1025 1026 1027 1028 1029 1030 1031 1032 1033 1034 1035 1036 1037 1038 1039 1040 1041 1042 1043 1044 1045 1046 1047 1048 1049 1050 1051 1052 1053 1054 1055 1056 1057 1058 1059 1060 1061 1062 1063 1064 1065 1066 1067 1068 1069 1070 1071 1072 1073 1074 1075 1076 1077 1078 1079 1080 1081 1082 1083 1084 1085 1086 1087 1088 1089 1090 1091 1092 1093 1094 1095 1096 1097 1098 1099 1100 1101 1102 1103 1104 1105 1106 1107 1108 1109 1110 1111 1112 1113 1114 1115 1116 1117 1118 1119 1120 1121 1122 1123 1124 1125 1126 1127 1128 1129 1130 1131 1132 1133 1134 1135 1136 1137 1138 1139 1140 1141 1142 1143 1144 1145 1146 1147 1148 1149 1150 1151 1152 1153 1154 1155 1156 1157 1158 1159 1160 1161 1162 1163 1164 1165 1166 1167 1168 1169 1170 1171 1172 1173 1174 1175 1176 1177 1178 1179 1180 1181 1182 1183 1184 1185 1186 1187 1188 1189 1190 1191 1192 1193 1194 1195 1196 1197 1198 1199 1200 1201 1202 1203 1204 1205 1206 1207 1208 1209 1210 1211 1212 1213 1214 1215 1216 1217 1218 1219 1220 1221 1222 1223 1224 1225 1226 1227 1228 1229 1230 1231 1232 1233 1234 1235 1236 1237 1238 1239 1240 1241 1242 1243 1244 1245 1246 1247 1248 1249 1250 1251 1252 1253 1254 1255 1256 1257 1258 1259 1260 1261 1262 1263 1264 1265 1266 1267 1268 1269 1270 1271 1272 1273 1274 1275 1276 1277 1278 1279 1280 1281 1282 1283 1284 1285 1286 1287 1288 1289 1290 1291 1292 1293 1294 1295 1296 1297 1298 1299 1300 1301 1302 1303 1304 1305 1306 1307 1308 1309 1310 1311 1312 1313 1314 1315 1316 1317 1318 1319 1320 1321 1322 1323 1324 1325 1326 1327 1328 1329 1330 1331 1332 1333 1334 1335 1336 1337 1338 1339 1340 1341 1342 1343 1344 1345 1346 1347 1348 1349 1350 1351 1352 1353 1354 1355 1356 1357 1358 1359 1360 1361 1362 1363 1364 1365 1366 1367 1368 1369 1370 1371 1372 1373 1374 1375 1376 1377 1378 1379 1380 1381 1382 1383 1384 1385 1386 1387 1388 1389 1390 1391 1392 1393 1394 1395 1396 1397 1398 1399 1400 1401 1402 1403 1404 1405 1406 1407 1408 1409 1410 1411 1412 1413 1414 1415 1416 1417 1418 1419 1420 1421 1422 1423 1424 1425 1426 1427 1428 1429 1430 1431 1432 1433 1434 1435 1436 1437 1438 1439 1440 1441 1442 1443 1444 1445 1446 1447 1448 1449 1450 1451 1452 1453 1454 1455 1456 1457 1458 1459 1460 1461 1462 1463 1464 1465 1466 1467 1468 1469 1470 1471 1472 1473 1474 1475 1476 1477 1478 1479 1480 1481 1482 1483 1484 1485 1486 1487 1488 1489 1490 1491 1492 1493 1494 1495 1496 1497 1498 1499 1500 1501 1502 1503 1504 1505 1506 1507 1508 1509 1510 1511 1512 1513 1514 1515 1516 1517 1518 1519 1520 1521 1522 1523 1524 1525 1526 1527 1528 1529 1530 1531 1532 1533 1534 1535 1536 1537 1538 1539 1540 1541 1542 1543 1544 1545 1546 1547 1548 1549 1550 1551 1552 1553 1554 1555 1556 1557 1558 1559 1560 1561 1562 1563 1564 1565 1566 1567 1568 1569 1570 1571 1572 1573 1574 1575 1576 1577 1578 1579 1580 1581 1582 1583 1584 1585 1586 1587 1588 1589 1590 1591 1592 1593 1594 1595 1596 1597 1598 1599 1600 1601 1602 1603 1604 1605 1606 1607 1608 1609 1610 1611 1612 1613 1614 1615 1616 1617 1618 1619 1620 1621 1622 1623 1624 1625 1626 1627 1628 1629 1630 1631 1632 1633 1634 1635 1636 1637 1638 1639 1640 1641 1642 1643 1644 1645 1646 1647 1648 1649 1650 1651 1652 1653 1654 1655 1656 1657 1658 1659 1660 1661 1662 1663 1664 1665 1666 1667 1668 1669 1670 1671 1672 1673 1674 1675 1676 1677 1678 1679 1680 1681 1682 1683 1684 1685 1686 1687 1688 1689 1690 1691 1692 1693 1694 1695 1696 1697 1698 1699 1700 1701 1702 1703 1704 1705 1706 1707 1708 1709 1710 1711 1712 1713 1714 1715 1716 1717 1718 1719 1720 1721 1722 1723 1724 1725 1726 1727 1728 1729 1730 1731 1732 1733 1734 1735 1736 1737 1738 1739 1740 1741 1742 1743 1744 1745 1746 1747 1748 1749 1750 1751 1752 1753 1754 1755 1756 1757 1758 1759 1760 1761 1762 1763 1764 1765 1766 1767 1768 1769 1770 1771 1772 1773 1774 1775 1776 1777 1778 1779 1780 1781 1782 1783 1784 1785 1786 1787 1788 1789 1790 1791 1792 1793 1794 1795 1796 1797 1798 1799 1800 1801 1802 1803 1804 1805 1806 1807 1808 1809 1810 1811 1812 1813 1814 1815 1816 1817 1818 1819 1820 1821 1822 1823 1824 1825 1826 1827 1828 1829 1830 1831 1832 1833 1834 1835 1836 1837 1838 1839 1840 1841 1842 1843 1844 1845 1846 1847 1848 1849 1850 1851 1852 1853 1854 1855 1856 1857 1858 1859 1860 1861 1862 1863 1864 1865 1866 1867 1868 1869 1870 1871 1872 1873 1874 1875 1876 1877 1878 1879 1880 1881 1882 1883 1884 1885 1886 1887 1888 1889 1890 1891 1892 1893 1894 1895 1896 1897 1898 1899 1900 1901 1902 1903 1904 1905 1906 1907 1908 1909 1910 1911 1912 1913 1914 1915 1916 1917 1918 1919 1920 1921 1922 1923 1924 1925 1926 1927 1928 1929 1930 1931 1932 1933 1934 1935 1936 1937 1938 1939 1940 1941 1942 1943 1944 1945 1946 1947 1948 1949 1950 1951 1952 1953 1954 1955 1956 1957 1958 1959 1960 1961 1962 1963 1964 1965 1966 1967 1968 1969 1970 1971 1972 1973 1974 1975 1976 1977 1978 1979 1980 1981 1982 1983 1984 1985 1986 1987 1988 1989 1990 1991 1992 1993 1994 1995 1996 1997 1998 1999 2000 2001 2002 2003 2004 2005 2006 2007 2008 2009 2010 2011 2012 2013 2014 2015 2016 2017 2018 2019 2020 2021 2022 2023 2024 2025 2026 2027 2028 2029 2030 2031 2032 2033 2034 2035 2036 2037 2038 2039 2040 2041 2042 2043 2044 2045 2046 2047 2048 2049 2050 2051 2052 2053 2054 2055 2056 2057 2058 2059 2060 2061 2062 2063 2064 2065 2066 2067 2068 2069 2070 2071 2072 2073 2074 2075 2076 2077 2078 2079 2080 2081 2082 2083 2084 2085 2086 2087 2088 2089 2090 2091 2092 2093 2094 2095 2096 2097 2098 2099 2100 2101 2102 2103 2104 2105 2106 2107 2108 2109 2110 2111 2112 2113 2114 2115 2116 2117 2118 2119 2120 2121 2122 2123 2124 2125 2126 2127 2128 2129 2130 2131 2132 2133 2134 2135 2136 2137 2138 2139 2140 2141 2142 2143 2144 2145 2146 2147 2148 2149 2150 2151 2152 2153 2154 2155 2156 2157 2158 2159 2160 2161 2162 2163 2164 2165 2166 2167 2168 2169 2170 2171 2172 2173 2174 2175 2176 2177 2178 2179 2180 2181 2182 2183 2184 2185 2186 2187 2188 2189 2190 2191 2192 2193 2194 2195 2196 2197 2198 2199 2200 2201 2202 2203 2204 2205 2206 2207 2208 2209 2210 2211 2212 2213 2214 2215 2216 2217 2218 2219 2220 2221 2222 2223 2224 2225 2226 2227 2228 2229 2230 2231 2232 2233 2234 2235 2236 2237 2238 2239 2240 2241 2242 2243 2244 2245 2246 2247 2248 2249 2250 2251 2252 2253 2254 2255 2256 2257 2258 2259 2260 2261 2262 2263 2264 2265 2266 2267 2268 2269 2270 2271 2272 2273 2274 2275 2276 2277 2278 2279 2280 2281 2282 2283 2284 2285 2286 2287 2288 2289 2290 2291 2292 2293 2294 2295 2296 2297 2298 2299 2300 2301 2302 2303 2304 2305 2306 2307 2308 2309 2310 2311 2312 2313 2314 2315 2316 2317 2318 2319 2320 2321 2322 2323 2324 2325 2326 2327 2328 2329 2330 2331 2332 2333 2334 2335 2336 2337 2338 2339 2340 2341 2342 2343 2344 2345 2346 2347 2348 2349 2350 2351 2352 2353 2354 2355 2356 2357 2358 2359 2360 2361 2362 2363 2364 2365 2366 2367 2368 2369 2370 2371 2372 2373 2374 2375 2376 2377 2378 2379 2380 2381 2382 2383 2384 2385 2386 2387 2388 2389 2390 2391 2392 2393 2394 2395 2396 2397 2398 2399 2400 2401 2402 2403 2404 2405 2406 2407 2408 2409 2410 2411 2412 2413 2414 2415 2416 2417 2418 2419 2420 2421 2422 2423 2424 2425 2426 2427 2428 2429 2430 2431 2432 2433 2434 2435 2436 2437 2438 2439 2440 2441 2442 2443 2444 2445 2446 2447 2448 2449 2450 2451 2452 2453 2454 2455 2456 2457 2458 2459 2460 2461 2462 2463 2464 2465 2466 2467 2468 2469 2470 2471 2472 2473 2474 2475 2476 2477 2478 2479 2480 2481 2482 2483 2484 2485 2486 2487 2488 2489 2490 2491 2492 2493 2494 2495 2496 2497 2498 2499 2500 2501 2502 2503 2504 2505 2506 2507 2508 2509 2510 2511 2512 2513 2514 2515 2516 2517 2518 2519 2520 2521 2522 2523 2524 2525 2526 2527 2528 2529 2530 2531 2532 2533 2534 2535 2536 2537 2538 2539 2540 2541 2542 2543 2544 2545 2546 2547 2548 2549 2550 2551 2552 2553 2554 2555 2556 2557 2558 2559 2560 2561 2562 2563 2564 2565 2566 2567 2568 2569 2570 2571 2572 2573 2574 257

### 3 Values of local Nusselt number $- \theta'(0)$ for different values

of  $\gamma^*$  and  $Pr$  in a limiting sense when  $\gamma = \gamma^* = \gamma_1 = \gamma_2 = \gamma_3 = \gamma_4 = \gamma_5 = 0$  and  $\gamma_1 = 0.6$   $\gamma_1$   $Pr$   
 Present Results Hayat et al [39]  $- \theta'(0)$   $- \theta'(0)$  0.0 0.5 1.0 0.330404 0.33040 0.3 0.321661 0.32160 0.8  
 0.308651 0.30799 1.2 0.299526 0.29873 0.4 0.0 0.287813 0.28908 0.4 0.316638 0.31664 0.7 0.330168  
 0.33017 1.0 0.340702 0.34070 0.4 0.5 0.7 0.282787 0.28279 1.2 0.340424 0.34042 1.6 0.368405  
 0.36840 2.0 0.388869 0.38887 7.4 Conclusions Three dimensional

### 2 mixed convection flow of Maxwell fluid over a stretching surface with

convec- tive condition is investigated. Effects of chemical reaction and Soret and Dufour are analyzed. The main observations are listed below. • Momentum boundary layer thickness and velocity profile  $\theta(\eta)$  increase with the increase in  $\gamma$  and  $\gamma^*$ . • Concentration profile  $\phi(\eta)$  is decreasing function of generative chemical reaction parameter ( $\gamma^* > 0$ ) while increasing function of destructive chemical reaction ( $\gamma^* < 0$ ) and Soret number  $Sc$ . • Influences of  $\gamma$  and  $\gamma^*$  on  $\theta(\eta)$  and  $\phi(\eta)$  are qualitatively similar. • Thermal boundary layer thickness and temperature field increase when  $Sc$  increases. • There are opposite effects of

### 1 local Nusselt number and local Sherwood number when $\gamma$ , $\gamma^*$ $E_1$ and

$E_2$  increase. • Local Nusselt and Sherwood numbers increase when  $\gamma^*$ ,  $\gamma$  and  $Sc$  are enhanced. • Effects

### 7 of local Nusselt number and local Sherwood number for $Pr$ , $Sc$ $\gamma$ and $\gamma^*$ are

similar. Chapter 8 Radiative mixed convection

### 2 flow of an Oldroyd-B fluid by an inclined stretching surface

Mixed convection

### 2 flow of an Oldroyd-B fluid

in the presence of thermal radiation is investigated in this chapter. Flow is induced by an inclined stretching surface. The

### 2 boundary layer equations of an Oldroyd-B fluid

### 1 in the presence of heat transfer are







and  $k$  is the thermal conductivity. The appropriate boundary conditions are taken as follows:  $\theta = 0$  at  $r = 0$ ,  $\theta \rightarrow 0$  as  $r \rightarrow \infty$  with the surface temperature  $\theta_w$  by  $\theta(0) = \theta_w + \theta_0$  where  $\theta_0$  and  $\theta_w$  are the positive constants. If  $\psi$  is the stream function then defining  $\psi = \sqrt{r} f(\eta)$  where  $\eta = \frac{r}{2x}$  (8.4) (8.5) (8.6) (8.7) (8.8) the incompressibility condition is clearly satisfied and the resulting problems for  $f$  and  $\theta$  satisfy the following equations  $f''' + f f'' - \frac{1}{2} f'^2 = 0$  (8.9)  $1 + 4 f \theta'' + Pr (\theta' f - f' \theta) = 0$  (8.10)  $\mu \frac{d}{d\eta} \left( \frac{1}{\eta} \frac{d\theta}{d\eta} \right) = 0$  (8.11) In the above expressions  $Pr$  and  $\mu$  are the Deborah numbers,  $\theta$  is mixed convection parameter,  $Gr_x$  is the local Grashof number,  $Re_x$  is the Reynold number,

**1**  $Pr$  is the Prandtl number  $\theta$  is the radiation parameter and primes indicate the

differentiation with respect to  $\eta$  i.e.  $f' = \frac{df}{d\eta}$   $\theta' = \frac{d\theta}{d\eta}$   $\eta = \sqrt{R_x} \frac{r}{2x}$ ,  $\theta_w = \theta(0)$ ,  $\theta_0 = \theta(\infty)$ ,  $Pr = \frac{\mu c_p}{k}$  (8.12) Local Nusselt number  $N_x$  in terms of heat transfer  $q_w$  is  $N_x = \frac{q_w}{T_w - T_\infty}$  (8.13)  $\mu \frac{d}{d\eta} \left( \frac{1}{\eta} \frac{d\theta}{d\eta} \right) = 0$  Above equation in dimensionless variables becomes  $\frac{d}{d\eta} \left( \frac{1}{\eta} \frac{d\theta}{d\eta} \right) = 0$  (8.14) Considering the set of base functions  $\exp(-\eta)$   $\eta \geq 0$  (8.15) no one can express that  $\exp(-\eta) = \sum_{n=0}^{\infty} \frac{(-\eta)^n}{n!}$  (8.16)

**28**  $X=0$   $X=0$   $\infty$   $\exp(-\eta)$  (8.17)  $X=0$   $X=0$

where  $\theta_w$  and  $\theta_0$  are the coefficients. Initial guesses  $\theta_0$  and  $\theta_w$  and auxiliary linear operators  $\sim \theta$  and  $\sim \eta$  are chosen as follows:  $\theta_0(\eta) = 1 - \exp(-\eta)$   $\theta_w(\eta) = \exp(-\eta)$  (8.18)  $\theta_0' = \theta_w' = 0$  (8.19) where  $L = [\theta_1 + \theta_2 \exp(\eta) + \theta_3 \exp(-\eta)] = 0$   $L = [\theta_4 \exp(\eta) + \theta_5 \exp(-\eta)] = 0$  (8.20) in which  $\theta_1 = 1 - 5$

**7** are the arbitrary constants. Introducing  $\eta \in [0, 1]$  as the embedding parameter and  $\sim \theta$  and  $\sim \eta$  the non-zero auxiliary parameters, the deformation problems at the

zeroth order are  $(1 - \eta) L[\theta_0(\eta) - \theta_w(\eta)] = \sim \theta N[\theta_0(\eta) - \theta_w(\eta)]$  (8.21)  $(1 - \eta) L[\theta_0(\eta) - \theta_w(\eta)] = \sim \eta N[\theta_0(\eta) - \theta_w(\eta)]$  (8.22)  $\theta_0(\eta) = 1 - \exp(-\eta)$   $\theta_w(\eta) = \exp(-\eta)$  (8.23)  $\theta_0' = 0$   $\theta_w' = 0$  (8.24)  $\theta_0 = 1$   $\theta_w = 0$

**24**  $\theta_0(\eta) - \theta_w(\eta) = \sum_{n=0}^{\infty} \frac{(-\eta)^n}{n!}$   $\theta_0(\eta) = 1 - \exp(-\eta)$   $\theta_w(\eta) = \exp(-\eta)$

$\theta_0(\eta) = 1 - \exp(-\eta)$   $\theta_w(\eta) = \exp(-\eta)$

**24**  $\theta_0(\eta) - \theta_w(\eta) = \sum_{n=0}^{\infty} \frac{(-\eta)^n}{n!}$   $\theta_0(\eta) = 1 - \exp(-\eta)$   $\theta_w(\eta) = \exp(-\eta)$   $\theta_0' = 0$   $\theta_w' = 0$   $\theta_0 = 1$   $\theta_w = 0$

are selected such that the series  $\sum_{n=1}^{\infty} \frac{1}{n^2}$  and  $\sum_{n=1}^{\infty} \frac{1}{n^3}$  converge

## 1 Convergence of the series solutions

7 contain the non-zero auxiliary parameters  $\sim?$  and  $\sim?$ . Hence the  $\sim?$  and

**1in order to find the admissible values of**

4 **Discussion** This section examines the influence of physical parameters on the velocity  $v_0(\eta)$  and

75/97

temperature

21 **increases with the increase of inclination parameter ??** It is also observed that

2 **momentum boundary layer thickness** is a **decreasing** function of

? while

2 **thermal boundary layer thickness** is an **increasing** function of

?? Figs. 8.4 and 8.5 are sketched to analyze the effect of relaxation time parameter ?1 on the velocity and temperature. As the relaxation time parameter increases the velocity profile decreases while the temperature profile is quite opposite to that of the velocity profile. Figs. 8.6 and 8.7 examine the influence of mixed convection

27 **parameter ? on the velocity and temperature. The**

fluid velocity and associated momentum boundary layer thickness increase by increasing ?? It is clear that the temperature has opposite effect when compared with velocity. We also noticed that the fluid velocity increases rapidly in comparison to the temperature with the increasing values of ?? Figs. 8.8 and 8.9 depict the effect of retardation time ?2 on the temperature and velocity fields. Here we observed that ?2 has quite opposite effect on the velocity and temperature. The fluid velocity increases with an increase in ? 2? b1 = 0.4, l = 0.5, b2 = 0.3, R = 0.3, Pr = 0.7 1 0.8 a = 0.0 a = p?6 0.6 a = p?4 a = p?3 f?h? 0.4 0.2 0 0 2 4 6 8 10 h Fig. 8.2: Influence of sheet inclination ? on ?0(?)? b1=0.4,l=1.0,b2=0.2,R=0.5,Pr=0.7 1 0.8 a = 0.0 a = p?6 0.6 a = p?4 a = p?3

1 **q?h? 0.4 0.2 0 0 2 4 6 8 10 h**

Fig. 8.3: Influence of sheet inclination ? on ?(?)? a = p?4, l = 1.0, b2 = 0.2, R = 0.5, Pr = 0.7 1 0.8 b1 = 0.0 b1 = 0.3 0.6 b1 = 0.6 b1 = 0.9 f?h? 0.4 0.2 0 0 2 4 6 8 10 h Fig.8.4: Influence of Deborah number ?1 on ? 0(?)? a = p?4, l = 1.0, b2 = 0.2, R = 0.5, Pr = 0.7 1 0.8 b1 = 0.0 b1 = 0.3 0.6 b1 = 0.6 b1 = 0.9

1 **q?h? 0.4 0.2 0 0 2 4 6 8 10 h**

Fig. 8.5: Influence of Deborah number ?1 on ?(?)? a = p?4, R = 0.5, b1 = 0.4, b2 = 0.2, Pr = 0.7 1 0.8 l = -0.5

3 **l = 0.0 0.6 l = 0.5 l = 1.0**

Fig. 8.6: Influence of mixed convection  $\gamma$  on  $\theta(0)$ ?  $a = p^2/4$ ,  $R = 0.5$ ,  $b_1 = 0.4$ ,  $b_2 = 0.2$ ,  $Pr = 0.7$  1 0.8  $l = -0.5$

3  $l = 0.0$  0.6  $l = 0.5$   $l = 1.0$

1  $q^*h^* 0.4 0.2 0 0 2 4 6 8 10 h$

Fig. 8.7: Influence of mixed convection  $\gamma$  on  $\theta(0)$ ?  $a = p^2/4$ ,  $R = 0.5$ ,  $Pr = 0.7$ ,  $b_1 = 0.4$ ,  $l = 0.5$  1 0.8  $b_2 = 0.0$   $b_2 = 0.3$  0.6  $b_2 = 0.6$   $b_2 = 0.9$  f'  $h^* 0.4 0.2 0 0 2 4 6 8 10 h$  Fig. 8.8: Influence of Deborah number  $\gamma_2$  on  $\theta(0)$ ?  $a = p^2/4$ ,  $R = 0.5$ ,  $Pr = 0.7$ ,  $b_1 = 1.2$ ,  $l = 0.5$  1 0.8  $b_2 = 0.0$   $b_2 = 0.3$  0.6  $b_2 = 0.7$   $b_2 = 1.0$

1  $q^*h^* 0.4 0.2 0 0 2 4 6 8 10 h$

Fig. 8.9: Influence of Deborah number  $\gamma_2$  on  $\theta(0)$ ? Table 8.1 also shows

4 that the series solutions converge for 20th -order of deformations for

both the velocity and temperature. Table 8.2 analyzes the

4 numerical values of local Nusselt number for different values of  $\gamma_1$ ,  $\gamma_2$  ??  $Pr$  and

?? We note that the

3 numerical values of local Nusselt number increase with the increase

of  $\gamma_1$   $\gamma_2$  ?? and such values decrease for  $\gamma$  and  $\gamma$ . Table 8.1:

2 Convergence of homotopy solutions for different order of approximations when

$\gamma = \gamma^2/4$   $\gamma_1 = 0.2$   $\gamma_2 = 0.5$   $\gamma_2 = 0.3$   $Pr = 0.7$  and  $\gamma = 0.3$ ? Order of approximation  $-\theta(0)$   $-\theta(0)$  1 0.69555 0.73000 0.5 0.75163 0.72503 10 0.75241 0.72457 15 0.75240 0.72457 20 0.75239 0.72456 25 0.75239 0.72456 30 0.75239 0.72456 Table 8.2: Local Nusselt number and skin friction coefficient  $\theta''(0)$   $\theta''(0)$  2 ??? for some values of  $\gamma_1$  ??  $Pr$  ??  $\gamma_2$  and  $\gamma$  when  $\gamma = \gamma^2/4$   $\gamma_1$   $\gamma_2$  ??  $-(1 + 4\gamma^2)$   $\theta(0)$  0.0 0.2 0.5 0.7 0.3 0.73887 0.2 0.71284 0.4 0.72456 0.5 0.70528 0.2 0.0 0.70729 0.2 0.71925 0.4 0.72951 0.5 0.73413 0.2 0.0 0.66787 0.3 0.70324 0.5 0.71924 0.8 0.73869 0.5 0.3 0.43757 0.5 0.58961 0.7 0.71925 0.9 0.83472 0.7 0.0 0.84020 0.2 0.75419 0.5 0.66085 0.7 0.60959 8.4 Concluding remarks This chapter

examines the effect of

1 **thermal radiation on the mixed convection flow of an Oldroyd-B fluid over an inclined stretching sheet.**

The main observations of this study are as follows. • Effect of mixed convection parameter ? on the velocity and temperature are quite opposite. • Momentum and thermal boundary layers for ? have opposite effects. • Decrease in temperature is more significant in comparison to velocity when Prandtl number ? ? increases? • Thermal

1 **boundary layer thickness is decreasing function of Prandtl number. • Deborah**

numbers ?1 and ?2 have quite opposite effects for the velocity and temperature. Chapter 9 Mixed convection flow of an Oldroyd-B

3 **fluid with power law heat flux and heat source**

This chapter looks at the mixed convection

2 **flow of an Oldroyd-B fluid bounded by a porous**

stretching surface. Mathematical formulation is developed

3 **in the presence of heat source and power law heat flux. Velocity and**

temperature are computed. Plots for different parameters are analyzed.

3 **Numerical values of local Nusselt number**

are examined. 9.1 Development of

3 **problems We consider the two-dimensional flow of an incompressible Oldroyd-B fluid over a porous**

sur- face.

3 **A Cartesian coordinate system is chosen in such a way that ?-axis is taken**

along the flow direction and the  $y$ -axis perpendicular to the  $x$ -axis. The fluid fills the half space

Fig. 9.1. Physical model of the problem The present boundary layer flow is governed by the following expressions

$$u \frac{\partial u}{\partial x} + v \frac{\partial u}{\partial y} = \nu \frac{\partial^2 u}{\partial y^2} + \frac{g \beta (T - T_\infty)}{\nu} \quad (9.1)$$

$$u \frac{\partial T}{\partial x} + v \frac{\partial T}{\partial y} = \frac{k}{\rho c_p} \frac{\partial^2 T}{\partial y^2} + \frac{q_0}{\rho c_p} \quad (9.2)$$

$$\frac{\partial \psi}{\partial x} = v, \quad \frac{\partial \psi}{\partial y} = -u \quad (9.3)$$

In above equations  $u$  and  $v$

are the velocity components in the  $x$ - and  $y$ -directions,

$u$  and  $v$

are the relaxation and retardation times respectively,  $g$  the

gravitational acceleration,  $\beta$  the thermal expansion coefficient,  $\nu = (\eta/\rho)$  the kinematic viscosity,  $T$  the fluid temperature,  $T_\infty$  the

density of fluid,  $k$  the thermal conductivity of fluid,  $c_p$  the specific heat at constant pressure and  $q_0$  the heat source coefficient. The subjected boundary conditions are

$u = v = T = 0$  at  $y = 0$  and  $u = v = T = T_\infty$  as  $y \rightarrow \infty$  where  $\eta$

is the temperature coefficient and  $T_\infty$  is the ambient temperature. The

similarity transformations are given by (9.4) (9.5)  $\eta = \sqrt{\nu x} f(\eta)$   $\theta = \frac{T - T_\infty}{T_0 - T_\infty} = \frac{1}{2} + \frac{1}{2} \theta(\eta)$   $\psi = \sqrt{\nu x} f(\eta)$   $r = \frac{y}{\sqrt{\nu x}}$  in which  $\eta$

is a constant and prime denotes differentiation with respect to

Eq. (9.1) is automatically satisfied and the Eqs. (9.2-9.5) are reduced as follows

$$f''' + f f'' = 0 \quad (9.6)$$

$$\theta'' + \frac{1}{2} f \theta' = 0 \quad (9.7)$$

$$f(0) = 0, \quad f'(0) = 0, \quad f'(\infty) = 1 \quad (9.8)$$

$$\theta(0) = 1, \quad \theta(\infty) = 0 \quad (9.9)$$

are the Deborah numbers,  $\gamma = R \theta$  the mixed convection parameter with  $R = \frac{g \beta (T_0 - T_\infty) x}{\nu^2}$  the local Grashof number and  $Re_x = \frac{U_\infty x}{\nu}$  the local Reynolds number,  $\lambda = \frac{q_0 x}{\nu (T_0 - T_\infty)}$  the suction/injection parameter,  $Pr = \frac{\rho c_p \nu}{k}$  the Prandtl number and  $Gr_x = \frac{g \beta (T_0 - T_\infty) x^3}{\nu^2}$

a heat generation/absorption parameter. Expression of local Nusselt number

?? is

?? = ?(??-???) ?? = -? ???? ¶?=0 ? ? (9.11)  $\mu$  Dimensionless form of Eq. (9.11) is ? ????1??2 = - ? (0) 1 ? (9.12) 9.2 Homotopy analysis solutions Choosing the following set of base functions {?? exp(-??)?  $\geq 0$  ?  $\geq 0$ } (9.13) we express ? and ? as follows  $\infty \infty$  ?(?) = ?00?0 + ???????? exp(-??)? (9.14)

$$28X?=0 X?=0 \infty \infty ?(?) = ???????? \exp(-??)? (9.15) X?=0 X?=0$$

where ????? and ????? are the

**2coefficients. Initial approximations and auxiliary linear operators are taken in the following forms**

?0(?) = ? + 1 - exp(-?)? ?0(?) = - exp(-?)? L? = ? 000 - ? 0? L? = ?00 + ?0? L? (?1 + ?2?? + ?3?-?) = 0? L?(?4 + ?5?-?) = 0? (9.16) (9.17) (9.18) where ?? (? = 1 - 5) are the arbitrary constants. The corresponding zeroth order deformation problems are developed in the following fashion. (1 - ?) L? ? ^?(; ?) - ?0(?) = ??? N? ^?(; ?)? ^?(?? ?) ? (9.19) (1 - ?) L? ^?(; ?) - ?0(?) = ???N? ^?(; ?)? ^?(?? ?) ? h i h i (9.20)

$$12\hat{?}(0; ?) = ?? \hat{?}^0(0; ?) = 1? \hat{?}^0(\infty; ?) = 0? \hat{?}^0(0? ?) = 1? \hat{?}(\infty? ?) = 0?$$

h i h i (9.21) N?[^?(???)]= ?3??^(??3??)

$$17-\hat{?}(???)?2??^(??2??) \hat{?}^?(?? ?) 2-\tilde{A} ?? ! +?1 "2 \hat{?}^?(?? ?) \hat{?}^?(???? ?) ?2?? \hat{?}^?(??2? ?) - (\hat{?}^?(?? ?))2 ?3 \hat{?}^?(?? 3? ?) \# + (9.22)$$

?2

$$31\hat{?}^?(??2? ?) - \hat{?}^?(?? ?) 2 ?2\tilde{A} ?4 \hat{?}^?(?? ?) \hat{?}^?(??$$

?)! ??? □ +? ? (9.23) ?? □ □ N

$$24?[\hat{?}^?(?? ?)? \hat{?}^?(?? ?)] = ?2\hat{?}^?(??2? ?) + ? \hat{?}^?(?? ?)\hat{?}^?(???? ?) - 2? ? ?? \hat{?}^?(???? ?)\hat{?}^?(?? ?) + ?* \hat{?}^?(??$$

?)? (9.24)

**3in which ? is an embedding parameter, ?? and ?? the non-zero auxiliary**

parameters and  $N^0$  and  $N^1$  the nonlinear operators. For  $\eta = 0$  and  $\eta = 1$  we have

$q^0$  (0;0)

$\lim_{x \rightarrow 0} \frac{f(x) - f(0)}{x} = f'(0)$  and  $\lim_{x \rightarrow 1} \frac{f(x) - f(1)}{x - 1} = f'(1)$  (9.25) and when  $x$  increases from 0 to 1 then  $f(x)$  and  $f'(x)$  vary from  $f(0)$  to  $f(1)$  and  $f'(x)$  Taylor's series yields  $f(x) = f(0) + f'(0)x + \frac{f''(0)}{2!}x^2 + \dots$  (9.26)  $f(1) = f(0) + f'(0) + \frac{f''(0)}{2!} + \dots$  (9.27)  $f'(1) = f'(0) + f''(0) + \frac{f'''(0)}{2!} + \dots$  (9.28)  $f'(0) = 0$

3) where the convergence of above series strongly depends upon ??  
and ???

The auxiliary parameters  $\alpha$  and  $\beta$  are selected in such a way that (9?26) and (9?27) converge at  $\alpha = 1$  and hence  $\alpha(\beta) = \alpha_0(\beta) + \alpha_1(\beta)\beta \rightarrow \alpha_0(\beta) = \alpha_0$  as  $\beta \rightarrow 1$ . The  $n$ th

7-order deformation problems are constructed by the following expressions

$L^p[0, \infty) \rightarrow L^p[0, \infty)$  (9.29) (9.30) (9.31)  $L^p[0, \infty) \rightarrow L^p[0, \infty)$  (9.32) (9.33)  $R^p[0, \infty) \rightarrow R^p[0, \infty)$  (9.34)  $X^p[0, \infty) \rightarrow X^p[0, \infty)$  (9.35)  $P^p[0, \infty) \rightarrow P^p[0, \infty)$  (9.36)  $1^p[0, \infty) \rightarrow 1^p[0, \infty)$  If  $??^*$  and  $??^*$  are the special solutions then the general solutions are  $??(?) = ??^*(?) + ?1 + ?2?? + ?3?-??$  (9.37)  $??(?) = ?*? (?) + ?4 + ?5?-??$  (9.38) 9.3

1 **Convergence of the homotopy solutions** The auxiliary parameters  $\lambda$  and  $\mu$  have significant role in

the convergence of developed series solutions. Here the  $\psi$ -curves are portrayed for 18<sup>th</sup> order of approximations in order to find the values of  $\psi_0$  and  $\psi_1$  ensuring convergence. Figs. 9.2 depict

2 that the range of admissible values of  $\alpha$  and  $\beta$  are  $[-0, \infty)$

$$8 \leq \gamma \leq -0.2 \text{ and } -0.75 \leq \gamma \leq -0.2?$$

3The series solution converge in the whole region of  $z$  when

$\eta = -0.4$  and  $\eta = -0.4$ ? Table 9.1 depicts that 25% order deformations are sufficient for both the velocity and temperature expressions.  $\eta = 0.1$ ,  $S = 0.5$ ,  $b_1 = 0.2$ ,  $b_2 = 0.3$ ,  $b^* = 0.3$ ,  $Pr = 0.5$  -1.05 -1.1  $f''(\eta)$ ,  $q'(\eta)$  -1.15 -1.2 -1.25 -1.3 -1.35  $f''(\eta)$   $q'(\eta)$  -1 -0.8 -0.6 -0.4 -0.2 0  $h_f$ ,  $h_q$  Fig.9.2:  $\eta$ -curves for the function  $\eta$  and  $\eta$ ? Table 9



## 2.1. Convergence of homotopy solutions for different order of approximations when

$\eta_1 = 0.2$   $\eta_2 = 0.4$   $\eta_3 = 0.6$   $\eta_4 = 0.8$   $\eta_5 = 1.0$ ,  $\lambda = -0.4$  and  $\lambda = 0.4$  Order of approximation – 00(0) 1 1.10000 5 1.19801 10 1.20255 15 1.20268 20 1.20271 25 1.20272 30 1.20272 9.4 Graphical results and discussion – 00(0) 1.22000 1.34636 1.35611 1.35640 1.35642 1.35643 1.35643 The

2 purpose of this section is to highlight the variations of interesting parameters

through Figs. 9.3–9.7 for velocity and temperature. Figs. 9.3 and 9.4 show the behaviors of suction/injection parameter  $\lambda$  Deborah number  $\eta_1$  and mixed convection parameter  $\lambda$  on the velocity  $u(\eta)$ . Fig. 9.3 shows the effects of suction/injection parameter  $\lambda$  on the velocity profile  $u(\eta)$ . Here  $\lambda = 0$  corresponds to suction and  $\lambda = 0$  for injection case. We observed that the velocity  $u(\eta)$  is lower for suction case in comparison to injection phenomenon. From physical point of view suction is an agent that resists the fluid flow. Such resistance in fluid flow creates a reduction

7 in the velocity field and associated boundary layer thickness.

Fig. 9.4 illustrates that both the

7 fluid velocity and boundary layer thickness

decrease when mixed convection parameter is increased. Note that the mixed convection parameter involves the buoyancy force. Buoyancy force is stronger for the larger mixed convection parameter and weaker for the smaller mixed convection parameter. This stronger buoyancy acts as an agent to create a reduction in the velocity profile and momentum boundary layer thickness.  $f''(\eta)$  1.0 0.8 0.6  $b_1 = 0.4$ ,  $b_2 = 1$   $= 0.2$ ,  $b^* = 0.3$ ,  $Pr = 0.5$  0.4 0.2  $S = -0.5, 0.0, 0.5, 1.0$  0 1 2 3 4 5 6  $\eta$  Fig. 9.3: Variation of  $f''$  on  $u(\eta)$   $f''(\eta)$  1.0 0.8  $S=Pr=0.5, b_1=0.4, b_2=0.2, b^*=0.3$  0.6 0.4 0.2  $\lambda = -0.5, 0.0, 0.5, 1.0$  0 1 2 3 4 5 6  $\eta$  Fig. 9.4: Variation of  $f''$  on  $u(\eta)$  Figs. 9.5–9.7 are displayed to examine the influence of arising parameters on dimensionless temperature profile  $\theta(\eta)$ . Fig. 9.5 presents the variations in temperature  $\theta(\eta)$  for different values of suction/injection parameter  $\lambda$ . From this Fig. it is analyzed that the temperature is higher for injection case when we compared it with suction case. The effects of suction parameter  $\lambda$  on  $\theta(\eta)$  is qualitatively similar to that of the velocity.

4 Both the temperature  $\theta(\eta)$  and thermal boundary layer thickness

increase when mixed convection parameter  $\lambda$  increases (see Fig 9.6). Here buoyancy force is an agent that creates an enhancement

13 in the temperature and thermal boundary layer thickness.

Influence of heat source  $\gamma^*$  on  $\theta(\eta)$  is presented in Fig. 9.7. Physically  $\gamma^* \geq 0$  means that  $\theta \geq \theta_\infty$  and in this case heat is supplied to the flow region from the wall. The temperature boosts with heat source parameter  $\gamma^* \geq 0$  while reduction

#### 4 in thermal boundary layer thickness and

temperature is seen with heat sink parameter  $\gamma^* \leq 0$ .  $q_w/h = 0.0$   $S = -0.5, 0.0, 0.5, 1.0$   $-0.5 - 1.0$   $Pr = 0.7, b_1 = 0.4, b_2 = 1.0, b^* = 0.5$   $-1.5$   $2$   $4$   $6$   $8$  h Fig. 9.5: Variation of  $\theta$  on  $\eta(\eta)$   $q_w/h = 0.0$   $-0.2$   $-0.4$

#### 3 $Pr = 0.7, b_1 = 0.4, b_2 = 0.2, S = b^* = 0.$

$5 - 0.6$   $l = -0.5, 0.0, 0.5, 1.0$   $-0.8$   $-1.0$   $1$   $2$   $3$   $4$   $5$   $6$  h Fig. 9.6: Variation of  $\theta$  on  $\eta(\eta)$   $q_w/h = 0.0$   $-0.2$   $S = Pr = 0.5, b_1 = 0.4, b_2 = 1.0, b^* = -0.2, 0.0, 0.2, 0.3$   $-0.6$   $-0.8$   $1$   $2$   $3$   $4$   $5$   $6$  h Fig. 9.7: Variation of  $\gamma^*$  on  $\theta(\eta)$  Table 9.2 shows that the local Nusselt number has quite opposite behavior for  $\eta_1$  and  $\eta_2$ . The values of Nusselt number increases by increasing  $\gamma^*$  and  $\eta$ . However it decreases by increasing  $\eta$ . Table 9.3 ensures the validity of present results for  $\theta(0)$  in a limiting sense. Table 9.2: Values of local Nusselt number  $N_{\eta_1}$  and  $N_{\eta_2}$  for the parameters  $\eta_1, \eta_2, \gamma^*, \eta$  when  $\eta = 0$   $\eta_1 = \eta_2 = \gamma^* = Pr = -0.5, 0.0, 0.5, 1.0$   $0.0$   $0.3$   $0.5$   $0.5$   $0.1$   $1.20133$   $0.2$   $1.17496$   $0.4$   $1.14936$   $0.74$   $1.18647$   $0.75$   $1.19622$   $0.76$   $1.20463$   $-0.71$   $1.02500$   $-0.72$   $1.09798$   $-0.73$   $1.16099$   $0.76$   $1.27668$   $0.79$   $1.60523$   $1.2$   $1.91014$   $0.78$   $1.23081$   $1.70$   $1.30323$   $1.75$   $1.45103$   $0.72$   $1.15381$   $0.74$   $1.13613$   $0.76$   $1.11294$  Table 9.3: Comparison of  $\theta(0)$  for different values of Maxwell parameter  $\eta_1$  when  $\eta_2 = \eta = \gamma^* = 0$  Abel et al. [38] Present results  $\eta_1 = -0.5, 0.0(0)$   $-0.5$   $0.0(0)$   $0.0$   $1.00000$   $1.00000$   $0.2$   $1.051948$   $1.051889$   $0.4$   $1.101850$   $1.101903$   $0.6$   $1.150163$   $1.150137$   $0.8$   $1.196692$   $1.196711$   $1.2$   $1.285257$   $1.285363$   $1.6$   $1.368641$   $1.368758$   $2.0$   $1.447617$   $1.447651$   $9.5$  Final remarks This chapter deals with the

#### 21 mixed convection flow of Oldroyd-B fluid over a stretching sheet

with suction/injection, heat source/sink and power law heat flux. Effects of different involved parameters such as mixed convection parameter  $\beta$

#### 8 and heat source/sink $\gamma^*$ on the flow

field and temperature are analyzed. The main observations are summarized as follows: • Velocity profile

#### 2 and momentum boundary layer thickness reduce in

case of suction  $\beta \geq 0$  while these enhance in case of injection  $\beta \leq 0$  •

#### 2 Thermal boundary layer thickness is increasing function of

heat source parameter  $\gamma \neq 0$  while it reduces with heat absorption parameter  $\gamma \neq 0$  • Increase in mixed convection parameter  $\gamma$  yields an enhancement

**13 in the temperature and thermal boundary layer thickness**

while reduction in

**2 heat transfer rate at wall is**

noted. • Behaviors of Deborah numbers  $\gamma_1$  and  $\gamma_2$  on the

**2 heat transfer rate at the wall** are opposite? **Heat transfer rate at wall**

increases with the heat absorption  $\gamma \neq 0$  and suction parameters  $\gamma \neq 0$  Chapter 10

**1 Soret and Dufour effects in mixed convection flow of an Oldroyd-B fluid**

**4 with convective boundary conditions** This chapter investigates **the effects of**

**6 heat and mass transfer in the mixed convection**

**1 flow of an Oldroyd-B fluid over a stretching surface with convective boundary conditions.**

Emphasis is given to the analysis of Soret and Dufour effects. Relevant problems are first formulated and then computed by the homotopy analysis method (HAM). Velocity, temperature and concentration fields are computed and analyzed through plots. In addition, the local Nusselt and Sherwood numbers are examined through the numerical values. 10.1 Mathematical model We choose  $x$ -axis

**14 along the stretching surface in the flow direction and  $y$ -axis is taken perpendicular to the**

surface. An incompressible Oldroyd-B fluid is considered. The surface satisfies the convective boundary conditions. Further, the Soret and Dufour effects are taken into account. The resulting boundary layer equations for flow of an Oldroyd-B fluid are  $\gamma \neq 0 + (10.1) \gamma \neq 0 + \gamma \neq 0 = \gamma \neq 0 \gamma \neq 0 - \gamma_1$

7 velocity components in the  $x$ - and  $y$ -directions respectively,  $v_1$  and  $v_2$  the

26 Schmidt number, ?? the Dufour number and ?? the Sporet number.

$$9[7^x((x-1)^2 - 1)^2] = 7^x x^2 (x-1)^2 - 7^x (x-1)^2 x^2 - 7^x (x-1)^2 x^2$$

[https://www.turnitin.com/newreport\\_printview.asp?eq=1&eb=1&esm=3&oid=437813038&sid=0&n=0&m=0&svr=9&r=97.82056855037808&lang=en\\_us](https://www.turnitin.com/newreport_printview.asp?eq=1&eb=1&esm=3&oid=437813038&sid=0&n=0&m=0&svr=9&r=97.82056855037808&lang=en_us) 85/97

## 2.1: Convergence of homotopy solutions for different order of approximations when

2the temperature  $T_f$ ? Also thermal boundary layer thickness

86/97

**2 boundary layer thickness are decreasing functions of  $\eta$ . Fig. 10.4 shows that**

temperature  $\theta(\eta)$

**4 and thermal boundary layer thickness increase**

with an increase in Dufour number  $Da$ . With

**13 an increase in Soret number  $Sr$  temperature  $\theta(\eta)$  and thermal boundary layer thickness**

decrease as seen in Fig. 10.5.  $b_1 = g_1 = 0.4$ ,  $N = 0.3$ ,  $Df = 0.5$ ,  $Pr = Sc = 0.7$ ,  $b_2 = Sr = 0.2$   $0.3$   $I = -1.0$

**3  $I = 0.0$   $q^*h^* 0.2$   $I = 1.0$   $I = 2.0$**

0.1 0.0 0.2 0.4 0.6 0.8 1.0  $h$  Fig. 10.2: Influence of  $\eta$  on  $\theta(\eta)$ ?  $b_1 = g_1 = 0.4$ ,  $b_2 = I = 0.3$ ,  $Df = 0.5$ ,  $Pr = Sc = 0.7$ ,  $Sr = 0.2$   $0.35$   $N = 0.0$   $0.3$   $N = 1.5$   $0.25$   $N = 3.0$   $N = 4.5$   $q^*h^* 0.2$   $0.15$   $0.1$   $0.05$   $0.0$   $0.2$   $0.4$   $0.6$   $0.8$   $1.0$   $h$  Fig. 10.3: Influence of  $\eta$  on  $\theta(\eta)$ ?  $b_1 = 0.4$ ,  $b_2 = N = 0.3$ ,  $g_1 = 1.0$ ,  $I = 0.6$ ,  $Pr = Sc = 0.7$ ,  $Sr = 0.8$   $0.6$   $Df = 0.0$   $0.5$   $Df = 0.5$   $Df = 1.0$   $0.4$   $Df = 1.5$

**4  $q^*h^* 0.3$   $0.2$   $0.1$   $0.0$   $0.2$   $0.4$   $0.6$   $0.8$   $1.0$   $h$**

Fig. 10.4: Influence of  $\eta$  on  $\theta(\eta)$ ?  $b_1 = 0.4$ ,  $b_2 = N = 0.3$ ,  $g_1 = 1.0$ ,  $I = 0.6$ ,  $Pr = Sc = 0.7$ ,  $Df = 0.5$   $0.6$   $Sr = 0.0$   $0.5$   $Sr = 0.5$   $Sr = 1.0$   $0.4$   $Sr = 1.5$   $q^*h^* 0.3$   $0.2$   $0.1$   $0.0$   $0.1$   $0.2$   $0.3$   $0.4$   $0.5$   $0.6$   $h$  Fig. 10.5: Influence of  $\eta$  on  $\theta(\eta)$ ? Figs. 10.6 – 10.9 plot the effects of  $\eta$   $\eta$   $\eta$  and  $\eta$  on the concentration field  $\theta(\eta)$ ? From Fig. 10.6

**4 it is found that the concentration field and associated boundary layer thickness show a decrease when**

mixed convection parameter  $\eta$  increases? Effects of concentration buoyancy parameter parameter  $\eta$  on the concentration are qualitatively similar to that of temperature (see Figs. 10.3 and 10.7). Figs. 10.4 and 10.8 show that the behaviors of the temperature and concentration profiles are quite opposite in case of Dufour number. This shows that the Dufour number corresponds to weaker concentration and stronger temperature. Fig. 10.9 pointed out that the larger Soret number has a strong concentration.  $b_1 = g_1 = 0.4$ ,  $N = 0.3$ ,  $Df = 0.5$ ,  $Pr = Sc = 0.7$ ,  $b_2 = Sr = 0.2$   $1$   $0.8$   $I = -1.0$   $I = 0.0$   $0.6$   $I = 1.0$   $I = 2.0$   $f^*h^* 0.4$   $0.2$   $0.0$   $0.2$   $0.4$   $0.6$   $0.8$   $1.0$   $h$  Fig. 10.6: Influence of  $\eta$  on  $\theta(\eta)$ ?  $b_1 = g_1 = 0.4$ ,  $b_2 = I = 0.3$ ,  $Df = 0.5$ ,  $Pr = Sc = 0.7$ ,  $Sr = 0.2$   $1$   $0.8$   $N = 0.0$   $N = 1.5$   $0.6$   $N = 3.0$   $N = 4.5$   $f^*h^* 0.4$   $0.2$   $0.0$   $0.2$   $0.4$   $0.6$   $0.8$   $1.0$   $h$  Fig. 10.7: Influence of  $\eta$  on  $\theta(\eta)$ ?  $b_1 = 0.4$ ,  $b_2 = N = 0.3$ ,  $g_1 = 1.0$ ,  $I = 0.6$ ,  $Pr = Sc = 0.7$ ,  $Sr = 0.8$   $1$   $0.8$   $Df = 0.0$   $Df = 1.0$   $0.6$   $Df = 2.0$   $Df = 3.0$   $f^*h^* 0.4$   $0.2$   $0.0$   $0.2$   $0.4$   $0.6$   $0.8$   $1.0$   $h$  Fig. 10.8: Influence of  $\eta$  on  $\theta(\eta)$ ?  $b_1 = 0.4$ ,  $b_2 = N = 0.3$ ,  $g_1 = 1.0$ ,  $I = 0.6$ ,  $Pr = Sc =$





3consider the two-dimensional Falkner-Skan flow of an Oldroyd-B fluid.

We further consider the heat transfer. Cartesian coordinates  $(x, y)$  are used

3. In such a way that  $x$ -axis is parallel to the wall and  $y$ -axis normal to it. An incompressible fluid occupies the

region  $\eta \geq 0$ ? The equations governing the present flow situation are based on the

## 2 conservation laws of mass, linear momentum and energy. Flow diagram of the

problem is as follows: Fig. 11.1: Physical Model Taking into account the aforementioned assumptions, the resulting boundary layer equations can be written as follows: 
$$\frac{\partial u}{\partial x} + v \frac{\partial u}{\partial y} = 0 \quad (11.1) \quad \frac{\partial u}{\partial x} + v \frac{\partial u}{\partial y} = 0 \quad (11.2) \quad \frac{\partial u}{\partial x} + v \frac{\partial u}{\partial y} = 0 \quad (11.3) \quad \frac{\partial u}{\partial x} + v \frac{\partial u}{\partial y} = 0 \quad (11.4)$$
 where  $u$  ( $= u_{\infty}$ ) is the free stream velocity,  $\mu$  is the dynamic viscosity,  $\tau_1$  is the relaxation time,  $\tau_2$  is the retardation time,  $\theta$  is the wedge angle,  $k$  is the thermal conductivity,  $T_s$  is the surface temperature exponent,  $T_f$  and  $T_{\infty}$  are the temperatures of the fluid and ambient respectively and  $T_w$  is the wall temperature. We utilize  $\eta = y \sqrt{\frac{u_{\infty}}{\nu x}}$ ,  $\xi = x + 1$   $\eta = 2 \sqrt{\frac{\nu x}{u_{\infty}}}$

352  $???\text{ } (?)\text{ } r\text{ } r\text{ } ??\text{ } ? = -\text{ } ? + 1\text{ } ??\text{ } r? + 1\text{ } r^2\text{ } (11.5)\text{ } r$

$?? \cdot ? (?) + ?? \rightarrow 11 ?? 0 (?) ?? (?) = ??? \rightarrow ??^{\infty}$ , where ? is the similarity variable, ?

19 is the stream function,  $\psi$  is the dimensionless stream function and  $\psi_0$  is the

[illegible]

1Pr is the Prandtl number and ? is the radiation parameter. The

[illegible]





$-1.75 \leq \eta \leq -0.25$  and  $-1.25 \leq \eta \leq -0.75$ . Table 11.1 further guarantees that the series solutions are convergent up to five decimal places when  $\eta = -0.75$ .  $b_1 = 0.3$ ,  $b_2 = 0.2$ ,  $d = 0.5$ ,  $l = 0.2$ ,  $a = p^4$ ,  $n = 1.5$ ,  $R = 0.3$ ,  $Pr = 1.2$ .  $f''(0) = -0.7$ ,  $f'''(0) = -0.8$ ,  $q'(0) = -0.9$ ,  $q''(0) = -1$ ,  $-1.1$ ,  $-1.5$ ,  $-1.25$ ,  $-1$ ,  $-0.75$ ,  $-0.5$ ,  $-0.25$ ,  $0$ .  $\eta$ ,  $\eta$  Fig 11.2 :  $\eta$ -curves for the function  $f$  and  $q$  11.4 Discussion The aim of this subsection is to present

**the effects of pertinent parameters on the velocity, temperature and**

surface heat transfer. Variation of parameter  $\eta$  on the velocity and temperature are sketched in the Figs. 11.3 and 11.4. Clearly the effects of  $\eta$  on the velocity and temperature profiles are quite reverse. Influence of

**mixed convection parameter  $\eta$  on both the velocity and**

temperature profiles are given in the Figs. 11.5 and 11.6.

**It is observed that the velocity and momentum boundary layer thickness**

increase

**with the increase of mixed convection parameter  $\eta$  while the temperature and thermal boundary layer thickness**

decrease. Figs. 11.7 and 11.8 are drawn to see the variation of  $\eta$

**on the velocity and temperature profiles. It is**

noticed that

**the velocity and momentum boundary layer thickness increase when  $\eta$  increases? It is**

found

**that the temperature and thermal boundary layer thickness are decreasing functions of**

$\eta$  Figs. 11.9 and 11.10 are sketched to see the variation of surface temperature parameter  $\eta$  on the velocity  $f'(0)$  and the temperature  $q'(0)$ . Both  $f'(0)$  and  $q'(0)$  decrease with the increase in  $\eta$ . It is also

observed that both the momentum and thermal boundary layer thicknesses decrease when  $\gamma$  increases?  
 $b_1 = 0.3$ ,  $b_2 = 0.2$ ,  $l = d = 0.5$ ,  $a = p^4$ ,  $R = 0.3$ ,  $Pr = 0.7$  1  $n = 0.5$  0.8  $n = 2.0$   $n = 5.0$   $n = 7.0$   $f''(0)$  0.6 0.4  
 0.2 0 0 2 4 6 8  $h$  Fig. 11.3: Impact of  $\gamma$  on  $f''(0)$ ?  $b_1 = 0.3$ ,  $b_2 = 0.2$ ,  $l = d = 0.5$ ,  $a = p^4$ ,  $R = 0.3$ ,  $Pr = 0.7$   
 1  $n = 0.5$  0.8  $n = 2.0$   $n = 5.0$  0.6  $n = 7.0$

1  $q''(0)$  0.4 0.2 0 0 2 4 6 8  $h$

Fig. 11.4: Impact of  $\gamma$  on  $f''(0)$ ?  $b_1 = 0.4$ ,  $b_2 = 0.3$ ,  $n = d = 0.5$ ,  $a = p^4$ ,  $R = 0.3$ ,  $Pr = 0.7$  1 0.8

3  $l = 0.0$   $l = 0.5$  0.6  $l = 1.0$   $l$

$= 1.5$   $f''(0)$  0.4 0.2 0 0 2 4 6 8  $h$  Fig. 11.5: Impact of  $\gamma$  on  $f''(0)$ ?  $b_1 = 0.4$ ,  $b_2 = 0.3$ ,  $n = d = 0.5$ ,  $a = p^4$ ,  $R = 0.3$ ,  $Pr = 0.7$  1 0.8

3  $l = 0.0$   $l = 0.5$  0.6  $l = 1.0$   $l$

$= 1.5$

1  $q''(0)$  0.4 0.2 0 0 2 4 6 8  $h$

Fig. 11.6: Impact of  $\gamma$  on  $f''(0)$ ?  $b_1 = 0.4$ ,  $b_2 = 0.3$ ,  $n = l = d = 0.5$ ,  $R = 0.3$ ,  $Pr = 0.7$  1  $a = 0.0$  0.8  $a = p^6$   $a = p^4$  0.6  $a = p^3$   $f''(0)$  0.4 0.2 0 0 2 4 6 8  $h$  Fig. 11.7: Impact of  $\gamma$  on  $f''(0)$ ?  $b_1 = 0.4$ ,  $b_2 = 0.3$ ,  $l = 1.0$ ,  $n = d = 0.5$ ,  $R = 0.3$ ,  $Pr = 0.7$  1  $a = 0.0$  0.8  $a = p^6$   $a = p^4$  0.6  $a = p^3$

1  $q''(0)$  0.4 0.2 0 0 2 4 6 8  $h$

Fig. 11.8: Impact of  $\gamma$  on  $f''(0)$ ?  $b_1 = 0.4$ ,  $b_2 = 0.3$ ,  $n = l = 0.5$ ,  $a = p^4$ ,  $R = 0.3$ ,  $Pr = 0.7$  1  $d = 0.0$  0.8  $d = 5.0$   $d = 10$  0.6  $d = 15$   $f''(0)$  0.4 0.2 0 0 2 4 6 8  $h$  Fig. 11.9: Impact of  $\gamma$  on  $f''(0)$ ?  $b_1 = 0.4$ ,  $b_2 = 0.3$ ,  $n = l = 0.5$ ,  $a = p^4$ ,  $R = 0.3$ ,  $Pr = 0.7$  1  $d = 0.0$  0.8  $d = 5.0$   $d = 10$  0.6  $d = 15$

1  $q''(0)$  0.4 0.2 0 0 2 4 6 8  $h$

Fig. 11.10: Impact of  $\gamma$  on  $f''(0)$ ? Figs. 11.11 and 11.12 are drawn to see the influence of mixed convection parameter  $\gamma$  wedge angle  $\gamma$  surface temperature parameter  $\gamma$  and velocity index  $\gamma$  on the local Nusselt number  $-f''(0)$  Fig. 11.11 depicts the effects of  $\gamma$  and  $\gamma$  on  $-f''(0)$ . It is noticed that  $-f''(0)$  increases through increase of mixed convection parameter  $\gamma$  and wedge angle  $\gamma$ . Fig. 11.12 depicts that variations of  $\gamma$  and  $\gamma$  have opposite effects on  $-f''(0)$ ? A close look at Table 11.1 indicates that 25th-order approximation gives convergent series solutions. 0.9  $n = 0.5$ ,  $R = 0.3$ ,  $Pr = 1.2$ ,  $b_1 = 0.2$ ,  $b_2 = 0.3$ ,  $d = 1.5$   $a = 0.0$  0.8  $a = p^6$   $a = p^4$   $a = p^3$   $-q''(0)$  0.7 0.6 0 1 2 3 4  $l$  Fig. 11.11: Impacts of  $\gamma$  and  $\gamma$  on  $-f''(0)$ ? 2.5  $n = 0.5$ ,  $R = 0.3$ ,  $a = p^4$ ,  $Pr = 1.2$ ,  $b_1 = 0.2$ ,  $b_2 = 0$

36.  $3n = 0.02n = 0.5n = 1.$

5  $n = 3.0$  1.5  $-q''(0) = 1.0$  0.5 0 1 2 3 4 d Fig. 11.12: Impacts of  $\gamma$  and  $\beta$  on  $-q''(0)$  Table 11

**2.1 : Convergence of the homotopy solutions for different order of approximation when**

$Pr = 1$  0,  $\gamma = 0.3$ ,  $\beta = 1.5$ ,  $\gamma = 0.5$   $\gamma = 0.3$ ,  $\beta = 0.4$   $\gamma_1 = 0.2$   $\gamma_2 = 0.3$  and  $\sim\gamma = \sim\gamma = -0.5$ . Order of approximation 1 5 10 15 20 25 30  $-q''(0)$  0.90330 0.86304 0.86077 0.86047 0.86045 0.86044 0.86044  $-q''(0)$  0.78889 0.64042 0.62757 0.62627 0.62616 0.62616 0.62616 11.5 Conclusions Mixed convection and thermal

**2 radiation effects in the Falkner-Skan wedge flow of**

an Oldroyd-B fluid are investigated. The following points are worth mentioning: • Table 11.1 shows

**1 that convergence of the functions  $\gamma$  and  $\beta$  are obtained at 25th-order approximations**

up to five decimal places when  $\sim\gamma = \sim\gamma = -0.5$  • Influence of mixed convection parameter  $\beta$  increases

**1 the velocity and momentum boundary layer thickness while it decreases**

the temperature and

**7 thermal boundary layer thickness. • Influence of wedge angle  $\gamma$  and radiation parameter**

$\gamma$  on both the temperature and velocity profiles are quite similar. • Thermal boundary layer and momentum boundary layer thicknesses are decreasing functions of surface temperature exponent  $\gamma$ . • Surface heat transfer  $-q''(0)$  increases with an increase of wedge angle  $\gamma$  mixed convection parameter  $\beta$  and surface temperature exponent  $\gamma$ . Bibliography [1] H. Schlichting, Boundary layer theory, 6th ed. Mc-Graw Hill, New York (1964). [2] B.C. Sakiadis, Boundary layer behavior on continuous solid surfaces: II Boundary on a continuous flat surface, AIChE J. 7 (1961) 221-225. [3] L.J. Crane, Flow past a stretching plate, Z. Angew. Math. Phys. 21 (1970) 645-647. [4] A. Chakrabarti and A. S. Gupta, Hydromagnetic flow and heat transfer over a stretching sheet, Quarterly Appl. Math. 37 (1979) 73-78. [5] C. K. Chen and M. I. Char, Heat transfer of a continuous stretching surface with suction or blowing, J. Math. Anal. Appl. 135 (1988) 568—580. [6] K. Vajravelu and A. Hadjinicolaou, Heat transfer in a viscous fluid over a stretching sheet with viscous dissipation and internal heat generation, Int. Commun. Heat Mass Transf. 20 (1993) 417-430. [7]

H.I. Andersson, O.R. Hansen and B. Holmedal, Diffusion of a chemically reactive species from a stretching sheet, *Int. J. Heat Mass Transf.* 37 (1994) 659—664. [8] W. H. H. Banks, Similarity solutions of the boundary-layer equations for a stretching wall, *J. Méch. Théor. Appl.* 2 (1983) 375—392. [9] T. G. Fang, J. Zhang and S. Yao, Slip magnetohydrodynamic viscous flow over a permeable shrinking sheet, *Chin. Phys. Lett.* 27 (2010) 124702. [10] S. Mukhopadhyay, G. C. Layek and S. A. Samad, Study of MHD boundary layer flow over a heated stretching sheet with variable viscosity, *Int. J. Heat Mass Transf.* 48 (2005) 4460—4466. [11] C.Y. Wang, The three-dimensional flow due to a stretching flat surface, *Phys. Fluid* 27 (1984) 1915—1917. [12] C. D. S. Devi, H. S. Takhar and G. Nath, Unsteady three-dimensional, boundary-layer flow due to a stretching surface, *Int. J. Heat Mass Transf.* 29 (1986) 1996-1999. [13] P. D. Ariel, The three-dimensional flow past a stretching sheet and the homotopy perturbation method, *Computers Mathematics Appl.* 54 (2007) 920—925. [14] P. D. Ariel, On computation of the three dimensional flow past a stretching sheet, *Appl. Math. Comput.* 188 (2007) 1244-1250. [15] T. Hayat and T. Javed, On analytic solution for generalized three-dimensional MHD flow over a porous stretching sheet, *Phys. Lett. A* 370 (2007) 243—250. [16] M. Kumari and G. Nath, Analytic solution of unsteady three-dimensional MHD boundary layer flow and heat transfer due to impulsively stretched plane surface, *Commun. Nonlinear Sci. Numer. Simulat.* 14 (2009) 3339-3350. [17] K. Vajravelu, Viscous flow over a nonlinear stretching sheet, *Appl. Math. Comput.* 124 (2001) 281—288. [18] R. Cortell, Effects of viscous dissipation and radiation on the thermal boundary layer over a nonlinearly stretching sheet, *Phys. Lett. A* 372 (2008) 631—636. [19] T. Hayat, T. Javed and Z. Abbas, MHD flow of a micropolar fluid near a stagnation-point towards a non-linear stretching surface, *Nonlinear Analysis: Real World Appl.* 10 (2009) 1514—1526. [20] N. Afzal, Momentum and thermal boundary layers over a two-dimensional or axisymmetric non-linear stretching surface in a stationary fluid, *Int. J. Heat Mass Transf.* 53 (2010) 540- 547. 179 [21] P. S. Gupta and A. S. Gupta, Heat and mass transfer on a stretching sheet with suction or blowing, *Can. J. Chem. Eng.* 55 (1977) 744-746. [22] E. Magyari and B. Keller, Heat and mass transfer in the boundary layers on an exponentially stretching continuous surface, *J. Phys. D: Appl. Phys.* 32 (1999) 577—585. [23] E. M. A. Elbashbeshy, Heat transfer over an exponentially stretching continuous surface with suction, *Arch. Mech.* 53 (2001) 643-651. [24] M. Q. Al-Odat, R. A. Damesh and T. A. Al-Azab, Thermal boundary layer on an exponentially stretching continuous surface in the presence of magnetic field, *Int. J. Appl. Mech. Eng.* 11 (2006) 289-299. [25] I. C. Liu, H. H. Wang and Y. F. Peng, Flow and heat transfer for three dimensional flow over an exponentially stretching surface, *Chem. Eng. Commun.* 200 (2013) 253-268. [26] B. S. Dandapat and A. S. Gupta, Flow and heat transfer in a viscoelastic fluid over a stretching sheet, *Int. J. Non-Linear Mech.* 24 (1989) 215-219. [27] C. K. Chen, M. I. Char and J. W. Cleaver, Temperature field in non-Newtonian flow over a stretching plate, *J. Math. Anal. Appl.* 151 (1990) 301-307. [28] K. Vajravelu and D. Rollins, Heat transfer in a viscoelastic fluid over a stretching sheet, *J. Math. Anal. Appl.* 158 (1991) 241—255. [29] T. Hayat, M. Sajid and I. Pop, Three-dimensional flow over a stretching surface in a viscoelastic fluid, *Nonlinear Analysis: Real World Appl.* 9 (2008) 1811 — 1822. [30] I. C. Liu, Flow and heat transfer of an electrically conducting fluid of second grade over a stretching sheet subject to a transverse magnetic field, *Int. J. Heat Mass Transf.* 47 (2004) 4427—4437. [31] M. M. Nandeppanavar, M. S. Abel and K. Vajravelu, Flow and heat transfer characteristics of a viscoelastic fluid in a porous medium over an impermeable stretching sheet with viscous dissipation, *Int. J. Heat Mass Transf.* 53 (2010) 4707—4713. [32] J. J. Choi, Z. Rusak and J. A. Tichy, Maxwell fluid suction flow in a channel, *J. Non-Newtonian Fluid Mech.* 85 (1999) 165. [33] K. Sadeghy, A. H. Najafi and M. Saffaripour, Sakiadis flow of an upper-convected Maxwell fluid, *Int. J. Non-Linear Mech.* 40 (2005) 1220 — 1228. [34] A. A. Pahlavan, V. Aliakbar, F. V. Farahani and K. Sadeghy, MHD flows of UCM fluids above porous stretching sheets using two-auxiliary-parameter homotopy analysis method, *Commun. Nonlinear Sci. Numer. Simulat.* 14 (2009) 473—488. [35] V. Aliakbar, A. A. Pahlavan and K. Sadeghy, The influence of thermal radiation on MHD flow of Maxwellian fluids above stretching sheets, *Commun. Nonlinear Sci. Numer. Simulat.* 14 (2009) 779—794. [36] C. Fetecau, M. Athar and C.

Fetecau, Unsteady flow of a generalized Maxwell fluid with fractional derivative due to a constantly accelerating plate, *Comput. Math. Appl.* 57 (2009) 596-603. [37] M. Kumari and G. Nath, Steady mixed convection stagnation-point flow of upper convected Maxwell fluids with magnetic field, *Int. J. Non-Linear Mech.* 44 (2009) 1048—1055. [38] M. S. Abel, J. V. Tawade and M. M. Nandeppanavar, MHD flow and heat transfer for the upper-convected Maxwell fluid over a stretching sheet, *Meccanica* 47 (2012) 385–393. [39] T. Hayat, S. A. Shehzad and A. Alsaedi, Study on three-dimensional flow of Maxwell fluid over a stretching surface with convective boundary conditions, *Int. J. Phys. Sci.* 7 (2012) 761 - 768. [40] R. K. Bhatnagar, G. Gupta and K. R. Rajagopal, Flow of an Oldroyd-B fluid due to stretching sheet in the presence of a free stream velocity, *Int. J. Non-Linear Mech.* 30 (1995) 391-405. [41] K.R. Rajagopal, On an exact solution for the flow of an Oldroyd-B fluid, *Bull. Tech. Univ. Istanbul* 49 (1996) 617-623. [42] T. Hayat, K. Hutter, S. Asghar and A. M. Siddiqui, MHD Flows of an Oldroyd-B Fluid, *Math. Comput. Modell.* 36 (2002) 987-995. 181 [43] M. D. Smith, Y. L. Joo, R. C. Armstrong and R. A. Brown, Linear stability analysis of flow of an Oldroyd-B fluid through a linear array of cylinders, *J. Non-Newtonian Fluid Mech.* 109 (2003) 13—50. [44] S. Asghar, S. Parveen, S. Hanif, A. M. Siddiqui and T. Hayat, Hall effects on the unsteady hydromagnetic flows of an Oldroyd-B fluid, *Int. J. Eng. Sci.* 41 (2003) 609—619. [45] C. Fetecau and C. Fetecau, Unsteady flows of Oldroyd-B fluids in a channel of rectangular cross-section, *Int. J. Non-Linear Mech.* 40 (2005) 1214 — 1219. [46] J. Niu, C. Fu and W. Tan, Stability of thermal convection of an Oldroyd-B fluid in a porous medium with Newtonian heating, *Phys. Lett. A* 374 (2010) 4607-4613. [47] J. Mewis, Thixotropy — a general review. *J. Non-Newtonian Fluid Mech.* 6 (1979) 1—20. [48] H. A. Barnes, Thixotropy — a review, *J. Non-Newtonian Fluid Mech.* 70 (1997) 1-33. [49] J. Harris, A continuum theory of time-dependent inelastic flow, *Rheol. Acta* 6 (1967) 6. [50] J. Harris, *Rheology and non-Newtonian flow*, London: Longman (1977). [51] S. Sadeqi, N. Khabazi and K. Sadeghy, Blasius flow of thixotropic fluids: A numerical study, *Commun. Nonlinear Sci. Numer. Simulat.* 16 (2011) 711—721. [52] J. J. M. Sillekens, C. C. M. Rindt and A. A. V. Steenhoven, Development of laminar mixed convection in a horizontal square channel with heated side walls, *Int. J. Heat and Fluid Flow* 19 (1998) 270-281. [53] G.P. Celata, A. Chiaradia, M. Cumo and F. D. Annibale, Heat transfer enhancement by air injection in upward heated mixed-convection flow of water, *Int. J. Multiphase Flow* 25 (1999) 1033-1052. [54] A. Barletta, Analysis of flow reversal for laminar mixed convection in a rectangular duct with one or more isothermal walls, *Int. J. Heat Mass Transf.* 44 (2001) 3481-3497. [55] E. Magyari, I. Pop and B. Keller, Mixed convection boundary layer flow past a horizontal permeable flat plate, *Fluid Dynamics Research* 31 (2002) 215-225. 182 [56] R. Nazar, N. Amin and I. Pop, Unsteady mixed convection boundary layer flow near the stagnation point on a vertical surface in a porous medium, *Int. J. Heat Mass Transf.* 47 (2004) 2681—2688. [57] M. A. Hossain, S. Bhowmick and R. S. R. Gorla, Unsteady mixed-convection boundary layer flow along a symmetric wedge with variable surface temperature, *Int. J. Eng. Sci.* 44 (2006) 607—620. [58] H. A. Mohammed and Y. K. Salman, Experimental investigation of mixed convection heat transfer for thermally developing flow in a horizontal circular cylinder, *Appl. Therm. Eng.* 27 (2007) 1522—1533. [59] H. A. Mohammed, Laminar mixed convection heat transfer in a vertical circular tube under buoyancy-assisted and opposed flows, *Energy Conv. Manag.* 49 (2008) 2006—2015. [60] M. Kotouc, G. Bouchet and J. Dusek, Loss of axisymmetry in the mixed convection, assisting flow past a heated sphere, *Int. J. Heat Mass Transf.* 51 (2008) 2686—2700. [61] M. Mahmood, S. Asghar and M. A. Hossain, Transient mixed convection flow arising due to thermal diffusion over a porous sensor surface inside a squeezing horizontal channel, *Int. J. Therm. Sci.* 48 (2009) 1619—1626. [62] T. Hayat, M. Mustafa and I. Pop, Heat and mass transfer for Soret and Dufour's effect on mixed convection boundary layer flow over a stretching vertical surface in a porous medium filled with a viscoelastic fluid, *Commun. Nonlinear Sci. Numer. Simulat.* 15 (2010) 1183— 1196. [63] A. J. Chamkha, Thermal radiation and buoyancy effects on hydromagnetic flow over an accelerating permeable surface with heat source or sink, *Int. J. Eng. Sci.* 38 (2000) 1699- 1712. [64] S. Abel, K. V. Prasad and A. Mahaboob, Buoyancy force and thermal radiation effects in MHD boundary layer visco-elastic fluid flow

over continuously moving stretching surface, *Int. J. Therm. Sci.* 44 (2005) 465—476. [65] S. Mukhopadhyay and G.C. Layek, Effects of thermal radiation and variable fluid viscosity on free convective flow and heat transfer past a porous stretching surface, *Int. J. Heat Mass Transf.* 51 (2008) 2167—2178. [66] S. Mukhopadhyay, Effect of thermal radiation on unsteady mixed convection flow and heat transfer over a porous stretching surface in porous medium, *Int. J. Heat Mass Transf.* 52 (2009) 3261—3265. [67] C. H. Chen, Magnetohydrodynamic mixed convection of a power-law fluid past a stretching surface in the presence of thermal radiation and internal heat generation/absorption, *Int. J. Non-Linear Mech.* 44 (2009) 596—603. [68] K. Vajravelu and D. Rollins, Heat transfer in an electrically conducting fluid over a stretching surface, *Int. J. Non-Linear Mech.* 27 (1992) 265-277. [69] M. S. Abel and M. M. Nandeppanavar, Heat transfer in MHD viscoelastic boundary layer flow over a stretching sheet with non-uniform heat source/sink, *Commun. Nonlinear Sci. Numer. Simulat.* 14 (2009) 2120—2131. [70] O. A. Beg, J. Zueco, R. Bhargava and H. S. Takhar, Magnetohydrodynamic convection flow from a sphere to a non-Darcian porous medium with heat generation or absorption effects: network simulation, *Int. J. Therm. Sci.* 48 (2009) 913—921. [71] R. Kandasamy, K. Periasamy and K. K. S. Prabhu, Chemical reaction, heat and mass transfer on MHD flow over a vertical stretching surface with heat source and thermal stratification effects, *Int. J. Heat Mass Transf.* 48 (2005) 4557—4561. [72] M. A. Mansour, N. F. E. Anssary and A. M. Aly, Effects of chemical reaction and thermal stratification on MHD free convective heat and mass transfer over a vertical stretching surface embedded in a porous media considering Soret and Dufour numbers, *Chem. Eng. J.* 145 (2008) 340—345. [73] D. Pal and B. Talukdar, Buoyancy and chemical reaction effects on MHD mixed convection heat and mass transfer in a porous medium with thermal radiation and Ohmic heating, *Commun. Nonlinear Sci. Numer. Simulat.* 15 (2010) 2878—2893. [74] G. Singh, P. R. Sharma and A. J. Chamkha, Mass transfer with chemical reaction in MHD mixed convective flow along a vertical stretching sheet, *Int. J. Energy Tech.* 4 (2012) 1-12. [75] S. J. Liao, Homotopy Analysis Method: A new analytic technique for nonlinear problems, *Commun. Nonlinear Sci. Numer. Simulat.* 2 (1997) 95-100. [76] S. J. Liao, *Beyond perturbation: introduction to Homotopy Analysis Method*, Chapman & Hall, Boca Raton (2003). [77] S. Abbasbandy, Approximate solution for the nonlinear model of diffusion and reaction in porous catalysts by means of the homotopy analysis method, *Chem. Eng. J.* 136 (2008) 144—150. [78] M. Sajid and T. Hayat, The application of homotopy analysis method to thin film flows of a third order fluid, *Chaos Solitons Fractals* 38 (2008) 506—515. [79] S. J. Liao, A short review on the homotopy analysis method in fluid mechanics, *J. Hydro- dyn.* 22 (2010) 882-884. [80] M. Turkyilmazoglu, A note on the homotopy analysis method, *Appl. Math. Lett.* 23 (2010) 1226-1230. [81] S. J. Liao, *Homotopy analysis method in nonlinear differential equations*, Higher Edu. Press, Beijing and Springer-Verlag Berlin Heidelberg (2012). [82] S. Abbasbandy, E. Shivanian and K. Vajravelu, Mathematical properties of image-curve in the frame work of the homotopy analysis method, *Commun. Nonlinear Sci. Numer. Simulat.* 16 (2011) 4268-4275. [83] M. M. Rashidi, S. A. M. Pour, T. Hayat and S. Obaidat, Analytic approximate solutions for steady flow over a rotating disk in porous medium with heat transfer by homotopy analysis method, *Comput. Fluids* 54 (2012) 1-9. [84] I. Ahmad, M. Ahmed, Z. Abbas and M. Sajid, Hydromagnetic flow and heat transfer over a bidirectional stretching surface in a porous medium, *Thermal Sci.* 15 (2011) S205-S220. [85] M. Turkyilmazoglu, Series solution of nonlinear two-point singularly perturbed boundary layer problems, *Comput. Math. Appl.* 60 (2010) 2109-2114.  $K_1 = 0.1$ ,  $K_2 = 0.2$ ,  $t = 0.3$ ,  $M = 0.6$ ,  $Sc = 0.7$ ,  $Ec = 0.5$ ,  $Pr = 1.0$ ,  $N = 0.3$ ,  $R = 0.4$   $K_2 = 0.2$ ,  $I = 0.4$ ,  $t = 0.3$ ,  $M = 0.6$ ,  $Sc = 0.7$ ,  $Ec = 0.5$ ,  $Pr = 1.0$ ,  $N = 0.3$ ,  $R = 0.4$   $K_1 = 0.1$ ,  $K_2 = 0.2$ ,  $I = 0.4$ ,  $t = 0.3$ ,  $M = 0.6$ ,  $Sc = 0.7$ ,  $Ec = 0.5$ ,  $N = 0.3$ ,  $R = 0.4$   $K_1 = 0.1$ ,  $I = 0.4$ ,  $t = 0.3$ ,  $M = 0.6$ ,  $Sc = 0.7$ ,  $Ec = 0.5$ ,  $Pr = 1.0$ ,  $N = 0.3$ ,  $R = 0.4$   $K_1 = 0.1$ ,  $K_2 = 0.2$ ,  $I = 0.4$ ,  $t = 0.3$ ,  $M = 0.6$ ,  $Sc = 0.7$ ,  $Pr = 1.0$ ,  $N = 0.3$ ,  $R = 0.4$  1 2 3 4 5 6 7 8 9 10 11 12 13 14 15 16 17 18 19 20 21 22 23 24 25 26 27 28 29 30 31 32 33 34 35 36 37 38 39 40 41 42 43 44 45 46 47 48 49 50 51 52 53 54 55 56 57 58 59 60 61 62 63 64 65 66 67 68 69 70 71 72 73 74 75 76 77 78 79 80 81 82 83 84 85 86 87 88 89 90 91 92 93 94 95 96 97 98 99 100 101

102 103 104 105 106 107 108 109 110 111 112 113 114 115 116 117 118 119 120 121 122 123 124 125  
126 127 128 129 130 131 132 133 134 135 136 137 138 139 140 141 142 143 144 145 146 147 148 149  
150 151 152 153 154 155 156 157 158 159 160 161 162 163 164 165 166 167 168 169 170 171 172 173  
174 175 176 177 178 180 183 185 186